Development and Evaluation of Criteria for the Comparison and Optimization of Bottom Hole Assemblies

by

Florian Aelfers

Submitted to the

Chair of Drilling and Completion Engineering

in Partial Fulfillment of the Requirements for the Degree of

MASTER OF SCIENCE

at the

Montanuniversität Leoben

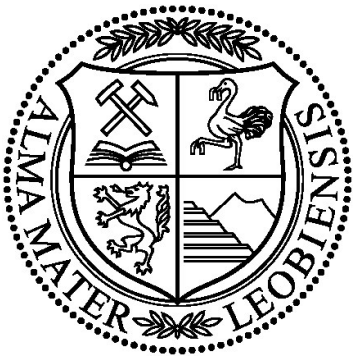

Industry Advisor:

Dr.-Ing. Hanno Reckmann

Dr.-Ing. Andreas Hohl

Dipl.-Ing. Ilja Gorelik

Dipl.-Ing. Claus Grafelmann

Dipl.-Ing. Olof Hummes

Dipl.-Ing. Christian Linke

University Advisor:

Univ.-Prof. Dipl.-Ing. Dr.mont. Gerhard Thonhauser

Scope of this Thesis

This thesis should provide a better understanding of lateral vibration phenomena encountered in directional drilling. A variation of simple model configurations is used to show the impact of geometry and excitation changes on the vibration system. These simulations are also useful for the identification of key parameters which could build the foundation of new optimization algorithms and procedures. The model builds upon existing software tools and methods to analyze beam structures and BHA components in terms of lateral vibrations. The occurring displacements, bending moments and strain energies are calculated and are presented in an easy understandable plotting format. Vibrational countermeasures, such as stabilizer placement should be identified while considering the overall functionality and purpose of the BHA design. Lateral vibration design criteria are developed, which consider the mechanical constraints such as dimensions, maximum allowable stresses and natural frequencies of the used components. Another set of criteria is based on operational requirements like steerability and BHA tool sequence.

The result should represent a platform for an easy and fast to perform lateral vibration analysis. Furthermore, should the new BHA optimization and design comparison criteria provide a better support for application engineers during the selection process.

"It is time to stop paving the cow paths. Instead of embedding outdated processes in silicon and software, we should obliterate them and start over. We should 'reengineer' our businesses: use the power of modern information technology to radically redesign our business processes in order to achieve dramatic improvements in their performance."
Michael Hammer: Harvard Business Review July/August 1990

Eidesstattliche Erklärung

Ich erkläre an Eides statt, dass ich diese Arbeit selbständig verfasst, andere als die angegebenen Quellen und Hilfsmittel nicht benutzt und mich auch sonst keiner unerlaubten Hilfsmittel bedient habe.

Affidavit

I declare in lieu of oath that I wrote this thesis and performed the associated research myself, using only literature stated in this volume.

19.01.2016
Datum / Date

Florian Aelfers
(Florian Johann Aelfers)
Matriculation number: 1035276

Acknowledgement

Special thanks to Dipl.-Ing. Claus Grafelmann who offered me a great internship opportunity with Baker Hughes first and later this master thesis project. I am very grateful for his trust into my abilities as an ongoing engineer and for micro-managing my thesis in the background. Thank you very much for very warm welcome and a friendly ear for my problems and concerns.

I owe great gratitude to Univ.-Prof. Dipl.-Ing. Dr. mont. Gerhard Thonhauser. His dedication for teaching drilling and drilling related management skills has been enrichment for my studies at the University of Leoben and helped me a lot during my studies. Thank you for the trust in me for writing my thesis abroad in Germany.

I would like to express my thanks to Dr.-Ing. Hanno Reckmann and Dipl.-Ing. Olof Hummes for their great advice and intellectual input which resulted in many interesting conversations. Their trust in my skills and knowledge helped me in fully developing my potential in merging research and application engineering into one thesis.

Further, I want to thank Dipl.-Ing. Ilja Gorelik, Dipl.-Ing. Christian Linke and Dipl.-Ing. Dr. Andreas Hohl for supervising my work. Ilja and Andreas put a lot of effort into teaching me the beauty and depth of MATLAB and research work which contributed to a very interesting work environment in which it was fun to work at. Christian supported me with is vast knowledge of drilling engineering, BHA design a drilling applications on the more practical side of my thesis. His charming and funny character helped me through some troublesome moments.

Many thanks to my family and friends for supporting me during my whole life, for making me laugh and helping me up when life was sorrowful. They have supported every decision of mine and stood behind my career decisions. I love you mom, dad and Max.

Kurzfassung

Laterale Schwingungen stellen ein großes Problem für den Bohrprozess dar. Bohrlochgarnituren (Abkürzung in Englisch: BHA) können zum Beispiel durch Schwingungen verursachte Wandkontakte und Biegebelastungen versagen und Untertagemessungen, sowie die Echtzeit-Datenübertragung, werden durch laterale Schwingungen stark beeinflusst. Obwohl laterale Schwingungen einen massiven Einfluss auf die Bohreffizienz ausüben, ist es durch ihre spezielle Ausprägung schwierig, diese zu modellieren und vorherzusagen. Laterale Schwingungen setzen sich nicht bis an die Oberfläche fort, was die Notwendigkeit von Untertagemessungen hervorruft, um diese Schwingungen zu erfassen. Dynamische Wandkontakte verändern laufend das Schwingungssystem in Bezug auf Eigenfrequenzen und Eigenformen, was zu Unterschieden in der physikalischen Auslenkung führt.

Diese wissenschaftliche Arbeit zeigt den Einfluss von Stabilisatoren, Geometrie und Unterschieden in der Erregerkraftart und Position. Eine Parameterstudie untersucht, anhand eines einfachen Balkenmodelles, welchen Einfluss Stabilisierungspunkte, Biegesteifigkeits- und Massenänderungen auf die laterale Schwingungsanfälligkeit haben. Das Modell nutzt das analytische Verfahren der Transfermatrizen, um alle modalen Eigenschaften und physikalischen Amplituden zu berechnen. Dieses analytische Modell ermöglicht, für eine einfache Balkengeometrie, eine schnelle Berechnung und eignet sich daher hervorragend für das Auswerten verschiedener Konfigurationen. Diese Parameterstudie zeigt die hohe Bedeutung einer geeigneten Stabilisierung für eine effektive Schwingungsminderung und dass Elemente mit einer geringeren Biegesteifigkeit, so genannte Flex-Subs, die meist für die Verringerung des statischen Biegemoments verwendet werden, einen nicht unbedeutenden Beitrag zu Schwingungsdämpfung leisten können. Diese Eigenschaft hängt jedoch stark von der geometrischen Beschaffenheit dieser Elemente ab. Zusätzlich zeigen die Berechnungen, dass die Formänderungsenergie, in Verbindung mit einer auf dem dynamischen Biegemoment basierenden kritischen Frequenzanalyse, eine gute Kennziffer für einen Optimierungsprozess ist. Ein Optimierungsprozess vergleicht verschiedene mögliche BHA-Konfigurationen auf deren laterale Schwingungsanfälligkeit und erlaubt somit die Auswahl der Konfiguration mit den kleinsten Schwingungsamplituden.

Das auf der Formänderungsenergie basierende Optimierungsverfahren ist eingebettet in einen Ansatz der die gesamte BHA-Leistungsfähigkeit berücksichtigt. Dazu zählen die statische und dynamische Belastung, Steuerbarkeit und geometrische Eigenschaften. Für das Richtbohrsystem ist die Steuerbarkeit von größerer Bedeutung als eine optimale statische und dynamische Belastung. Jedoch sollte keine der in Betracht gezogenen BHAs durch die Belastungsfälle versagen. Dieser Gesamtvergleich basiert auf verschiedenen Verhältnissen zwischen der geplanten Vorgabe oder Bohrparametern und den eigentlichen Belastungsgrenzen der BHA. Diese Arbeit zeigt die Auswirkungen von BHA-Änderungen auf die laterale Schwingungsanfälligkeit und wie verschiedene Designs am besten verglichen werden können.

Abstract

Lateral vibrations pose a major problem in drilling. Bottom Hole Assembly (BHA) failures, for example due to wellbore wall interactions and high bending stresses, can directly be related to vibration phenomena. Downhole measurement and real-time data transmission are also affected by vibrations and pose a problem in drilling performance. Although lateral vibrations can have severe consequences, their nature makes modeling and prediction quite challenging, especially in the pre-well design phase and BHA performance comparison. Lateral vibrations are not recognized at surface. Only downhole measurement systems can provide information about the downhole environment. Dynamic changes in wall contacts alter the vibration system in terms of natural frequencies and mode shapes, leading to different physical deflections. This makes dynamic modeling a difficult process.

This thesis demonstrates the impact of stabilization, geometry changes and excitation source variations on lateral BHA vibrations. In a parameter study on a beam structure model, different model configurations are simulated, analyzing the impact of stabilizer placement, bending stiffness and mass on vibration susceptibility. The model utilizes the given transfer matrix method as an analytical approach to compute all modal properties and physical amplitudes. This implementation enables a much faster computation than finite element method simulations, thus more model variations can be conducted in a given time frame.

The parameter study proves the importance of appropriate stabilizer placement to mitigate lateral vibration susceptibility. Flex-subs, mainly considered to reduce static bending loads, are found to greatly impact the vibration system, depending on their geometric properties. Moreover, the study identifies the most suitable presentation format for lateral vibrations. The strain energy, coupled with a dynamic-bending-moment-based critical speed analysis, is formed to a key parameter in the BHA optimization process to decrease lateral vibration susceptibility already in the planning phase.

The strain energy and dynamic bending moment based dynamic optimization procedure is integrated into an overall drilling performance criterion which incorporates BHA steerability, statics, dynamics and geometric properties. In directional wells, BHA steerability is more important to a drilling project than an optimized static or dynamic load performance. However, every BHA under comparison must not exceed their allowable load limitations. The properties represent ratios between well plan or operation parameters and BHA limitations. The parameter study and optimization criteria are demonstrating the effect of BHA alterations on lateral vibrations and how BHA designs can be optimized and compared.

Table of Contents

List of Acronyms

BHA	Bottom Hole Assembly	
MWD	Measurement While Drilling	
LWD	Logging While Drilling	
RSS	Rotary Steerable System	
PDC	Polycrystalline Diamond Compact	
WOB	Weight on Bit	[N]
DLS	Dog Leg Severity	[°/30 m]
BUR	Build Up Rate	[°/100 m]
OD	Outside Diameter	[m]
ID	Inside Diameter	[m]
ECD	Equivalent Circulating Density	[kg/m^3]
ROP	Rate of Penetration	[m/h]
RPM	Revolutions per Minute	[1/min]
MAC	Modal Assurance Criterion	
$(\dot{a})$	Time Derivative $\frac{\partial}{\partial t}$	
$(a)'$	Derivative with respect to the location $\frac{\partial}{\partial x}$	
M	Mass Matrix	[kg]
D	Damping Matrix	[kg/s]
S	Stiffness Matrix	[kg/s²]
$\mathbf{I_m}$	Modal mass Matrix	[-]
Λ	Spectral Matrix	[1/s²]
Φ	Modal Matrix	[-]
T	Transfer Matrix	
x	Physical Amplitude Vector	[m]
q	Vector of Modal Amplitudes	[m]
w	Lateral Displacement	[m]
M	Momentum	[Nm]
B	Bending Stiffness	[Nm^2]

Q	Shear Force	[N]
E	Young's Modulus	[N/m^2]
I	Area Moment of Inertia	[m^4]
ω	Frequency	[1/s]
p	Excitation Force	[N]
P	Point Load	[N]
μ	Mass Distribution	[kg/m]
Ω	Excitation Frequency	[1/s]
α	Damping Decay Factor	[-]

1 Introduction

Deep drilling requires thousands of meters of heavy steel pipe and even stiffer and more complex components at the very bottom of the borehole. This bottom hole assembly (BHA) includes all necessary tools to follow the desired well trajectory and to hit the right spot within the hydrocarbon bearing formation. Such wells can become very complex with different inclinations, turns and horizontal sections, greatly differing from historical vertical well drilling. An engineer can draw on a large variety of different BHA components which would fulfill the needs for every hole section. The available components range from bits, steering units, measurement tools, to components which alter the stiffness and stabilization of the BHA. Although heavy steel components, of up to several tons, are being used, the drilling conditions induce high loads on the BHA, moving and bending the components with ease.

This dynamic behavior leads to increased tool wear and damage of the installed components, reducing tool life time and increasing the risk of mechanical and electronic BHA failure. A major dynamic concern is drilling induced vibration. This vibration can be divided into axial, torsional and lateral vibration. Axial vibration induces a longitudinal BHA and string motion increasing bit wear and reducing ROP. Torsional vibration originates from a periodic acceleration and deceleration of the bit and string rotation, leading to a so-called stick-slip motion of the string. Lateral vibration can originate from different sources such as mass imbalance, eccentricity of the BHA or due to coupling between vibration types. Lateral vibration can be the cause for severe BHA damages and failures but is hard to detect on surface. This enforces the need of downhole vibration measurements.

Hence, BHA designs should be optimized to minimize the risk of inducing drilling vibrations. The optimization of a BHA design in the planning phase is a fundamental requirement but is usually done on a design-by-design basis without any automated processes, thus leading to subjective decisions and eventually to long trial and error processes.

This thesis focuses on increasing the objectivity and automation of dynamic BHA optimization with regards to lateral vibrations. An analytical model, the transfer matrix method, will be used to determine the displacement and bending moment of a simplified BHA model under different parameter variations. A focus will be set on stabilizer placement, excitation source position and influence of diameter changes along the BHA model. Further quantities such as the strain energy and lateral acceleration are evaluated from the analytical model results, identifying the most suitable parameter for describing lateral vibrations. These parameters are then used to create design criteria which allow a more qualitative BHA comparison. Having a sound foundation for comparing BHAs allows the implementation of optimization algorithms, identifying the optimum BHA configuration in terms of vibrations, static limits and steering capabilities. This comparison should be made prior to drilling, allowing for an optimum BHA run without vibration related standby and troubleshooting. Further automation and implementation into advisor software for real-time and post well BHA vibration mitigation and overall optimization is going to be performed in the near future.

2 State of the Art BHA Design

Nowadays, BHAs have deviated from the sole drilling purpose into multifunctional downhole tools capable of performing a wide range of tasks, from steering, over measurement to formation evaluation and logging.

Those tasks require more complex tools which in turn need careful engineering and design at the component level itself but also at the overall BHA resolution. Thus, allowing a flawless interaction between the different BHA components such as bit, steering unit, MWD/LWD and telemetry system.

Unfortunately, all these designs are somehow constrained in one way or another. The range of available materials for downhole tools limits the overall strength and therefore the loads the component can endure before ultimate failure. The well plan demands BHAs which are capable of delivering high performance and cost effectiveness, resulting in an alteration or trade off from the most reliable and strongest design.

Unpredictable loads, especially vibrations, add further complexity to the design approach. Hence, different calculation methods are available which incorporate the various types of vibrations, axial, torsional and lateral vibrations in particular. Based upon these models, service companies and operators have come up with their own recommendations for addressing and mitigating vibrations.

2.1 Drilling Project Requirements

Well construction starts in the drilling engineering department of an operator, based on available rig surface locations within the acquired lease and on the desired target coordinates of the hydrocarbon bearing formation. The drilling department designs a well trajectory upon those two points and additional information such as offset wells, subsurface structures and formation pressures. A state of the art well trajectory has evolved from being strictly vertical into complex 3-D shapes with different inclinations and turns, ranging from medium to extended reach depths at various borehole sizes.

After completing the well design phase, the operator approaches one of the available service companies on the market for BHA and drillstring designs for the planned well. The service company selects the appropriate technologies and tools from their product catalog and combines them into BHA designs which would meet the client requirements. The client requirements and the usual approach of a service company can be seen in Fig. 2.1.

A detailed BHA analysis is crucial to the well planning phase. Especially fit for purpose designs and approaches that consider the overall well design goal of reservoir performance and production volumes will outperform designs solely focused on ROP. This also requires a sufficient resource allocation at the planning phase of a drilling operation (Mims, Krepp 2003).

Furthermore, the service company has to come up with a measurement strategy, satisfying the need for data acquisition, and with drilling parameters, meeting tool specifications and client requirements at the same time. *"The goal is to design a directional strategy that complements the 'system', and not simply to 'hit the target' or 'follow the line'. " (Mims, Krepp 2003).*

The selected approach has to pass simulation and verification of different load scenarios and working conditions, thus ensuring proper functionality over a wide range of possible downhole conditions. If the requirements cannot be met, the client has to be contacted and alterations to the well plan should be discussed. However, there should be a close collaboration throughout the entire planning process, not only when problems arise.

Different loads and conditions affect certain design steps more than others, as shown in Fig. 2.1, and not all loads are fully understood or exactly definable. The static drilling environment like torque and drag and BHA loads is routinely modeled in simulation and calculation software. The dynamic areas are based more on assumptions and case by case solutions compared to the static counterpart, which has been widely accepted by operators and service companies. The occurrence of dynamic phenomena and their magnitude and range is quite unpredictable but the impact on the BHA and its performance in case of appearance should be minimized. As shown in Tab. 2.1, dynamic conditions such as vibrations influence critical design steps with a great magnitude.

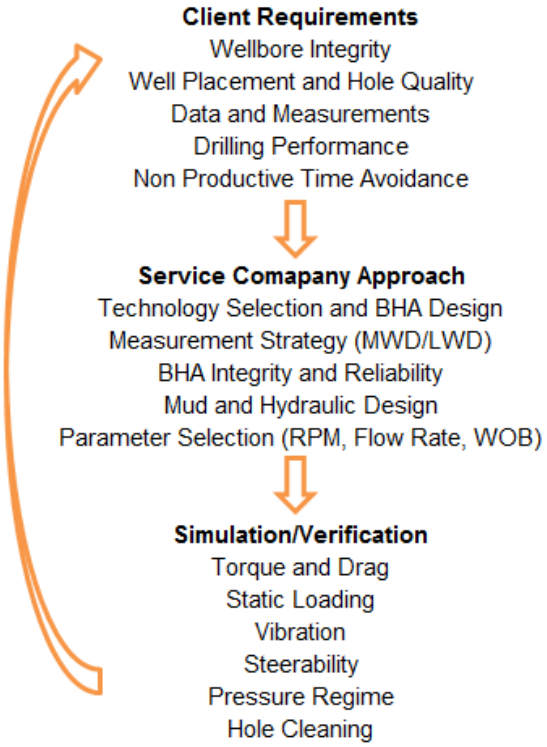

Fig. 2.1: Drilling project steps for BHA design.

Tab. 2.1: Impact of different calculation steps on BHA design. Note the huge influence of vibrations on the design. The weighting shown in this table is based solely on the considerations of the author.

		Service Company Approach			
		Technology Selection and BHA Design	BHA Integrity and Reliability	Mud Design	Parameter Selection (RPM, Flow Rate, WOB)
Simulation/ Verification	Torque and Drag	high	high	moderate	moderate
	Static Loading	high	high	moderate	moderate
	Vibration	high	high	low	high
	Steerability	high	moderate	low	moderate
	Pressure Regime	low	low	high	moderate
	Hole Cleaning	high	low	high	high

2.2 The BHA and its Purpose

Drilling tools are exposed on the one hand to a high pressure and temperature environment and on the other hand to high loads generated by the drilling operation. This very hostile combination has been tackled with the engineering solution of BHAs, enduring all the occurring loads whilst continuously driving the bit towards the target (Short 1993).

In drilling, the BHA is part of the drill string including all the drilling tools connected to the bottom of the drill pipes up to the bit. The BHA affects the loading of the bit in form of WOB and controlling the bit and consequently the well trajectory. Such an assembly can be constructed relatively simple, having only a drill bit and collars or more complicated including also stabilizers, different collar sizes and materials, positive displacement motors, rotary steerable systems, turbines, MWD/LWD systems, telemetry units and HWDPs (Mitchell et al. 2011; Bourgoyne et al. 1991).

The exchange and introduction of other components into a BHA allows for different configurations suitable for drilling different hole sections of a given trajectory no matter if they are vertical, inclined or long horizontal sections. BHA configurations with more advanced steering technology can also drill different sections without being pulled and reconfigured at the rig floor. The downsides of such drilling systems are the elevated costs and a higher degree of technological complexity, leading to a higher failure rate compared to conventional BHAs. However, modern complex trajectories rely on advanced steering technologies. Older systems may not even be considered as an alternative option for such wells (Aadnøy 2006; Mitchell et al. 2011).

2.2.1 Stabilizer Technology

The BHA can be comprised of different components depending on the BHA purpose. A special emphasis has been set on stabilizers due to their importance for the later vibration discussion.

Running a BHA made only from drill collars with a very similar gauge OD allowsjust a limited range of downhole operations. Such a BHA would be more susceptible to initiate buckling below the neutral point after a certain WOB threshold, thus greatly reducing deviation control and drilling performance up to total string lock-up. A greater deviation control can be achieved with the introduction of stabilizers. The first recorded BHA run with such stabilizers was in 1953, documented in a paper from Lubinski and Wood. Their investigations have shown that the stabilizer-bit distance and the annular gap at the stabilizer influence the side force and tilt angle of the bit. At that time stabilizers have been used to increase the distance from the bit to the tangency point for a maximum pendulum effect. A pendulum assembly was the first method for deviation control. This technology has been replaced with more modern and precise means of steering and hence has no significance anymore (Mitchell et al. 2011).

This primary use has been extended over the years alongside with the introduction of new steering technologies and other advanced downhole tools. Nowadays, stabilizers should also protect tools from wall contact which would lead to extensive wear on more expensive tools or subs. Furthermore, high side loads would damage or distort the sensitive electronics and antennas from MWD and LWD tools. Stabilizers provide means of predefining wall contacts within the BHA which greatly reduces the effort of steering predicable curves with RSS (Dueber, Gatzen 2013; Dueber 2008). Furthermore, stabilizers should not hang up on borehole perturbations and ledges of any size up to the diameter difference between the upset and nominal tool OD during drilling and tripping. The influence on drilling hydraulics should be kept at a minimum. Swab and surge effects should be avoided and the reduced annulus at the stabilizer should not impact ECD too much. Care should be taken that the stabilizer does not damage the casing or induces a side cutting action into the formation while drilling (Pastusek 2014).

Different stabilizer types are available from different manufacturers depending on their predetermined BHA position. Stabilizers can be divided into string or modular and motor bearing housing stabilizers. An example of a string or modular stabilizer is shown in Fig. 2.2 and a bearing housing stabilizer in Fig. 2.3.

Fig. 2.2: Example of a string or modular stabilizer. Stabilizers differ from the standard tubular length of 9 m. used in oil well drilling and are 1 to 2.5 m long. (Baker Hughes 2015)

Fig. 2.3: Bearing housing stabilizer on a downhole motor. (Baker Hughes 2015)

Stabilizers are available with different tool-body connections varying in manufacturing effort and area of application. Integral type stabilizers are the most common design in the oil industry. The blades are machined out of a larger diameter steel forging or steel bar, either standard steels or non-magnetic materials for the use close to MWD/LWD tools. Manufacturing integral type stabilizers requires high precision tools but the lack of weld seams or multiple components increases the overall mechanical strength of the stabilizer. Screw on type stabilizers consist of a sleeve carrying the stabilizer blades which is screwed onto the tool body. Thus, allowing the usage of one tool body for a larger number of borehole sizes. Clamp on types can be clamped on any position on a tool body. This has been originally developed for a more flexible stabilizer positioning in rotary BHAs. More recent designs are used for downhole motors, improving the directional and dynamic behavior. The blades can also be welded onto the tool body, producing the weld-on type stabilizer. Although cheap to produce, the pre-stressed weld seams are very prone to failure under drilling loads (Dueber, Gatzen 2013; Dueber 2008). The visual differences between the different tool-body connection types can be seen in Fig. 2.4.

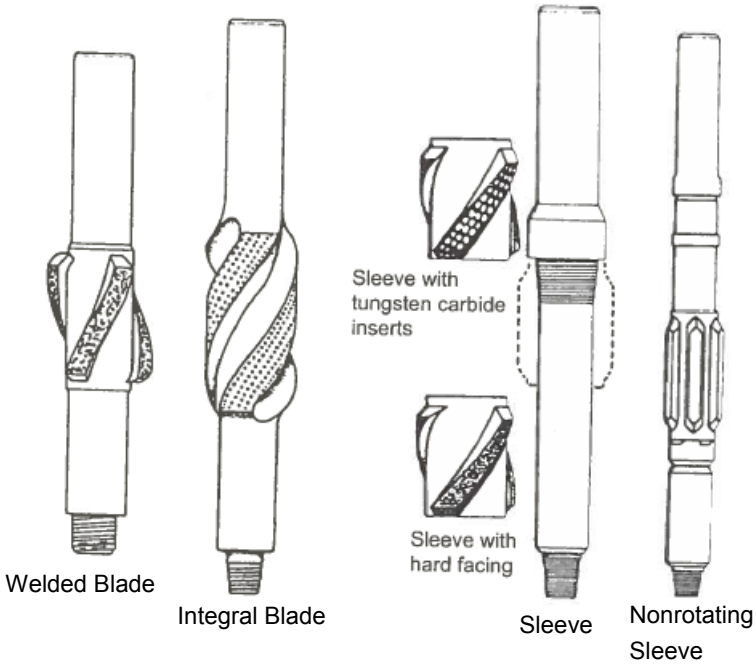

Fig. 2.4: Different stabilizer types. (modified after Mitchell et al. 2011)

Comparing Fig. 2.2 and Fig. 2.3 shows also a difference in stabilizer blades geometry. The stabilizer in Fig. 2.2 has a spiral design supporting string rotation with respect to a smoother movement and less vibration compared to straight blades (Dueber, Gatzen 2013; Dueber 2008). Most spiral stabilizers are manufactured with a right hand lead. Left hand leads are available but are more susceptible to pack-off because drilling in clockwise direction would force

the mud flow into much sharper direction changes as compared to right hand lead designs. Right hand design is mainly used in BHA configuration with an RSS (Dueber 2008).

Straight blade stabilizers, as shown in Fig. 2.3, are used with motor assemblies. The straight design has proven to be more beneficial during sliding compared to the spiral design. Different blade widths and gauge lengths are available, influencing the build rate of downhole motors. The most common blade designs are the so-called lateral designs with short blades for high build up rates and DTU2 designs which incorporate a standard gauge length for most of the motor applications. DTU2 stands for Double-Tilted U-joint housing, a special tilted sub of downhole motors. The blade geometry influences the contact area for side forces and the bending stiffness of the stabilizers. (Dueber, Gatzen 2013; Dueber 2008).

Regardless the stabilizer design, the blades are not in the middle of the stabilizer sub. This is due to the general requirement for the fishing necks of stabilizers to be at least 18” or 0.46 m. The tong length at the pin connection side has to be minimum 10” or 0.25 m (Ritter 2007). These geometries are shown in Fig. 2.5.

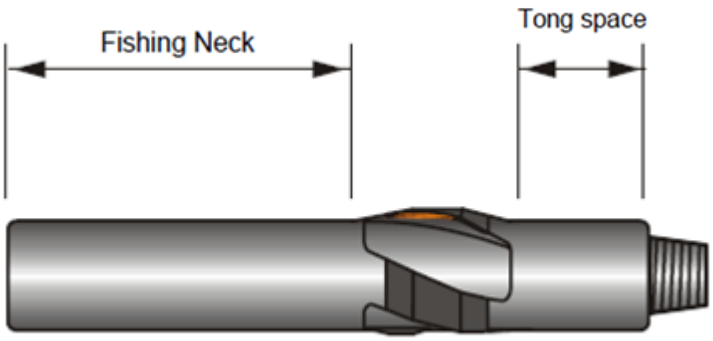

Fig. 2.5: Location of the stabilizer blades on the tool body considering enough space for fishing tools to interlock with the stabilizer and a tong space for the rig tongs during make-up and break-out of connections. (modified after Baker Hughes 2015)

2.2.2 Most Common BHA Configurations

“Stabilizers and other equipment should be connected in various combinations to the drill collars for building different assemblies … Small variations in tool spacing may have a large effect on BHA efficiency” (Short 1993). BHA designs must not only meet the directional objectives but should also be reliable enough to reduce the risk of expensive and time consuming downhole failures (Mitchell et al. 2011).

BHAs can be subdivided into rotary, motor and RSS types. All three classes are suitable for drilling vertical, deviated, tangent and horizontal hole sections but vary in their performance and reliability for different tasks and sections.

2.2.2.1 Rotary Type Assemblies

Rotary assemblies are the oldest type of BHAs and rotation is transferred to the bit by the top drive or rotary table only. They can vary in complexity as certain tasks require more specialized equipment and materials.

The simplest BHA is comprised of standard drill collars and a bit at the bottom, the so called slick or limber assembly configuration. Slick assemblies have been used for drilling vertical wells and for cleaning lower sections of a deviated or horizontal well where no directional control is required. They also serve as a design foundation for other assembly designs by exchanging some of the drill collars with other tools (Short, 1993). If the slick BHA is pulled off bottom in an inclined wellbore, the only force acting on the bit is the side force due to the weight of the collars between the bit and the tangency point. This side force acts in the direction of gravity and tends to bring the hole back to vertical, therefore called the pendulum effect. Reducing hook load and applying WOB, the BHA tends to push the bit away from its vertical direction. Depending on the WOB, the side force magnitude changes and holding or dropping tendencies can be achieved with the very same slick assembly (Mitchell et al. 2011). A typical slick assembly and the pendulum effect can be seen in Fig. 2.6.

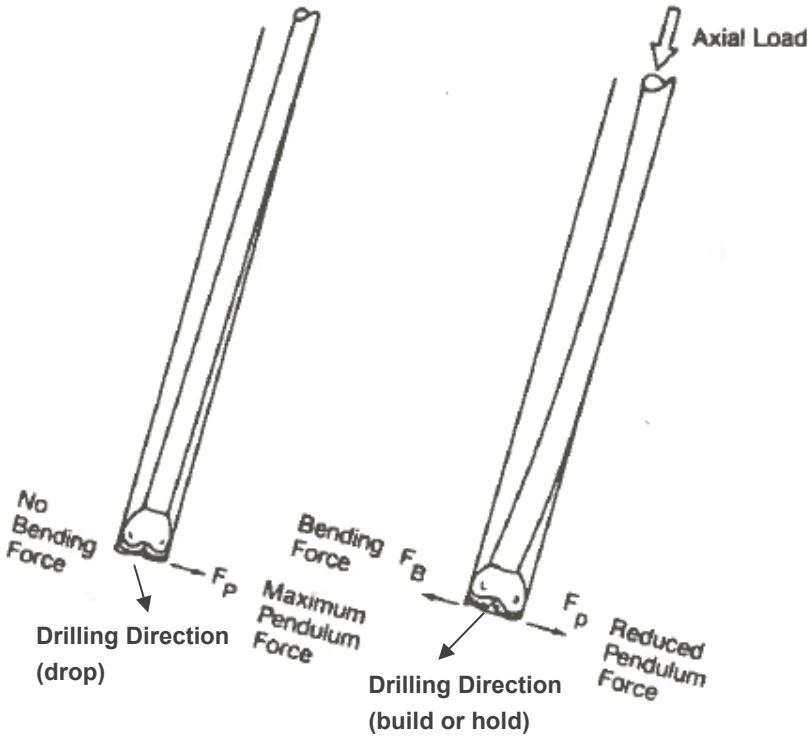

Fig. 2.6: A typical slick BHA configuration, consisting only of uniform drill collars. Without any WOB, the BHA sees the maximum side force and would drop back to vertical. Under a certain axial load, the pendulum side force is reduced and bending causes the BHA to hold or build. (modified after Bourgoyne et al. 1991)

Directional control has been greatly improved by the introduction of stabilizers into the assembly design. The position of one stabilizer inside a BHA greatly impacts the build, drop or hold tendencies under certain loads. An increase in the unsupported length between the bit and the stabilizer increases the side force at the bit, bringing the hole into a more vertical direction. Moving the stabilizer closer to the bit reduces the side force or changes its direction and the bit is pushed towards the high side of the hole. The stabilizer acts as a fulcrum and supports the build effort (Mitchell et al. 2011; Bourgoyne et al. 1991). Assemblies with building capacities have been classified as fulcrum assemblies and assemblies with a dropping tendency as pendulum assembly. Such assemblies follow the basic principle shown in Fig. 2.6.

Some well trajectories require more than a single stabilizer for accurate directional control. Usually two or three stabilizers placed at the right positions are sufficient to achieve the desired directional objectives. Adding more stabilizers does not further aid in directional control but reduces side forces and wear on other BHA components. Whether stabilizer placement can aid in vibration damping and mitigation is topic of this thesis. Multi stabilizer assemblies can also be configured to either build, hold or drop the hole angle as seen in Fig. 2.7 (Mitchell et al. 2011). Rotary assemblies are capable of drilling 2-D directional wells. More complex 3-D geometries require other steering methods and above all, measurement tools for a constant position update (Hummes 2010a).

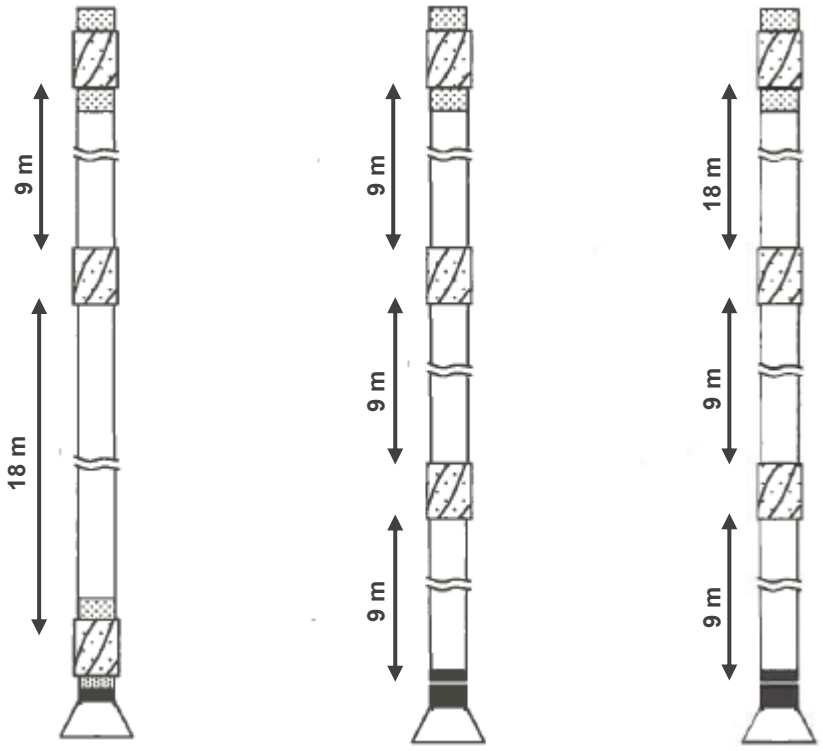

Fig. 2.7: From left to right: build or fulcrum BHA, hold or packed assembly and a drop or pendulum type BHA. (modified after Mitchell et al. 2011)

2.2.2.2 Motor Type Assemblies

Delivering mechanical power at the rig floor and transferring it through kilometers of drill string reaches its limitation at some point, since most of the available energy is needed to overcome friction as the whole string rotates. To tackle this problem, downhole motors have been introduced to the drilling industry. These tools convert hydraulic power from the rig pumps into rotational energy close to the bit, therefore reducing the required mechanical power input from the rig floor (Mitchell et al. 2011).

Introducing a bent sub or using a bent-housing motor for inclinations above 20° enhances directional control of motor assemblies. Furthermore, they allow, in combination with a MWD and telemetry system, for actively steering the bit into a desired direction. Two different modes are available for either drilling vertical or holding the inclination and for steering the well. In the so-called sliding mode drill string rotation is stopped and only the part below the motor section rotates. This points the bent section into the desired direction and changes in inclination and

azimuth can be made. In rotating mode the whole string rotates ignoring the directional capabilities of the bent housing and progress is made with the previously set direction. A schematic of the two working principles is shown in Fig. 2.8. Although motor assemblies are quite effective and inexpensive, the two modes are limited by axial force transfer, cuttings movement and differential sticking during sliding and vibrations in rotary mode (Mitchell et al. 2011).

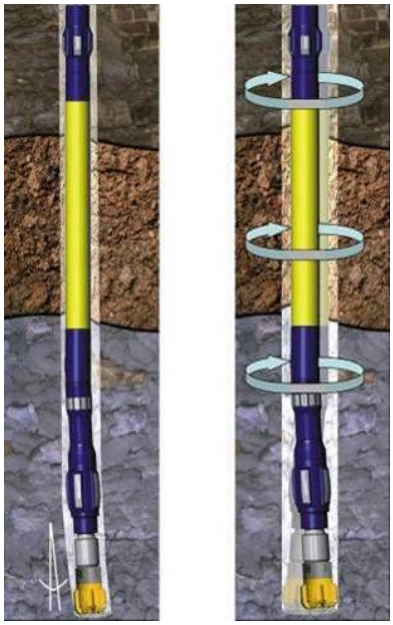

Fig. 2.8: Two different operating modes for downhole motors. Left: sliding mode for directional drilling. Right: rotary mode for drilling vertical or holding the direction in tangent and horizontal sections. (Baker Hughes 2015)

2.2.2.3 RSS Type Assemblies

Unlike a motor assembly, the RSS type does not rely on two different operational modes to change the hole direction. These tools are designed to drill with continuous rotation from surface, eliminating the need to change into sliding mode. Continuous rotation of the drill string allows for better transportation of cuttings to the surface resulting in a better hydraulic performance, weight transfer, and reduced well bore tortuosity due to a steadier steering model. An RSS assembly uses continuous steering adjustment, leading to smoother, less tortuous holes which are more in gauge compared to motor assemblies. Thus, greatly reducing torque and drag problems (Butt 2015).

All these features enable drilling of wells with more complex trajectories with a higher rate of penetration, especially in long tangent or horizontal sections. In combination with the right LWD services, it is possible to steer the well through the pay zone for maximum reservoir contact and drainage. Several companies have developed their own RSS design and working principle but typically they can be divided into push-the-bit and point-the-bit systems (Mitchell et al. 2011).

The point-the-bit system achieves directional control by generating a deflection angle between the low-end tool axis and the borehole axis. This bit tilt can be achieved in three different ways. The drive shaft can be bent inside a non-rotating housing (Fig. 2.9a). Tilt can also be made by holding a pre-set alignment with a geo-stationary unit inside a rotating housing (Fig. 2.9b) or with pads mounted on a non-rotating housing (Fig. 2.9c) (Sugiura 2008).

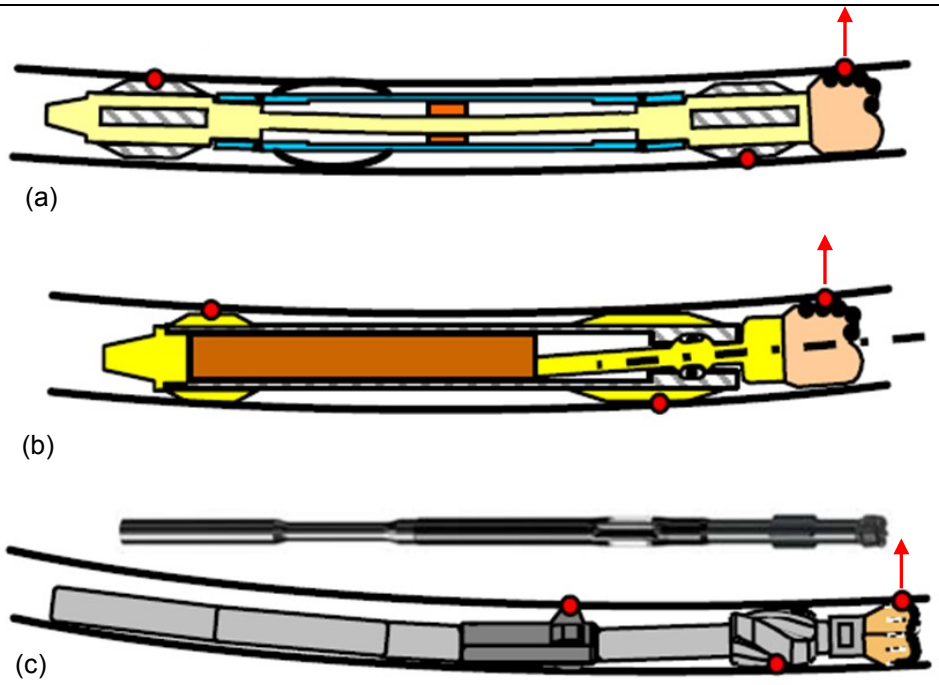

Fig. 2.9: Different point-the-bit systems. (a) The internally deflected shaft can be offset with eccentric cams, hydraulic pistons or packers. This type also includes a non-rotating mechanism which makes contact to the borehole wall. (b) A geo-stationary unit aligns the drive shaft internally while the outer housing rotates. (c) The non-rotating housing with pads utilizes a near bit stabilizer as a fulcrum for orientating the bit. (modified after Sugiura 2008)

Push-the-bit RSS change direction by applying a side load to the bit through multiple hydraulically expandable steering pads. This system can be subdivided into tools with pads mounted on a rotating and non-rotating housing (Sugiura 2008). Fig. 2.10 shows an example of a push-the-bit system with a non-rotating housing. Non-rotating should be understood as extremely low, in the orders of one to two full revolutions per hour.

Steering is achieved by either setting side force vectors using all available number of pads but with different hydraulic pressures or by actively positioning the pads and applying hydraulic pressure only to the desired pads instead to all. Push-the-bit systems use bits capable of actively side cutting into the formation (Gupta 2008).

Hybrid systems are using a combined working principle of steering the bit through the formation. They use pads or ribs for applying sufficient side force and the pushing action also points the bit into the right direction (Gupta 2008).

Powered RSS incorporate a straight motor section, increasing the available rotational energy at the bit and hence, rate of penetration. The downsides of this combination are increased vibrations, especially in hard formations, motor failures and higher overall costs (Butt 2015).

All of the above mentioned RSS can be operated in steering mode for changing hole direction or in the hold mode for maintaining the last set direction (Hummes 2010b).

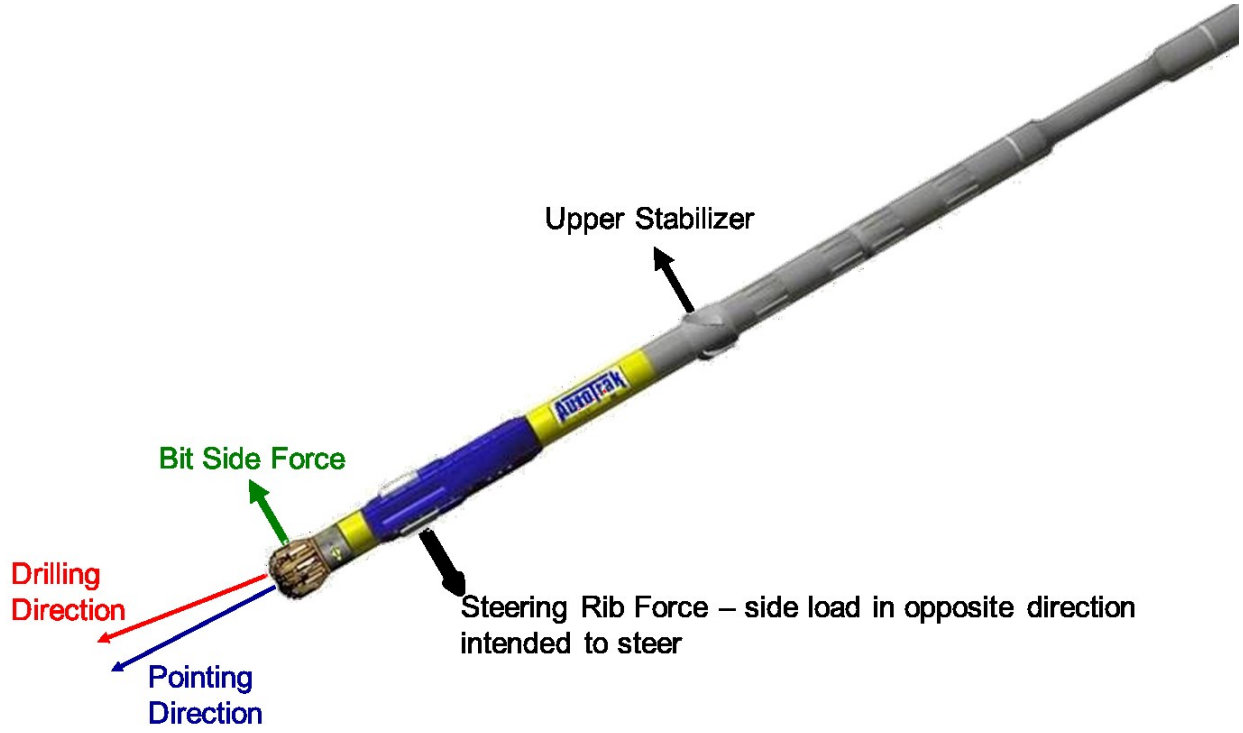

Fig. 2.10: A push-the-bit RSS with the steering pads mounted on a non-rotating housing (blue section). The three point geometry for steering the bit into the desired direction is indicated by the arrows. (Baker Hughes 2015)

2.2.3 Conflicting BHA Design Requirements

BHA design is highly application specific and depends on the customer expectations and well requirements. A BHA has to fulfill the basic requirement of drilling the assigned hole section from its starting point down to the target. Major BHA components such as steering or measurement units have a preset position within the most BHA designs and cannot be removed or placed on different positions. Furthermore, MWD tools require specific stabilizer spacing or have a stabilizer already incorporated in the collar. This narrows the possibilities of configuring the BHA to a limited number of exchangeable or removable components.

Assembly stabilization and stiffness are the two major parameters which can be altered with stabilizers and flexible components so-called flex-subs. Flex-subs are tools with a reduced outer diameter, allowing to reduce bending loads within the BHA (Aelfers 10/26/2015).

More stabilizers generate a tight or packed BHA, which centralizes the BHA inside the wellbore. This reduces undesired wall contacts on certain tools which can be crucial for some MWD measurement requirements. Further, a higher degree of stabilization allows for a better side force distribution, reducing the side force on every single stabilizer. However, more stabilization could also increase the side loads at a given stabilizer for example if the packed BHA is forced through a high local dogleg. Hence, a packed assembly is more susceptible to become stuck on micro-doglegs, leading to more drilling related challenges and possible down time. A limber assembly benefits from a reduction in bending stresses and better tripping / running capabilities in crooked hole sections. Long unstable sections are more prone to tool wear and measurement inaccuracies for certain MWD tools. Side forces could be localized at undesired positions. The eccentricity of the BHA could impact measurements and bending loads increase due to gravity effects between stabilizers (Aelfers 10/26/2015).

Flex-subs in combination with stabilizers can alter the stiffness of an assembly. BHA steerability requires flexibility to a certain extend. However, the predictability of the BHA movement is reduced as the BHA becomes more flexible. Assemblies, too stiff, could break under the drilling loads due to very high bending stresses (Aelfers 10/26/2015).

Eq. 2.1 shows that the natural frequency depends on the stiffness c and structure mass m. A stiffness increase generates higher ω_0 values whereas a higher mass would shift resonance to lower frequencies (Jürgler 2004):

$$\omega_0 = \sqrt{\frac{c}{m}} \qquad \textbf{Eq. 2.1}$$

A more stabilized and stiff BHA shifts the resonance frequencies towards higher frequency levels, whereas a flexible assembly could generate vibration problems at lower frequencies.

Common BHA design produces an assembly which is flexible enough for steering towards the desired target and sufficiently stiff to provide a stable and predictable drilling environment. Hence, design trade-offs have to be tolerated in both directions. An extremely stiff BHA would drill very predictable but steering the well would be hard to achieve. An entirely flexible design would have higher steering capabilities but no clearly defined wall contacts, reducing the predictability of the steering direction. Highly flexible sections are also more prone to buckling and string lock-up under high compression (Aelfers 10/26/2015).

2.3 The Dynamic Drilling System

BHA components have elastic properties and a specific mass and are therefore considered as vibration systems. The dynamic drilling environment can be divided into motion required for the drilling progress and unwanted, harmful phenomena which lead to a performance reduction or even failure. The most important requirement for drilling is rotation, whereas vibrations are an example for unwanted movement. Other dynamic forces include mud pressure fluctuations, WOB and torque changes, internal and external damping forces, centrifugal forces and borehole wall interactions.

Drilling vibrations can results in unwanted string motion ranging from small displacements to a significant motion compared to the required drilling motion and can become dangerous under certain circumstances. Severe damage can occur especially in the case of resonance between the excitation source frequency and natural frequency of the BHA. Even though resonance is not achieved, the BHA can be continuously exposed to unwanted dynamic loads (Dubbel et al. 2001, pp. O8-O9).

2.3.1 Vibrations

A process is periodic if it reoccurs after a certain time. A process is denoted as vibration, if a physical quantity, like tool displacement, appears periodically after the same time element (Jürgler 2004).

Vibrations have a starting point from which the displacement emerges and to which the system falls back after the kinetic energy has been dissipated, the zero-point. Vibrations can either be

free, where there is no energy transfer from or to the system, or “forced”, in which energy is constantly supplied to the system. Forced vibrations can either be self-excited or actuated from an external source. Undamped systems do not see any energy dissipation, whereas damped vibrations are losing energy due to internal or external friction. If more energy is introduced as dissipated the system is referred to as kindled vibration, where the amplitude grows with every period (Jürgler 2004).

The adverse length-diameter ratio of drill strings and BHAs causes the system to be excited with ease. Drilling induced vibrations are caused by bit and string interactions with the rock, mass imbalances, eccentricity of the BHA or due to coupling between vibration types. This can become quite complex due to the unpredictable nature of bit-formation interaction, string-wellbore interaction and hydraulics. Downhole conditions often induce multiple phenomena at once and one vibration mode can be transferred into other types (Aadnøy et al. 2009).

Excitation sources can create forces and stresses that oscillate at frequencies that are multiples of the applied rotational speed. The amplitude of the resulting BHA vibration depends on the magnitude of the excitation, the system damping and the proximity of the excitation frequency to a natural frequency of the BHA. When one or more excitation frequencies from the excitation bandwidth matches or is close to natural frequencies of the BHA, resonance has been achieved and the resulting amplitude intensifies (Aadnøy et al. 2009). An example for resonance within a given frequency bandwidth can be seen in Fig. 2.11. A peak in physical amplitude, here the strain energy of the whole BHA, at a certain frequency indicates that this excitation frequency matches one of the natural frequencies, leading to resonance.

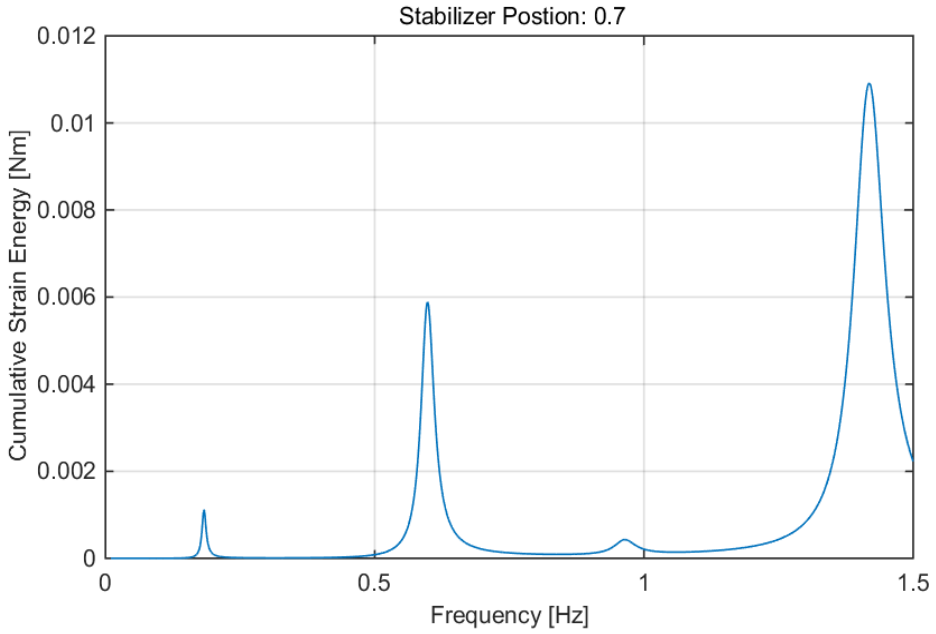

Fig. 2.11: Strain energy of a BHA with a single stabilizer. The high amplitudes occur where the excitation frequency matches the natural frequency of the BHA. These frequencies are called resonance frequencies.

High amplitude levels make the BHA susceptible to fatigue loading which can lead to localized or catastrophic failure. This can lead to numerous problems such as BHA twist-offs, premature

bit and tool failure, excessive tool joint wear and damage to the top drive and hoisting equipment. Furthermore, vibrations can cause a significant ROP reduction and hole enlargement leading to wellbore stability problems (Aadnøy et al. 2009).

Vibrations can induce three primary vibration modes. Axial vibration causes movement along the longitudinal axis of the BHA and string, torsional vibrations lead to twisting of the BHA and the lateral type precipitates a side to side motion of the BHA (Aadnøy et al. 2009). These three types lead to further phenomena such as bit bounce, whirl and stick-slip (Linke, Cardy 2009). The primary vibration types can be seen in Fig. 2.12.

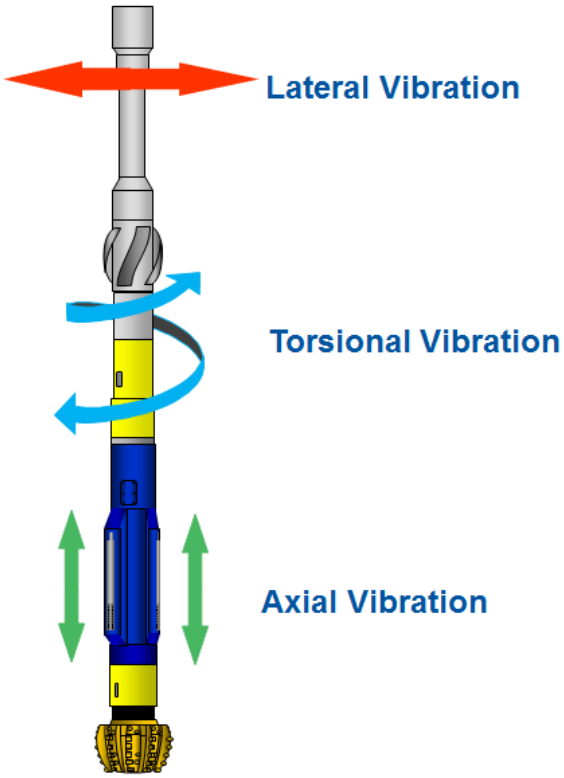

Fig. 2.12: Three primary types of vibrations. Lateral vibrations (red) could cause whirl, torsional vibrations (blue) can lead to stick slip problems and axial vibrations (green) move the whole string up and down. (Baker Hughes 2015)

2.3.1.1 Axial Vibrations

Axial vibration originates from erratic WOB fluctuations that cause the bit to lift off bottom and then drop down and impact the formation. The wellbore is not capable of restraining the axial movement of the BHA, resulting in large amplitude oscillations. This leads to an inconsistent rock breakage process, which in turn influences ROP. Such a behavior is called bit bounce. Typical bit bounce damage can be seen in Fig. 2.13, where the bit cutters are severely damaged or completely lost. This type of vibration has been observed first together with torsional modes before the lateral vibrations modes. Severe axial vibrations are quite common when drilling with roller cone bits due to their crushing behavior. A second source is the frequency tuning of mud pressure with the axial natural frequency of the BHA (Aadnøy et al. 2009).

Fig. 2.13: Severely damaged cutting structure of a roller cone bit due to high axial vibrations. This can also lead to the total loss a one or more roller cones. (Baker Hughes 2015)

Axial and torsional vibrations are transmitted up to the rig floor, whereas lateral modes are usually terminated at the neutral point. At the most severe cases of axial vibrations the top drive and hoisting system also sees axial movement, especially in shallow vertical wells where effective dampening is reduced. Axial vibrations can also initiate lateral vibration modes due downhole coupling of the different modes (Aadnøy et al. 2009).

2.3.1.2 Torsional Vibrations

This type of vibration originates from a periodic acceleration and deceleration of the bit and string rotation, triggered by high frictional torque at the bit and BHA. The low torsional stiffness of string components induces an instantaneous bit rotation different from the surface rotary speed. This causes a torsional pendulum effect due to the downhole friction along the BHA and drill pipes. A non-uniform bit motion arises in which the bit ceases to rotate for a short period at regular intervals, causing the whole string to torque up since constant rpm is supplied from surface. The string then spins free, accelerating to rotary speeds above the desired value and releasing the stored torque. Then, the string rotates freely and the rotary speed drops as the torque starts to build up until the system gets stuck again. Because of this movement action, this self-excited torsional vibration phenomenon is called stick-slip vibration. Fig. 2.14 shows the rotary speed and torque for a typical stick-slip situation. Stick-slip occurs quite often during drilling operations at low frequency levels without any severe damage and necessary countermeasures from the rig crew. High frequency torsional oscillations can also blend into lateral BHA vibrations. Torsional vibrations are common when running PDC bits because their shearing action induces a high bit friction which can damage the cutting structure as seen in Fig. 2.15. Other bit types and stabilizers can cause torsional oscillations too (Aadnøy et al. 2009).

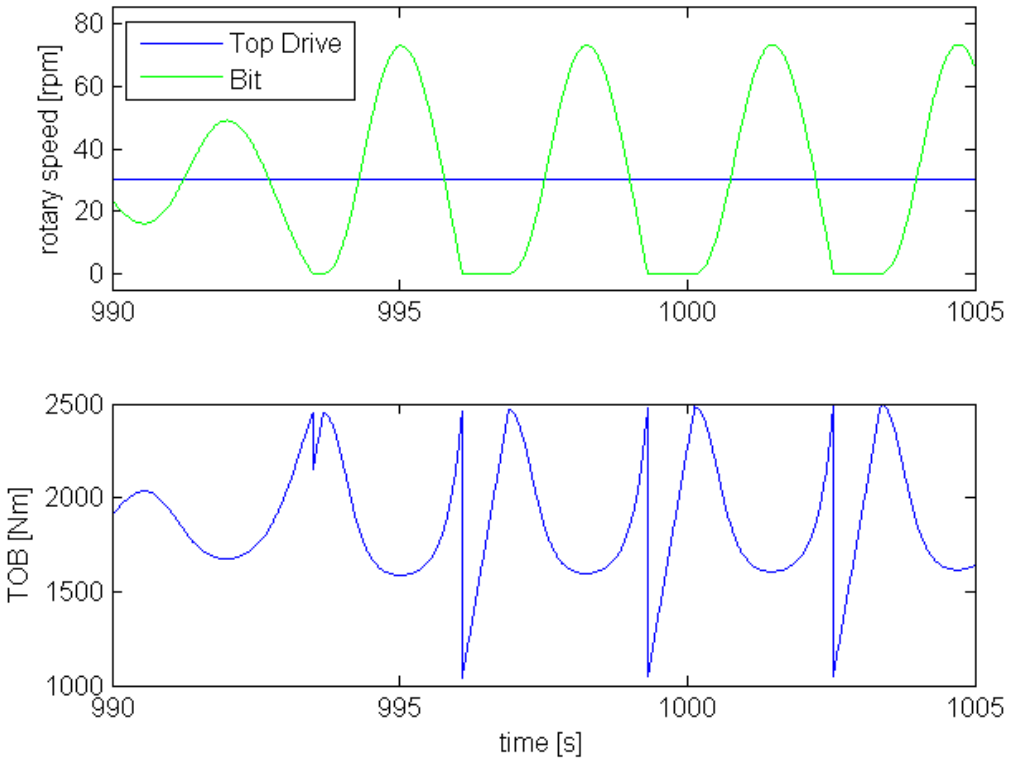

Fig. 2.14: Rotary speed and torque characteristics for a typical stick slip situation. Torque builds up as the bit motion is hindered and the top drive continuously rotates the string. The string then breaks free, increasing the rotary speed above the normal rotary speed and releasing the stored torque (Baker Hughes 2015).

Fig. 2.15: Damaged cutters of a PDC bit. Some cutters have been sheared off or have parted from their matrix connection and are lost. (Baker Hughes 2015)

Stick-slip vibration also increases tool connection wear and damage. Over-torqued connections above the recommended make-up-torque show severe thread damage and are difficult to break free at the rig floor. Backward rotation could even back-off properly torqued connection causing a risk for fish and lost in hole incidents. Top drives tend to stall at certain torsional vibrations (Aadnøy et al. 2009).

2.3.1.3 Lateral Vibrations

Lateral vibrations are also described as transverse, bending or flexural vibrations and walk of the bit or BHA in field terms. This vibration mode is widely recognized as one of the major causes of BHA failure but paradoxically the impact has been unknown for a long time, because lateral vibrations do not propagate up to the surface. Lateral vibrations are dispersive and of a higher frequency compared to the other vibration modes. Downhole accelerometer measurements are needed for detecting and recording vibrations, especially lateral vibrations (Aadnøy et al. 2009).

There are several downhole mechanisms which can lead to lateral vibrations, primarily bit-formation and BHA-borehole interactions. Two types of bending vibration result from coupling with axial forces, these are linear and parametric coupling in particular (Vandiver et al. 1990).

WOB fluctuations can lead to loss of mechanical stability which becomes evident as rapidly growing lateral vibrations. This is comparable to the induced snake motion of a vertical hanging rope as it is moved up and down at a particular frequency (Dunayevsky et al. 1993). Such a phenomenon, which is associated with specific axial fluctuations, is called parametric resonance (Magnus 1986). This can occur at WOB levels below the critical values obtained from a static buckling analysis (Dunayevsky et al. 1993). In parametric resonance the critical frequencies are not discrete sets of critical frequencies anymore (Magnus 1986). However, they are critical frequency bands which highly depend on the axial WOB fluctuations (Dunayevsky et al. 1993).

The source of linear coupling is the initial curvature of the BHA. An axial compressive load will cause a lateral deflection of such a bent assembly (Vandiver et al. 1990). Drilling with a slightly bent drill collar or an unbalanced MWD tool can result in violent lateral vibrations similar to the circular “whirling” motion of an unbalanced centrifuge (Jansen 1992). Destructive whirling has long been known to occur in rotating machinery when the rotation rate of the shaft is equal to the natural frequency of that shaft in bending. When this happens, the machine is known to be operating at a critical speed. However, whirling can also lead to an increased risk of failure or damage at non-resonant frequencies (Vandiver et al. 1990).

“The major source of excitation is the rotary speed. If the BHA has a natural transverse frequency close to that of the rotary speed, and the mode is not well damped, then there is a real danger of resonating the BHA and causing failure through fatigue” (Burgess et al. 1987).

The lateral resonance frequency highly depends on the drill collar size and stiffness, stabilizer location and hole inclination. More mass, less stiffness, greater stabilizer spacing and a vertical hole would lead to lower resonant frequencies. The inclination determines the point at which the drill collars above the last stabilizer contact the borehole wall. These wall contacts at the drill collars dampen lateral vibrations and eliminate their further propagation. Thus, lateral vibrations are terminated at this point and do not travel up to the surface. This contact point, called tie point, defines the length of the lateral vibration system (Burgess et al. 1987). This holds true for conventional assemblies based on heavy collars in inclined holes but extended reach BHAs show extended wall contacts if long drill collar or drill pipe sections are located in the horizontal section. The horizontal orientation increases the downward acting normal force, enabling the

BHA to sag to the low side of the hole. Despite these long wall contacts, BHAs in horizontal sections can still experience lateral vibrations. Running drill pipe under compression and high rotational speeds leads to a very high lateral vibration susceptibility. The termination of lateral BHA vibrations at the tie-point does not exclude that local areas of the drill pipes are susceptible to lateral vibrations. However, the drill pipes are rarely considered in vibration analyses (Heisig, Neubert 2000).

Although resonance between the excitation source and BHA frequency will lead to high amplitudes, it is not sufficient to look at the resonant conditions alone since once wall contact has been made, the system is charged and diverts from a harmonic oscillation. At wall contact, the rotational motion of the collars couples to the lateral motion of the drillstring. If the lateral kinetic energy gained from the rotation is greater than that lost in the impact, the drillstring will undergo a net lateral acceleration. As a result, the next interaction with the borehole can be more energetic than the last, with the magnitude of the shocks increasing with each impact until some limit is reached. Once the impacts have been initiated under these conditions, the impact interactions play a major role in the drillstring motion and the impacts become self-sustaining. The amount of energy transfer from rotation to lateral acceleration highly depends on the friction coefficient between the BHA and formation. As the friction coefficient increases, more energy is transferred (Aldred, Sheppard 1992).

A well-known category of lateral vibrations is the bit and collar whirl phenomenon. During whirling, the component shows an eccentric rotation around a point other than the geometric center of the borehole due to an over-gauge hole or bent collar. This whirl can occur either in a forward, backward or chaotic motion (Aadnøy et al. 2009). Forward synchronous whirl causes high wear on one side of BHA due to continuous rubbing on the full circumference of the wellbore. Backward whirl shows a frequency or direction that does not coincide with that of the excitation. A typical backward bit whirl pattern for a PDC bit is shown in Fig. 2.16 and the drill collar motion for both whirl conditions can be seen in Fig. 2.17. Wall contact during forward whirl will initiate a gradual change towards backward whirl. (Jansen 1992). This backward motion induces high frequency bending moment cycles and is therefore the most critical lateral vibration phenomena. The maximum possible bending moment amplitude is defined by the annular clearance between the BHA and borehole wall. This occurs especially at the joint between a collar and stabilizer. Bit whirl is a stable phenomenon which is difficult to eliminate by mere drilling parameter changes (Linke and Cardy 2009).

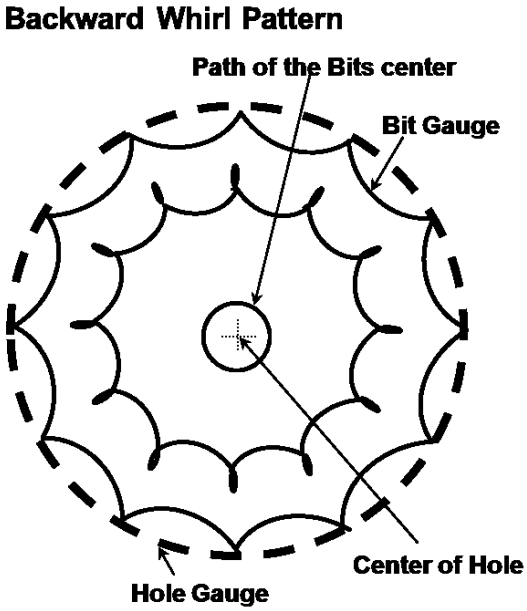

Fig. 2.16: Backward whirl pattern of a PDC bit as the bit center is offset towards the borehole center due to an over-gauge hole size. (Baker Hughes 2015)

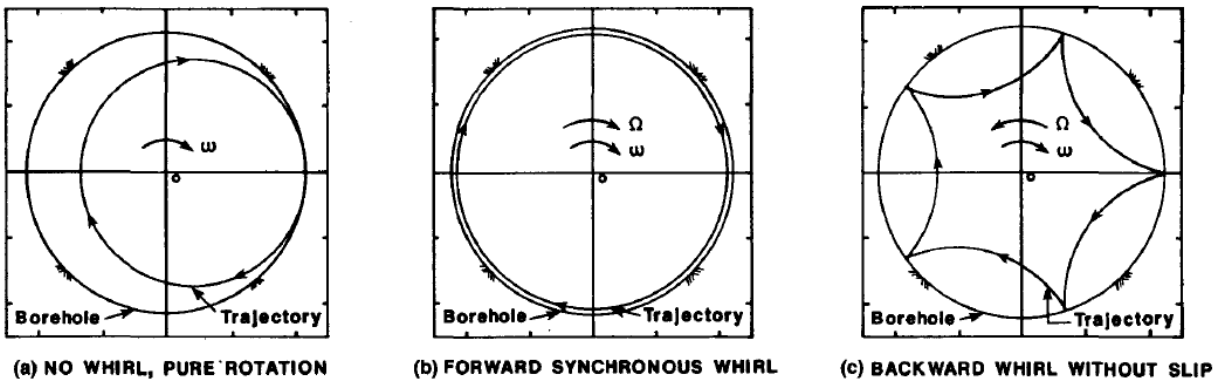

Fig. 2.17: (a) shows the no-whirl-rotation-only condition in an inclined hole where the drill collar lies on the low side of the well. (b) shows the forward whirl condition, which could be encountered when an initially bent collar deflects further as a result of the centrifugal force caused by rotation. (c) shows the backward whirl phenomenon, which results when the whirling drill collar contacts the borehole wall with a large frictional force, resulting in a tangential slip velocity of zero. (Vandiver et al. 1990)

Lateral vibrations can affect different BHA components. Bit damage results from excessive side forces and bit whirl which destroys the cutting structure or even the whole bit matrix (Aadnøy 2006). MWD/LWD tools can fail due to high bending loads on the measurement units or due to shock loads as the tool impacts with the borehole wall (Aadnøy et al. 2009; Reckmann et al. 2010).

A study conducted by (Reckmann et al. 2010) concludes that lateral vibrations and backward whirl are the most significant dynamic behavior responsible for MWD/LWD failure. 29 percent of all tool failures are vibration related but it should also be noted that vibration recording and transmitting tools are only run in high risk operations which contributes to this high number of failures.

Stabilizers can see an abnormal blade wear which can lead to breakage of the hard-facing (Fig. 2.18) and blade erosion. Furthermore, connection fatigue is increased during coupling of axial and transversal vibrations (Aadnøy et al. 2009).

Fig. 2.18: Chipped-off tungsten-carbide inserts of a stabilizer blade due to high lateral vibrations. (Baker Hughes 2015)

2.3.1.4 Summary

In summary, different downhole scenarios and excitation sources can lead to axial, torsional or lateral vibrations or various combinations of these phenomena. Some failure modes are characteristic for particular dynamic drilling dysfunctions. The identification of BHA failure and damage patterns during post well analysis can lead to the deduction of downhole vibrations which might have occurred during the operation. The plain occurrence of dynamic phenomena does not necessarily induce mechanical damage, as seen during low frequency torsional and axial oscillations (Linke, Hummes 2015a). A short overview of dynamic dysfunctions, their sources and failure modes can be seen in Fig. 2.19. The following chapter provides more information on the mentioned excitation mechanisms.

Dysfunction	Typical mechanical damage expected	Typical excitation sources	Typical scenario where it develops
Backward Whirl	Cracks, twist-offs	Bit or underreamer whirl, motor AKO, rotor of a motor, tools with eccentric mass, stabilizer blades, tools with blade-like upsets	high rpm, near-buckling loads, high friction
Fully-Syncronous Forward Whirl	Wear flats	bent motor, V-Stab, any tool with mass, stiffness, or geometry non-symmetrical	large diameter, low friction environments
Lateral Acceleration	Cracks, twist-offs, impact damage	High-friction environments, Bits and underreamers, motor bends, wobbling rotor inside stator, straight-bladed stabilizers, SDN, DCs and other heavy tools with slight eccentricities	high rpm, hard rock, high friction, light mud, low inclination tangents, inappropriate stabilization
Snaking	none	High-friction at BHA and string	horizontal tangents
Stick-Slip	Chipped PDC cutters, overheated bearings	Agressive PDC bit or friction along the borehole	High WOB or extended reach/tortuous wellbore
Low-Frequency Torsional Oscillation	none	Agressive PDC bit or friction along the borehole	High WOB or extended reach/tortuous wellbore
High-Frequency Torsional Oscillation	Electronics failures	PDC bit or stabilizer with strong contact force	Unknown
Bit Bounce	Bit damage: Tricone bearing damage, broken or chipped teeth; electronics failure; surface gear damage	Tricone: tri-lobe bottomhole pattern, PDCs at an angle of a hard interface, rig heave, shock subs and thrusters in compressible fluids, rig pump pressure spikes	Operations favoring a tri-lobe pattern, shallow wells, synchronized rig pumps
Low-Frequency Axial Oscillation	none	The same as for bit bounce	the same as for bit bounce.
High-Frequency Axial Oscillation	Electronics failures	Agitator tool. Tricone teeth.	Tricones: teeth tracking

Fig. 2.19: Overview of drilling dysfunctions and some typical excitation sources. The dysfunctions are related to axial, torsional, lateral or combinatorial vibrations. (Baker Hughes 2015)

2.3.1.5 Excitation Mechanisms

Rotation, imbalance, misalignment, bent components and BHA movement, as mentioned before, can create excitations that are at rotational frequency or multiples of the rotational frequency. If these frequencies match one of the BHA natural frequencies, a resonance condition with growing stresses occurs. The resonance inducing speeds are called critical speeds. The response to these excitation mechanisms is complex due to the large extent of coupling between the different vibration modes. Mass imbalance, misalignment and bent pipe typically raise lateral excitation of 1 to 2 times rpm. This lateral excitation can also induce secondary axial and torsional excitations with different multiples of rpm. (Besaisow, Payne 1988) and (Spanos, Payne 1992). Other excitation sources and their multiples of the rotational frequency can be found in Tab. 2.2. Fig. 2.20 shows the frequency bandwidth of common excitation sources and their response.

Tab. 2.2: Different excitation sources during a typical drilling operation. The mechanism describes how the source generates vibrations. Further, the direction or type of vibrations is given together with a typical frequency range and strength. The stated formulas should be seen as guidelines and are not suitable for exact calculations. (after Baker Hughes 2015)

Tool/Source	Mechanism	Direction	Frequency Formula	Typical Freq.	Excitation Strength
PDC or Tricone bit	fully developed whirl	lateral (whirling)	bit rpm * (blade# +1)	8…30 Hz	very strong
PDC bit	high-imbalance smooth	lateral (whirling)	bit rpm	2…6 Hz	low to medium
PDC bit	Frequent biting of cutters	torsional	unknown	<1Hz	depends on bit type
PDC or Tricone bit	snap (individual cutter chirp)	lateral/torsional	unknown	30+Hz	low to medium
PDC or Tricone bit	partially developed whirl	lateral (whirling)	bit rpm * (blade# +1)	20+Hz	strong to medium
Tricone bit	Tri-lobe pattern	axial	3x bit rpm	6…18Hz	none to strong
Reamer/hole opener	similar to bits	various	blade # * string rpm	various	strong to very strong
Motor	rotor wobbling	lateral	(motor rpm * rotor lobe#) - string rpm	3…6 Hz	rotor weight * ecc.
Motor	AKO (bent)	lateral	string rpm	0…3 Hz	medium to strong
Stabilizer	camshaft & leading edge	lateral	stabilizer rpm * blade #	0…6 Hz	depends on gauge and blade count
Drill Collar	bend, eccentric cut threads	lateral	string rpm	0…6 Hz	low to strong (mass * ecc)
Any eccentric tool	mass imbalance	lateral	tool/string rpm	0…6 Hz	low to strong (mass * ecc)
Soft Torque	maladjusted corrections	torsional	likely close to stick-slip frequency	<1 Hz	none to strong
Pumps	pressure pulses	mostly axial	strokes per minute	1…3 Hz	near surface significant
Heave	waves lifting rig	axial	f(ocean)	<< 1 Hz	none to excessive

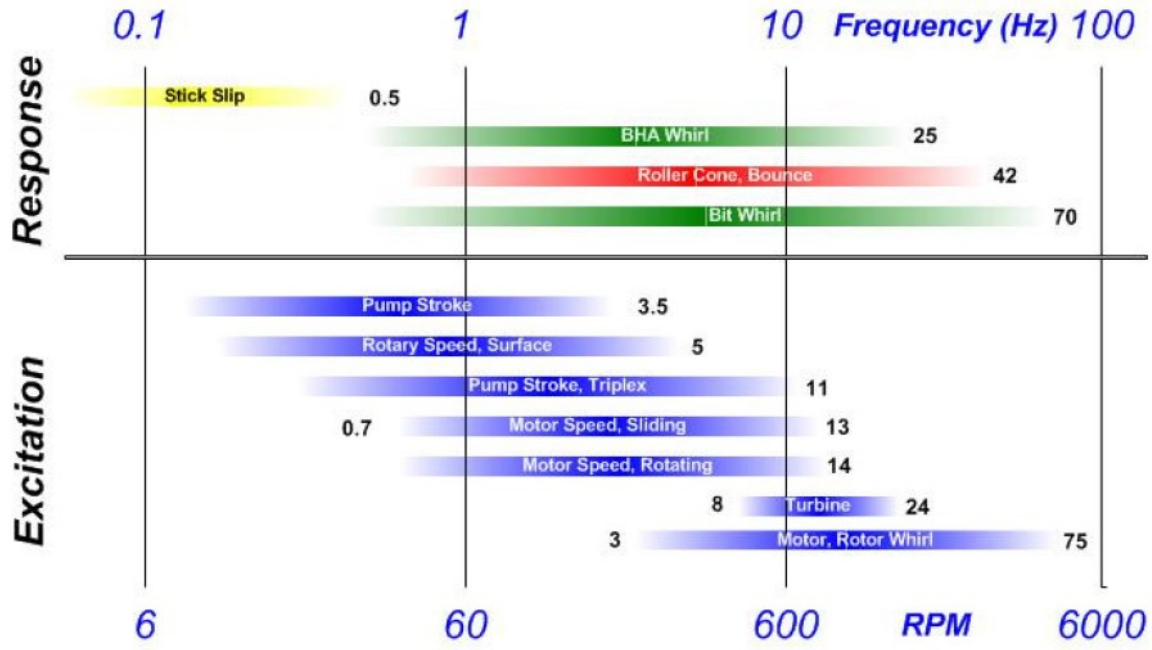

Fig. 2.20: Frequency range of common excitation sources and their vibration response. (Reckmann et al. 2010)

2.3.2 Computational Models

The calculation effort increases as the component diversity becomes bigger. Slick and single stabilizer BHAs can be determined with ease but complex geometries require special solution techniques, for example finite element methods (Heisig 1993) or transfer matrix approaches (Gasch et al. 2012). BHA vibrations can be investigated by the means of a structural dynamic analysis. Such an analysis contains a mathematical description of the assembly as a vibration system. The BHA under investigation is transferred into a simplified model which can be solved analytically or numerically (Gasch et al. 2012).

Analytical models have been extensively used in the past and are firmly established as state of the art computational models. The last two decades have seen a transition from these techniques towards a numerical approach to solve problems. Nowadays, finite element analyses and multi-body systems are the foundation for dynamic considerations. All statements, derivations and assumptions quoted in this chapter have been taken from (Gasch et al. 2012).

The base equation, which is incorporated into almost every dynamic model, is a second order differential equation of the linear equation of motion:

$$\boldsymbol{M}\ddot{u}(t) + \boldsymbol{D}\dot{u}(t) + \boldsymbol{S}u(t) = \boldsymbol{p}(t) \qquad \textbf{Eq. 2.2}$$

The mass, damping and stiffness matrices are denoted by $\mathbf{M}$, $\mathbf{D}$ and $\mathbf{S}$ respectively. The displacement vector and its derivatives are called $\mathbf{u}$. $\mathbf{p}$ is the force vector exciting the system.

BHAs have a continuous mass and elasticity distribution and hence, infinite degrees of freedom. Such a continuous system can be described through a partial time-location differential equation:

$$[EI(x)w''(x,t)]'' + \mu(x)\ddot{w}(x,t) = p(x,t) \qquad \textbf{Eq. 2.3}$$

This is the same equation as used in calculating beam forces. Here, EI describes the bending stiffness, μ the mass distribution, p a dynamic load and w the lateral displacement of the beam or the BHA. In addition to the time dependency, these parameters are location dependent. The location dependency is denoted by x and the time relationship by t. $(\dot{a})$ denotes the time derivative $\frac{\partial}{\partial t}$ and $(a)'$ the derivative $\frac{\partial}{\partial x}$ with respect to the location x. The result is bending vibrations w which are time and location dependent. Damping considerations, for example structural damping d, can be included, extending the equation to:

$$[EI(x)w''(x,t)]'' + d\dot{w}(x,t) + \mu(x)\ddot{w}(x,t) = p(x,t) \qquad \textbf{Eq. 2.4}$$

Closed analytical solutions for such a beam equation are very hard to obtain for complex systems but they can be a great assistant for conducting parameter studies on simple geometries due to a fast computation and traceable steps.

More complex continuous structures are not capable of providing an analytical solution, even with very aggressive simplification steps. Complex problems can be solved with the finite element method. The structure under investigation is divided into smaller elements with shape functions which can be handled more easily. Shape functions are used to obtain an approach solution to the exact solution as a linear combination of some kind of well-known functions. They describe how the dependent variables, which have to be determined, vary as a function of the spatial coordinates of the element. Then, a system of equations for the whole structure is set up, considering the boundary and transfer conditions of the elements. Such an equation system can be seen in Eq. 2.2. The number of equations is highly dependent on the element resolution of the model and can lead to very big systems which require a lot of computational power. This makes finite element methods unsuitable for parameter studies, where different model versions should be produced in an acceptable time frame. However, the implementation of the appropriate reduction method can also enable finite element methods for this purpose.

A predecessor of the modern finite element methods is the transfer matrix method. This method is very efficient in producing solutions for straight structures such as BHAs and allows the determination of natural frequencies, normal modes and system response for harmonic excited forces. The results of the transfer matrix method are based on exact solutions of the beam differential equations after Euler and Bernoulli. Thus, the transfer matrix method is the computation model of choice for this parameter study (Gasch et al. 2012).

2.3.2.1 The Transfer Matrix Method

The transfer matrix method has been developed in the 1920s for determining oscillations in piston engines and is suitable for determining straight structures at reasonable computation speeds.

The structure under investigation is divided into smaller segments for which the vibration equations are solvable through time and location shape functions. This solution is put into a form capable of determining the state variables at the end of a segment through the state variable of the segment onset. The state variables for this case are amplitudes of displacement w, inclination w', bending moment M and shear force Q:

$$\begin{Bmatrix} -w \\ -w' \\ M \\ Q \end{Bmatrix}_1 = [\boldsymbol{T}(\omega)] \begin{Bmatrix} -w \\ -w' \\ M \\ Q \end{Bmatrix}_0 \qquad \textbf{Eq. 2.5}$$

The transfer matrix $\mathbf{T}$ conveys this connectivity. Segment properties like mass, length and stiffness but also the frequency at which the system is vibrating is included in this matrix. The vibration equation of the whole structure is then assembled from the segment solutions, considering compatibility and equilibrium. This leads to loss of the inter-unknowns between the segment connections. The final equation system contains only the state variables from the start, position zero, and from the end point, which allows for an easy introduction of the boundary conditions at these locations (Gasch et al. 2012).

The numbers of unknowns are hereby independent of the number of segments which is the main reason for computational efficiency of the transfer matrix method but also the cause for some numerical flaws (Gasch et al. 2012).

The construction of the differential equations of motion requires two different sets of equations, the equilibrium conditions from the momentum and force balance (Eq. 2.6) and the laws of elasticity (Eq. 2.7).

$$M(t)'' + p(t) - \mu\ddot{w}(t) = 0 \qquad \textbf{Eq. 2.6}$$

$$M(t) = -Bw(t)'' \; with \; B(x) = EI(x) \qquad \textbf{Eq. 2.7}$$

The law of elasticity used here is the linear relationship between the momentum and beam curvature w'' with the bending stiffness B as proportionality constant. The bending stiffness and the mass distribution are location dependent. These equations are set up for each BHA segment as shown in Fig. 2.21. Combining these equations yields Eq. 2.3 and in the case of a constant bending stiffness this simplifies further to:

$$Bw(t)'''' + \mu\ddot{w}(t) = p(t) \qquad \textbf{Eq. 2.8}$$

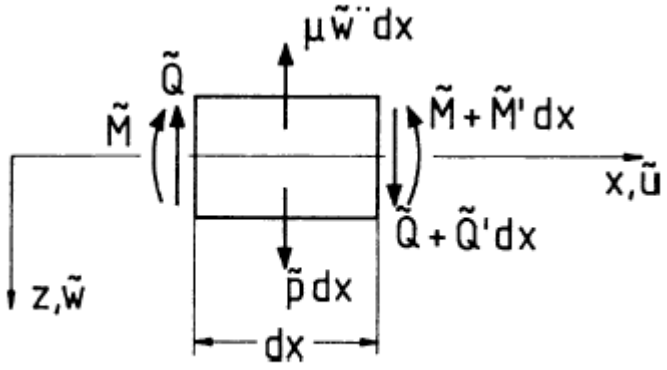

Fig. 2.21: Equilibrium conditions on a BHA segment. (Gasch et al. 2012)

In the differential equation of motion of Eq. 2.8, the fourth derivative occurs and hence four different boundary conditions are required, two on every end of the BHA. The type of boundary

condition depends on the model setup. Possible boundary conditions include a clamped $(w(0,t) = w'(0,t) = 0)$, free $(M(0,t) = Q(0,t) = 0)$ or limber mounted $(w(0,t) = M(0,t) = 0)$ end. The type of support on these ends is important for the boundary conditions. In addition to the boundaries, initial conditions have to be defined for time zero, for example an initial displacement and a velocity of zero.

The partial differential equation of motion in Eq. 2.8 can then be solved with the support of the Bernoulli separation approach. Instead of a partial differential equation, the separation approach provides two ordinary differential equations. This yields a solution for the variation of time and a more complicated solution for the location dependency which results in a characteristic equation with four solutions. Using an exponential approach and hyperbolic and trigonometric functions, called Rayleigh functions which are denoted by R, the equation system can then be written as:

$$\begin{Bmatrix} w(x) \\ w'(x) \\ M(x) \\ Q(x) \end{Bmatrix} = \frac{1}{2} \begin{bmatrix} R_1(x) & \frac{R_2(x)}{\lambda} & -\frac{R_3(x)}{\lambda^2 B} & -\frac{R_4(x)}{\lambda^3 B} \\ \lambda R_4(x) & R_1(x) & -\frac{R_2(x)}{\lambda B} & -\frac{R_3(x)}{\lambda^2 B} \\ -\lambda^2 B R_3(x) & -\lambda B R_4(x) & R_1(x) & \frac{R_2(x)}{\lambda} \\ \lambda^3 B R_2(x) & -\lambda^2 B R_3(x) & \lambda R_4(x) & R_1(x) \end{bmatrix} \begin{Bmatrix} w(0) \\ w'(0) \\ M(0) \\ Q(0) \end{Bmatrix} \qquad \textbf{Eq. 2.9}$$

or in a more reduced form:

$$\boldsymbol{x}(x) = \boldsymbol{T}(x, \lambda)\, \boldsymbol{x}(0) \qquad \textbf{Eq. 2.10}$$

Eq. 2.9 and Eq. 2.10 are valid for any beam structure with a constant bending stiffness and mass distribution. The input of the boundary conditions allows the determination of the eigenvalues λ and natural frequencies ω. The complex system is then reduced to a homogeneous equation system. Here for a cantilever beam excited by a free vibration:

$$\frac{1}{2} \begin{bmatrix} \cosh \lambda l + \cos \lambda l & \frac{\sinh \lambda l + \sin \lambda l}{\lambda} \\ \lambda(\sinh \lambda l - \sin \lambda l) & \cosh \lambda l + \cos \lambda l \end{bmatrix} \begin{Bmatrix} M(0) \\ Q(0) \end{Bmatrix} = \begin{Bmatrix} 0 \\ 0 \end{Bmatrix} \qquad \textbf{Eq. 2.11}$$

This equation system changes for different excitation types and other boundary conditions. For example for forced steady state harmonic oscillations as used in the conducted parameter study, the homogeneous equation system is written as:

$$\frac{1}{2} \begin{bmatrix} \cosh \lambda l + \cos \lambda l & \frac{\sinh \lambda l + \sin \lambda l}{\Lambda} \\ \Lambda(\sinh \lambda l - \sin \lambda l) & \cosh \lambda l + \cos \lambda l \end{bmatrix} \begin{Bmatrix} M(0) \\ Q(0) \end{Bmatrix} = \begin{Bmatrix} 0 \\ P \end{Bmatrix} \qquad \textbf{Eq. 2.12}$$

where P denotes the centrifugal force of a mass imbalance. For simplification, only the vertical force $P \sin \Omega t$, with the excitation frequency Ω, is considered for causing lateral vibrations of the beam structure. Λ is an abbreviation for:

$$\Lambda = \frac{\mu \Omega^2}{B} \qquad \textbf{Eq. 2.13}$$

The natural frequencies are the zero-points of the determinant of the coefficient matrix of this homogeneous equation system. The coefficient matrix yields zero for:

$$1 + cos\lambda l\ cosh\lambda l = 0 \qquad \textbf{Eq. 2.14}$$

An overview on the zero-points $\lambda_i l$ and the corresponding eigenfrequencies ω_i provides a graphical evaluation of Eq. 2.14, as shown in Fig. 2.22. By inserting the eigenvalues λ_i in Eq. 2.11, the corresponding natural modes can be determined.

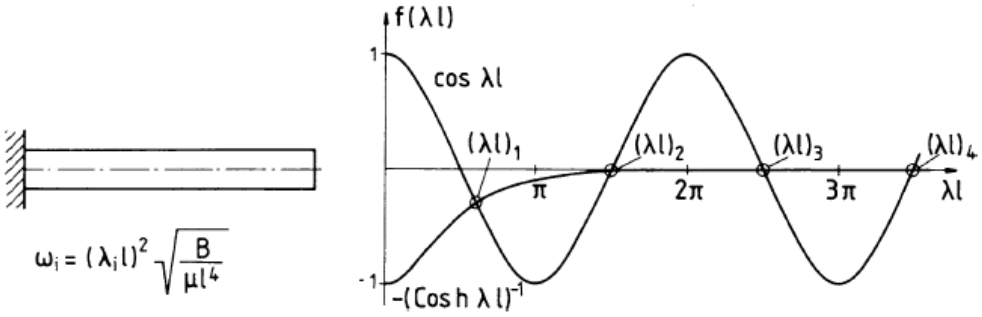

Fig. 2.22: Determination principle of natural frequencies of a cantilever beam. (Gasch et al. 2012)

Besides the eigenform, expressed through the curvature and displacement, the transfer matrix method yields directly the internal momentum and shear forces without any further calculations. This is one of the major advantages of the transfer matrix method. Additionally, these parameters are exact values and no approximations as in finite element methods which could lead to boundary discontinuities.

Determining higher natural frequencies can lead to numerical problems which can be compensated with double precision or with the introduction of more unknown variables by increasing the dimension of the transfer matrix. This decreases the contrast between extremely high and low values.

Direct elimination of the time dependency leads to certain limitations of this differential equation method. The introduction of dampers into the system generates a transfer matrix and a state variable vector which contains complex numbers. This does not influence the calculation schematic but the determination of zero crossings becomes tedious because a ω and decay factor α variation has to be performed for their determination:

$$\det(\lambda) = \det(\alpha + i\omega) = 0 \qquad \textbf{Eq. 2.15}$$

This procedure has not been really enforced since the finite element method provides a much more convenient way of solving this eigenvalue problem. A possible compensation for the computational expenditure is the coupling of the transfer matrix method with a modal analysis. Using modal analysis techniques, the normal modes and natural frequencies can be calculated with the transfer matrix method, in case of a conservative or proportional damped system. Afterwards a modal analysis is initialized, allowing faster computation of the results (Gasch et al. 2012). This coupling has been implemented into a MATLAB environment for conducting the parameter study.

2.4 Standard Tool Specification and BHA Design Procedure

Prior to drilling and deploying tools downhole, tool design should ensure the selection of the right materials, shape, manufacturing process and a proper mechanical or electronic functionality. This should ensure the expected downhole running hours for the used equipment.

The most common tool design approaches are based on static models which determine the maximum allowable static loads for given materials and designs. Further, a fatigue assessment should cover a broad variety of tool wear scenarios, such as corrosion and vibrations. A fatigue analysis is more complex and has a larger statistical spread compared to the static design which works with clearly defined loads and conditions. However, there is an uncertainty in both, statics and fatigue. The fundamentals of stress conditions and static and fatigue loading can be found in (Dubbel et al. 2001, pp. E2-E12).

Drilling itself is based on very few controllable operational parameters, namely block position, surface rotary speed, flow rate and mud properties. All other parameters such as WOB, ROP or vibrations are a response to those parameters and the prior BHA design which is comprised of different tools. A list of common drilling loads can be seen in Tab. 2.3.

Hence, trying to mitigate fatigue related drilling problems and damages by adjusting the drilling parameters might have little impact if the overall BHA design is not engineered for its actual purpose. Surface adjustments are burdened with uncertainties in load transfer and losses along the drill string, which could lead to ineffective decisions in vibration mitigation.

It might be challenging to optimize tool designs for vibration, especially if the tool is part of a multicomponent system such as a BHA. Changing the natural frequency or the excitation frequency, applying damping or eliminating certain excitation sources of a BHA design could reduce the occurring vibrations. Load data should represent downhole loading under actual or proposed service conditions. Simplified or worst case estimates should be made if these loads are unknown. Sources for load data are proposed tool specifications, tool data sheets, special calculations or downhole measurements (Dareing 1982; Ritter 2007).

Tab. 2.3: Possible downhole loads on drilling tools. They are distinguished between external/internal, monotone/cyclic and static/dynamic behavior. (Ritter 2007)

load type	explanations, causes and effects	examples	external or internal to assembly	monotone or cyclic behavior	static or fatigue assessment
bending	static bending sliding drill string in curved borehole	oriented drilling	ext	mono	stat
bending	alternating bending • rotating drill string in curved borehole • eccentric support of rotating shaft	rotary drilling eccentric support of rotating shaft	ext	cycl	fati
compression	axial force on bit	WOB	ext	mono	stat
compression	by pressure drop	rotor thrust thruster force	int	mono	stat
tension	pulling drill string	overpull, jarring	ext	mono	stat
pre-stress	by geometrical fit stretched or compressed parts or sections	thread pin/box sleeve, pre-stressed tie rod, mandrel	int	mono	stat
torsion	operating torque	Bit and Drag torque	ext	mono	stat
torsion	MUT (Make-Up torque)	torquing of thread connections	int	mono	stat
pressure	hydrostatic pressure	differential pressure	ext	mono	stat
pressure	oil hydraulics actuators pressure	rib piston	int	mono	stat
temperature strain	• by materials with different expansion coefficient • by temperature gradient	steel & CuBe	int	mono	stat
acceleration	Mass	Gravity	int	mono	stat
acceleration	by vibrations	Shaking	int	cycl	fati
spin	high speed rotation	turbine or generator rotors	int	mono	stat

2.4.1 Static Strength Assessment

Structural reliability is a basic functional requirement for drilling operations. The evaluation of material overloading resulting in local plastic deformation or global yielding of large areas is one of the major objectives of tool design. Large plastic deformations and possible structural instabilities, such as collapse and buckling, have to be evaluated to prohibit yielding without resistance, dysfunction, loss of preload, seal leakage and disassembly problems. Static tool strength assessment is usually performed for a worst case scenario. Harsh operating conditions like in high temperature and pressure wells and/or highly saturated mud environments decrease tool capacities by impaired material properties. Operating temperatures exceeding 150 °C lead to a progressive degradation of material properties, for example yield strength and Young‘s Modulus. A corrosive environment has only minor effects on the static strength of drilling tools but long term effects should not be neglected, like the reduction of the load bearing cross section (Ritter 2007).

For performing a static tool strength assessment two known concepts are usually considered. First the nominal stress concept, considering the nominal stress state, and secondly the local elastic stress concept which focuses on the local elastic notch stress. The nominal concept is only applicable if the geometry and loading conditions allow for a nominal stress value determination. Nominal stress is calculated on the basis of the net cross section of a specimen without taking into account the effect of geometric discontinuities such as holes, grooves, etc. Furthermore, this concept neglects local stress concentrations. Hence both concepts are integral parts of the static tool strength assessment (Ritter 2007; FKM 2012).

One fundamental safety criterion is based on the ductile material behavior of structural steel and its capacity to relieve local stress peaks exceeding yield strength by local plasticity and stress balancing. Local total strain values of up to 5 % are allowable for static plasticity which is known as the 5 % strain criterion. This criterion is the limit value of total strain for calculating the section factors, allowing for the influence of the stress gradient in bending and/or torsion in connection with the shape of the cross section. Thus, making best use of the load carrying capacity by accepting some yielding as the outside fiber stress exceeds the yield strength (Ritter 2007; FKM 2012).

Collapse load is usually determined by the nominal stress state, neglecting notch effects, reaching to the yield strength. For safe working conditions, a safety factor of 1.1 to 1.25 should be considered (Ritter 2007).

A static BHA analysis should deliver information about the occurring side forces, bending moment and wall contacts of the assembly under investigation. Finally, the maximum static loads and the safe working loads should be determined with the general aim of not exceeding the yield strength. A rate of capacity (ROC) should be defined (Eq. 2.16) which points out how much of the safe working range is used for the considered loads. A $\mathrm{ROC} > 1$ requires design optimization (Ritter 2007).

$$ROC = \frac{required\ load}{safe\ working\ load} \qquad \textbf{Eq. 2.16}$$

This static strength assessment can be used to develop operating specifications for different tools and sizes under static loading, as shown in Tab. 2.4.

Tab. 2.4: Operational Specifications for static load conditions. The parameters are given for different tool sizes. Such working ranges have not been defined for dynamic or combined loads yet. These values are only representative for the Baker Hughes drill collar based tool fleet. (modified after Dueber, Gatzen 2013)

		Tool Size			
Specification	**Unit**	**4 3/4**	**6 3/4**	**8 1/4**	**9 1/2**
Max. WOB	kN	1120	2990	2400	2250
Max. tool rotation	min^{-1}	400	400	300	300
Drilling torque (cont. operation)	kNm	12	32	48	72
Max. torque to failure	KNm	28	65	102	153
Overpull (cont. operation)	kN	2000	3900	5000	6000
Max. overpull to failure	kN	3000	5200	6700	8800
Max. dogleg severity (rot./slide)	°/100 ft.	Depending on BHA configuration			

2.4.2 Fatigue Strength Assessment

Fatigue is the most common failure in drilling. There are two different dynamic load conditions which can lead to BHA fatigue failure. The development of a low cycle-high stress condition, associated with stress levels near the yield strength of the used material, can be considered as one of the fatigue failure reasons. Stresses near the yield strength can lead to plastic deformation without material rupture. The second dynamic load condition is a high cycle-low stress condition significantly below the ultimate static strength which could also lead to fatigue failure. Stress levels exceeding the material yield strength can lead to overload breakage of the material. The total stress is comprised of the static and dynamic components. Considering only one component in the design process could prove disastrous since the monotonic loads are superimposed to the dynamic loads, thus reducing the fatigue limit. Such static loads can be connection preloading, constant torque, hydrostatic pressure or residual stress.(Dareing 1982).

Fatigue failure, in contrast to static failure of ductile materials, is a phenomenon of local stress and strain. A fatigue analysis is typically based on a constant amplitude loading such as bending under string rotation. The goal of the analysis is the identification of the acceptable loads which are below the fatigue limit or in other words infinite tool life. These results must be regarded as estimates towards the infinite life due to the hard predictability of the actual loading and wear conditions. In general, any predicable load should not exceed the fatigue limit. The fatigue limit is influenced by several different factors. The mud rheology has an impact on the corrosiveness of the environment. Wall contacts lead to marks which increase tool wear and induce fretting. Additionally, residual stresses from welding, surface treatment and manufacturing play a major role in tool life. Actual consideration of these factors is cumbersome and the uncertainty of exact environmental conditions, loads and random events require crack inspection for detecting unpredicted fatigue damage. Aiming for a more conservative approach would reduce fatigue failure occurrence but would also lead to very low acceptable operating limits (Ritter 2007).

The typical cyclic load in drilling operations to be considered in fatigue analysis is loading due to bending during drill string rotation. *“For example: At rotational speeds of about 100 to 300 rpm it will take about 56 to167 hours* (only about three “50-hours-jobs”) *to reach 1.000.000 bending cycles.”* (Ritter 2007). Torque variations can also induce cyclic loading on the drilling tools. Cyclic loads are loads which occur repetitively for a large number of cycles ($N >> 100$). Repetitive loads from several jobs or make-up and break-up of connections are considered as static loads only. Drill string vibrations also cause cyclic loading. Such load conditions are hard to determine and to consider in analyses and tool design. Therefore, operational conditions and BHA configurations must be adjusted to avoid vibrations. Overloading drilling tools above the preset load limit drastically reduces tool life and can lead to alternating local plastic deformation and micro cracking at comparatively low number of load cycles. High load cycles right at the beginning of the tool service life can also significantly reduce the overall life time. Overloading can be detected with downhole MWD tools. (Ritter 2007).

Cyclic bending load limits have been evaluated and are used in bending fatigue analysis for rotary applications. These limits may be considered for tools where it is known that the thread connection is the weakest part in terms of bending fatigue. Some connections require the

definition of two bending moment limits due to variations in the tubular thickness. Tools can either have a thick wall or a thin wall thread connection. For connections with dimensions in between, the thin-wall bending moment limit should be used. The bending moment limits are based on the assumption of the API drill collar material range and 2,000,000 load cycles as infinite life. Bending loads exceeding the limit may lead to material fatigue, crack, initiation and fracture (Linke, Hummes 2015b).

2.4.3 Critical Speed Analysis

The first line of defense for avoiding vibrational damage to the BHA would include the implementation of technical limits and the achievement of operational excellence during the planning and execution phase. However, state of the art vibration mitigation focuses on changing the drilling operational parameters, rotary speed and WOB in particular (Eltrissi 2009). This can happen during drilling with town-rig site cooperation, if real-time vibration data is available, or in the fashion of a post-well analysis, helping future BHA runs in the same well or field. Vibration measurements are used to identify the severity of vibration levels. Once high levels have been noted, the field personnel will reduce the rotary speed. Although vibration mitigation can be achieved by shifting the speed up or down, the speed reduction is preferred to mitigate lateral vibration due to the concept that a reduction in input energy solves the vibration problem best. But every vibration related drilling dysfunction has its own mitigation procedures. For example, on the contrary to mitigating lateral vibrations, mitigating stick-slip is performed by increasing rpm.

Another approach is to identify the natural frequencies of the BHA and to convert the frequency information into rotary speed values. This yields critical speed ranges directly related to the BHA natural frequencies which would lead to resonance if the excitation would match the natural frequency. These critical speed ranges are used for recommending safe top drive speed ranges. Solely using the natural frequencies eliminates the risk of wrong excitation sources and mechanisms. However, analyzing natural frequencies alone does not provide any information on how the BHA would react to downhole excitations.

Such a critical speed analysis, except for motors, does not yield any information about the amplitude, thus no statement about the vibration severity can be made in the case of resonance. Exact downhole vibration regimes depend on various parameters such as hole tortuosity, bit-wear status, actual side forces, local formation properties regarding stiffness and friction, and several other parameters. This leads to uncertainties in the determination the amplitude during resonance along the BHA since they are highly influenced by these downhole conditions (Linke, Hummes 2015a).

In contrast, critical speed analysis for motors is well understood since the motor mass imbalance and excitation frequency is well understood. A detailed approach to motor excited vibrations can be found in (Hohl et al. 2015). The same holds true for reamers. It has been found that the reamer excitation frequency follows the equation shown in Tab. 2.2 (Herbig 2015).

3 Dynamic Performance Characterization and Optimization of BHAs

The oil industry has developed design solutions for static load conditions over the past years which can be found in company manuals and API recommended practices. Despite drilling being a dynamic process the occurring dynamic loads are not fully considered within the overall BHA design. Extensive work has been done on vibration analysis, prediction and optimization of the drilling process in the past two decades and dynamic limits for single tools do exist, especially for electronics bearing tools. Monitoring vibrations downhole is a common practice and mitigation procedures are available. However, there is still room for further development. Vibrations are hard to incorporate due to their fluctuating nature and actual dynamic excitation sources are hard to detect. This study should identify suitable parameters for describing lateral dynamic phenomena on full size BHAs. These parameters can then be used to generate design criteria for comparing different BHA designs based on their lateral vibration susceptibility. This comparison should be made prior to drilling, allowing for an optimum BHA run without vibration related standby and troubleshooting.

3.1 Small Scale Parameter Study

It is hard to test and implement newly found concepts on full scale BHAs. Several different parameters and boundary conditions influence the results simultaneously and do not allow a proper study of the influences of every parameter. Considerations of material property changes, geometry, boundary conditions and excitation type, could lead to multiple unknowns and variables at a time which makes a distinct study of effects hard to perform. All possible influencing parameters can be seen in Tab. 3.1. This parameter study should identify the physical quantities and a suitable result output format for an optimization approach to mitigate lateral BHA vibrations. An overview of the behavior of possible BHA configurations under the influence of lateral vibrations is given and should demonstrate the effect of small configuration changes on vibration severity.

Tab. 3.1: Possible influencing parameters on lateral vibrations. The material properties have been kept constant for all models and the focus has been set on changing the stabilizer position and other geometry features.

Parameter
Density
OD (Outer Diameter)
ID (Inner Diameter)
Young's Modulus
Stabilizer Position
Number of Stabilizers
Excitation Location
Damping (mass, stiffness and structural)
Mass Distribution
Excitation Frequency
Boundary Conditions

Hence, different model configurations should investigate the effect of a single parameter on lateral vibrations at the time. All these models are based upon the same base case, representing a simplified BHA without any stabilizers and upsets. Material properties, mentioned in Tab. 3.1, such as density, Young's Modulus and damping are kept constant. The base model parameters can be seen in Tab. 3.2. The base case model configuration is shown in Fig. 3.1. The first five natural frequencies and associated mode shapes can be seen in Fig. 3.2. Each configuration is excited through a mass eccentricity located at a certain point in the model, leading to lateral vibrations. The system is designed to be already vibrating, thus eliminating the initial vibration build up. The excitation frequency range is rather small to allow for a higher resolution within this bandwidth, providing more accurate results. Actual downhole excitation sources could be at much higher excitation frequencies. Both ends are pinned, eliminating any additional excitations from a free moving end. These boundary conditions state that the lateral displacement and bending moment is zero at the BHA end points. Such a system is suspended at the nodes of its fundamental frequency. The model is positioned horizontally without any actual wellbore environment. This eliminates fluid interactions such as fluid damping and buoyancy. There are no possible wall contacts which could restrict the vibration system in displacement and bending. It should also be noted that no static loads, as for instance bending due to gravity, have been considered and are not represented within the following diagrams and values. Tab. 3.3 provides an overview of all state assumptions and boundary conditions.

Tab. 3.2: Base case model parameters. This model can be seen as a slick BHA comprised only of drill collars.

Parameter	Value and Unit
Length	100 [m]
OD	0.3 [m]
ID	0.16 [m]
Young's Modulus	2.07E11 [N/m²]
Density	7840 [kg/m³]
Excitation Location	25 [m]
Excitation Mass	100 [kg]
Excitation Eccentricity	0.1 [m]
Excitation Frequency Bandwidth and resolution	0.01 – 1.5 [Hz] in 0.001 steps
Damping Factor	0.05, only structural damping
Boundary Conditions	Both ends as pinned support

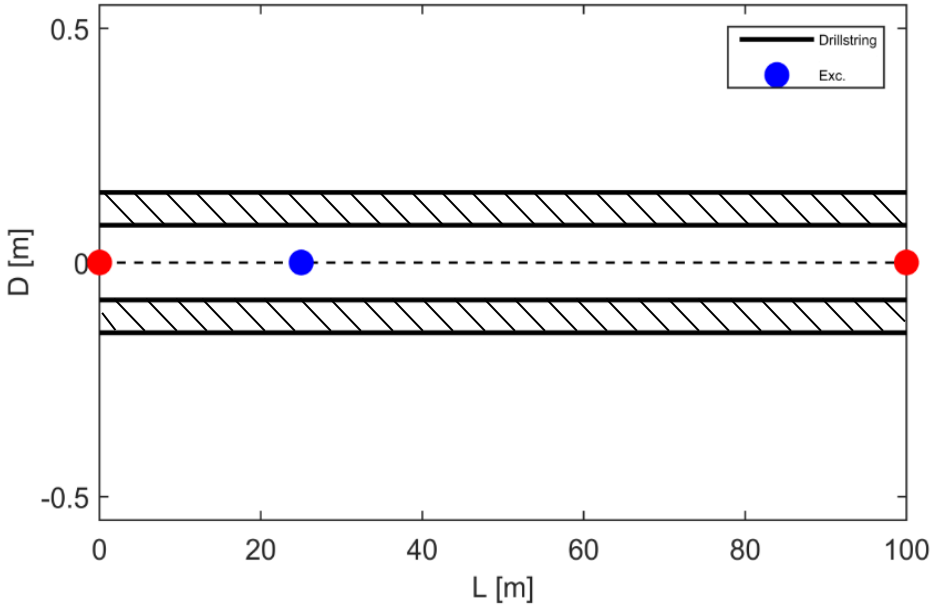

Fig. 3.1: Geometry of the base case. The excitation source (blue point) is located at 25 m, except for the excitation source variation model configuration. The red points on both ends illustrate the pinned boundary conditions.

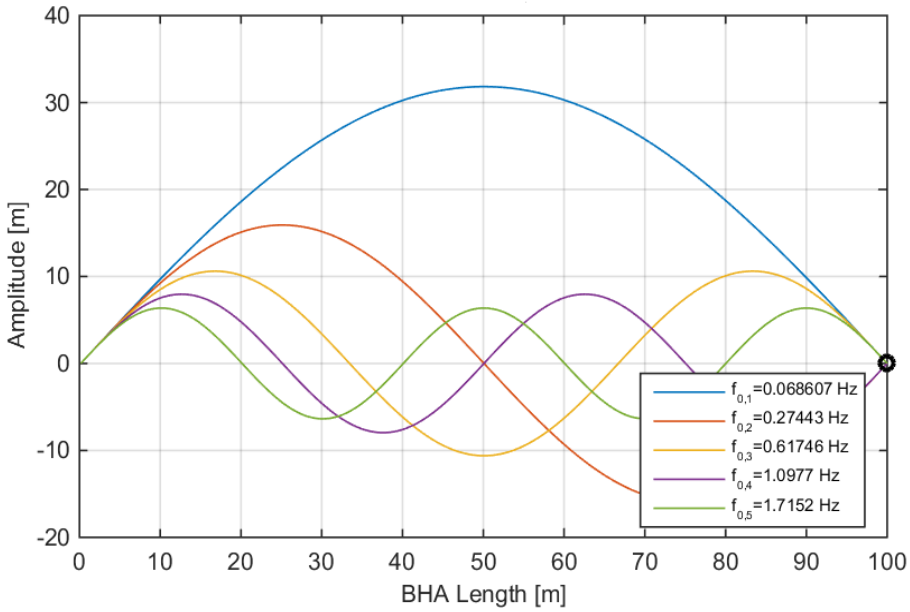

Fig. 3.2: The first five natural frequencies and appropriate mode shapes for the base case. The modal amplitude magnitude does not represent an actual physical displacement of the model.

Tab. 3.3: Assumptions and boundaries for all model configurations.

Assumptions and Boundaries	
Environment	Horizontal
	No fluids, wall contacts, buoyancy
Vibration	2-D
	Steady state
	Excitation frequency range
	Mass imbalance excitation
	Point source
	Only structural damping
Static forces	None
Material properties	Constant
Geometry	Constant length
	No stabilizer geometry
	Diameter and stabilizer changes
Boundary Conditions	Both pinned
	Free and pinned support

The conducted parameter study can be divided into three major model variations. The position of a single stabilizer, excitation source and diameter change has been changed along the structure length. The diameter change model is divided into a single diameter change run and one run which should simulate a flex-sub within a BHA.

The models use a MATLAB implementation of the transfer matrix method, as described in Chapter 2.3.2. The used code has been developed at the department of dynamics and vibrations of the Leibniz University Hannover. The transfer matrix method script has been used to determine the normal modes, natural frequencies and the state variables from Eq. 2.5. These state variables have been used to calculate further physical quantities which have been found useful for comparing different BHA cases. All physical quantities can be seen in Tab. 3.4.

The change in strain energy has been further investigated since the strain energy gives a good measure of the total energy stored in the BHA. Vibrations induce deformation and therefore an increase of the inner energy or strain energy can be observed. The total strain energy is the integral of the specific strain energy over the beam volume. Considering the corresponding stress state, for this case bending, and Hook's law leads to the following equation (Balke 2014):

$$U_B = \frac{1}{2}\int_V \frac{\sigma_b^2}{E}\, dV = \frac{1}{2}\int_l \int_A \frac{M_{bx}^2}{EI_{xx}^2} y^2 A dz = \frac{1}{2}\int_l \frac{M_{bx}^2}{EI_{xx}} dz \qquad \textbf{Eq. 3.1}$$

Furthermore, the lateral acceleration (Eq. 3.2) and velocity (Eq. 3.3) have been calculated based on the excitation frequency ω and lateral displacement w which is one of the four results of the transfer matrix method:

$$a = w\omega^2 \qquad \textbf{Eq. 3.2}$$

$$v = w\omega \qquad \textbf{Eq. 3.3}$$

Tab. 3.4: Physical quantities calculated and used in every parameter study.

Physical Quantity	Unit
Lateral Displacement	[m]
Lateral Velocity	[m/s]
Lateral Acceleration	[m/s²] or [g]
Bending Moment	[Nm]
Shear Force	[N]
Strain Energy	[Nm]

These quantities have been consolidated and arranged in different plots to evaluate the lateral vibration tendency of the model configurations under investigation.

3.1.1 Stabilizer Position Variation

This model variation moves a single stabilizer, realized as nodal point, along the BHA from left to right at the given excitation frequency range. All other influencing parameters are kept constant. In total, 101 different stabilizer positions are under investigation for the given BHA model. The stabilizer is assumed to be a rigid support with a defined stiffness of 10^{12} N/m² which corresponds to materials used for stabilizers. Excitation location and magnitude have not changed from the base case. Both, the impact on the physical deflection of various single stabilizer positions and possible physical quantities for describing these phenomena should be identified. Stabilizers are expected to show the biggest influence on the vibration system.

Modal Analysis

Assuming a discrete excitation force, a stabilizer directly placed at this force would create an additional node at this point in the vibration system and hence, renders the excitation source impact to zero. The BHA would not see any vibrations from this particular source. A stabilizer placed directly at one of the nodal points of a particular vibration mode does not influence the normal mode shape and natural frequency of this mode. However, as indicated in Fig. 3.3, a vibration system contains more than a single natural frequency and corresponding mode shapes and nodal points can vary for the different natural frequencies. Hence, a stabilizer, having no effect for a particular mode, can alter the shape and frequency of other normal modes. The introduction of a new nodal point, for example through adding a stabilizer, alters the vibration system and other normal mode shapes and natural frequencies are generated. Stabilizers act as a nodal point for all occurring normal mode shapes and natural frequencies, causing zero amplitude at its position. For example, a stabilizer positioned directly at 50 m would alter the first mode shape from Fig. 3.3 to the shape of the blue curve seen in Fig. 3.4. The first mode shape from the stabilizer position zero has been terminated and the new first mode looks similar to the second mode from position zero. A stabilizer directly at 50 m produces symmetric normal mode shapes. Normal modes are not necessarily symmetric for other stabilizer positions.

Proper stabilizer placement limits the displacement and the loads acting on the BHA. In addition, stabilizers alter the natural frequencies and normal modes of the BHA, thus shifting high load areas and resonance frequencies to different values and positions along the BHA.

The change of natural frequencies and mode shapes can be seen in Fig. 3.3 and Fig. 3.4 for two different stabilizer positions. The response for other configurations out of the 101 can be seen in the Appendix A. The stabilizer position, as indicated on the following figures, is given in meters and is referenced to the left boundary. A stabilizer at 0 m from the bit is indicated here by 10E-5 m due to MATLAB computation reasons.

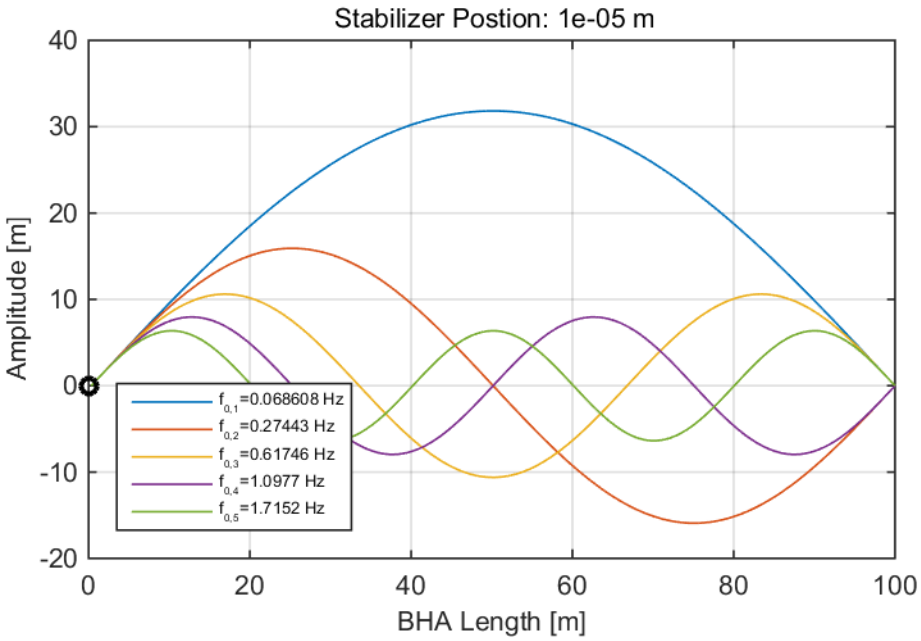

Fig. 3.3: First five natural frequencies and mode shapes for a stabilizer at zero m. This is the same result as for the base case.

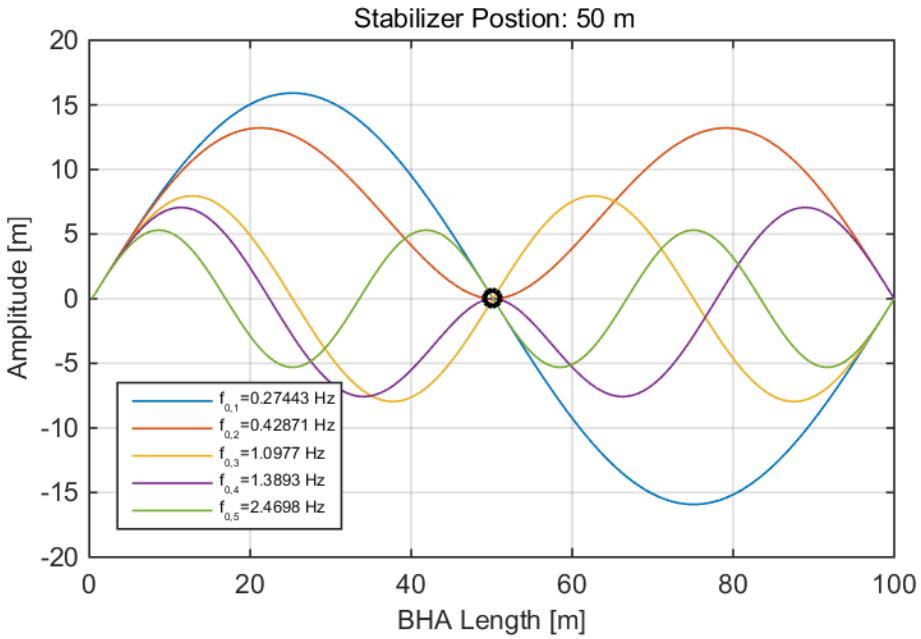

Fig. 3.4: Natural Frequencies and mode shapes for a stabilizer at 50 m from the bit. The first mode shape from position 0 m has been terminated and the new first mode is the same as the second mode from position 0 m. The normal modes do not have to be symmetric around the stabilizer position.

The influence of the stabilizer position on the normal mode shapes can be further investigated with the modal assurance criterion (MAC). The MAC allows the comparison of modal properties before and after a change in the physical structure caused by a wanted modification. The MAC is calculated as the normalized scalar product of the two sets of vectors $\{\varphi_A\}$ and $\{\varphi_X\}$. The resulting scalars are arranged into the MAC matrix:

$$MAC(r,q) = \frac{|\{\varphi_A\}_r^T\{\varphi_X\}_q|^2}{(\{\varphi_A\}_r^T\{\varphi_A\}_r)(\{\varphi_X\}_q^T\{\varphi_X\}_q)} \qquad \textbf{Eq. 3.4}$$

r and q indicate two modal vectors, for example from two different stabilizer positions. The MAC implies the degree of mode shape similarity between different model configurations. One normal mode shape of a particular configuration is compared with all other same order normal mode shapes from the other configurations. For example a configuration with a stabilizer at 12 m is compared against all other 101 positions, including the 12 m configuration. This least square based form of a linear regression analysis yields an indicator that is most sensitive to the largest difference between comparative values. It results in a modal assurance criterion that is insensitive to small changes or small magnitudes. The criterion takes value between zero, representing no similarity and one, representing full similarity. *"Values larger than 0.9 indicate strong similarity whereas small values indicate poor resemblance of the two shapes."* (Pastor et al. 2012). For this investigation the criterion is zero when the mode shapes are linearly independent or orthogonal (Pastor et al. 2012). Fig. 3.5 shows the modal assurance criterion for all 1st normal modes. Plots for other normal modes can be found in Appendix A.

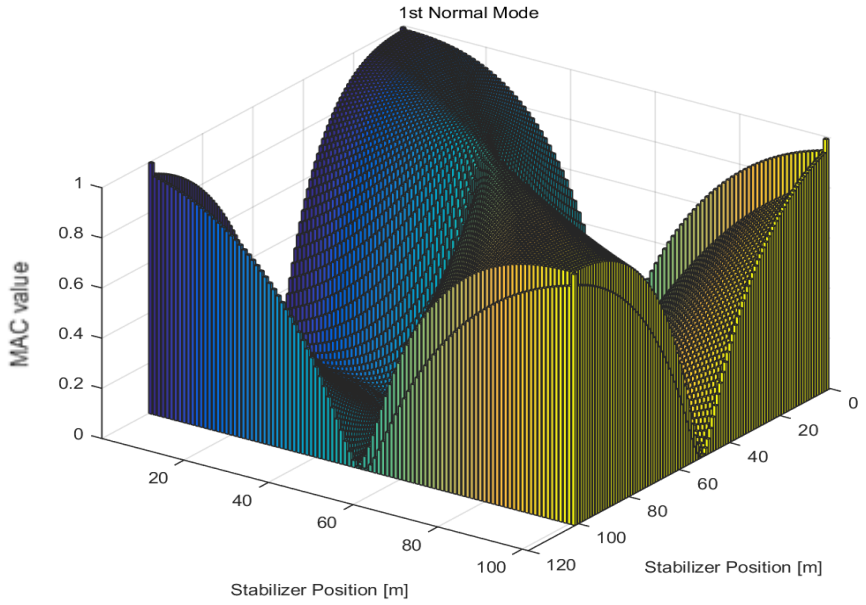

Fig. 3.5: Modal assurance criterion for all 1st normal modes of every stabilizer position. The elevated values at the edges result from the stabilizer being too close to the boundaries of the model, thus transforming the stabilizer into a clamp which can also bear a moment. Values of one means that the mode shapes are coherent and zero that the shapes are orthogonal.

The criterion yields one where the mode shapes are equal which is for example for the stabilizer location 0 m and 100 m because these two positions produce the very same normal mode shape. Stabilizers producing a completely mirrored normal mode shape are entirely non-

coherent and yield zero as value. This phenomenon can also be seen in Fig. 3.6, where the normalized mode shapes of ten different first normal modes are plotted. The term first mode refers to the first mode occurring at different stabilizer positions and not to the first mode from the base case. Position 0 m and 100 m produce exactly the same mode shape and have therefore a criterion index of 1. The purple curve of position 100 m is directly above the blue curve from stabilizer position 0 m and therefore not visible. Note also that some mode shapes show a lower slope towards the left or right BHA end. In this case the stabilizer is placed too close to the end and acts as a clamping point which can also receive a bending moment.

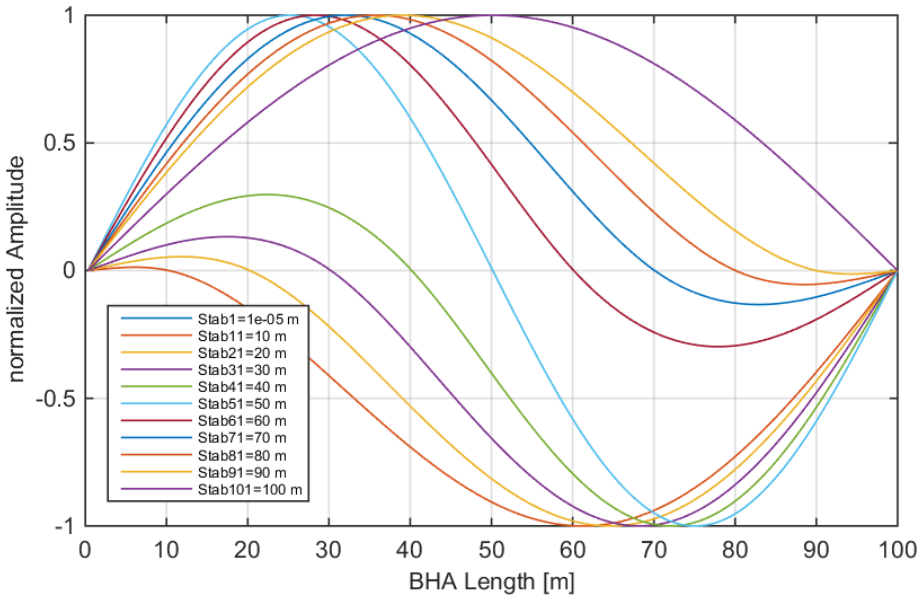

Fig. 3.6: Normalized mode shapes of ten 1st modes for 10 different stabilizer positions.

This change in natural frequency and normal mode shape generates a new vibration system for every stabilizer position. A normal mode shape change severely influences its excitation and resulting physical amplitudes, thus altering the prerequisites for resonance and high loads.

The dependency of the physical amplitude on the normal mode shapes can be studied using the equation of motion in a modal domain. From Eq. 2.2 the equation of motion in the modal domain can be written as:

$$\boldsymbol{I_m\ddot{q} + D\dot{q} + \Lambda q = \Phi^T f = f_{modal}} \qquad \textbf{Eq. 3.5}$$

This can be calculated with the transformation:

$$\boldsymbol{x = \Phi q} \qquad \textbf{Eq. 3.6}$$

$\mathbf{I_m}$, $\mathbf{D}$ and $\mathbf{\Lambda}$ are the modal mass matrix or unity matrix, the modal damping matrix and the spectral matrix of the system. The diagonal spectral matrix $\mathbf{\Lambda} = \mathbf{diag}(\omega_{0,i}^2)$ is comprised of the eigenvalues of the BHA. $\boldsymbol{x}$ is the physical deflection at a given point of the BHA, $\mathbf{\Phi}$ is the mass-normalized and orthogonal modal matrix containing the eigenvectors and $\mathbf{q}$ is the vector of modal amplitudes. The term $\boldsymbol{f_{modal} = \Phi^T f}$ can be seen as the modal force vector of all external forces. The full derivation of Eq. 3.5 can be found in (Silva 2007). As Eq. 3.6 states, the physical amplitude at a specific point is a resultant of all modes and modal amplitudes at this

point of interest. The stabilizer position changes the modal amplitude, shape and whether certain modes are present or suppressed, thus impacting the physical amplitude at a specific location. The actual excitation of the different modes depends on the modal force vector $\mathbf{f}_{\mathbf{modal}}$. The vector components which are unequal zero will result in an excitation of the corresponding mode.

Forced Response

The physical deflection leads to a lateral displacement of the BHA which depends on the stabilizer position and on the excitation frequency as shown in Fig. 3.7 for a stabilizer at 20 m. The system reacts different to various excitation frequencies. High amplitudes in lateral displacement imply the excitation of resonance frequencies. Also note that there is no displacement directly at the stabilizer through the whole frequency bandwidth. This position is indicated by the red dashed line.

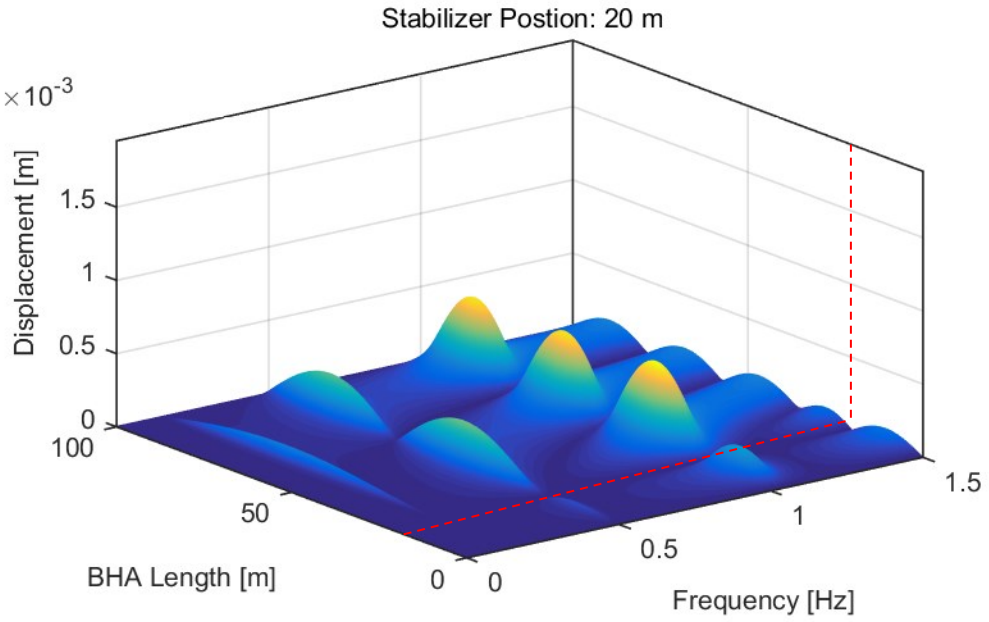

Fig. 3.7: Lateral displacement of a BHA with a single stabilizer at 20 m from the bit. The dashed red line indicates the stabilizer position.

The 3-D plot shown in Fig. 3.7 is only valid for one stabilizer position. Since 101 stabilizer positions are under investigation, 101 different plots are available. For better comparison of the individual stabilizer positions, a more consolidated plotting approach is required. This also minimizes the risk of misinterpreting results. The picked diagram type is shown in Fig. 3.8. It shows the maximum displacement along the BHA for all stabilizer positions for the given excitation frequency bandwidth. The maximum lateral displacement has been determined for every frequency step along the entire length of the BHA, thus highlighting the location and frequency of critical displacements which could damage assembly components. One stabilizer position can have multiple resonance frequencies and thus several frequencies where lateral displacement could be of concern. The computed vertical line in Fig. 3.8 directly at 25 m marks the position of the excitation force and a stabilizer directly at this point renders the excitation effects to zero. The observable wave form in Fig. 3.8 is the frequency response of the first four normal modes.

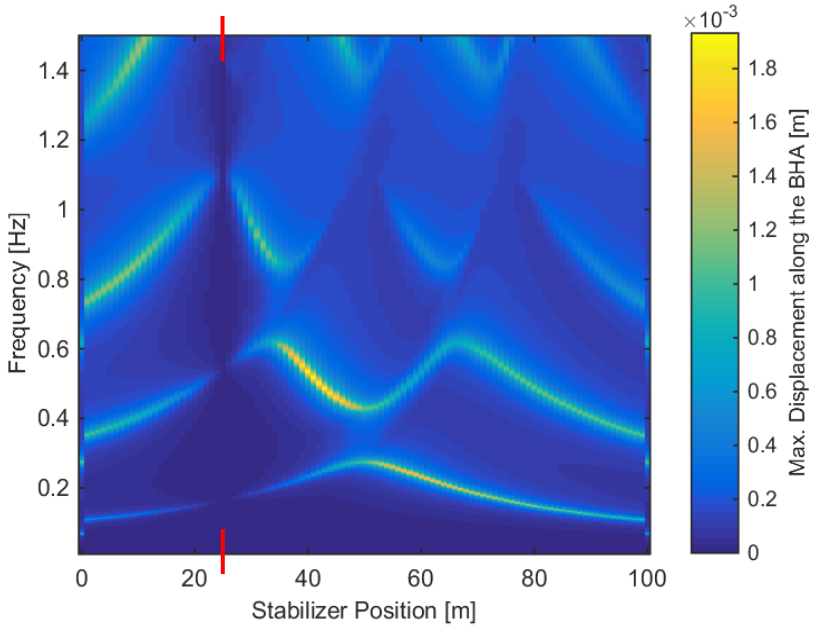

Fig. 3.8: Maximum displacement along the BHA for all stabilizer positions through the whole frequency band. The red marker indicates the excitation source location.

This plot eliminates the ability of viewing all displacements along the BHA for a given stabilizer position. Fig. 3.8 lacks the location information of the maximum lateral displacement and an additional plot is required. The presentation format remains the same and can be seen in Fig. 3.9. The computed vertical line at 25 m from the bit indicates that a stabilizer directly placed at the point of excitation eliminates the impact of this particular force on lateral vibrations. The scalar product $\mathbf{\Phi}^T\mathbf{f}$ becomes zero if the eigenvector of a given mode is zero. The stabilizer produces a node for all modes along the BHA. Hence, no mode is going to be excited if the stabilizer is placed directly at the excitation source. This graphical presentation method could be used to highlight tolerable or critical positions of the maximum displacement or other physical quantities. Placement of tools, sensitive to lateral vibrations, into areas of high physical amplitudes could be avoided which in turn enhances tool reliability.

Fig. 3.7 and Fig. 3.8 show the maximum displacement for every frequency, thus for all resonances within the bandwidth. This information could be further reduced to the overall maximum displacement along the BHA and its corresponding resonance frequency as shown in Fig. 3.10, producing only one value for a given stabilizer position and frequency. The maximum values along the model length have been determined for all physical quantities and the overall maximum value with its resonance frequency is presented in this plot type. Hence, one model configuration yields just only one value over the complete frequency bandwidth and not a single value for every frequency step. This provides an easier understandable plot but neglecting other resonances which does not eliminate the potential vibration problems at these frequencies. Similar plots are available for the other physical quantities and are shown in Appendix A. The red curve shows the corresponding resonance frequency at the overall maximum lateral displacement for every stabilizer position. The shape of the red curve illustrates a change in the frequency response at which the highest amplitude occurs. The frequency information from Fig. 3.8 has been consolidated into one curve which contains all maxima and the slope changes with the frequency at which the maxima occur. The blue curve indicates the maximum lateral

displacement determined across the whole frequency spectrum and along the length of the BHA.

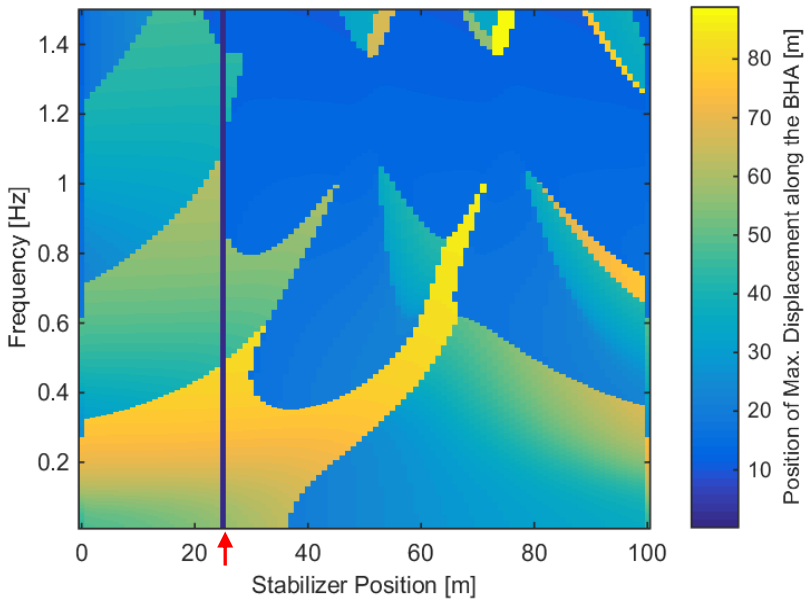

Fig. 3.9: Position of the maximum displacement for every stabilizer position and across the frequencies under investigation. The computed vertical line at 25 m, indicated by the red arrow, expresses a displacement of zero for a stabilizer directly at the excitation source.

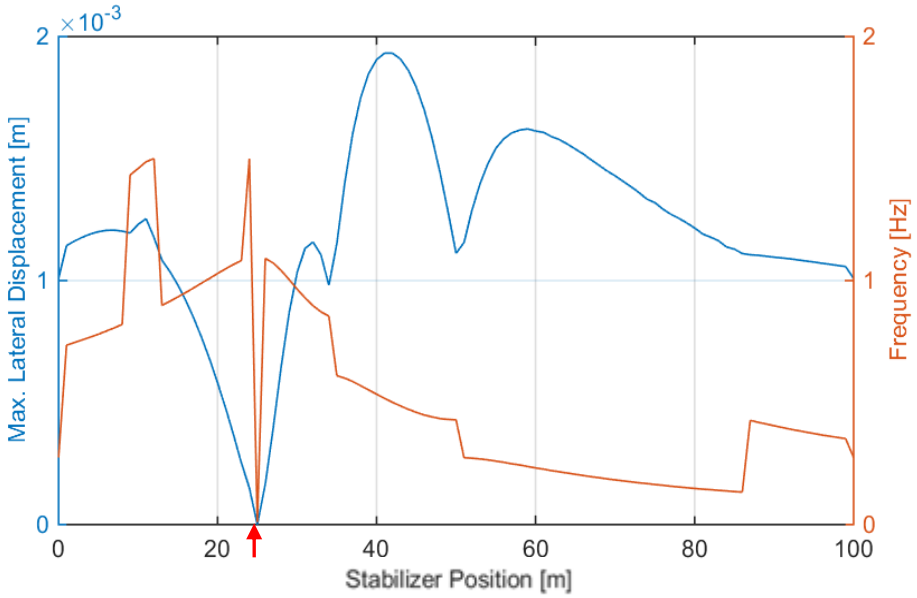

Fig. 3.10: Max. lateral displacement along the BHA and across all frequencies. The red arrow indicates the excitation source location.

Lateral displacement and bending moment follow the same trend, although the maxima occur at different frequencies and stabilizer positions. This phenomenon has been expected since bending is the 2nd derivative of the deflection curve from the beam equation as shown in Chapter 2.3.2. The maximum bending moment for all stabilizer positions is shown in Fig. 3.11 and the location of the maximum bending moment in Fig. 3.12.

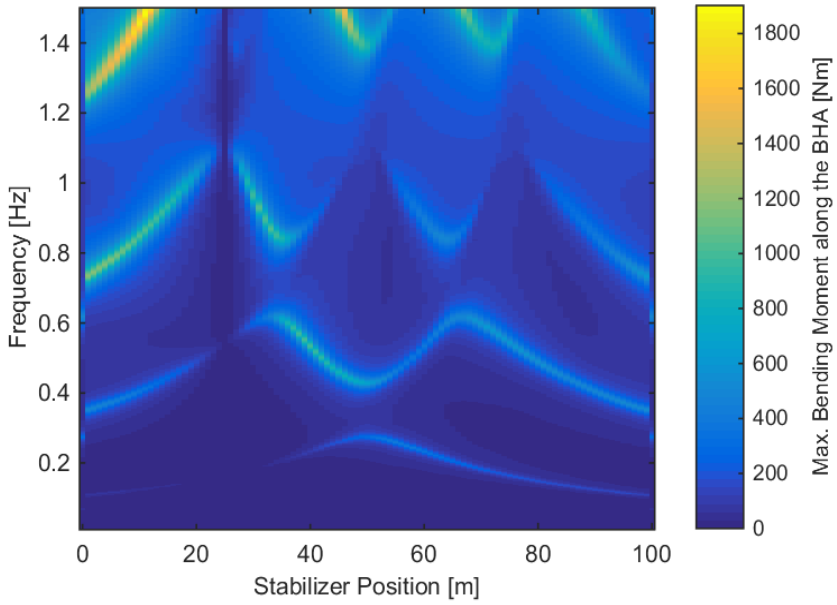

Fig. 3.11: Max. bending moment along the BHA for every stabilizer position across the given frequency bandwidth. The trend correlates perfectly with the lateral displacement but the maxima occur at different frequencies and stabilizer positions.

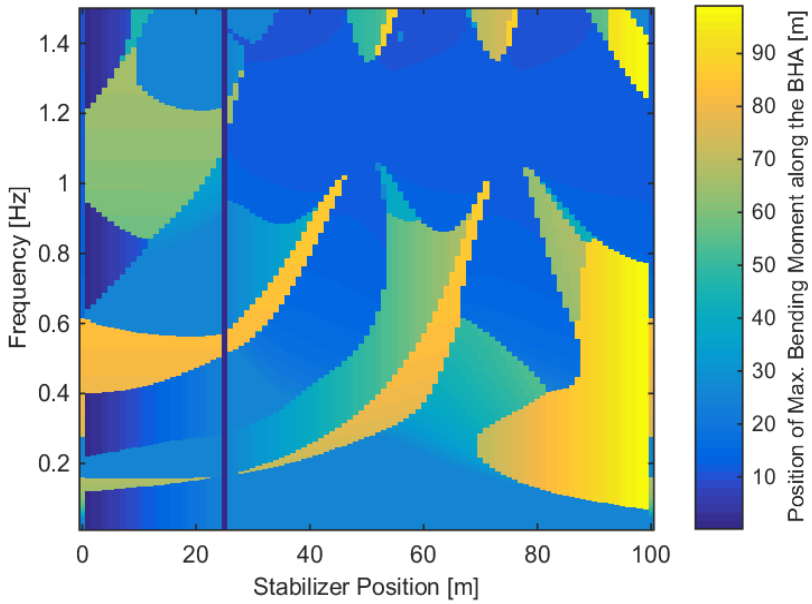

Fig. 3.12: Position of the max. bending moment along the BHA for all stabilizers. The maximum bending moment occurs on different positions compared to the lateral displacement due to the second order derivative relationship between displacement and bending.

Eq. 3.2 and Eq. 3.3 yield the lateral acceleration and velocity based on the lateral displacement and excitation frequency. Both parameters follow the same trend as the lateral displacement and bending moment. However, the additional multiplication with the excitation frequency for the velocity and squared excitation frequency for the acceleration increases the frequency dependency of the results. This shifts results with higher values into areas of higher frequencies, although the lower resonances are still present within the system. The acceleration response of the system can be seen in Fig. 3.13 and Fig. 3.14. The velocity plots are not going to be presented here and can be found in Appendix A.

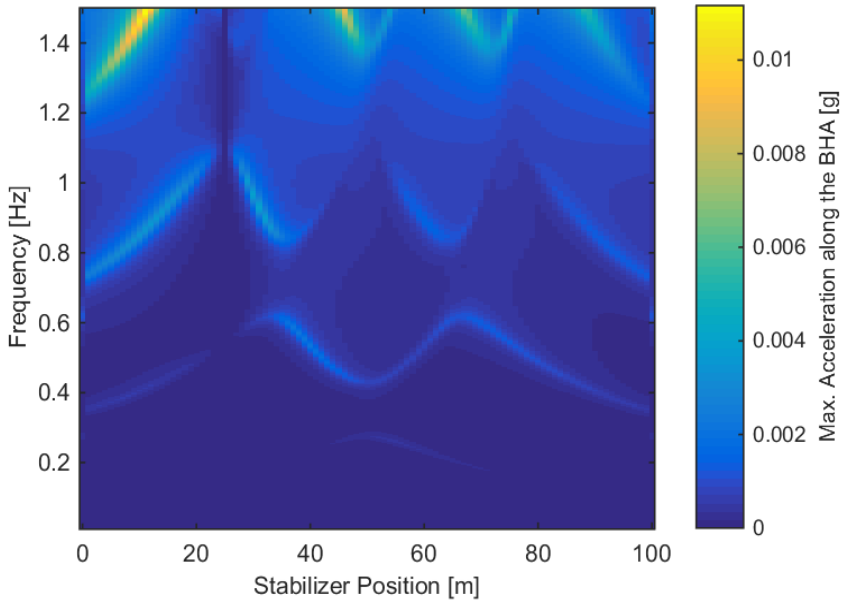

Fig. 3.13: Max. acceleration along the BHA for every stabilizer position. Note the shift to areas of higher frequencies compared to the lateral displacement. This is due to the multiplication with the squared excitation frequency to obtain the lateral acceleration.

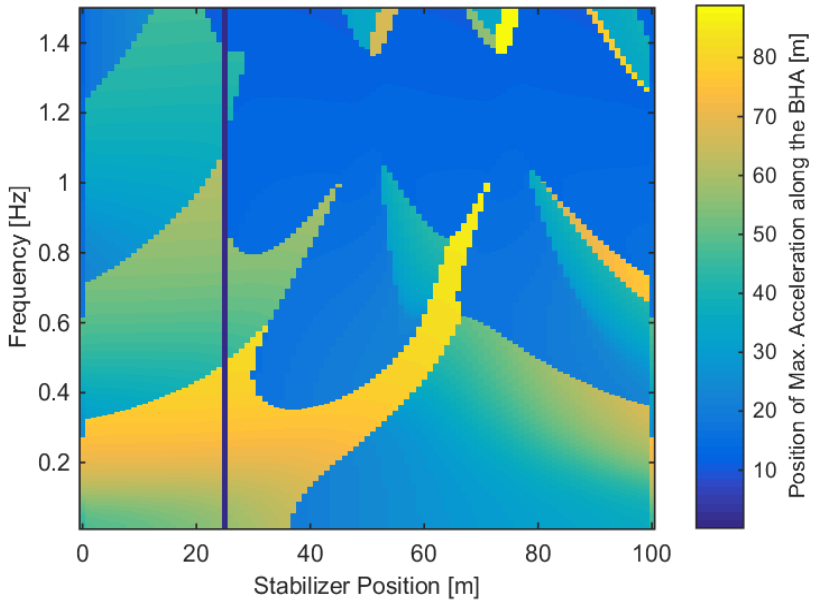

Fig. 3.14: Position of the max. lateral acceleration along the BHA for different stabilizer positions. The location of high lateral accelerations is identical to the lateral displacement.

Using Eq. 3.1 the cumulative strain energy along the BHA has been calculated for every stabilizer position. The sum of the strain energy is a good indicator of the total energy stored within the complete BHA. This sum contains all strain energy values along the BHA length for every frequency step and for one BHA configuration, thus eliminating the requirement of plotting the BHA length. The maximum strain energy would not deliver any new results compared to the other parameters and would be unsuitable for a complete BHA assessment. Maxima contain only local information and do not cover the energy stored within the entire assembly. However, the analysis of maxima, as for the lateral displacement and bending moment, provides valuable information about exceeding certain tool limits. Fig. 3.15 shows the sum of the strain energy for

every stabilizer position across the whole excitation frequency bandwidth. As expected, the cumulative strain energy follows the same trend as the bending moment with respect to the frequency response and resonance. Therefore, these frequency responses have been further investigated and are presented in Fig. 3.15. This plot for the first four mode shapes reveals that the sum of the strain energy shows the highest values exactly at the same frequencies as the acceleration and bending moment. The values are just too small compared to the high frequency values and are therefore not clearly visible in Fig. 3.15. Fig. 3.16 provides a magnification of the first three mode shapes. However, these plots provide no statement about the local distribution of the strain energy.

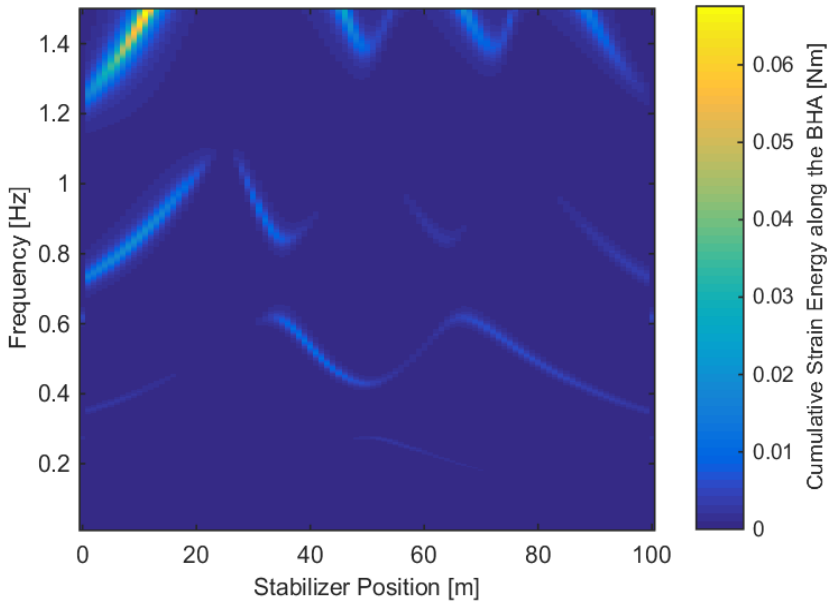

Fig. 3.15: Cumulative strain energy along the BHA for every stabilizer and across the whole frequency band. Note that higher frequencies yield a higher parameter response due to the quadratic influence of the excitation force.

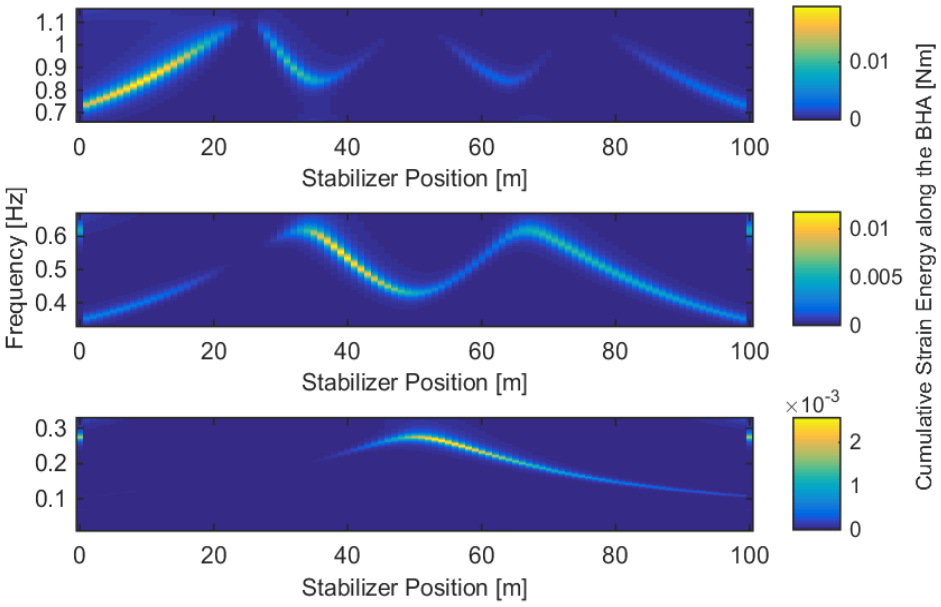

Fig. 3.16: Cumulative strain energy along the BHA for the first three frequency responses, providing a magnified version of Fig. 3.15. The frequencies at which high stain energy values occur corresponds with those of high acceleration and bending moment values.

Summary

This study leads to the conclusion that some stabilizer positions are more favorable compared to others. Proper stabilizer placement can limit the harmful effects of lateral vibrations such as high accelerations and bending moments which could lead to tool damage or failure. Furthermore, a stabilizer could reduce the total strain energy of a BHA, thus reducing the amount of energy stored in the system due to vibrations. However, the selection of the optimum stabilizer position is highly dependent on the excitation type, excitation frequency and location. The excitation amplitude, frequency and location impacts the physical deflection and resonance phenomena of the system. Furthermore, a stabilizer alters the normal mode shape and natural frequencies, as shown above. This changes the vibration system with every new stabilizer position, shifting the resonance frequencies and high amplitude locations.

Under the assumption that only lateral vibration mitigation are of interest for optimum stabilizer position, the investigating engineer should consider the parameter response across the entire available frequency bandwidth, ensuring that all possible resonance problems are covered. Comparing different stabilizer positions across the whole frequency range could eventually lead to the best stabilizer configuration for a BHA.

The cumulative strain energy provides a good indicator for the overall BHA performance and allows a comparison of different BHA designs. The one design with the lowest strain energy could outperform the other assemblies in terms of vibration reduction. The same concerns and dependencies, as discussed for other parameters, hold true for the strain energy consideration. Similar strain energy reflections have already been made by Jeff Bailey and information about his related work can be found in (Bailey et al. 2008), (Bailey, Remmert 2010) and (Bailey et al. 2010).

3.1.2 Excitation Source Location

The exact position of a downhole excitation source is hardly known and can only be determined in very rare cases. Downhole motors and reamers are well known excitation sources and can be incorporated in dynamic calculations accordingly. Motor vibrations are directly related to the rotor stator configuration, motor speed and surface rotation. Reamer dynamic behavior has been derived empirically from field studies (Tab. 2.2). However, other sources such as mass imbalance or eccentricity can occur at any location within a BHA due to certain load conditions and assembly configurations. The frequency or frequency bandwidth of most downhole excitations is unknown and educated guesses and estimates have been made as discussed in Chapter 2.3.1.5. Even the assumption of multiple discrete excitation sources does not reflect the actual downhole conditions since different operations could generate or terminate certain excitations. An excitation source distribution would be capable of representing a more realistic scenario, especially if the distribution occurs randomly at certain locations. These excitation source assumptions have not been covered within this work yet and are under investigation.

This parameter model configuration builds upon the previous stabilizer position alteration and introduces a change in the excitation location along the string. Eleven different excitation locations have been calculated for all 101 stabilizer positions, leading to 11x101 different scenario configurations in total. The findings of the first parameter study are now going to be discussed for different excitations source locations. This case should validate, if the approach can be implemented on a wider variety of model configurations as just for stabilizer positions. This model configuration should demonstrate whether a change in excitation location could outweigh the significance of stabilizers on the vibration system.

Modal Analysis

The excitation source and location does not influence the natural frequencies and normal modes. Stabilizers on the contrary greatly impact mode shape and frequencies. This simulation run has also shown that a stabilizer does not only create an additional node at its own position but also alters certain modes to have nodes at other positions different form the stabilizer position. These additional nodes occur for certain stabilizer configurations only in a specific BHA length range at the left and right side of the BHA. Fig. 3.17 illustrates this phenomenon. Regardless the nodes directly at the shown stabilizer positions, there is a high density of nodal points between 25 m – 33 m and between 70 m close to 80 m.

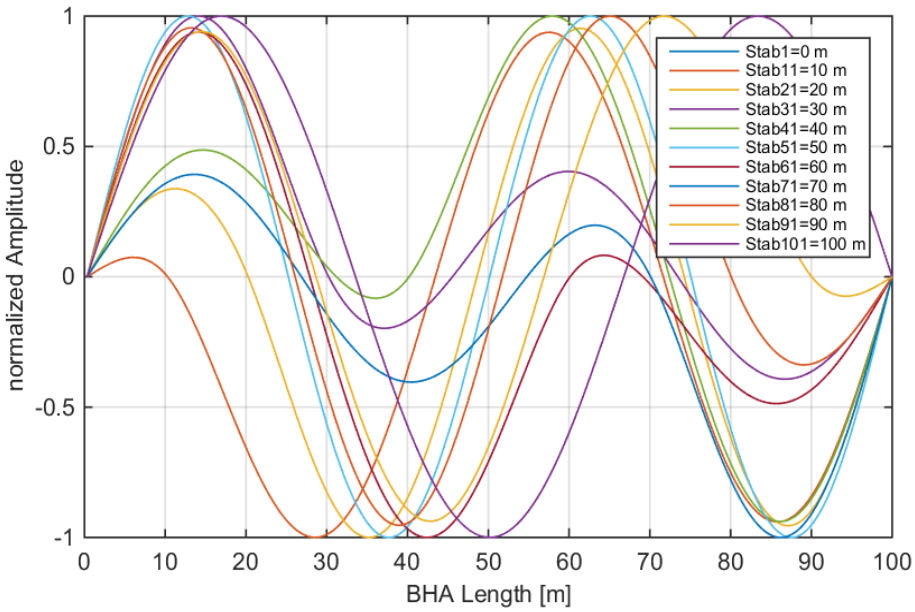

Fig. 3.17: A selection of ten distinct 3rd normalized normal modes. Note the clear indication of a symmetry effect due to the repetition of stabilizer-excitation position configuration above 50 m.

This additional node reduces the impact of the excitation force if the excitation position is shifted close to one of these nodes. The modal amplitudes are smaller and hence the physical amplitude becomes less, following the principles of Eq. 3.5.The excitation source effect can also be rendered to zero if the excitation position is directly at this node.

This phenomenon of an additional node has been observed at the first and third normal mode. The second normal mode does not follow this trend of an additional node on the left and right side of the BHA. This can be clearly seen when comparing Fig. 3.18 with Fig. 3.19 where the excitation sources are shifted from 18 m to 26 m. The amplitude response of the 3rd mode is reduced as almost all 3rd normal modes of all stabilizer configurations have a node close to 26 m. The 2nd mode shows a full amplitude response across all stabilizer positions for both excitation positions. The mode shapes of the 2nd normal modes do not have an additional node close to the excitation sources and therefore generate a similar response for these two excitations. However, the node produced by the stabilizer affects all normal modes regardless of other normal mode dependent nodes.

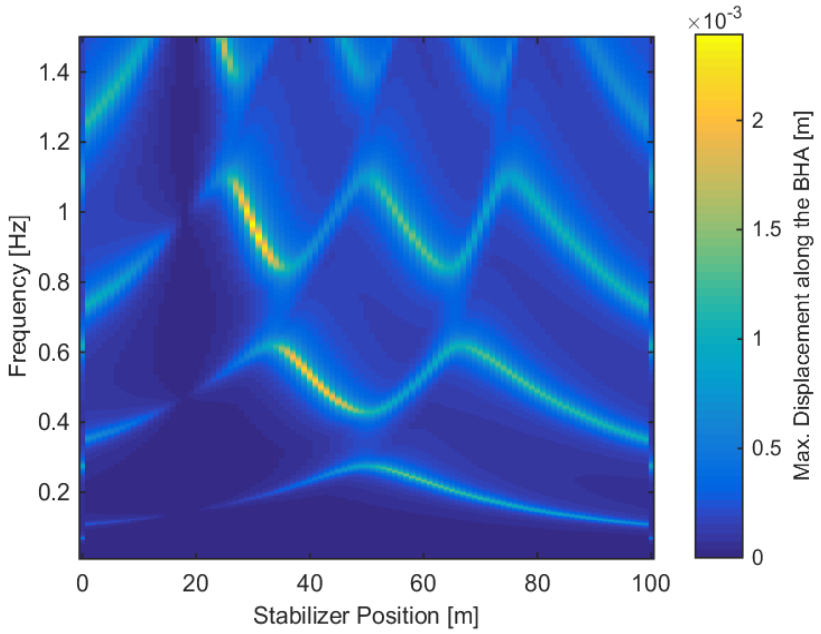

Fig. 3.18: Max. lateral displacement for all stabilizer positions and an excitation source at 18 m from the bit. All modes show an amplitude response to the excitation except for a stabilizer directly at 18 m which renders the impact of the excitation source to zero.

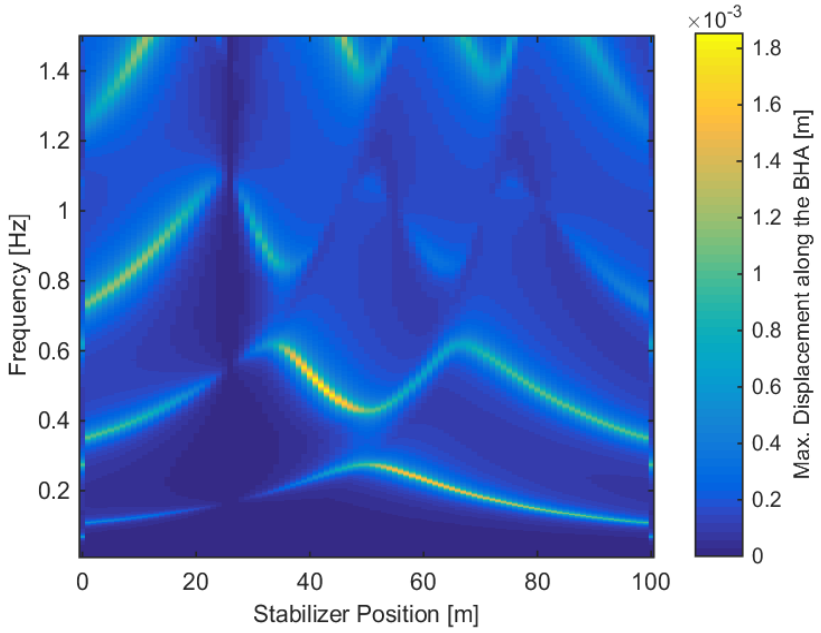

Fig. 3.19: Max. lateral displacement for all stabilizer positions and an excitation source at 26 m from the bit. Note the amplitude response reduction for the 3rd mode as almost all 3rd normal modes of all stabilizers have a node close to 26 m. The 2nd mode shows a full amplitude response across all stabilizer positions

The first mode shows a reduced amplitude response for stabilizers close to the bit. This is related to the generation of a smaller antinode on the left and a bigger antinode on the right side of such a stabilizer. Fig. 3.20 illustrates this phenomenon for a stabilizer at 29 m distance from the bit. Smaller antinodes tend to have smaller modal amplitude and thus lead to reduced physical amplitude at the same frequency.

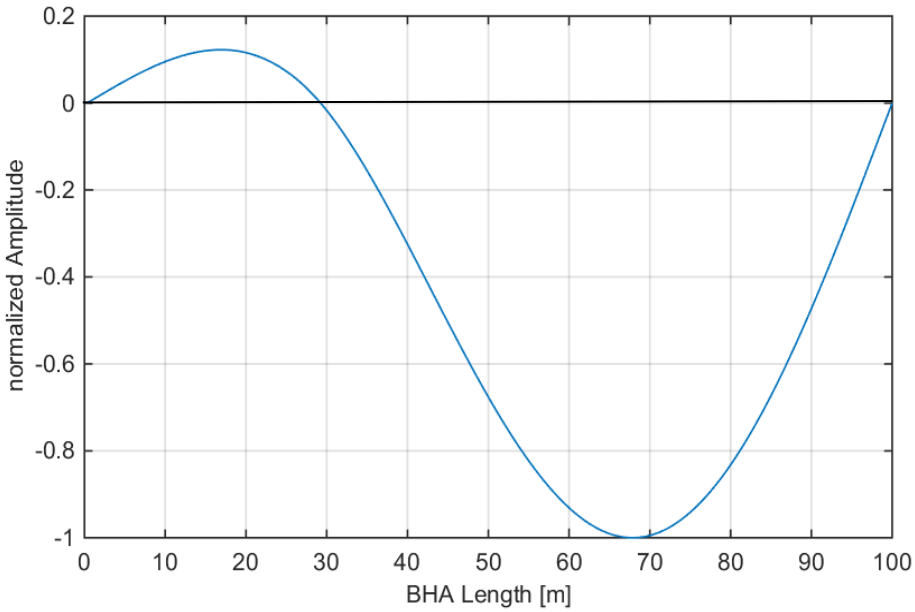

Fig. 3.20: 1st normalized normal mode for a stabilizer located 29 m from the bit. The first antinode on the left side of the stabilizer is evidently smaller than the antinode on the right side, leading to a smaller physical response closer to the bit as indicated in the first frequency response in the figure above.

Forced Response

The excitation location influences the occurrence of high loads, regardless of the influence of the stabilizer position on the physical response and location of high and low values. As the excitation source is shifted from left to right, the position of the maximum displacement, bending moment and other physical quantities is relocated according to the new excitation position. Fig. 3.21 and Fig. 3.22 show the maxima shift for the lateral displacement at two different excitation locations. The shown excitation positions of 18 m and 82 m demonstrate the symmetry effect of the model. Using the same stabilizer position distribution and boundary conditions, a change in excitation location yields mirrored physical amplitudes if the distances from the left and right boundary are identical.

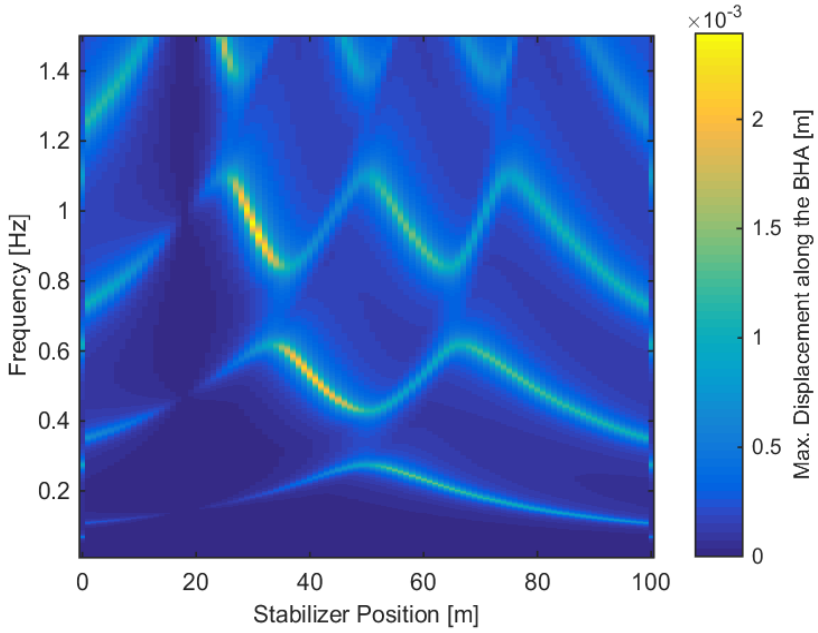

Fig. 3.21: Max. lateral displacement for all stabilizer positions and an excitation source at 18 m.

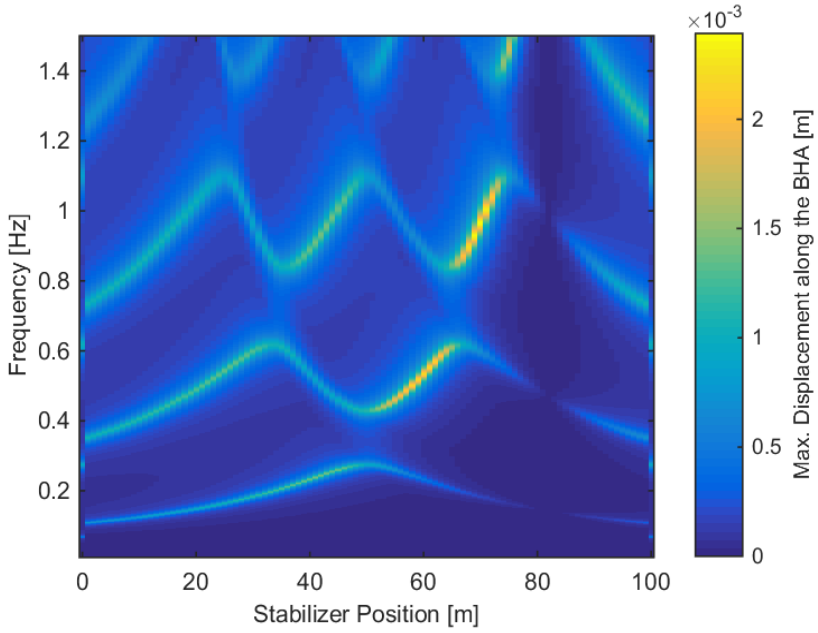

Fig. 3.22: Max. lateral displacement for all stabilizer positions and an excitation source at 82 m from the bit. Note the maxima shift towards the left compared to the figure shown above.

This shift is even more evident when investigating the actual position of the maximum values. Fig. 3.23 and Fig. 3.24 show the positions of the maximum lateral displacement for two different excitation source locations. The other parameters under investigation follow the same trends as described for the lateral displacement. The diagrams for those can be found in Appendix B.

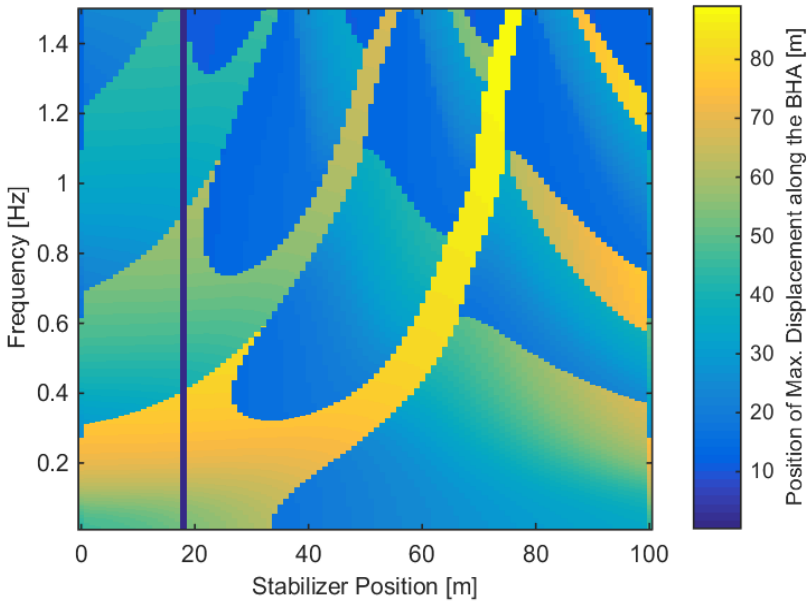

Fig. 3.23: Position of the max. lateral displacement for all stabilizers and an excitation source at 18 m. Most maxima are located near the bit.

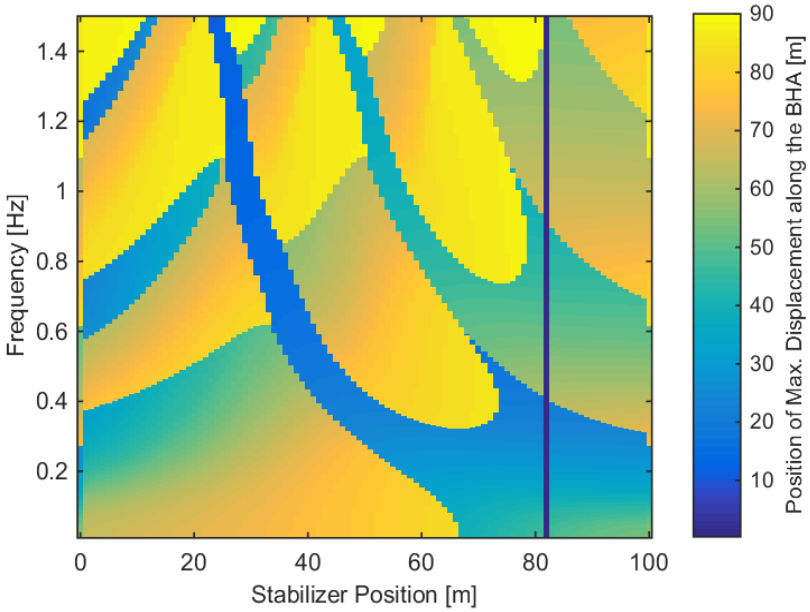

Fig. 3.24: Position of the max. lateral displacement for all stabilizers and an excitation source at 82 m. The maxima are shifted further away from the bit, following the position change of the excitations source.

Summary

This study of different excitation source locations on the physical parameters demonstrates their impact on lateral vibrations. The position of the highest values is greatly influenced by the excitation position. The presented charts show that symmetric excitation sources produce a symmetric physical response. This study also validates the results from the first parameter study. Stabilizers impact the lateral vibration susceptibility the most. Stabilizers alter the normal mode shape and amplitude, thus determining how excitation sources impact the severity of lateral vibrations. This phenomenon has been clearly seen due to the additional node for the 3rd normal modes and their reduced impact on displacement and other quantities.

Hence, proper stabilizer placement remains the far most reasonable vibration mitigation method, especially since the excitation magnitude and location are hard to identify. This study is based on a point excitation through mass imbalance but other excitation types and combinations should be expected downhole.

3.1.3 Bit Excitation

To investigate the effects of different excitation types, combined with a range of possible stabilizer positions, on lateral vibrations, the excitation source has been moved to emulate an excitation directly at the bit. Such a bit excitation has been realized through a mass imbalance with the same eccentricity and mass as for the other configurations. The location of the mass imbalance is 0.05 m right of the left end of the BHA model. The left side is simulated as a free end which does not restrict lateral movement. The right end is realized as a pinned bearing, identical to the other model configurations. The stabilizer is the only pinned support along the 100 m long BHA and is shifted between 1 m and 20 m away from the bit. Fig. 3.25 shows the geometry with the boundaries, excitation source and a stabilizer position. Previous excitation location variations have shown only a minor influence on the vibration system compared to alterations in stabilizer placement. A bit excitation introduces another excitation type into the parameter study, showing the vibration behavior of a single stabilizer BHA excited directly at the bit. This alters stabilizer requirements and the overall oscillation system due to different boundary conditions, leading to different mode shapes and natural frequencies.

Modal Analysis

The difference between a free and pinned end is reflected in the normal mode shapes. The boundary condition on the left allows for deflections in the normal mode shapes and can therefore lead to physical deflection at this point. The first normal mode shapes show a minor influence during the stabilizer position variation. Lacking a pinned boundary condition at the bit, the stabilizer is the only node on the left side. The change of the 1st normal mode shape for different stabilizer positions is shown in Fig. 3.26. The 1st normal mode is now suspended at the stabilizer and the right boundary. Normal mode shapes and natural frequencies undergo changes, if the stabilizer is not in a node, as the stabilizer is moved from the starting position towards the right. The natural frequencies of the first 5 normal modes increase, whereas the others decrease or stay nearly the same. The changes in normal mode shape and natural frequencies are crucial for an optimum stabilizer placement to mitigate the effects of this particular excitation source. Some stabilizer positions alter the normal modes in a way which increases the total physical amplitude and hence deflection, acceleration and bending stresses. The changes in normal mode shape and natural frequencies are shown in Fig. 3.27 and Fig. 3.28. Fig. 3.29 shows the modal amplitude for every normal mode, thus indicating which normal modes contribute most at specific excitation frequencies. The first three normal modes are the main contributors to the overall physical amplitude. The remaining normal modes, of the 12 under investigation, contribute less to the overall physical displacement. Other normal mode shape and natural frequency plots can be found in Appendix C.

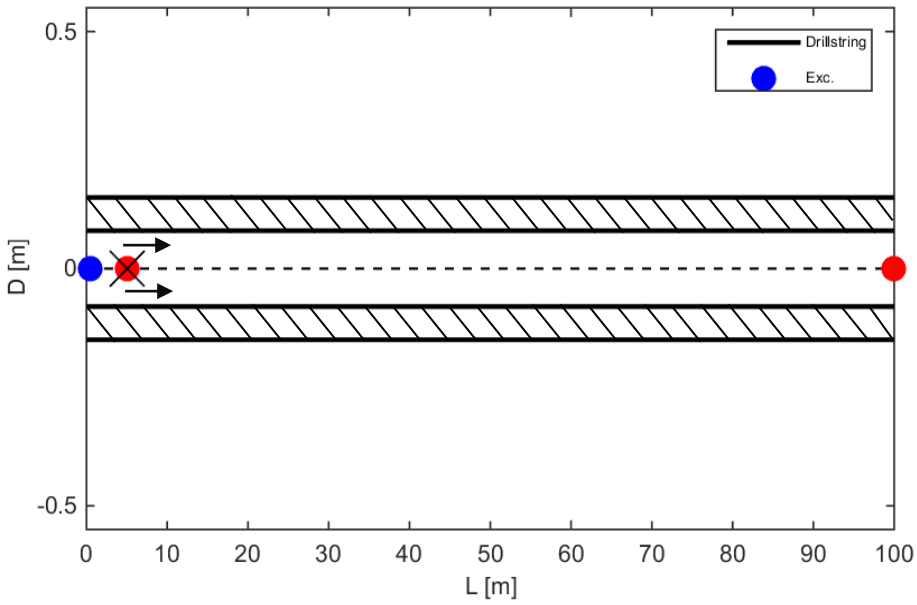

Fig. 3.25: BHA model with a mass imbalance directly at the bit. The position of the excitation, 0.5 m from the left boundary, is shown in blue and the variable stabilizer, here at 5 m from the bit, in red. The pinned boundary on the right end is also shown in red. Note that there is no movement restriction on the left boundary.

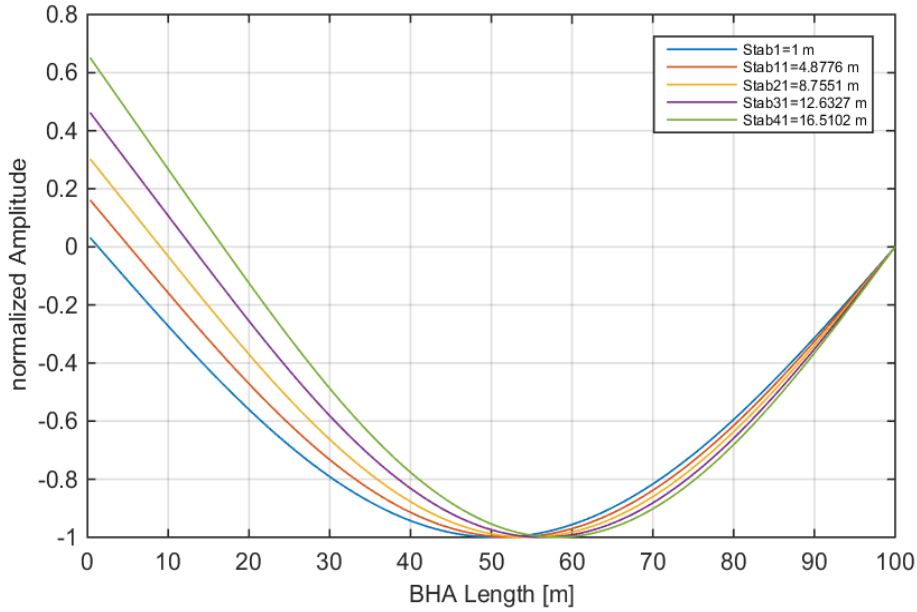

Fig. 3.26: Normalized 1st normal modes for selected stabilizer positions. The change in mode shape is minor compared to mode shapes of higher frequencies.

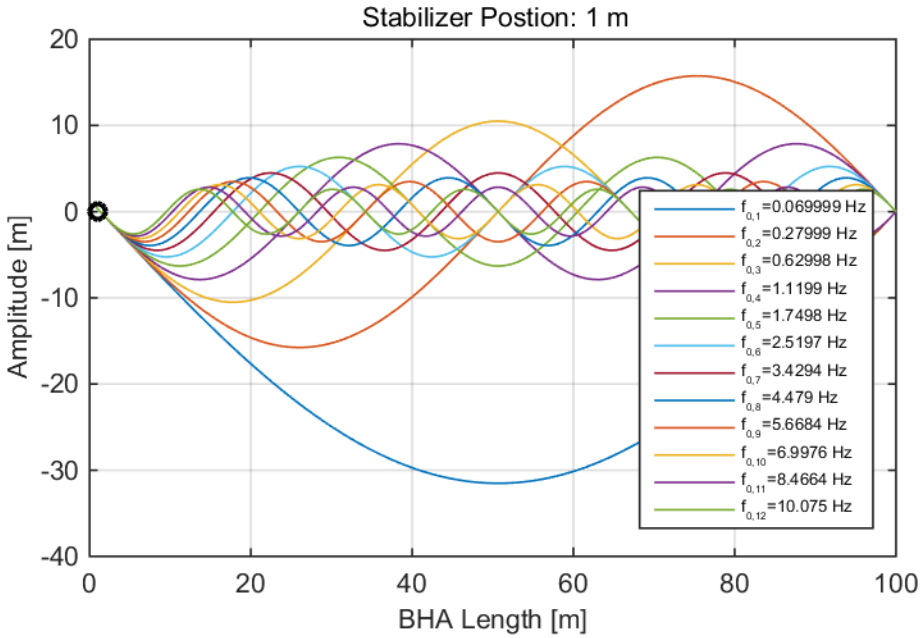

Fig. 3.27: Normal mode shapes and their corresponding natural frequencies for a stabilizer at 1 m from the bit.

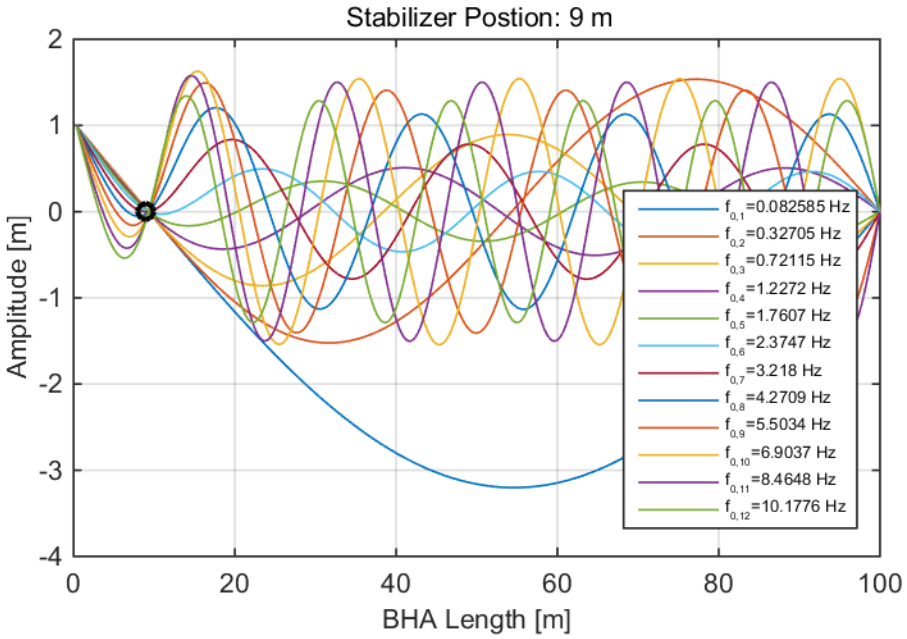

Fig. 3.28: Normal mode shapes and natural frequencies for a stabilizer at 9 m from the bit. The normal modes shapes are more erratic at higher natural frequencies. The first few normal modes show only a minor change in shape as the stabilizer is being moved.

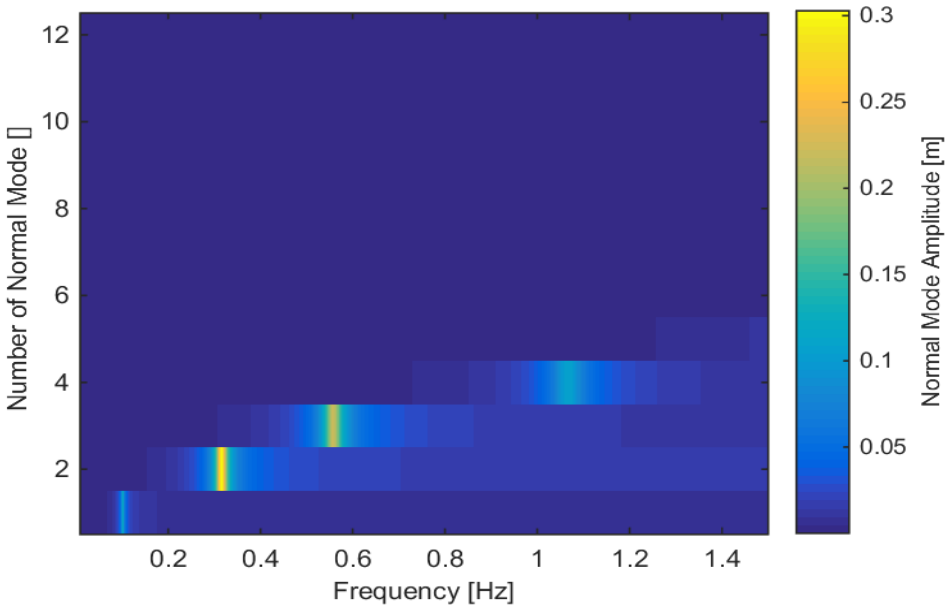

Fig. 3.29: The first 12 normal modes and their modal amplitude at various excitation frequencies. The first three normal modes show the highest contribution to the overall physical amplitude in this frequency range. The higher normal modes are outside of the frequency range of interest.

Forced Response

A stabilizer close to the position of the excitation force reduces the lateral displacement. The normal modes and modal amplitudes for these stabilizer configurations lead to smaller physical amplitudes compared to placements further away from the bit. Fig. 3.30 and Fig. 3.31 illustrate the difference in lateral displacement between two stabilizer positions. Stabilizer positions ranging from 5 m to 9 m show the smallest displacement values.

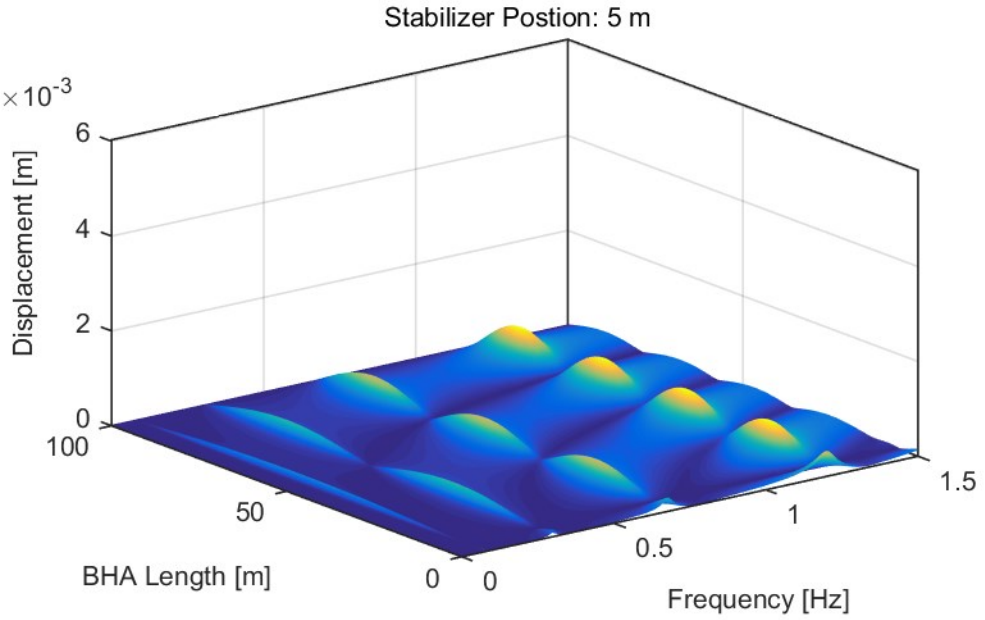

Fig. 3.30: Lateral displacement for a stabilizer at 5 m from the bit. This configuration yields a relatively small lateral displacement.

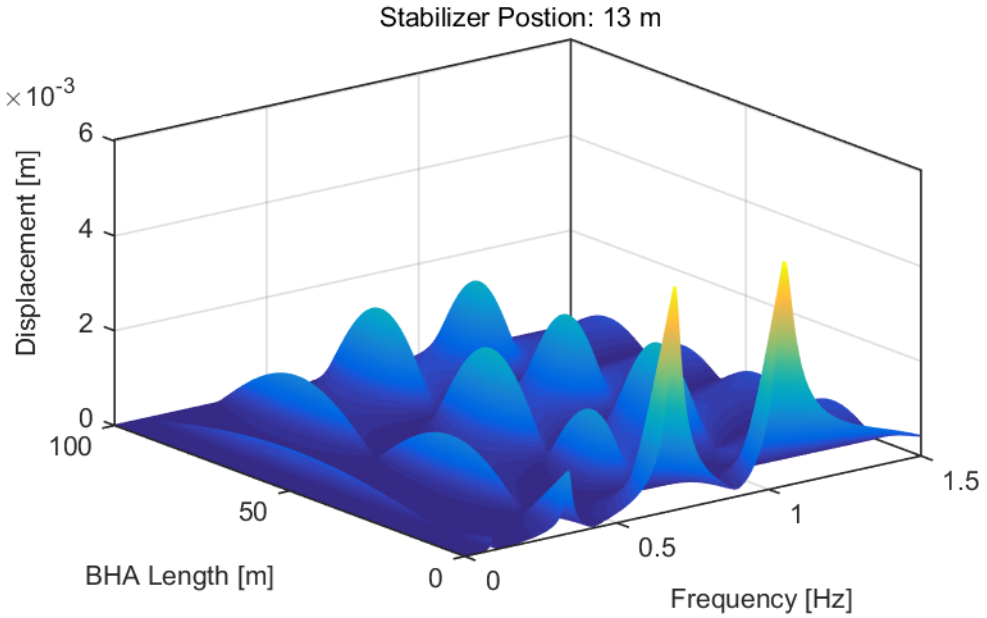

Fig. 3.31: Lateral displacement for a stabilizer at 13 m. This configuration shows higher displacement values compared to the configuration with a stabilizer at 5 m.

This trend is also noticeable on the combined representation of all maximum lateral displacement values for all stabilizer positions under investigation. This plot is shown in Fig. 3.32. Stabilizer positions close to the excitation location show the smallest maxima. However, the frequency response at which the highest displacement value occurs is shifted to lower frequencies as the stabilizer is moved further away from the bit. This is directly related to the length increase of the free moving section below the stabilizer. As this section becomes longer, the modal amplitudes of the lower frequencies gain in proportion. Further consolidating the amplitude information across the entire selected frequency bandwidth provides a more distinct presentation of the change in frequency response and optimum stabilizer positions. The change in frequency response for the maximum lateral displacement is indicated by the steep slope change of the red line in Fig. 3.33. The blue curve represents the maximum lateral displacement across the BHA length and frequency range. The position of the maximum lateral displacement for every frequency step along the assembly length is shown in Fig. 3.34. Higher frequencies lead to maxima close to the bottom of the BHA whereas lower frequencies produce maxima further away from the bit. Charts for lateral acceleration and velocity can be found in Appendix C.

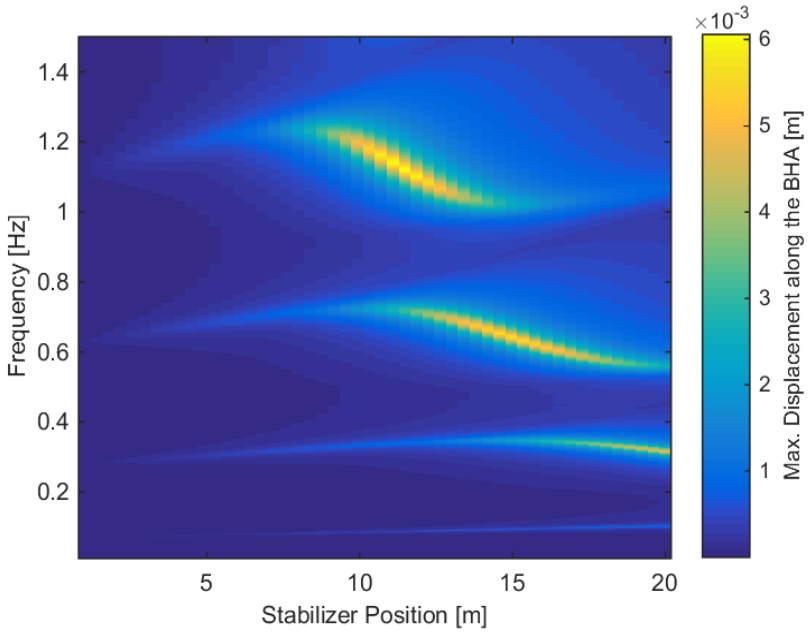

Fig. 3.32: Max. lateral displacement for all stabilizer positions investigated during the bit excitation simulation. The frequencies at which the maximum occurs are shifted to lower values as the stabilizer is moved further away from the excitation source.

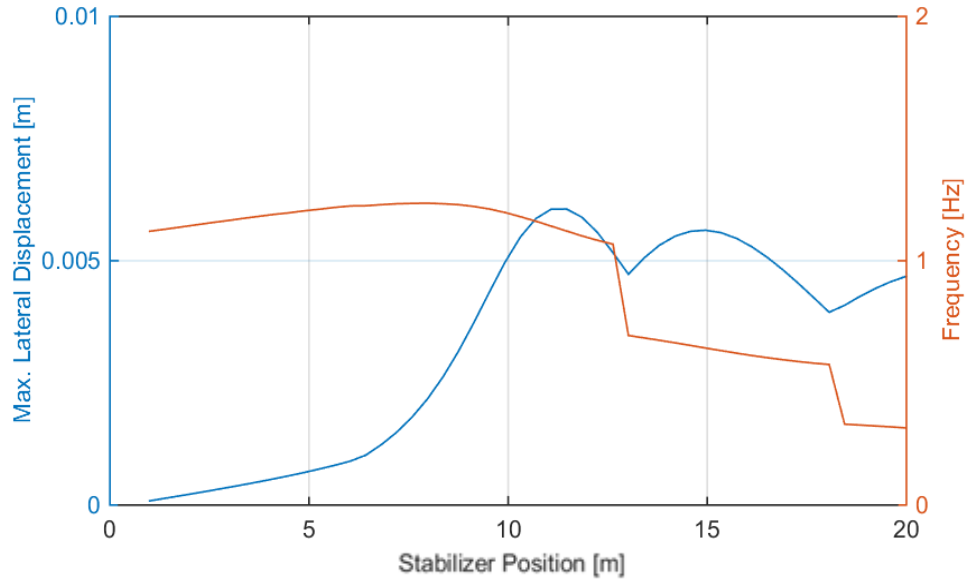

Fig. 3.33: Max. lateral displacement across the BHA length and entire frequency range. The steps in max. lateral displacement and corresponding frequency are at the same stabilizer positions as in Fig. 3.32.

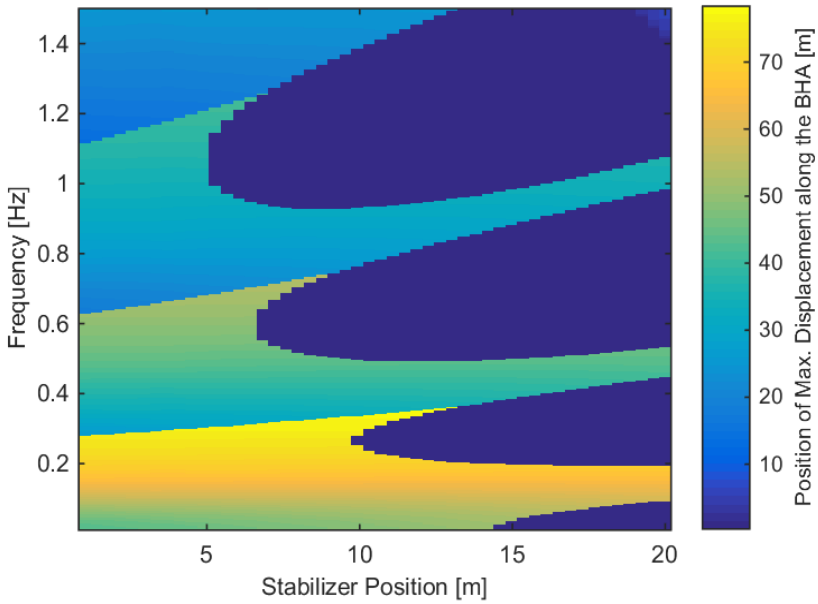

Fig. 3.34: Position of the maximum lateral displacement for every frequency step and stabilizer position. Lower frequencies show maxima further away from the bit.

Maximum bending moment and cumulative strain energy follow the same trend, as shown for the maximum lateral displacement in Fig. 3.32. The maximum values, occurring at the highest frequency response, dominate the results and let the other responses appear smaller. This big difference in values allocates the color blue to most of the bending moment and strain energy values although they represent results unequal to zero. Fig. 3.35 and Fig. 3.36 show the maximum bending moment and cumulative strain energy for this model configuration. This concentration of the highest bending moment and strain energy values is pinned to a particular frequency response and stabilizer positions. These assembly configurations are also visible in Fig. 3.37 and Fig. 3.38. Stabilizers close to the bit excitation yield the smallest maximum bending moment and cumulative strain energy. As shown in Fig. 3.39, certain frequencies generate high bending moments close to the bottom of the BHA and others higher up the assembly.

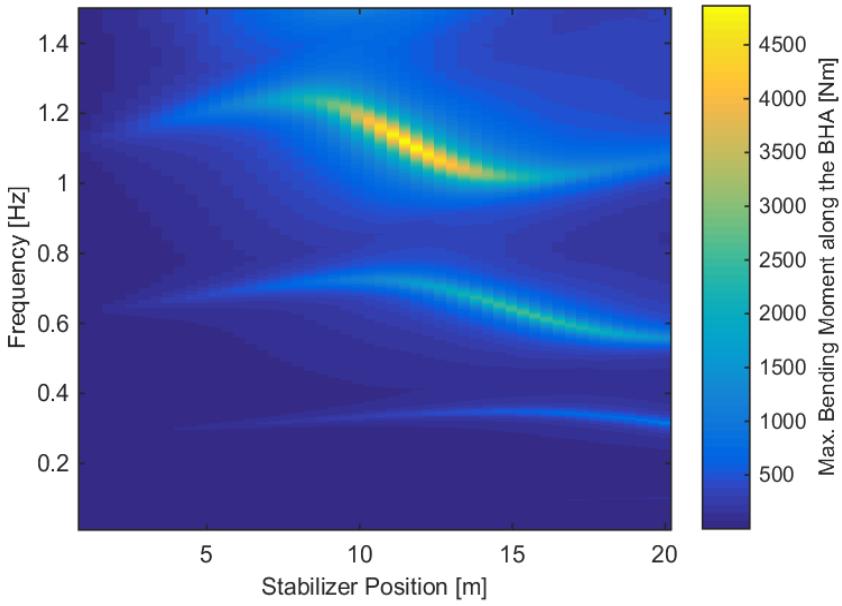

Fig. 3.35: Max. bending moment for all stabilizer positions and every frequency step.

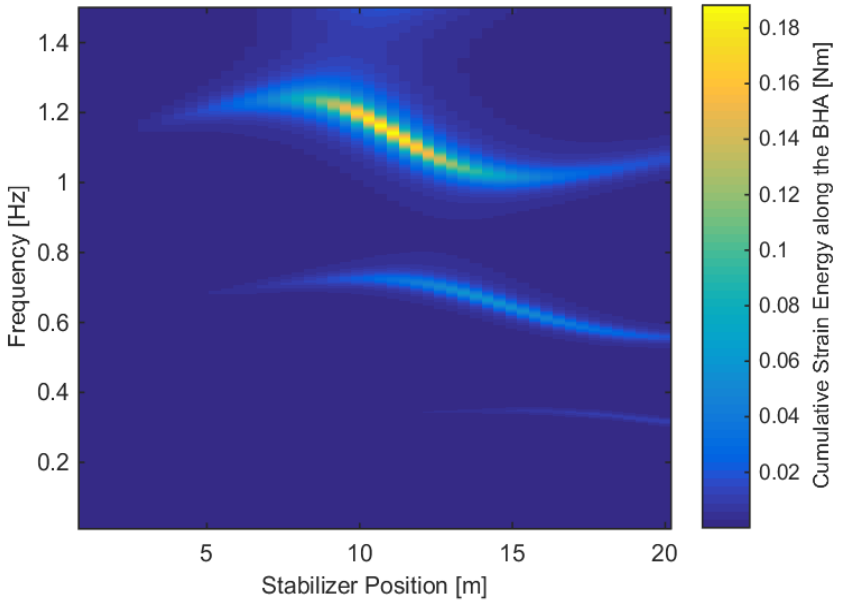

Fig. 3.36: Cumulative strain energy for every stabilizer position and frequency step. As for the maximum bending moment, the highest values occur at certain assembly configurations and frequency steps.

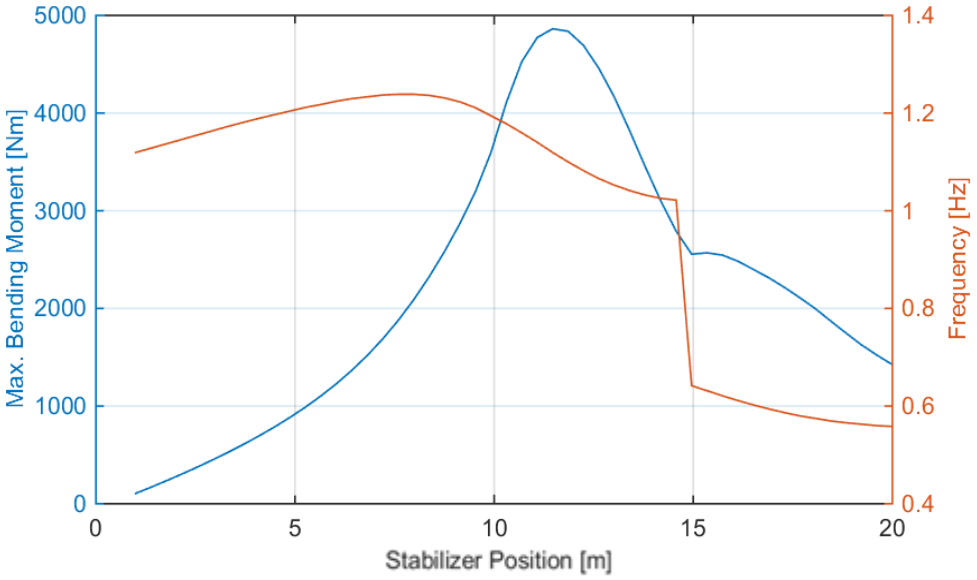

Fig. 3.37: Max. bending moment for all stabilizer positions across the BHA length and frequency range. The smallest values occur for stabilizers close to the bit excitation.

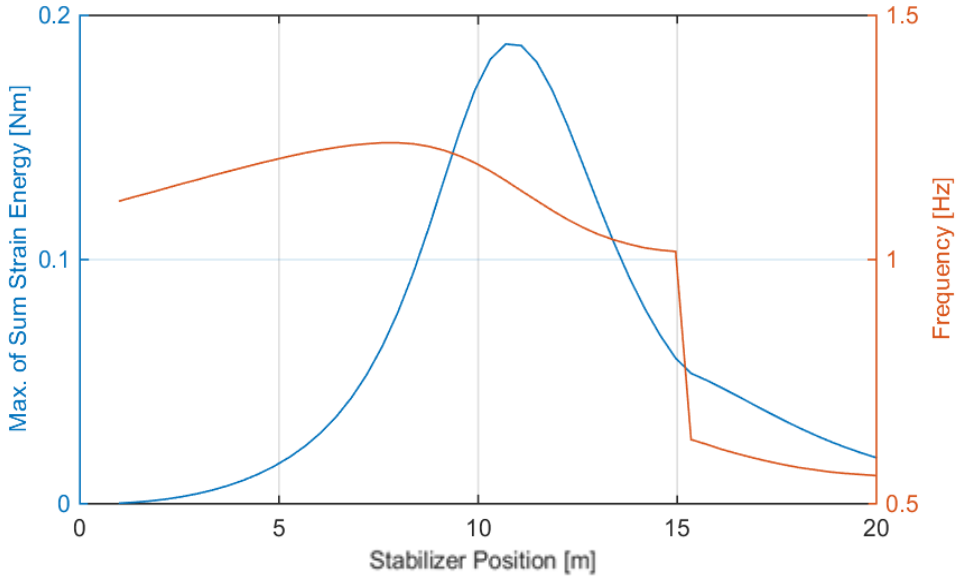

Fig. 3.38: Max. cumulative strain energy for all stabilizer positions across the BHA length and frequency range.

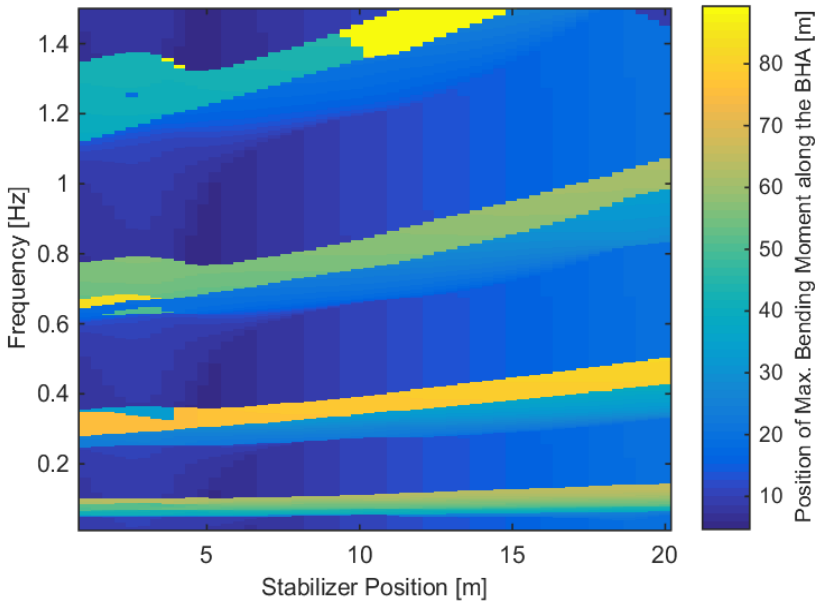

Fig. 3.39: Position of the max. bending moment for all stabilizers and frequency steps. Different frequency responses generate maxima at different locations along the BHA.

Summary

The bit excitation model has shown the impact of near bit stabilization on lateral vibrations. Stabilizers directly at the bit or within a certain distance from the bit have shown a reduction in physical amplitude. Furthermore, this parameter study demonstrates that a stabilizer, placed in a certain spacing from a bit excitation would lead to higher bending moment and strain energy values than a near bit stabilizer or a stabilizer placed even further away from the bit. This leads to the conclusion that lateral vibrations, generated by mass imbalances at the bit, can be compensated best with stabilization directly at the bit or within a certain distance. This model configuration confirms the necessity of near bit stabilizers which have already been introduced to the drilling industry. RSS systems also contribute to near bit stabilization.

3.1.4 Geometry Effects

A change in wall thickness impacts BHA flexibility as mentioned in Chapter 2.2.3 and hence influences the drilling capabilities of an assembly. Furthermore, geometric properties can also change within a single component. For example some tools are machined with different upsets, slots, cut-offs or effective flow areas to meet certain stabilization, flow rate or measurement criteria. These changes can influence the vibration susceptibility of a BHA, since wall thickness is directly related to mass and bending stiffness of a component. In addition, a geometry change affects natural frequencies and normal mode shapes of the vibration system.

To investigate the effect of changes in geometry on lateral vibrations, this parameter study is divided into three different modulations of a diameter variation. The cases should represent a tapered BHA, a tapered BHA with a constant mass distribution and an assembly with a so-called flex-sub component. Other parameters, such as the excitation location at 25 m and structural damping are identical to the base case. The constant mass distribution model configuration does not reflect any realistic BHA designs and should be seen as a sole academic configuration for studying the influences of certain parameters. To reduce the model complexity

and to avoid multiple changes at a time, no stabilizers have been simulated for the diameter change configurations. Solely the impact of geometrical modifications on lateral vibrations should be investigated. The effect of stabilizers has been shown in the previous configurations.

3.1.4.1 Tapered BHA

A smaller diameter is introduced on the left side of the model and the section length of this thinner section increases with every computation step. The principle of such a diameter change can be seen in Fig. 3.40. The model OD is altered from 0.3 m to 0.2 m at the diameter change position. The ID is constant over the whole length and all steps. This diameter change causes a change in area moment of inertia and mass between the two different sections. This study demonstrates the impact of real dimension alterations of BHAs.

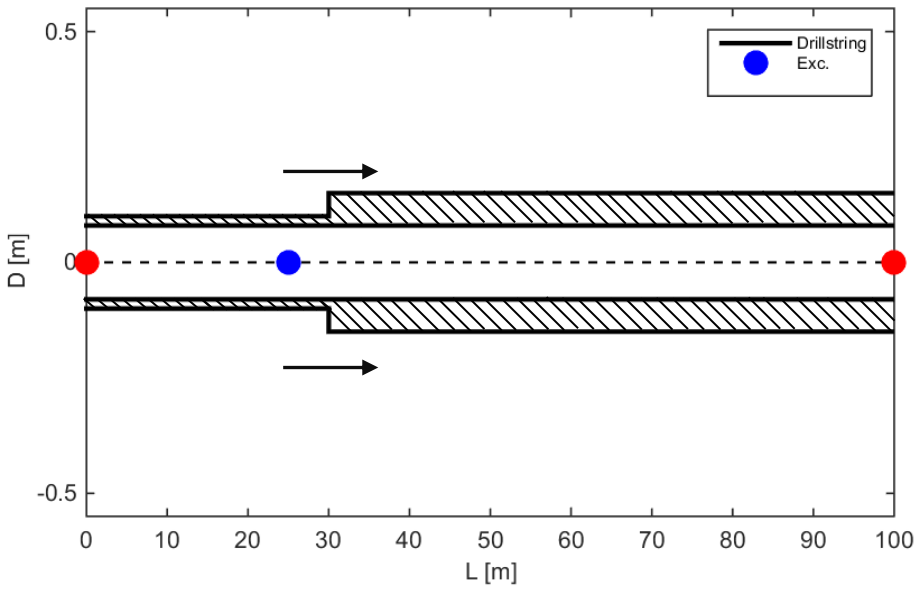

Fig. 3.40: Tapered BHA model with a single diameter change. The length of the thinner section increases with every computation step. The diameter change is here at 30 m distance from the bit. The red points indicate the boundary conditions of the model.

Modal Analysis

The normal mode shapes show only a slight impact of the diameter change and its progression compared to an introduction and variation of stabilizers. However, the natural frequencies decrease continuously as the BHA becomes thinner and thus more flexible. The change of the first 5 normal modes and their natural frequencies for a selected diameter change position can be seen in Fig. 3.41. Fig. 3.42 shows the normalized 1st mode shape for ten diameter change positions. The 2nd normalized mode shape and other natural frequency plots can be found in the Appendix D.

A tapered BHA with a short reduced OD section leads to a change in slope of the normal mode shape close to the diameter change position. This phenomenon is related to the variation in section stiffness. However, a shorter and thinner section can also yield the same stiffness as a longer and thicker element since bending stiffness is dependent on segment length.

As the diameter change progresses further, the normal mode shapes tend to level off with a smaller slope. The point, where the change in slope occurs, is shifted alongside with the diameter change position. The remaining thicker BHA section with its higher bending stiffness reduces the modal amplitude of the normal mode shapes, thus altering the shape at the excitation location as well. The normal mode shape does not change significantly over the last few steps. However, the natural frequency values continue to drop until the whole BHA is at an OD of 0.2 m. This change in normal modes impacts the physical amplitudes such as displacement and bending moment and alters their response accordingly. Hence, the physical quantities show the highest response close to the midpoint of the BHA model and smaller values close to the end points. The effect on lateral displacement and bending moment are going to be discussed on the following pages.

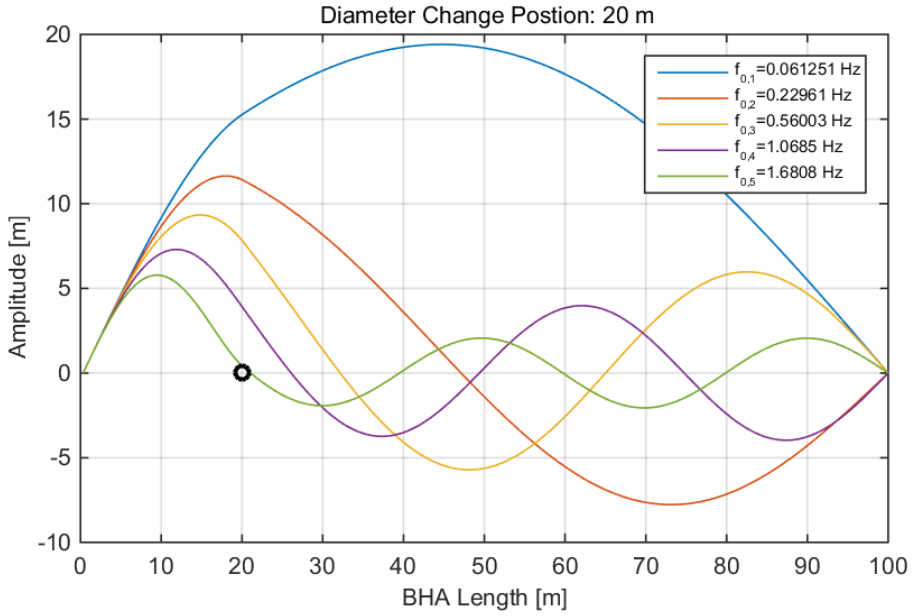

Fig. 3.41: The first 5 normal modes and natural frequencies for a diameter change at 20 m distance from the bit. Note the change in the slope on the left side due to a change in weight and stiffness of the BHA.

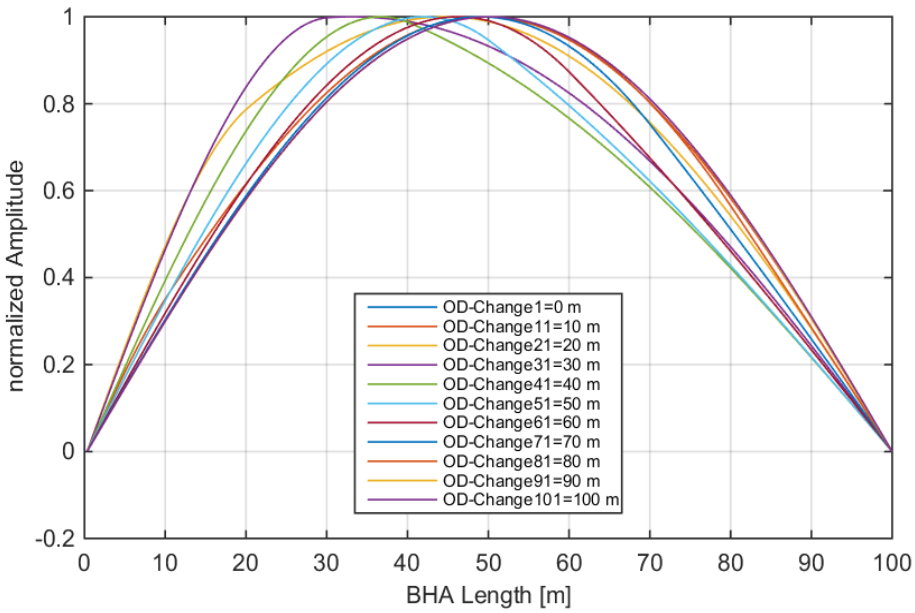

Fig. 3.42: Normalized 1st normal modes for selected diameter change positions. The shapes show some response to the change but not as severe as seen in the stabilizer position variation where the modes change significantly.

The modal assurance criterion yields the same statement that small diameter changes have only little significance for the normal mode shapes. The criterion is not influenced by boundary phenomena which have been observed for the stabilizer positions, where a stabilizer placed close the BHA end points causes a criterion value of 1. Fig. 3.43 shows the modal assurance criterion for all 101 1st normal modes of the model.

The implementation of a threshold for the modal assurance criterion at 0.95 provides a more detailed insight into the small mode shape changes of this model. As already indicated by Fig. 3.42 the normal modes show a higher degree of consistency compared to the stabilizer position variation. A stabilizer introduces an additional node to the system, whereas a geometry change does not require the normal modes to pass the base line at that point. However, this geometry alteration changes the normal mode shape by shifting it in the horizontal direction. The modal assurance criterion for all 2nd normal mode shapes can be found in Appendix D.

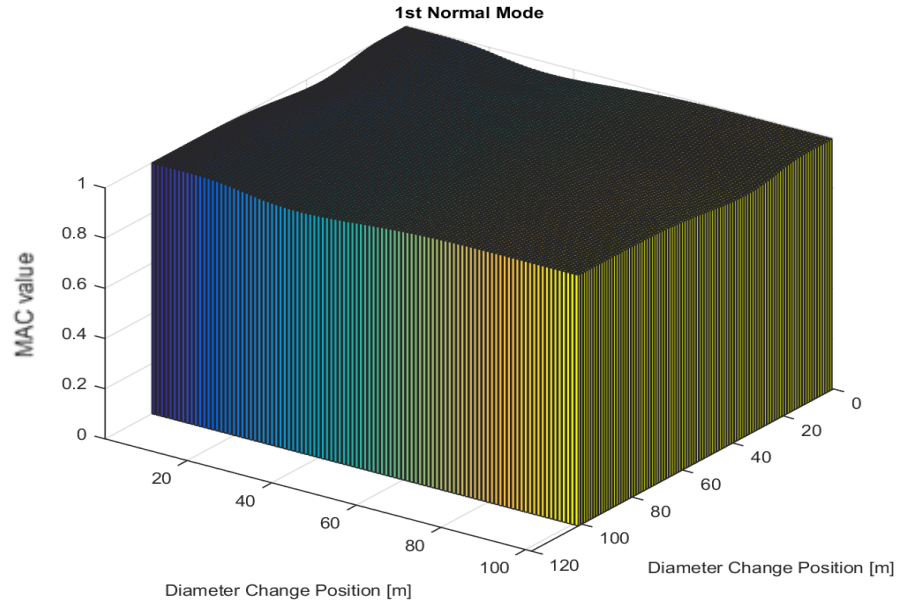

Fig. 3.43: Modal assurance criterion for all 101 1st normal modes. The criterion shows that there are only small mode shape modifications present during the diameter position change.

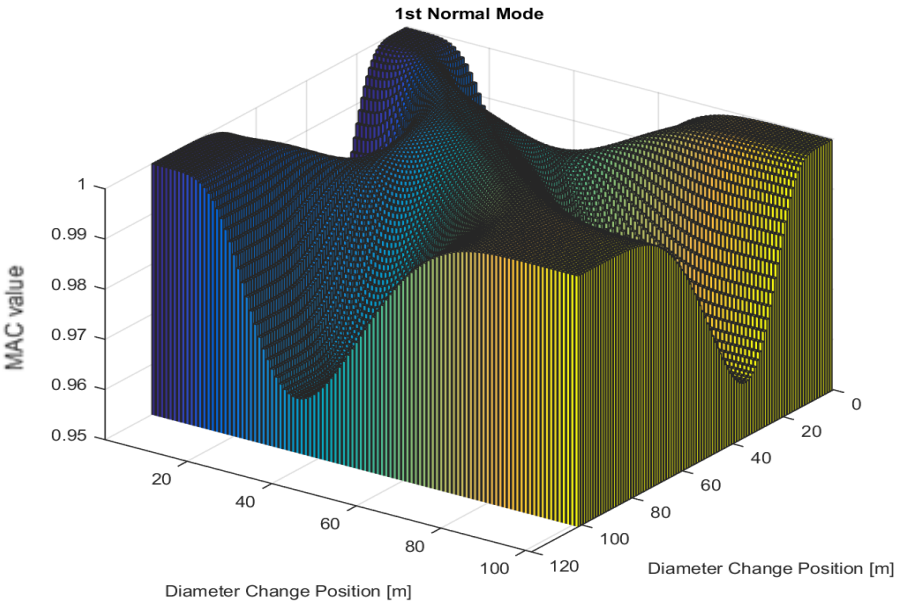

Fig. 3.44: Modal assurance criterion for all 101 1st normal modes with a threshold set at 0.95 to increase the resolution for the remaining values.

Forced Response

Lateral displacement tends to increase as the BHA becomes thinner and lighter. The highest displacement values can be found at a diameter change position close to the middle of the BHA model. The displacement becomes less as the diameter change position is shifted above the midpoint until it reaches the end. Fig. 3.45 shows all diameter change positions and their lateral displacement in one plot. This plot illustrates the increase in lateral displacement as the model becomes thinner. The lateral displacement for selected diameter change positions can be found in Appendix D. Resonance occurs at smaller frequency values as the diameter change progresses along the BHA and effects from the OD reduction become more significant. The OD

change reduces the stiffness of the model leading to smaller natural frequencies. Lower frequencies have been recognized to generate high displacement values close to the top end of the BHA model. The locations of the maximum lateral displacement can be seen in Fig. 3.46. In general, lower frequencies show the highest displacement values. This fact is associated with the selected damping model which consists only of structural damping. Structural damping is constant across the whole frequency range. The lateral acceleration and velocity yield the same results as the lateral displacement since both are based on the displacement. The results for both parameters can be found in Appendix D. Plots for the overall maxima across the length and frequencies are also shown in the appendix.

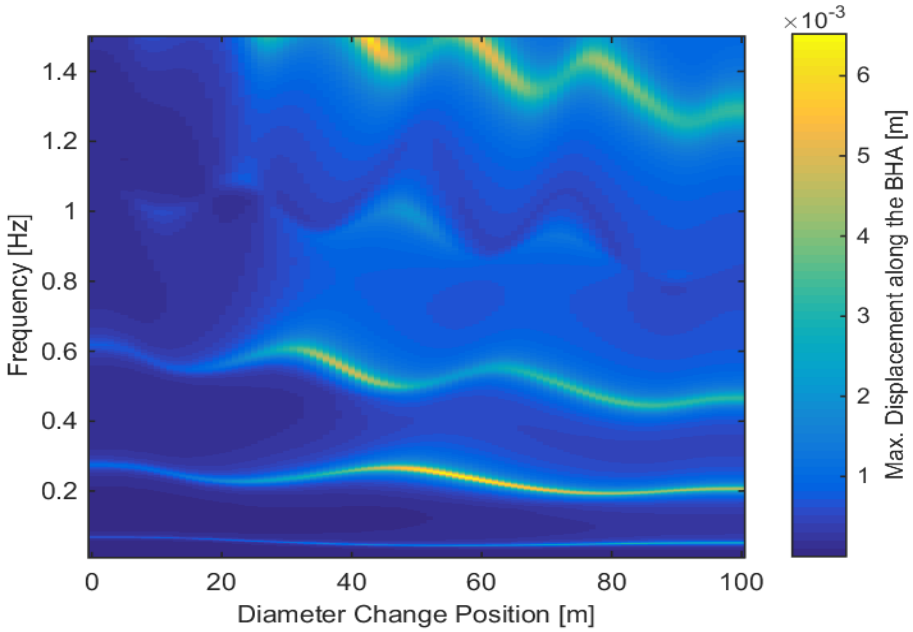

Fig. 3.45: Max. lateral displacement for all diameter change positions. The highest displacement values are related to positions around the middle section of the BHA. The change in frequency response with a progressing diameter change from left to right can be associated with a decrease in stiffness as the OD is being reduced.

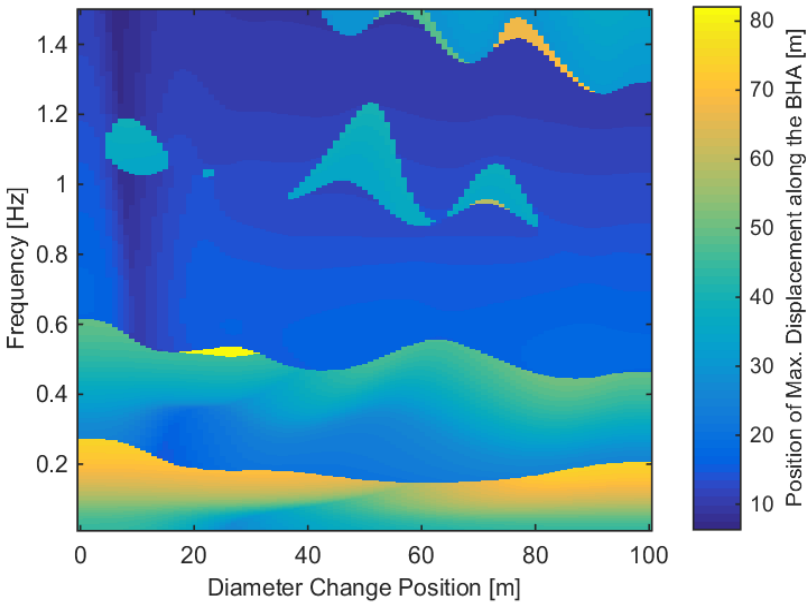

Fig. 3.46: Location of the maximum lateral displacement for all diameter change positions. Note that lower frequencies tend to generate a maximum close to the top end of the BHA model.

Bending moment results are highly dependent on the bending stiffness of the model and its segments. Therefore, it has been noted that the bending moment decreases in the thinner BHA segment. The highest bending moment values are concentrated in the stiffer element of the BHA which corresponds to the segment with the larger OD. Fig. 3.47 shows the bending moment for a given diameter change position. It is clearly visible that the change in bending moment amplitude is directly related with the diameter change. As the stiffer section becomes shorter, the bending moment values tend to increase in this particular area, leading to high stresses in this short section. A bending moment plot for a different diameter change position can be found in Appendix D.

Investigating the maximum bending moments and their locations for different diameter change positions along the BHA, as shown in Fig. 3.48 and Fig. 3.49, concludes that the majority of high bending moments occur at high frequencies and in the top area of the BHA. This combination is equivalent to the stiffer section of the BHA model. As these figures indicate, the bending moment values drop as the diameter change approaches the top end of the BHA model. This phenomenon can be explained with a change in the normal mode shapes. The stiffness alteration impacts the normal mode shapes and therefore influences the physical amplitude according to Eq. 3.7. The highest bending moments occur at the highest simulated frequency which is related to the frequency dependency of the amplitude of the excitation force. Hence, the physical deflection becomes more severe at higher frequencies.

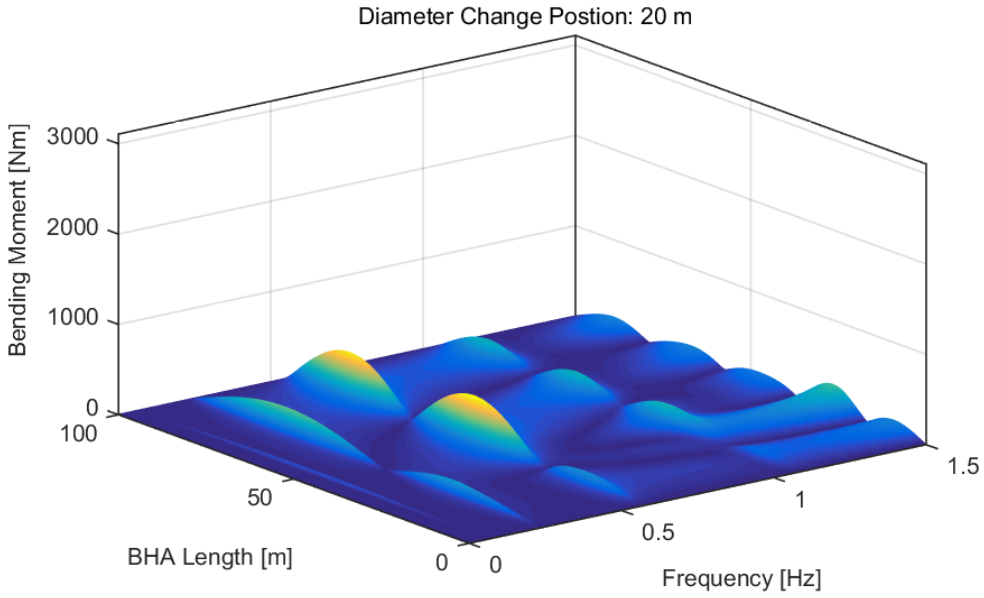

Fig. 3.47: Bending moment for a diameter change at 20 m from the bit. The highest bending moment amplitudes occur in the stiffer section of the BHA.

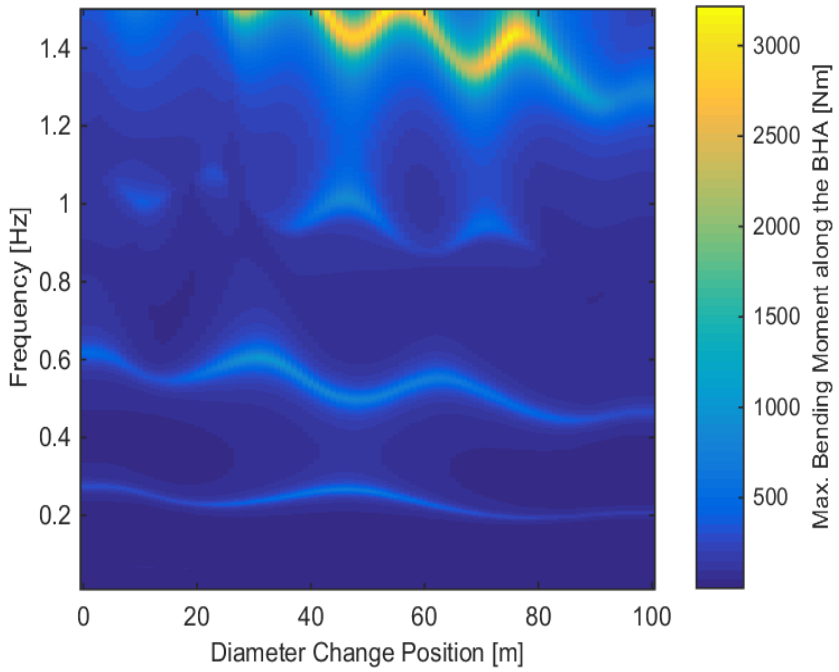

Fig. 3.48: Maximum bending moment for all diameter change positions. The highest values occur at high frequencies.

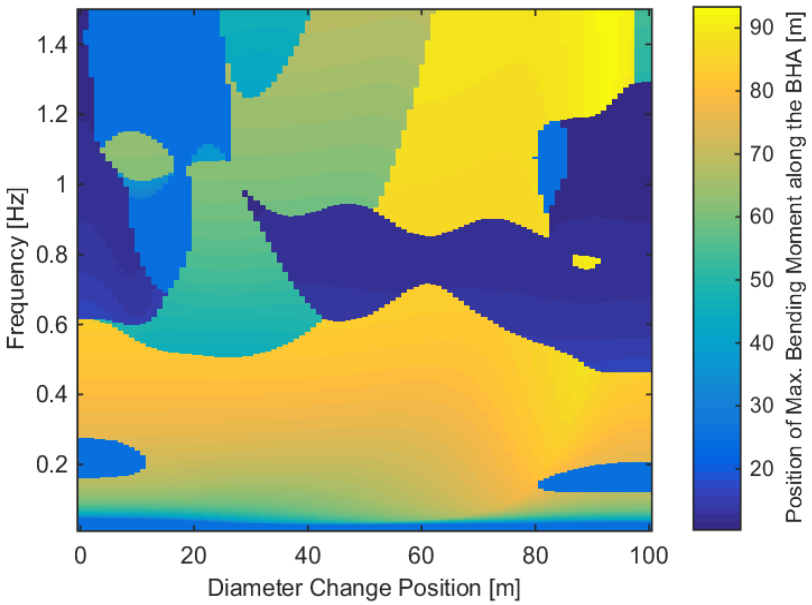

Fig. 3.49: Position of the maximum bending moment for all diameter change positions. The majority of high values are located on the stiffer section of the BHA.

The cumulative strain energy along the BHA length yields higher values for the diameter change model configurations compared to the stabilizer position modifications. Cumulative strain energy maxima for the stabilizer position configuration are at 0.06 Nm, whereas this model configuration shows values up to 0.25 Nm. The exact values depend on the excitation amplitude but the relative difference can be interpreted. The smaller diameter leads to a reduction of the area moment of inertia for this section which in turn increases the fraction of Eq. 3.1 and thus the strain energy values. Furthermore, the deficiency of any stabilization points within this model configuration does not allow for any vibration restriction or dampening effects to occur. Stabilizer absence contributes to higher strain energy values, which again highlights the importance of proper BHA stabilization for vibration control. The frequency at which the strain energy values occur drops identical to the maximum displacement and bending moment values, caused by a reduction in BHA stiffness as the diameter change progresses to the top end. Fig. 3.50 and Fig. 3.51 show the progression of the cumulative strain energy with the continuous change in diameter along the BHA length.

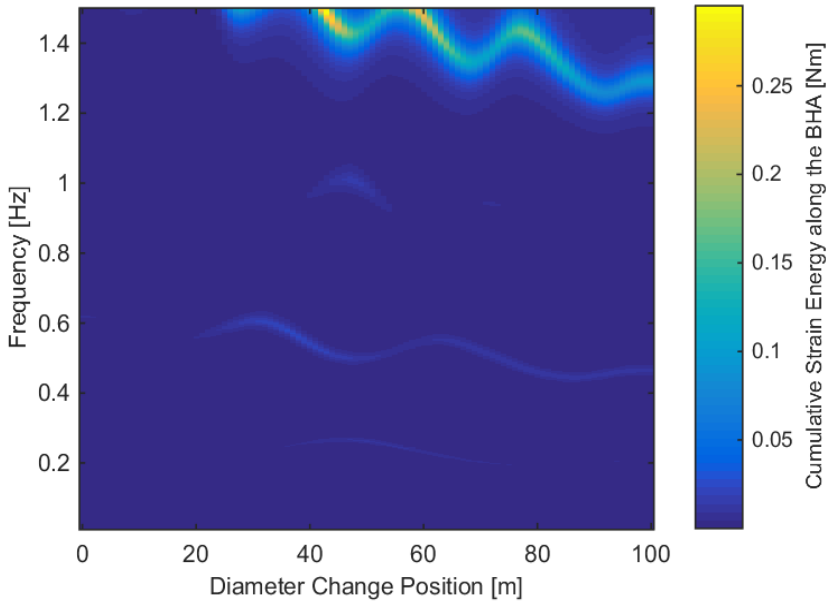

Fig. 3.50: Cumulative Strain Energy for all diameter change positions. A reduction in OD increases the strain energy values due to a reduction in area moment of inertia.

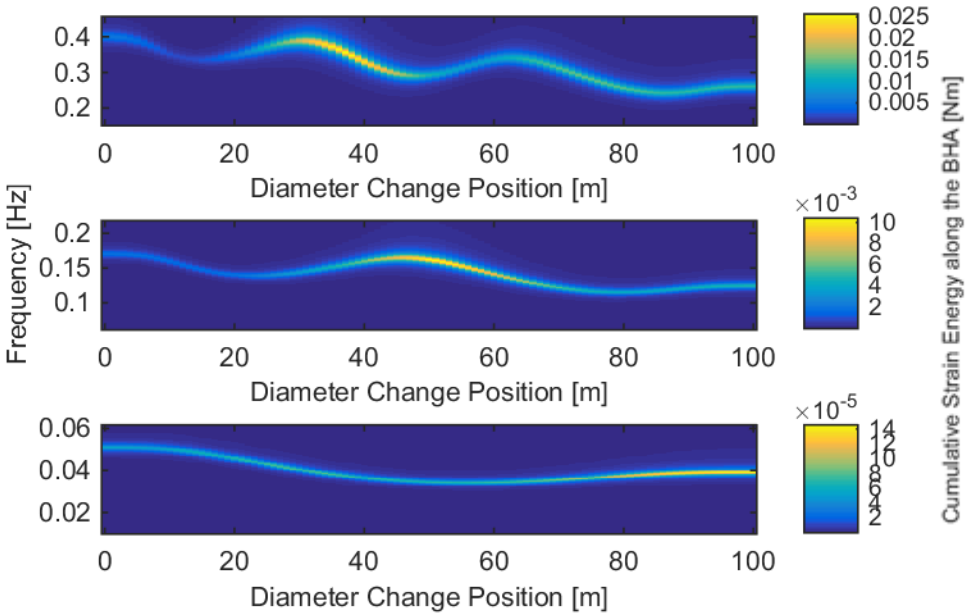

Fig. 3.51: Cumulative strain energy along the BHA for the first three frequency responses, providing a magnified version of Fig. 3.50.

Summary

This study shows that an OD change impacts the area moment of inertia and therefore element stiffness. These two parameters are responsible for the magnitude and corresponding frequencies at which these magnitudes occur. Hence, lateral displacement, bending moment, strain energy and all other parameters under investigation tend to increase as the diameter change progresses from the bottom to the top of the BHA model. The results are highly dependent on the normal mode shape and natural frequencies which determine whether the given normal modes contribute to the overall lateral vibration amplitude. The normal modes are influenced by the length ratio of the two different OD sections. A short small OD section

produces a steeper slope and a short large OD element at the top generates a smaller slope of the normal mode shapes. This phenomenon can be related to a sudden change in element stiffness.

3.1.4.2 Constant Mass Tapered BHA

This parameter study builds upon the same input as the tapered BHA model. However, the mass reduction related to the OD change has been neglected in this model. The mass distribution μ has been set to a constant value of 396.54 kg/m which represents the mass distribution of the base case:

$$\mu = \frac{\rho\pi(OD^2 - ID^2)}{4} \qquad \textbf{Eq. 3.7}$$

The constant mass distribution does not alter the segment mass according to the diameter change. Hence, the BHA remains at the mass of the initial configuration. Effects of this thinner but equally heavy BHA are investigated and compared with the variable mass configuration. This simulation clarifies whether a plain geometry change or mass related effects influence lateral vibrations to a greater extent. Such a constant mass configuration is comparable with an assembly comprised of different materials.

Modal Analysis

The smaller diameter reduces the area moment of inertia and thus the bending stiffness of the BHA model. This creates a more flexible structure which is still as heavy as the base case due to the constant mass. This configuration produces lower natural frequencies compared to the OD variation without mass adjustment (variable mass). More mass, at smaller diameters, decreases the natural frequencies. The natural frequencies and normal mode shapes for selected diameter change positions can be seen in Fig. 3.52 and Fig. 3.53. If these results are now being compared with the variable mass model, the natural frequency values decrease as the diameter change position progresses to the top of the BHA model. As a result, higher normal modes are then also within the 1.5 Hz range. Additional diagrams can be found in Appendix E. The modal assurance criterion shows the same trend as for the variable mass model. The same affected pairs show a lower degree of correspondence for the diameter change under constant mass considerations. The degree of correspondence between all 1st normal mode shapes can be seen in Fig. 3.54. The change in normal mode shape is more severe for a constant element mass, leading to a lower degree of correspondence. However, the normal mode difference between these two BHA models is small. The criterion for all 2nd normal mode shapes can be found in Appendix E.

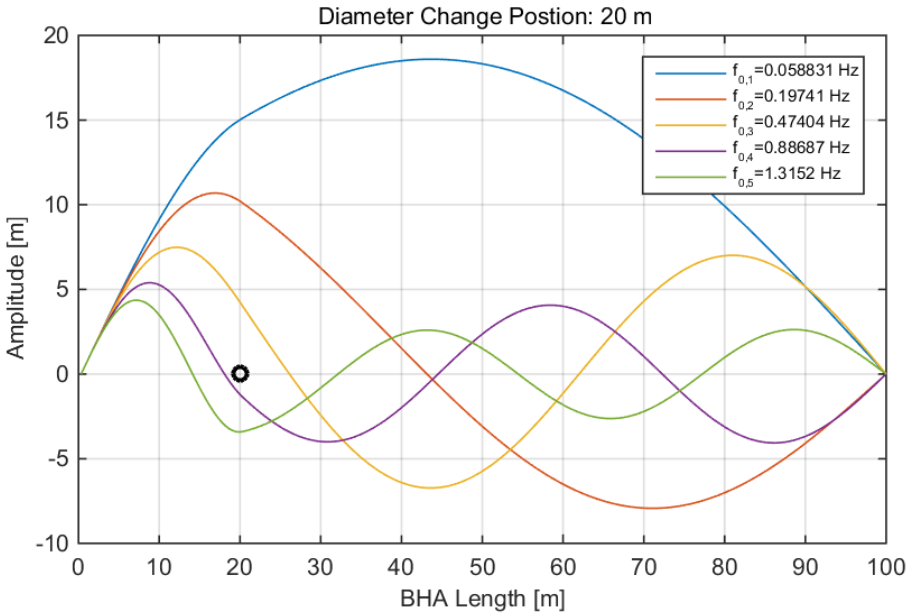

Fig. 3.52: The first 5 normal modes and natural frequencies for a diameter change at 20 m distance from the bit. The mode shape is identical to the model with a variation in mass. However, the natural frequencies are lower than in the other BHA model configuration.

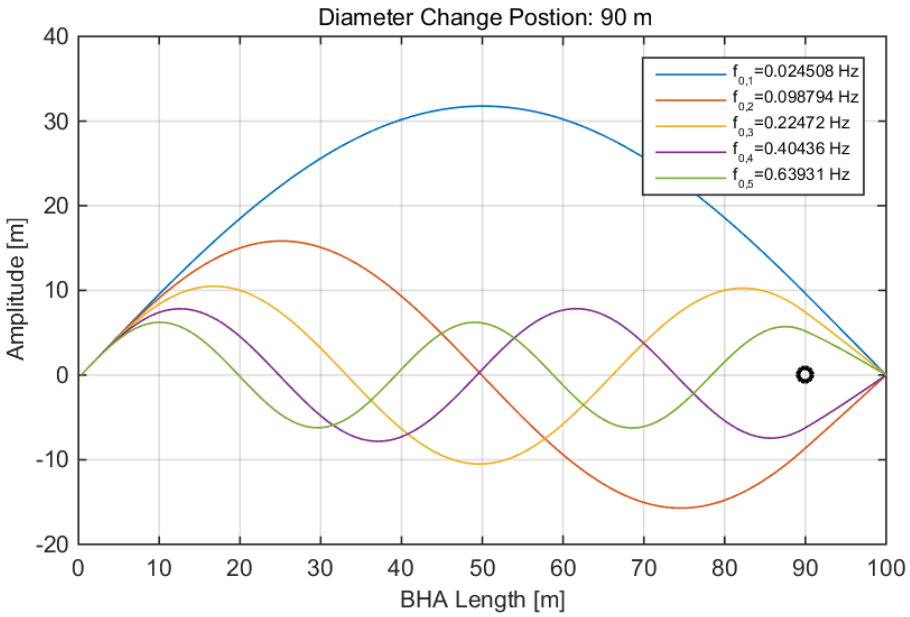

Fig. 3.53: The first 5 normal modes and natural frequencies for a diameter change at 90 m distance from the bit. Note that the natural frequency values change more significantly compared to the variable mass model as the diameter change position progress to the top of the BHA.

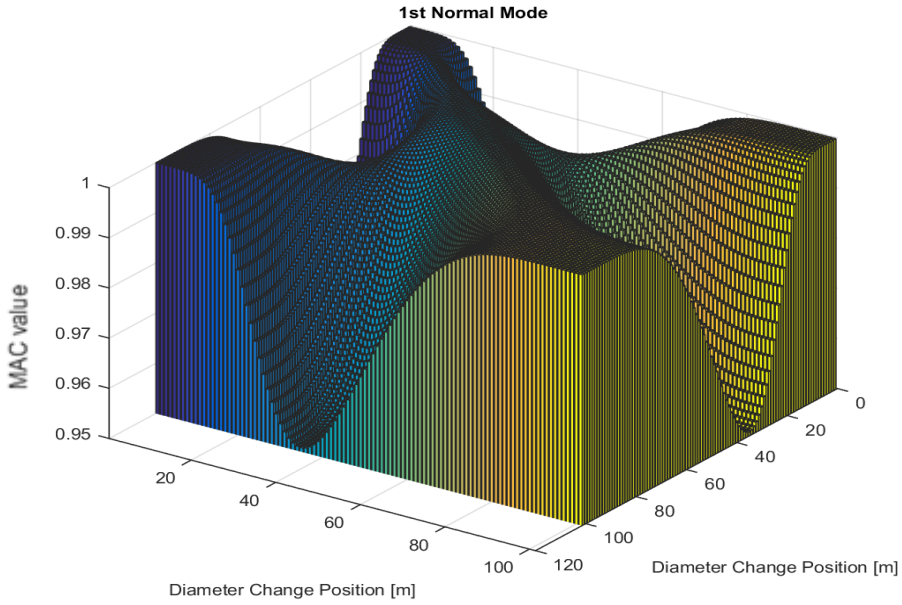

Fig. 3.54: Modal assurance criterion for all 1st normal mode shapes of the constant mass model. The same pairs as for the variable mass models are affected. They show a lower degree of correspondence.

Forced Response

The sole geometric change has been identified to show only little influence on the lateral displacement, acceleration and velocity for this model. Fig. 3.55 and Fig. 3.56 show the lateral displacement for two different diameter change positions. The increase in number of peaks in Fig. 3.56 is related to the excitation of higher normal modes within the given frequency range which are shifted into the bandwidth due to a reduction of the natural frequency values for every normal mode. Fig. 3.57 illustrates the maximum lateral displacement along the BHA and across the whole frequency bandwidth. A constant mass leads to a steeper drop in the frequency response at which the maximum displacements occur. Given the frequency bandwidth, more than the previously considered natural frequencies, which could cause resonance related vibration damage, have to be considered. The higher mass hinders the lateral BHA movement even though the model shows a reduced bending stiffness. Hence, changing the geometry does not necessarily lead to more severe vibrations. A larger diameter difference may lead to bigger physical amplitudes on the vibration system. However, this was not part of the conducted simulations.

The position of the maximum lateral displacement also reflects the steeper drop in the frequency response. The maxima positions are slightly shifted further to the top of the BHA for the same diameter change positions compared to the variable mass BHA model. The lower section of the frequency bandwidth generates maximum values close to the top of the BHA model whereas the maxima at other frequencies are located in the mid area of the model. The visibility of low frequency amplitudes can be related to the selected structural damping model as described earlier. Fig. 3.58 shows the position of the maximum lateral displacement. Plots for the acceleration and velocity can be found in Appendix E.

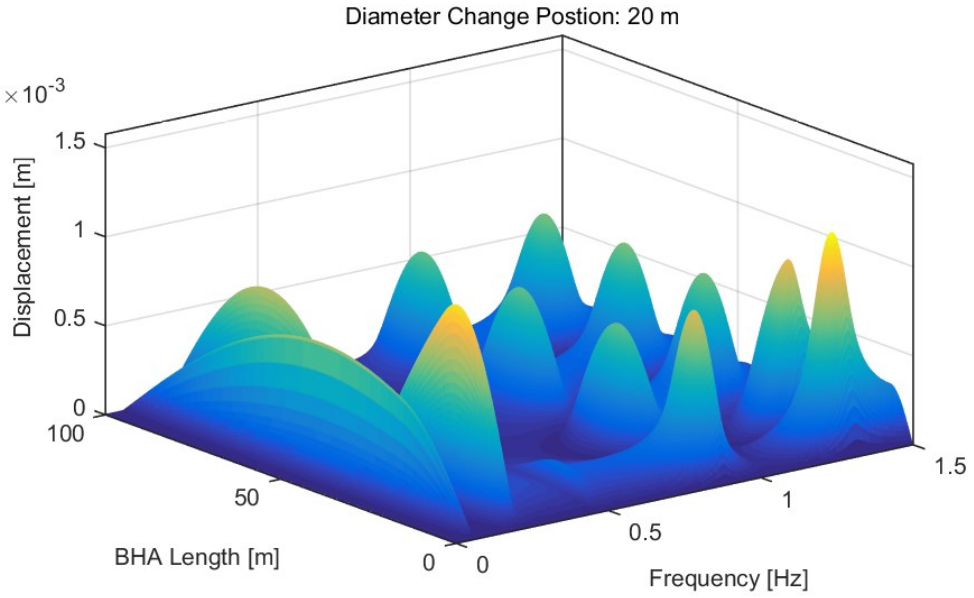

Fig. 3.55: Lateral displacement for a diameter change 20 m from the bit and a constant mass distribution.

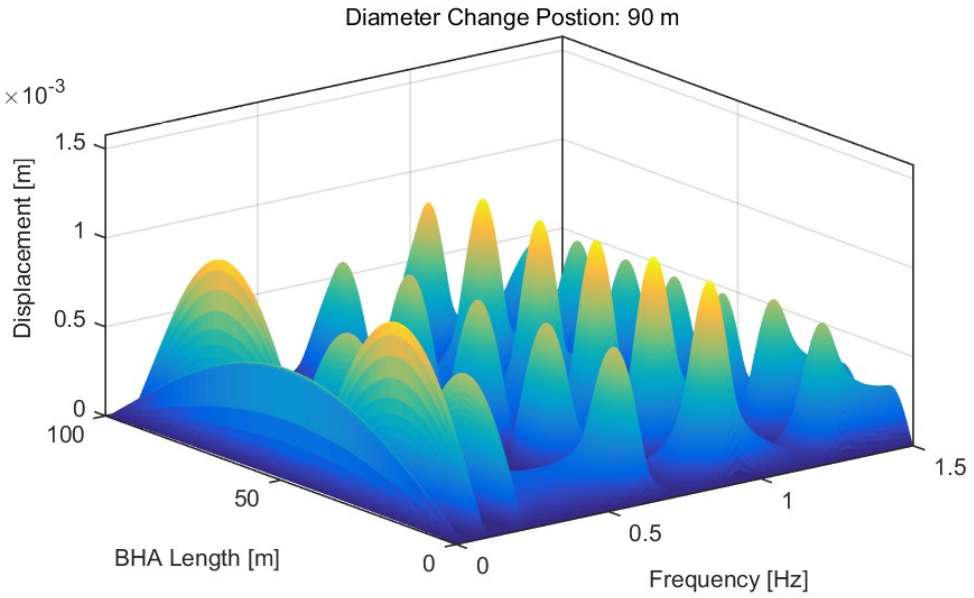

Fig. 3.56: Lateral displacement for a diameter change 90 m from the bit. Note that the displacement magnitude only shows a small change compared to the previous figure.

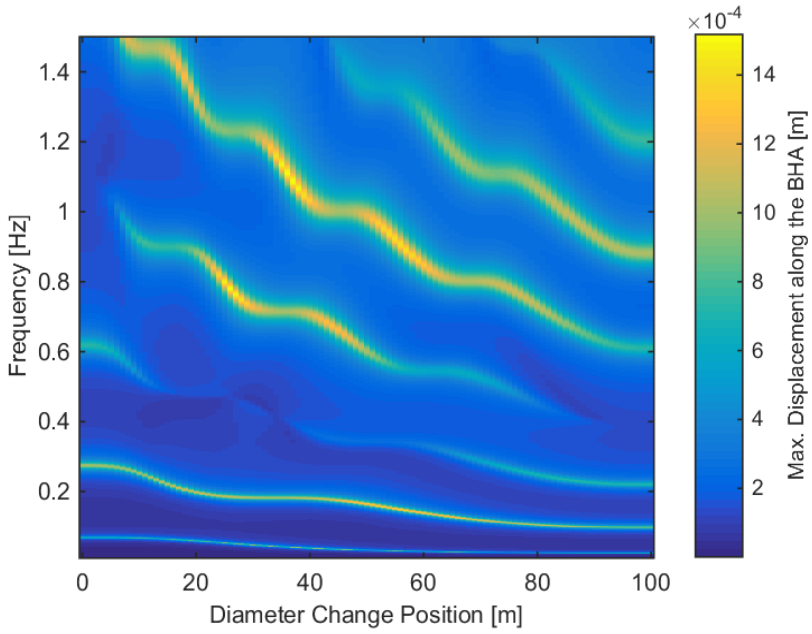

Fig. 3.57: Max. lateral displacement for all diameter changes under constant mass conditions. The lateral displacement shows only a little variation as the diameter change progresses from the bottom to the top of the BHA. However, the frequencies at which those values occur tend to drop much steeper and more resonance frequencies are within the investigated frequency range.

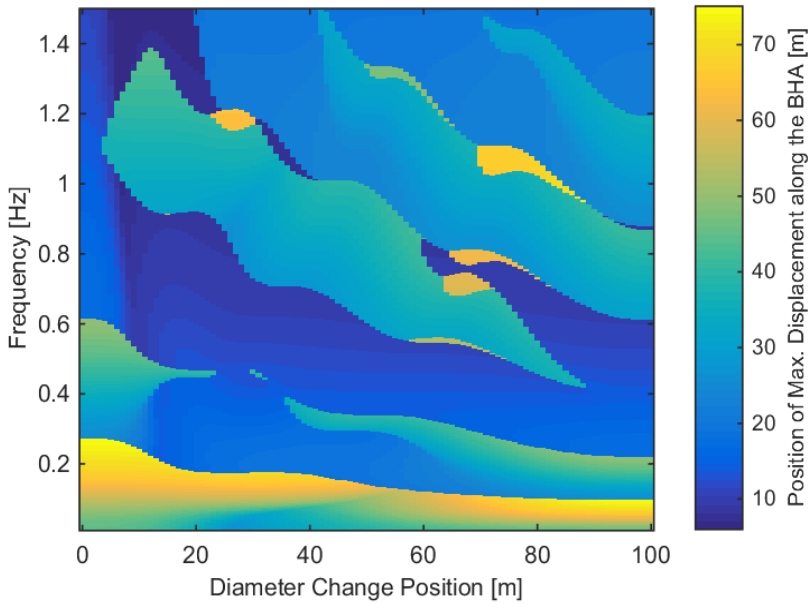

Fig. 3.58: Position of the max. lateral displacement for all diameter changes and a constant mass distribution.

The bending moment is reduced by almost 50 percent along all diameter changes for a constant mass distribution. However, the first few diameter change positions show higher bending moment values for the constant mass case compared to the variable mass model. This implies that small and short but heavy sections cause a concentration of high bending moments in this area. Boundary interaction could also influence the results of the first few computations. Bending stiffness is length dependent and becomes smaller as the thinner OD section becomes longer. This peak for diameter changes close to the bottom of the BHA can be seen in Fig. 3.59.

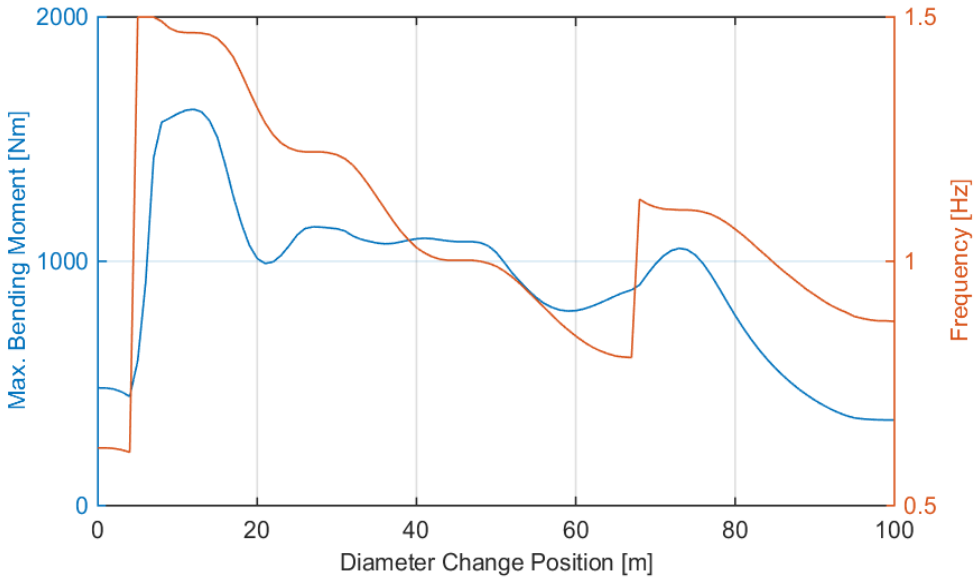

Fig. 3.59: Max. bending moment for all diameter change positions and across all frequencies. The progression of the diameter change towards the top of the BHA reduces the stiffness whilst maintaining a certain mass inertia due to the constant mass, thus reducing the bending moment amplitudes.

The frequency, at which maximum bending moments occur, drops faster as in the variable mass model configuration. This phenomenon shows the contribution of mass inertia on the frequency response. A reduced wall thickness but equally heavy BHA decreases the frequency response and bending moment amplitudes significantly. This trend is shown in Fig. 3.60 for the maximum bending moments for all diameter changes. The occurring plateaus are related to the encounter of nodal points of the normal modes as the BHA is excited. The dense resolution of diameter change positions causes several diameter changes to be affected by these nodes, thus creating these plateaus. Changes in the slope of the red curve are related to the consolidation of the resonance frequency information. All eigenfrequencies from Fig. 3.57 are used to generate one curve. Hence the sharp slope change reflects a shift in the resonance frequency where the maximum bending moments occurs. For diameter changes close to the left end, lower frequencies lead to high bending moment amplitudes. As the diameter change position is moving further to the right, the resonance frequencies of the maximum amplitudes become higher.

The strain energy follows the same trend as the bending moment in relation to the frequency drop. However, the absolute values show more similarities towards the stabilizer position variation. The denominator in Eq. 3.1 is influenced by the area moment of inertia and should increase the strain energy as the OD is reduced but the constant mass impacts the numerator, the bending moment, by keeping the values comparatively low. This dominance leads to an overall reduction in strain energy values. The strain energy results for this BHA model can be seen in Fig. 3.61. Bending moment itself depends on the natural frequencies of the configuration and the normal modes which influence the magnitude of the physical amplitude.

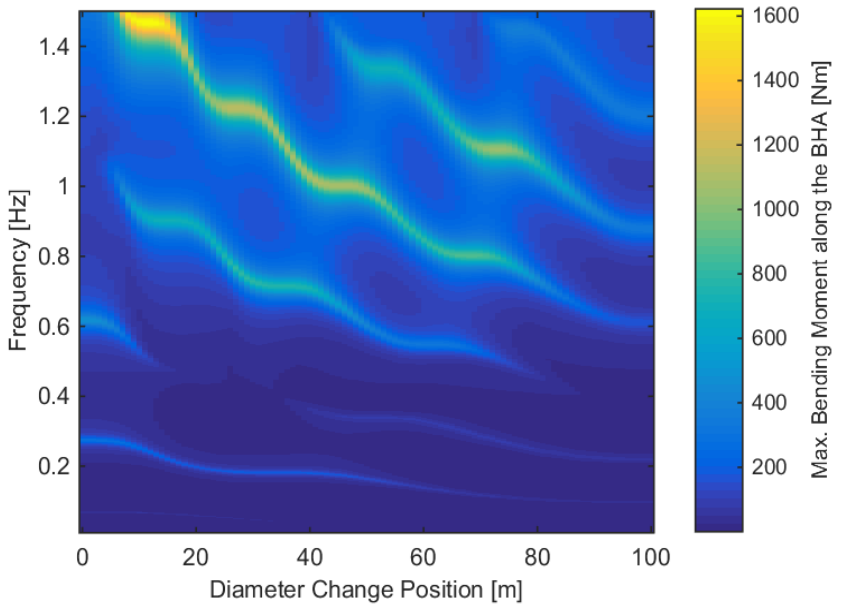

Fig. 3.60: Max. bending moment for all diameter change positions at a constant mass distribution. The frequency at which the max. bending moments occur drops more significantly for this case.

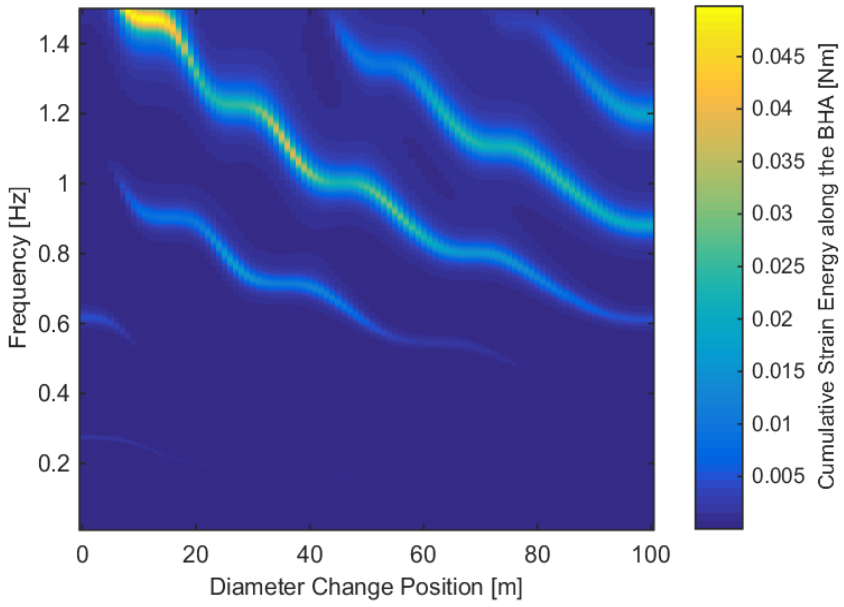

Fig. 3.61: Cumulative strain energy for all diameter changes with a constant mass distribution. Note the significantly lower strain energy values compared to the variable mass model.

Summary

This parameter study shows that mass inertia greatly impacts natural frequencies and the frequency response of the physical amplitude. This phenomenon can be explained with Eq. 2.1. A higher mass reduces the fraction within the square root, thus reducing the natural frequencies. The OD reduction decreases the bending stiffness of the BHA model. However, the constant mass counteracts these flexibility effects and reduces the physical amplitudes such as lateral displacement and bending moment. A higher mass would require more energy to be displaced by the same amount as for the variable mass case. The selection of more dense materials for certain BHA components could reduce lateral vibrations and could shift resonance phenomena to lower frequencies by maintaining a smaller overall BHA geometry compared to

lighter materials. A ratio between the bending stiffness and mass distribution, as indicated by Eq. 3.8, illustrates the difference between the constant mass and variable mass BHA model.

$$R = \frac{\frac{1}{301}\sum_{i=1}^{301} EI}{\frac{1}{301}\sum_{i=1}^{301} \mu} \qquad \text{Eq. 3.8}$$

This ratio is based on the arithmetic mean of the bending stiffness EI and mass distribution μ. The values for every single element out of 301 length elements have been calculated and are used for averaging across the total BHA length. As indicated in Fig. 3.62, the ratio of the constant mass model configuration shows a steeper slope as the variable mass BHA model. The constant mass of 396.54 kg/m as a denominator decreases the ratio much faster than the variable mass which adapts to the diameter change. This observation is comparable with a change in Young's Modulus or in other words with a material variation for the smaller OD section.

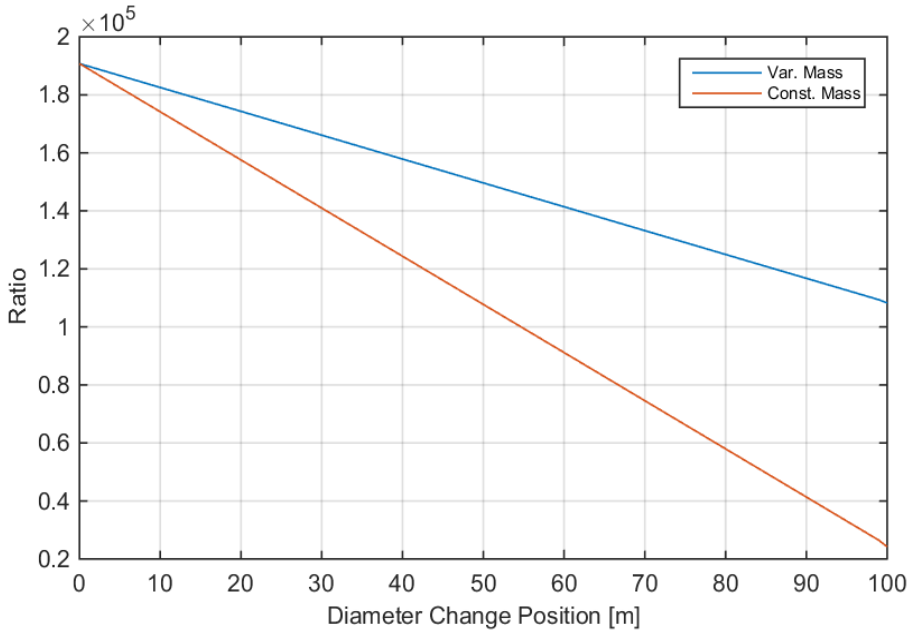

Fig. 3.62: Bending stiffness and mass distribution ratio for the variable and constant mass BHA model. The constant mass distribution causes a much larger denominator and thus reducing the ratio of the constant mass model much faster.

3.1.4.3 Flex – Sub BHA

Flex-subs are tools with a smaller outer diameter which reduces the bending stiffness of a particular area. On the contrary to a tapered BHA, the smaller OD section is placed in between components with larger dimensions. The flex-sub model configuration combines two diameter change positions in one simulation run, creating a short segment with a reduced OD. The residual BHA remains at the initial OD of 0.3 m. This model configuration allows the generation of a smaller OD section with an adjustable length which can be placed at different positions along the BHA. Fig. 3.63 shows an example of one of the calculated flex-sub positions. The flex-sub OD has been set to 0.2 m, the same OD reduction as for the other two diameter change models. The length of every flex-sub is 5 m. This length has been found to be a

reasonable tradeoff between length and number of flex-subs, allowing for a suitable investigation and data resolution. All further parameters and assumptions are adopted from the base configuration. State of the art BHA optimization steps recommend the usage of flex-subs to decrease the bending moment in certain BHA sections and to allow higher dogleg severities due to a higher local flexibility of the BHA. This test case should quantify the effects of these components on a lateral vibration system and how the findings fit into the overall dynamic optimization process. Some papers and companies recommend a flex element, as described in Chapter 2.2.3, to reduce lateral vibrations. Whether a low stiffness element with a restricted length could prove beneficial to vibration mitigation should be clarified within the next parameter study.

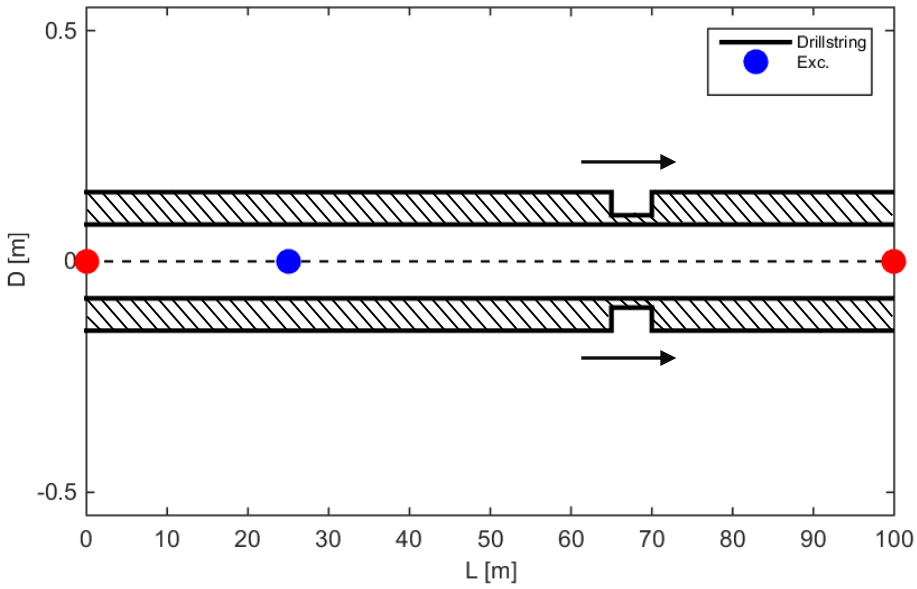

Fig. 3.63: BHA model with a flex-sub starting at 65 m with a total length of 5 m.

Modal Analysis

The normal mode shapes of the first five natural frequencies show a shape variation in form of a discontinuity directly at the flex-component location. This is related to the sudden change in bending stiffness of the element. However, the section is too small compared to the remaining BHA to have an impact on the natural frequencies, thus the values vary only after the second decimal digit. Fig. 3.64 shows the natural frequencies and normal modes for a flex-sub at 65 m. This model configuration produces an almost symmetric effect for the normal mode shapes. For example the mode shapes of a flex-sub at 35 m are symmetric to a sub at 65 m. Fig. 3.65 shows that the normal mode shapes of all 1st modes are symmetric for symmetric flex-sub positions such as for 35 m and 65 m. That these positions are not entirely symmetric can be seen in the MAC plot (Fig. 3.67). The natural frequencies do not follow this symmetry-effect and show different values for both positions. Further normal mode and natural frequency diagrams can be found in Appendix F. The modal assurance criterion, as shown in Fig. 3.66, yields a high degree of correspondence between all 1st normal mode shapes of this flex-sub variation. Fig. 3.67 provides a magnified version of Fig. 3.66, highlighting the small changes of the criterion. The reasons for such a high degree are the same as for the diameter change models. Similar to

a single diameter change, a flex-sub does not introduce an additional node to the vibration system. Comparing normal mode shapes with another, produces only small deviations from a high degree of correspondence. However, the normal mode shapes are shifted horizontally. The pair where the criterion deviates from a value of one is different to the diameter change model configuration. The comparison of the normal mode shapes from second to the ninth and the last four flex-sub variations show the least degree of correspondence. The modal assurance criterion for all 2nd normal mode shapes can be seen in Appendix F.

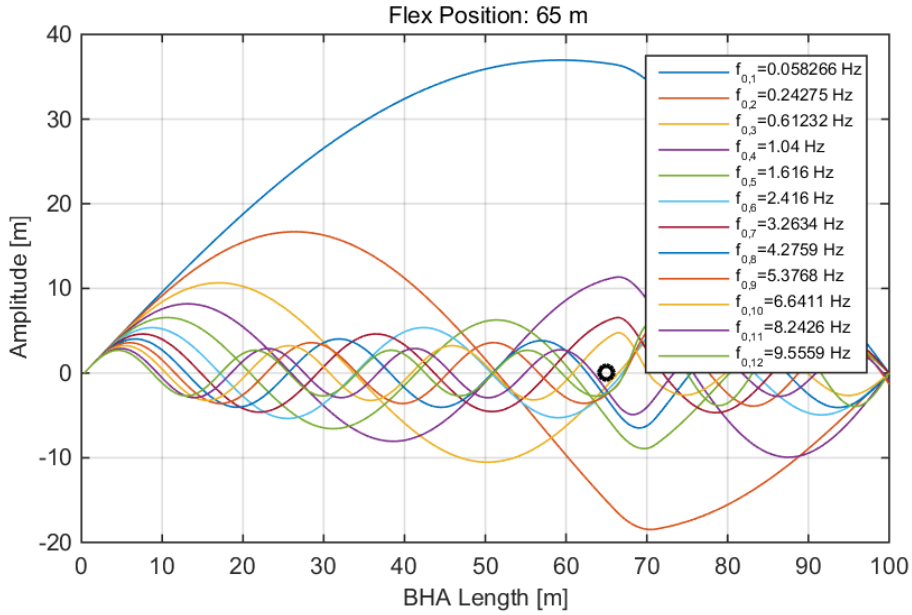

Fig. 3.64: The first 12 natural frequencies and normal model shapes for a 5 m flex-sub starting at 65 m from the bit. The shape and frequencies for different locations tend to vary only in the decimal places.

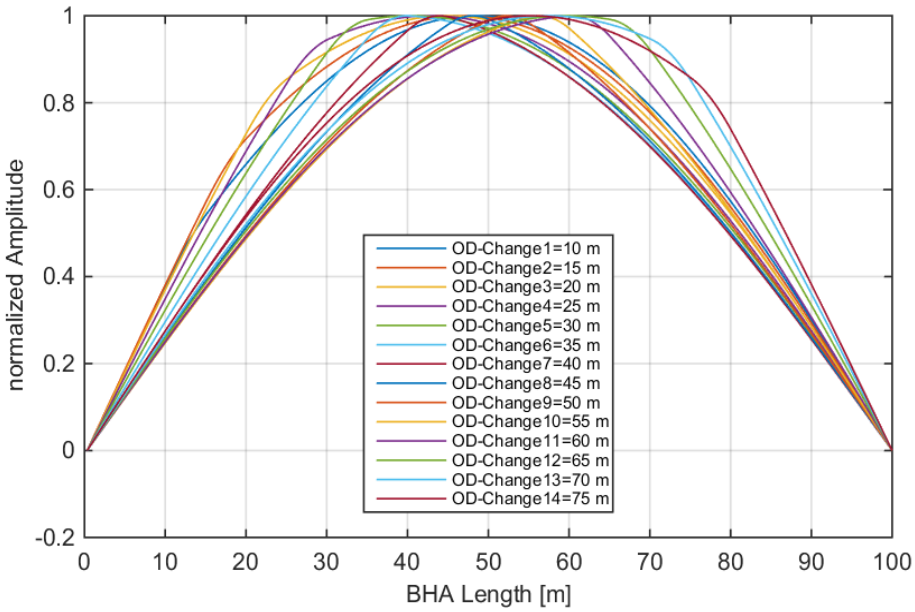

Fig. 3.65: Selection of normalized 1st normal modes of selected flex-sub positions. The symmetry of given flex-subs is reflected in the symmetrical normalized normal mode shape.

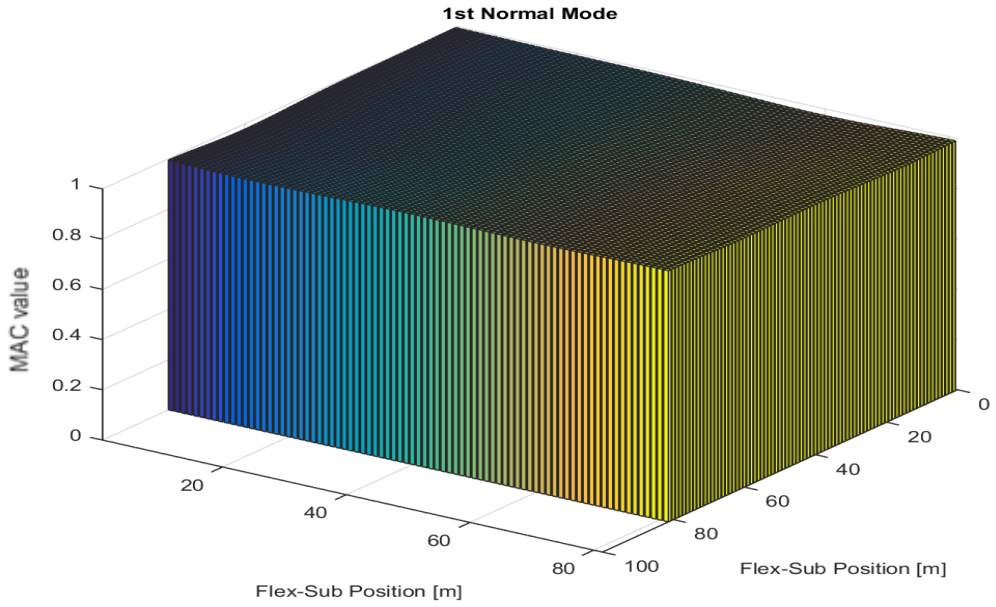

Fig. 3.66: Modal assurance criterion for all 1st normal modes of all flex-subs. There is a high degree of correspondence between all flex-sub positions.

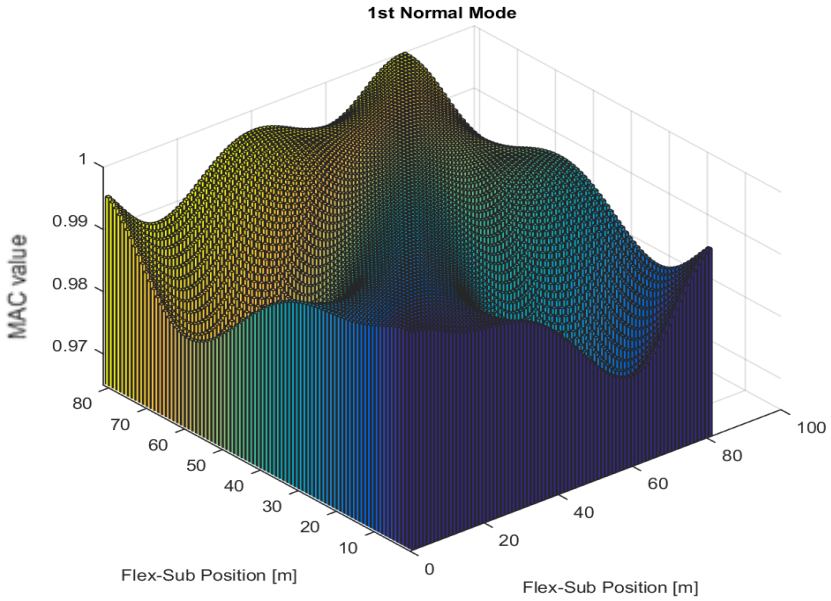

Fig. 3.67: Magnified view of the modal assurance criterion for all 1st normal modes of all flex-subs. Comparison of the first and last flex-sub positions with each other yields the least degree of correspondence between the normal mode shapes.

Forced Response

Flex-subs close to the excitation source yield the highest lateral displacement values. These relatively high displacement values occur at low frequencies below or at 0.5 Hz as shown in Fig. 3.68. Fig. 3.68 presents the maximum lateral displacement for all flex-sub positions and across the whole frequency bandwidth. An excitation location shift to 50 m from the bit has shown that this phenomenon is consistent and reoccurs for different locations (Fig. 3.69). Fig. 3.70 shows the lateral displacement for one particular flex-sub position. This does not exclude higher frequencies from having a physical displacement, albeit their response is comparatively low to the lower frequencies and is therefore not clearly visible in the shown plots. Especially since not

all of the considered natural frequencies are within the frequency bandwidth under investigation. Discontinuities in the frequency response of the maximum amplitudes are mode dependent. A change of the maximum amplitude from one mode to another causes the frequency to change accordingly. Fig. 3.71 shows that the maximum lateral displacement alternates between the second and third mode, producing the frequency discontinuities seen in Fig. 3.68. However, all modes contribute to the overall physical displacement.

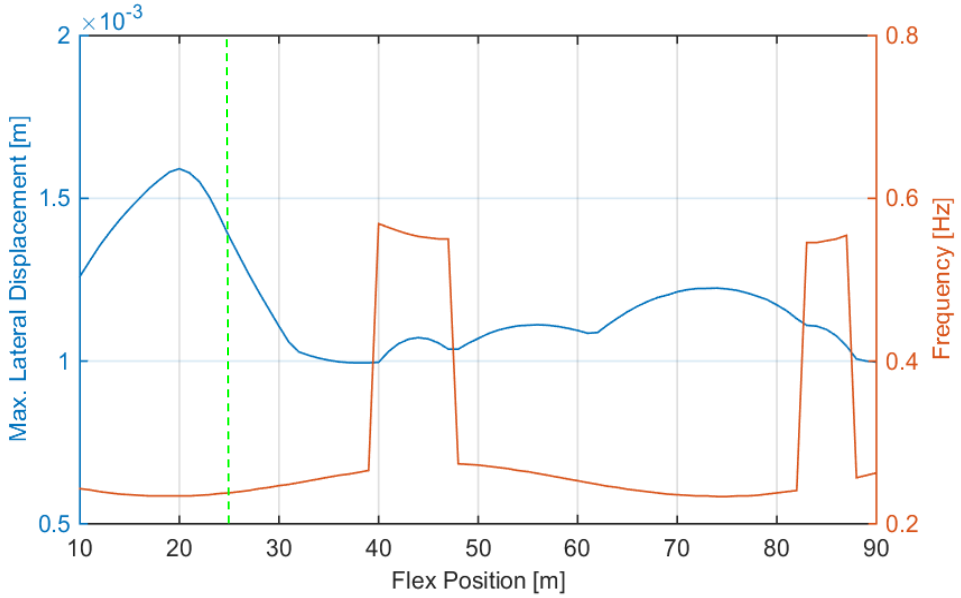

Fig. 3.68: Max. lateral displacement for all flex-sub positions and across the whole frequency range. The highest lateral displacements occur for a flex-sub at the excitation location (dashed green line) and in front of it.

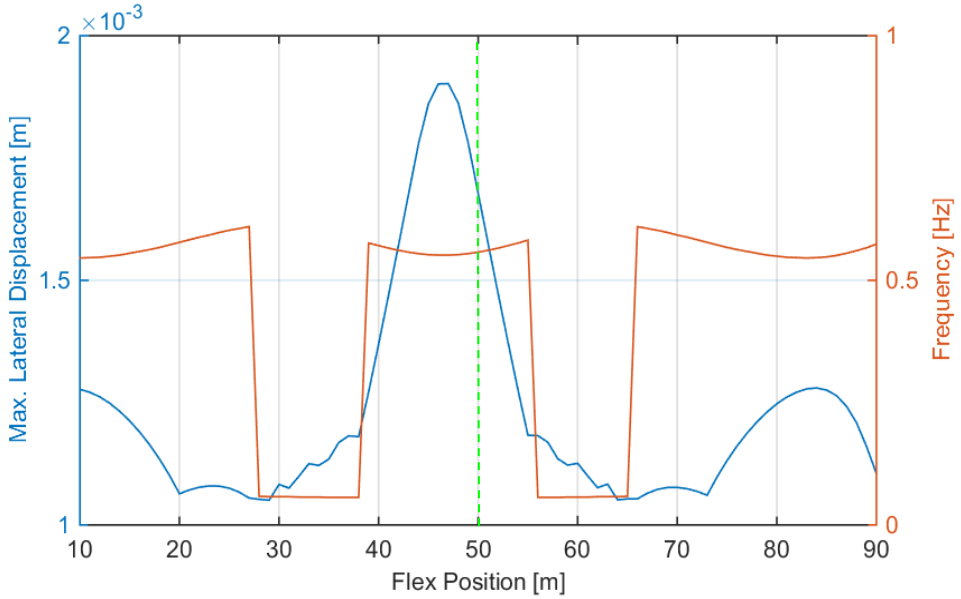

Fig. 3.69: Max. lateral displacement for all flex-sub positions. The excitations source (dashed green line) has been moved from 25 m to 50 m from the bit.

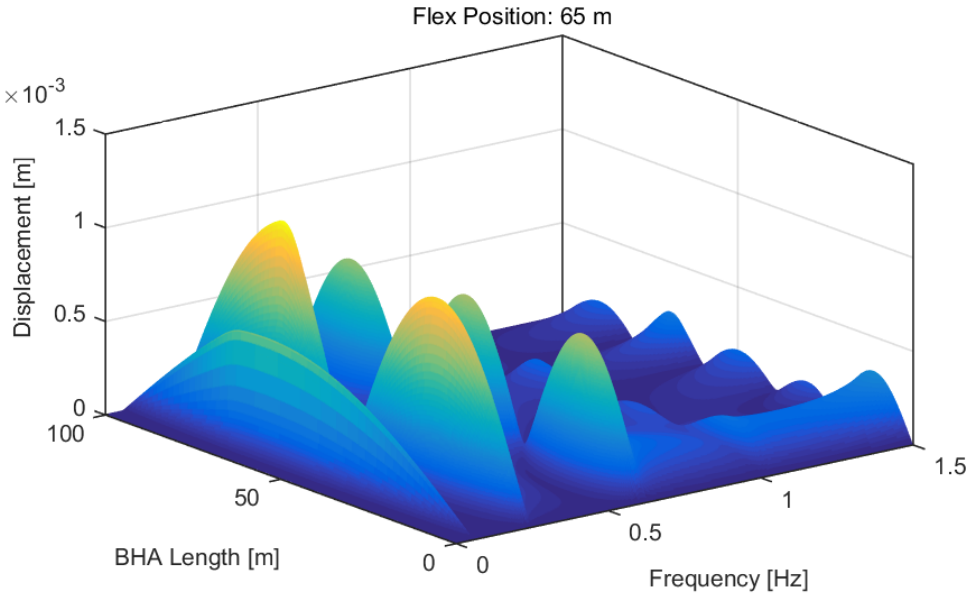

Fig. 3.70: Lateral displacement for a 5m long flex-sub starting at 65 m from the bit. Note that the highest amplitudes occur at relatively low frequencies.

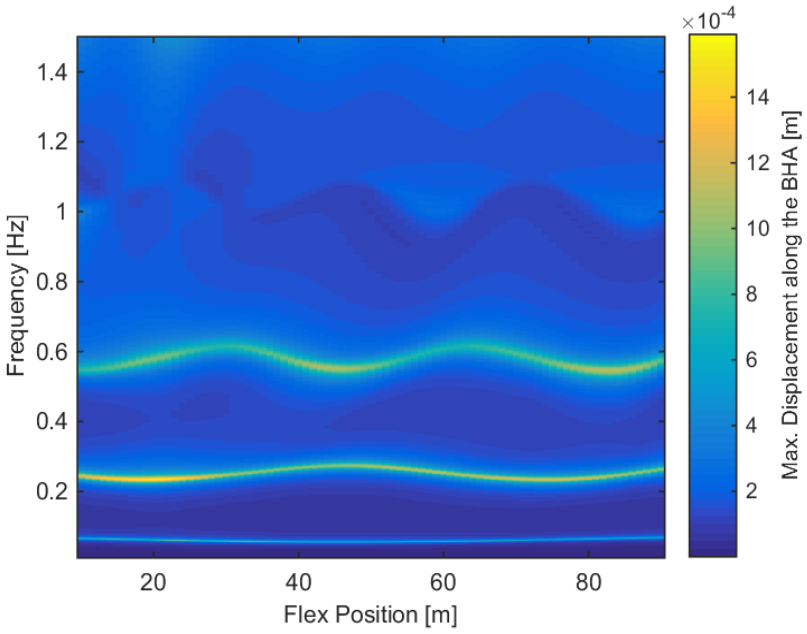

Fig. 3.71: Max. lateral displacement for all flex-sub positions The excitation source is located at 25 m from the bit. The highest displacement values occur at relatively low frequencies and alternate between the second and third mode.

It has been observed that bending moment values show only a small variation along the different flex-sub positions. This phenomenon can be related to the constant bending stiffness distribution along the BHA model. The flex-component reduces the bending stiffness but its length remains constant and the impact is rather small compared to the overall model bending stiffness. The variation of the overall maximum bending moment along the length and frequency range can be seen in Fig. 3.72. Fig. 3.73 illustrates the constant behavior of the ratio between bending stiffness and mass distribution. The highest bending moment values occur also at

relatively low frequencies and for flex-component positions close to the excitation source. Plots for the acceleration and velocity can be found in Appendix F.

A flex-sub decreases the strain energy of the BHA model, especially if the component is placed at a certain distance from the excitation source. This optimum is highly dependent on the excitation location and type of excitation. For this particular excitation the optimum flex-sub placement is located between 50 m and 60 m from the bit and directly behind the bit. A flex-sub starting or terminating directly at the excitation source has proven to be disadvantageous. Such a configuration, as shown in Fig. 3.74, has resulted in the highest amplitude response. Further plots for all physical quantities can be found in Appendix F. Comparing Fig. 3.72 with Fig. 3.68 shows a difference in the bending moment maxima and the maximum lateral displacement curve. This is related to the mathematical computation of these two parameters. Displacement is calculated from the first derivative of the beam equation, whereas the bending moment depends on the second order derivative of the same equation.

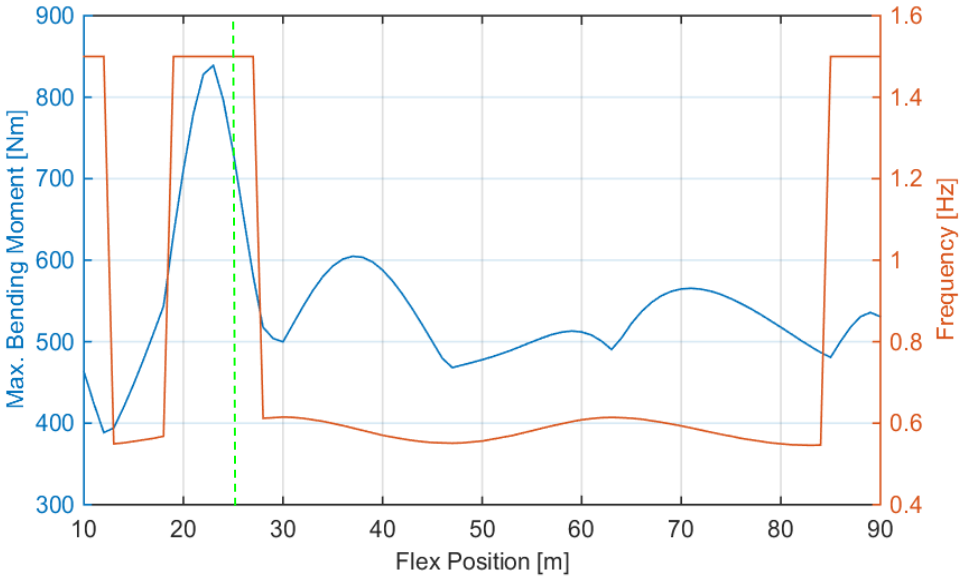

Fig. 3.72: Max. bending moment for all flex-sub positions and across the whole frequency range. Most of the maximum values occur at frequencies around 1 Hz and higher. The dashed green line indicates the excitation source position.

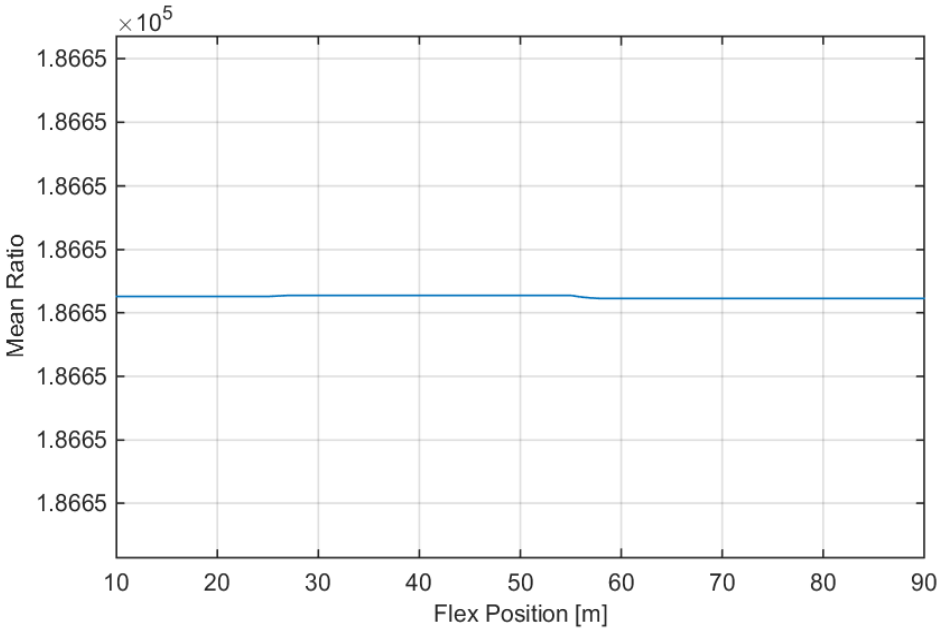

Fig. 3.73: Mean ratio between bending stiffness and mass distribution for all flex-sub positions. The ratio produces a constant value for every position due to the constant length of the flex-sub, thus the y-axis shows a constant value. The inconsistency in the shown horizontal line is related to the used MATLAB plotting function and not to the data set.

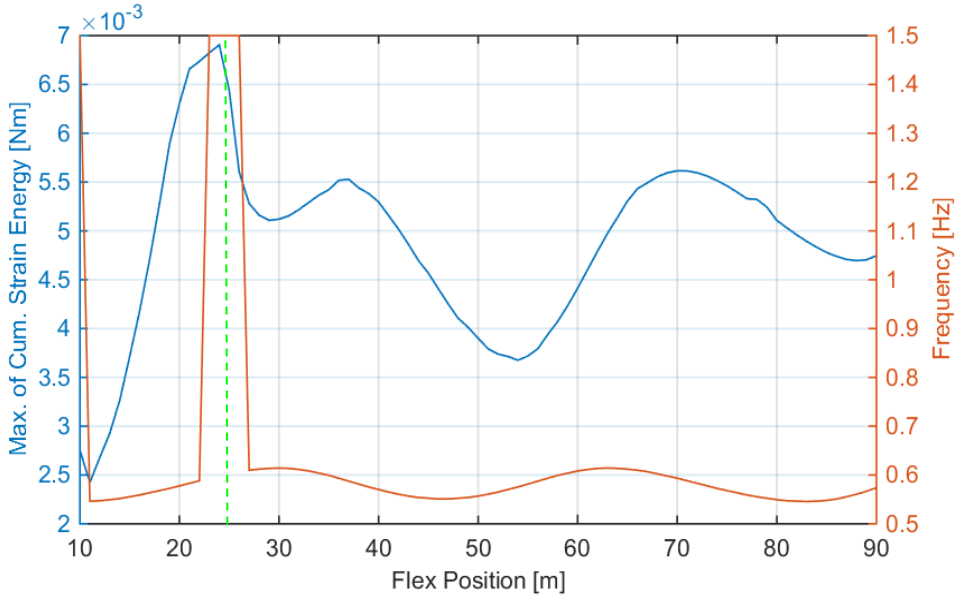

Fig. 3.74: Maxima of the cumulative strain energy across all frequencies for all flex-sub positions. The highest strain energy value occurs directly at the excitation source (dashed green line).

Summary

A flex-sub decreases the natural frequencies and influences the normal mode shapes due to a reduction in bending stiffness. This effect is comparable to the observations from the other diameter change configurations. The impact of the flex-sub on the overall bending stiffness is limited since the component length of 5 m remains constant throughout every calculation step whereas the bending stiffness of the other diameter change models decreases as the simulation proceeds. A change in the flex-sub length changes the magnitude in bending

stiffness and mass reduction. Therefore, the overall natural frequency behavior is directly dependent on the flex-sub length. This small shift in natural frequencies of the whole BHA could be beneficial in mitigating resonance problems and protecting critical areas from harmful lateral vibrations. However, this would require accurate knowledge of the excitation amplitude and location. The fact that a reduction in bending stiffness can be achieved through a tapered BHA or a flex-sub leaves the decision of the appropriate selection up to the engineer in charge. A design which can mitigate lateral vibrations due to a mass imbalance somewhere in the BHA could be ineffective to compensate vibrations excited through the bit or otherwise. A flex-sub placement provides another way of mitigating lateral vibrations but might not be the only possible option available. Stabilizer placement could also lead to the same amount of vibration reduction. The choice of mitigation procedure is also influenced by other BHA requirements such as steering capabilities, tool limits, spacing and measurement requirements. These features could outweigh slight dynamic advantages.

3.1.5 Parameter Study Summary and Conclusion

The transfer matrix method has been validated by means of this small scale parameter study on simple model configurations. Examination of different display formats for the presentation of the physical response of lateral vibrations has led to the selection of the diagram styles deemed most suitable for later interpretation and analysis. The color coded presentation is most useful for showing the maxima of every configuration and their corresponding frequencies. Further consolidation has led to the line plot of the overall maximum amplitude and related frequency. This provides an easier identification of critical configurations and is therefore used for the optimization steps. The parameter study has highlighted the impact of small configuration changes on the lateral vibrations system.

The model is capable of demonstrating the impact of stabilizers and the influence of various stabilizer positions on lateral vibrations. The obtained results reflect and confirm industry wide expectations of stabilizer impact on a dynamic drilling system. Excitation source positions and different excitation types significantly affect the system response. A certain BHA design is not necessarily effective in mitigating lateral vibrations from different excitations. BHA Design and performance is highly excitation dependent and no general purpose design, incorporating all possible vibration sources, can be defined. The application of adding stabilization close to the bit in assemblies has been justified. These components can reduce the magnitude of lateral vibrations, originating directly from the bit, under the prerequisite of appropriate stabilizer spacing. A stabilizer could increase physical amplitudes if positioned too far away from the bit. Diameter changes show less influence on the vibration system as stabilizers since these changes do not introduce any additional nodes to the system. However, the model configurations have shown a dependency of natural frequencies and normal mode shapes on mass distribution and bending stiffness changes. Mass and stiffness alterations have shown to shift higher resonance frequencies into the frequency range under investigation. This is essential for BHA design considerations and should not be neglected. The integration of flex-subs has been justified through a static BHA analysis so far. Flex-subs are used to reduce the static bending moment in critical areas and to alter BHA steering capabilities by changing the

overall BHA stiffness. The used Flex-Sub model configuration shows that these components can deliver a decisive contribution to the mitigation of lateral vibrations.

The highly simplified model length and configurations are not directly related to real BHA applications. Real systems allow only discrete stabilizer positions and other modifications and no changes within physical tools. The validation of a generalized model with a continual parameter variation confirms that the methodology can be performed on more detailed BHA models with discrete variations. The configuration variations have enabled the generation of high resolution diagrams which allow a better visualization of small changes along the model length and frequency spectrum. Care should be taken with the amplitude response of the model configuration. A mass imbalance was used as the excitation source. In reality, lateral vibrations are not necessarily introduced from a mass imbalance, e.g. a whirling bit. However, modeling for example a whirling bit as a mass imbalance is a good enough approximation of reality. The parameter study provides the foundation for a presentation method, showing the general trend and behavior of lateral vibrations. The introduction of well-known excitation sources and real BHA geometries would deliver more realistic results in terms of vibration severity and amplitude location. The simple parameter study model was validated with the Baker Hughes in-house FEM software BHASYSPro. An identical model setup has shown the same results for natural frequencies and normal modes. This validation has been done prior this study. The validity of the results in terms of real drilling applications should be done with field data.

All conducted modifications have demonstrated that certain configurations, under the given excitation source, lead to a reduction in lateral vibrations. Other configurations have contributed to an amplification of lateral vibrations and should therefore be omitted. These insights have been used to construct optimization approaches which can be used during the BHA design planning phase. The consolidated line plot of the overall configuration maxima provides the basis for the optimization considerations.

3.2 Formulation of a Design Criterion for Lateral Vibrations

Drilling vibrations are to some extend inevitable. Loads and motion required for the well bore construction process are directly linked to vibrational phenomena and other manifestations of energy dissipation. Whether BHA components fail, depends on the magnitude and duration of different vibration modes. Hence, BHAs can be run at vibrations under certain circumstances and limitations. These limitations depend on the assembly properties such as used materials, component configuration, flexibility and stabilization. Furthermore, operational parameters such as rotary speed and WOB impact the vibration tendency of a BHA.

Hence, some design criteria incorporate operational parameters and others build upon BHA properties. Both aim for comparability between different BHA designs based on their vibration susceptibility. This should allow the selection of the best BHA design from a broader selection of possible configurations. Criteria can also include a threshold value for certain parameters which indicate ranges for safe drilling loads and areas where drilling would lead to severe vibration problems. The formulation of design criteria is not a new concept and attempts for different vibration types have been made during the past decades.

The conducted parameter study shows the influence of different configurations on lateral vibrations and which physical quantities are most useful for constructing a new design criterion for mitigating lateral vibrations in drilling assemblies. The strain energy has been found to be most useful for quantifying and comparing different model configurations and is the foundation of the following criterion proposal. Additionally, other parameters are included to incorporate local tool limitations which would be neglected by a plain strain energy consideration. Stabilizers have shown to have the biggest influence on the vibration system of the model configurations under investigation.

Every optimization criterion is based on assumptions and uses selected input parameters. The results are only valid for the given environment. If the real world application differs from the computed results, all chosen optimum positions become irrelevant and the model validity is questionable. This does not necessarily lead to the conclusion that the assumptions and computations are wrong, stating only, that they do not match the real drilling environment. Hence, every optimization criterion should be used with care and the fundamental assumptions should be cross-checked with the actual drilling operation.

3.2.1 Assembly Optimization – Vibration Mitigation (AOVM) – Procedure

If vibrations occur during drilling, their magnitude and destructive nature can be restricted. Minimizing the susceptibility of BHAs to lateral vibrations starts with the planning and design phase. Proper stabilizer placement and tool geometries can reduce the likelihood and severity of lateral vibrations by shifting natural frequencies and introducing additional nodes to the vibration system. The enforcement of dynamic load limits and safe operating windows should serve as a follow-up control on the optimization steps.

Such a procedure is highly dependent upon assumptions and underlying computational models. The results obtained from such an optimization hold only true for this particular case. The optimization output has limited validity, if the downhole conditions deviate significantly from the modeled parameters, especially in terms of excitation source properties and BHA configuration. The presented assembly optimization and vibration mitigation procedure (AOVMP) should be used as a tool for reducing the overall probability of severe vibration impact on the BHA under investigation.

The BHA vibration mitigation utilizes the strain energy allocated in the assembly components. The strain energy depends on the BHA length segment and excitation frequency under investigation. Since the overall BHA performance is of interest, the strain energy values of every length segment are used to construct a cumulative strain energy value. This cumulative sum represents the stored energy inside a BHA for one particular frequency and BHA configuration. These values can be represented on a frequency versus strain energy plot as shown in Fig. 3.75 to compare the cumulative strain energy across the whole frequency bandwidth.

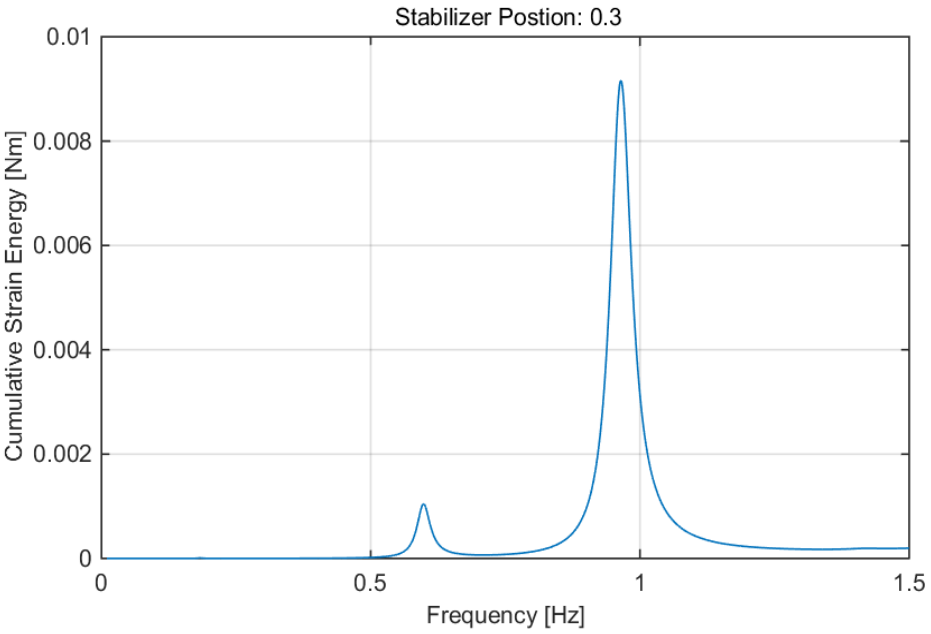

Fig. 3.75: Cumulative strain energy for every frequency step. This particular BHA configuration has a single stabilizer at 30 m from the bit.

The plot shown in Fig. 3.75 is useful for analyzing one specific BHA configuration. This stabilizer position from Fig. 3.75 is not necessarily the best position along the BHA for mitigating lateral vibrations. To find the optimum stabilizer position in terms of lateral vibrations, such a plot would have to be generated for all possible stabilizer or geometry configurations. This approach would lead to several plots, making it difficult to find out the optimum placement.

To incorporate all possible assemblies in one plot, the frequency dependent strain energy information has to be consolidated into one value for every BHA configuration. The length cumulative strain energy values are summated across the entire frequency range. This generates one strain energy value for every BHA configuration. These single values can now be compared with each other to determine the assembly with the lowest strain energy value. The strain energy values are normalized to the maximum strain energy value to allow a better comparison of different designs. Fig. 3.76 shows an example of such an optimization plot for various stabilizer configurations. This plot is generated using the stabilizer position variation model as stated in Chapter 3.1.1. Similar plots for the bit excitation, diameter change and flex-sub model configurations can be found in Appendix G. Comparing various positions on one graph allows a quick identification of the optimum position which would result in the lowest strain energy. The normalization process directly ranks the different designs, stating for example that Design A is ten times better than Design B due to lower strain energy values by a factor of ten across the whole frequency bandwidth.

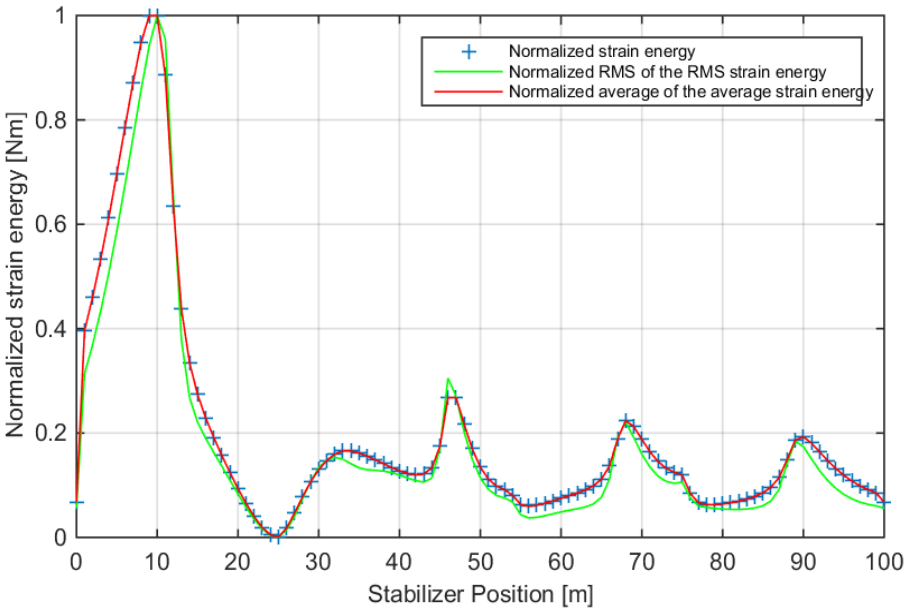

Fig. 3.76: Normalized summated strain energy values across the length and frequency for every configuration. The strain energy value yields zero for a stabilizer located directly at the excitation location. Three different calculation methods have been used. The average, sum and root mean square of the strain energy across the length and frequency range.

The obtained optimum position states that this location would yield the lowest strain energy inside the BHA across the entire frequency spectrum under investigation. This diagram type eliminates the possibility of determining resonance frequencies for any position, since the summation along the frequency incorporates resonance and out of resonance steps. The so found optimum states that, even in the case of resonance, the vibrations are considered less harmful to the drilling system compared to other stabilizer or geometry positions. Fig. 3.76 shows 101 different BHA configurations. Real drilling assemblies do not provide the same degree of freedom in stabilizer placement or geometry alterations as shown here. Other tools such as MWD/LWD, motors or telemetry and power generation units reduce the possible options for stabilizer placement. Some tools have already a stabilizer incorporated in their body. This reduces the data density of the plot, rupturing the smooth line presentation. Therefore, a bar diagram should be used to provide better means of visualization. The results of a stabilizer parameter study with four different stabilizer positions can be seen in Fig. 3.77.

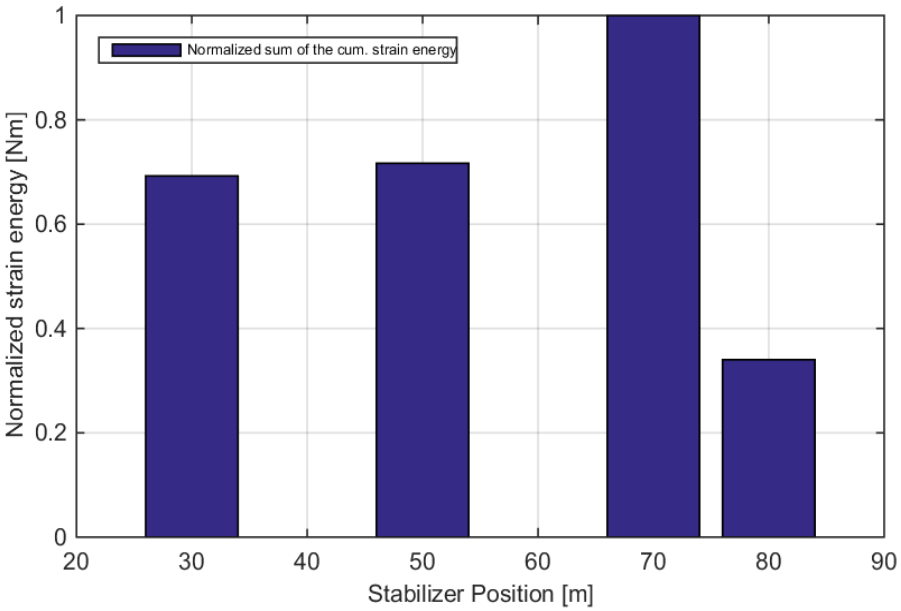

Fig. 3.77: Normalized summated strain energy values across the length and frequency for four selected stabilizer positions. This plot represents four possible choices for single stabilizer on a given BHA. The simulation suggests that a stabilizer located at 80 m from the bit would yield the lowest strain energy value across the investigated frequency spectrum.

However, this does not guarantee that the BHA will not fail due to lateral vibrations because of the lack of distinction between resonances and out of resonance frequencies. The magnitude of the occurring dynamic loads determines if vibration related failure is probable.

The identification of resonance frequencies for the selected optimum requires the investigation of the frequency plot, similar to Fig. 3.75, for that particular BHA configuration. This allows the determination of critical frequencies or, if multiplied by 60, critical rotary speeds. The employment of this optimization makes a comparison between various BHA designs possible. Plain critical speed analyses are limited in this regard.

If resonance frequencies are found, the critical loads should be investigated in addition to the standard critical speed analysis execution. As previously stated in Chapter 2.4.2, a BHA can endure vibrations up to a certain level and duration. State of the art dynamic design from a mechanical engineering point of view relies on running hour and load cycle recommendation to incorporate maximum dynamic loading limits. Application engineering focuses on the identification of critical rotary speeds and assurance of avoiding these speeds by all means. The proposed dynamic load limit should bridge the gap between the mechanical and application engineering approach.

The total BHA load is comprised of an alternating bending moment due to rotation and vibration loading. If the overall load exceeds the limit of a particular component, the given BHA is exposed to an increased failure risk. Hence, the total load must not exceed the defined load limits. The total dynamic bending moment for every BHA component can be defined as the rotating bending moment, superimposed by the lateral vibrations bending. (Eq. 3.9) (Linke 2014):

$$M_{b,total} = M_{b,rotating} + M_{b,lateral} \qquad \textbf{Eq. 3.9}$$

This total dynamic bending moment must not exceed the maximum allowable bending moment:

$$M_{b,total} \leq M_{b,allowable} \qquad \textbf{Eq. 3.10}$$

Or in terms of a safety factor:

$$SF = \frac{M_{b,allowable}}{M_{b,total}}, \qquad SF \geq 1 \qquad \textbf{Eq. 3.11}$$

A safety factor of 1 is recommended for standard operations but should be increased to higher limits for sensitive sensor components and critical operations with an increased risk of failure. The bending moment has been used since tool limits cannot be defined through the strain energy stored inside the BHA. Local bending moments could exceed the component limits whereas the overall strain energy of the entire assembly might be at non critical levels. This bending moment threshold can be implemented into the frequency charts as shown in Fig. 3.78 and Fig. 3.79. Such an investigation should follow directly after the identification of the optimum position.

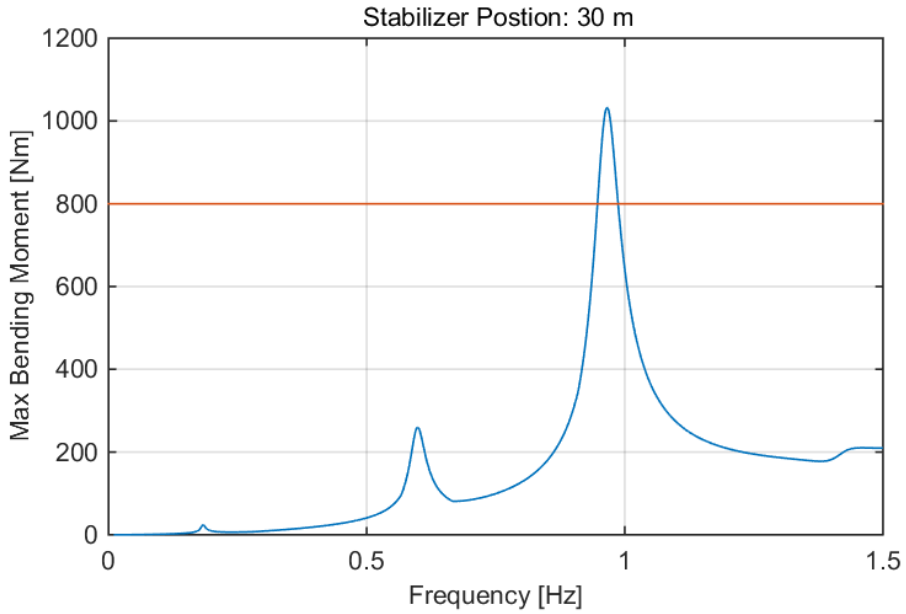

Fig. 3.78: Critical frequency plot for a BHA configuration with a stabilizer 30 m from the bit. The max. bending moment threshold has been set at 800 Nm which identifies frequencies around 1 Hz to be critical to the BHA. Note that this bending moment represents only the lateral vibration component without the rotating bending moment.

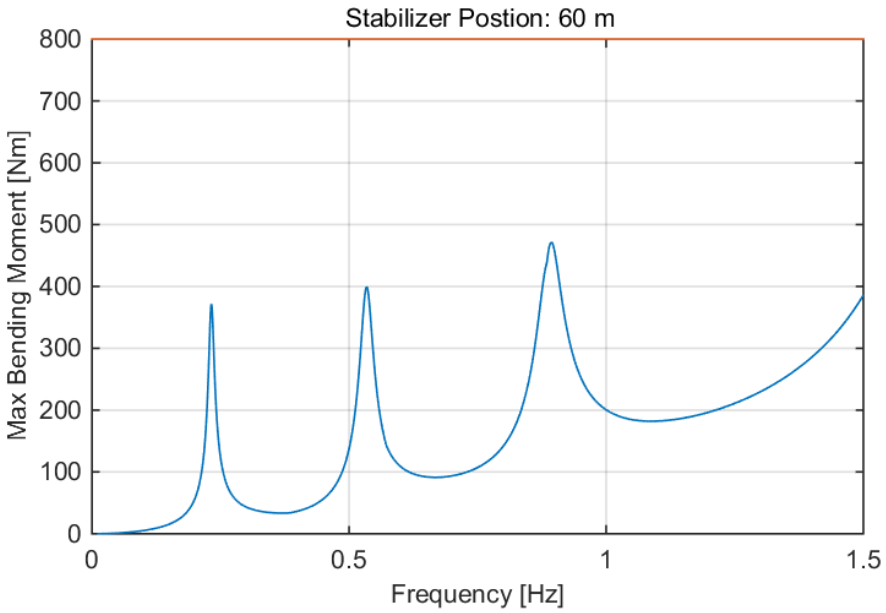

Fig. 3.79: Critical frequency plot for a BHA configuration with a stabilizer 60 m from the bit. The max. bending moment threshold of 800 Nm indicates that this particular BHA configuration will not fail under the given excitation and within the presented frequency range.

The relative strain energy based comparison between two or more BHAs is not influenced by the excitation amplitude. However, if the dynamic bending moment exceeds tool specifications, depends on the amplitude of the excitation force. As shown in Fig. 3.78 and Fig. 3.79 some resonances are far below the set tool limitation for bending moment. An increase in mass imbalance leads directly to an increase in physical amplitude. This could elevate previously non-critical frequency areas above the set tool limit.

Excitation amplitudes are hardly known for actual downhole conditions, making precise decisions beyond the scale of a parameter study impossible to do. Though unknown, the maximum possible physical amplitude is limited by the borehole wall. The parameter study is not restricted by any wall contacts and can generate for example displacements of 0.5 meters which would not be possible in an actual drilling environment. This displacement limitation can be used to approximate the maximum possible amplitudes. Scaling the excitation source to these specifications improves the applicability of the bending moment analysis. Downhole bending moment data acquired via strain gauges or tool memory aids in assessing the maximum amplitudes and can serve as a baseline for future BHA designs. If no amplitude statements are possible, the application engineer should focus on relative BHA comparisons.

3.2.2 Overall BHA Design Optimization

The vibration mitigation and optimization steps should be imbedded into a BHA specification catalog which combines steering, static, dynamic and other assembly requirements and limits. The selected parameters should allow for a proper BHA design comparison and serve as a foundation for the implementation of automated optimization processes.

Above all, BHAs under investigation have to meet the steering requirements of achieving the planned build up rates and tolerate the dog leg severities.

A BHA which cannot drill to the desired target coordinates should not be investigated any further and adjustments should be made to enhance steerability. Static load limits and the degree of capacity utilization should be determined prior to the dynamic analysis, since dynamic load scenarios are superimposed on the static loads. BHA designs which cannot withstand sole static wellbore conditions require thorough re-engineering. A contact force limitation should be incorporated into the static BHA criterion. Side forces acting on critical and sensitive areas such as electronic sleeves or measurement sections could damage the tool during operation and hence compromise BHA integrity and service deliverability. The dynamic loads should also remain within the specifications of every component. Furthermore, BHA design should aim for a strain energy minimization since this parameter is directly related to vibration severity. If all these criteria are met by more than one BHA configuration, the assembly with the least amount of modular connections and other geometry changes should be preferred. A reduction in modular connections and diameter changes reduces the risk of BHA failure due to stress concentration and parting connections. The proper radial clearance for every BHA size should be achieved to avoid unnecessary wall contact which in turn could lead to contact forces in sensitive areas and changes in dynamic behavior. Tab. 3.5 provides an overview of the corner stones in BHA comparison and optimization. The layout of Tab. 3.5 represents the importance of every optimization category from top to bottom. During engineering, this top-down sequence should be followed to ensure a quick elimination of BHA designs unsuitable for the assigned drilling project.

Tab. 3.5: Specification catalog for BHA comparison and optimization steps.

Category	Parameter	Description
Steering	build up rate	Target BUR +/- uncertainties
Static Loading	dog leg severity and static bending	$\mathrm{DLS} < \mathrm{DLS}_{\mathrm{critical}}$ $\mathrm{M_b} \leq \mathrm{M_{b,allowable}}$
	contact forces	$\mathrm{F_{lat.}} \leq \mathrm{F_{lat.,allowable}}$
Dynamic Loading	dynamic bending	$\mathrm{M_b} \leq \mathrm{M_{b,allowable}}$
	strain energy	$\mathrm{E_{strain}} \rightarrow \min$
Geometry	radial clearance	Avoid wall contacts in critical areas
	No. of modular connections	$\sum \mathrm{mod.\,connections} \rightarrow \min$
	No. of OD/ID changes	$\sum {}^{\mathrm{OD}}/_{\mathrm{ID}}\ \mathrm{changes} \rightarrow \min$

These 4 categories can be used to set up an evaluation guideline to analyze a given BHA design based on its overall performance in steering, static and dynamic loading.

Well plan and operational loads are normalized to certain BHA requirements and properties based on simple ratios. Ratios close to 1 indicate a BHA design which fulfills all mandatory requirements but its full optimization potential has not been exploited yet. BHAs with values close to 0 show a higher degree of optimization and should be favored compared to designs with values close to 1.

Ratios concerning the steering capabilities of an assembly are put in relation with the BUR requirements (Eq. 3.13) and BHA DLS limitations (Eq. 3.14).

BUR predictions exhibit a certain inaccuracy and therefore a safety factor should be included when working with these values. Field experience has shown that a safety factor of 2 °/100 ft is sufficient. This new parameter is indexed as “pseudo well plan” (Eq. 3.12). The BUR_{ratio} demands: $DLS_{pseudo\ well\ plan} \leq BUR_{BHA\ capabilty}$. Very similar values, producing a BUR_{ratio} close to 0, indicate a BHA with an optimum stiffness – flexibility relationship. An excess of BHA capability shows an assembly too flexible and potentially difficult to steer along the planned trajectory. BHAs with capabilities below the set DLS goal are not suitable for achieving the desired steering performance and must not be considered.

The DLS_{ratio} is used to investigate if the static bending load limits are exceeded or not. A BHA configuration could achieve the desired BUR but material limitation could increase the risk of failure above a certain bending moment threshold. The smaller the DLS_{ratio} the smaller the bending loads for this particular design. BHA DLS tolerances must not be smaller than the well DLS. Otherwise the BHA is exceeding its bending moment limit. Investigating small $DLS_{well\ plan}$ values in the range of 0.1 to 1°/30 m would lead to unusual small ratios, since even stiff BHAs allow DLS of values higher than 2°/30 m. This, however, is tool size dependent. It is not necessary to apply this DLS_{ratio} in tangent sections or if the planned DLS is below 1°/ 30 m.

$$DLS_{pseudowell\ plan} = DLS_{well\ plan} + 2°/100ft \quad \textbf{Eq. 3.12}$$

$$BUR_{ratio} = 1 - \frac{DLS_{pseudo\ well\ plan}}{BUR_{BHA\ capability}} \quad \textbf{Eq. 3.13}$$

$$DLS_{ratio} = \frac{DLS_{pseudo\ well\ plan}}{BHA\ DLS_{max,allowable}} \quad \textbf{Eq. 3.14}$$

The next parameter ratio considered is contact forces (Eq. 3.15). All contact forces are evaluated against their allowable threshold. Then the ratio yielding the highest value is selected to account for the worst case scenario of the entire BHA. As for the steering parameters, an excess of the allowable loads leads to a drop out of the BHA design under considerations and reengineering is required. In Eq. 3.15 n indicates the number of contact forces under investigation. For example 20 different contact forces might be considered and then the contact force yielding the highest ratio (worst case) should be selected for further considerations.

$$Contact\ Force_{ratio} = \frac{\max(Contact\ Force_n)}{allowable\ Contact\ Force_n} \quad \textbf{Eq. 3.15}$$

A ratio for the dynamic loads (Eq. 3.16) uses the bending moment due to lateral vibrations, superimposed on the rotating bending moment as stated in Eq. 3.9. The dynamic bending moment ratio is bound to the same limitations as stated for the AOVM procedure, especially to the uncertainties concerning the excitation amplitude. It is not possible to state if a system with more resonance frequencies but small amplitudes is more or less severe than a system with fewer resonance frequencies but high amplitudes. The only real indicator is BHA failure.

$$M_{b,dynamic} = \frac{BHA\ M_{b,dyn}}{allowable\ M_{b,dyn}}$$ **Eq. 3.16**

The geometry input, of both, the number of connections and diameter changes, is based on the total BHA length:

$$No.Connections_{ratio} = \frac{\sum Connections}{L_{BHA}}$$ **Eq. 3.17**

$$No.Diameter\ Changes_{ratio} = \frac{\sum Diameter\ Changes}{L_{B\ HA}}$$ **Eq. 3.18**

A BHA design with fewer connections would have increased downhole reliability due to a reduction in possible connections failures. Diameter changes, especially upsets could reflect stick-slip vibrations, causing more severe downhole vibrations than initially present. *"It has further been discovered that torsional waves traveling along the drill string vary the sensitivity of the drill string to backward rotation of the bit. Indeed, such torsional waves can travel up and down the drill string and lead to backward rotation of the bit even after the bit has become stuck." (Reckmann et al. 2011)* Furthermore, the chance of hanging up the BHA with a high number of diameter changes is increased and pack-offs could occur through cuttings accumulation (Warren 1940). This could counteract stabilizer placement for vibration mitigation. These phenomena depend on hole quality and other drilling parameters. Hence, this parameter should be used with great care and can be excluded from the considerations for an overall drilling performance parameter.

It should be noted that this optimization approach should not be used to compare BHAs of different wells or well sections. A proper comparison is only possible for BHAs within the same well environment and operational parameters. Changing these boundary conditions would alter the foundation for this BHA comparison.

4 Conclusion and Outlook

The parameter study shows the behavior of simple tubulars under the influence of mass imbalance induced lateral vibrations. Variations in geometry and stabilization have led to a better understanding of vibration effects, especially which components and configurations mitigate or enhance lateral vibrations. These different modifications yield a selection of the most suitable representation methods and the definition of key parameters for further BHA vibration optimization steps. An indicator, which describes BHA vibration susceptibility best, is the cumulative strain energy. The strain energy is an indicator of how much energy from the excitation source is transferred into BHA deformation. The smaller this energy value becomes the smaller the overall vibration severity is. This approach considers the entire assembly and neglects tool limitations and does not consider frequency dependent information. Furthermore, a plain energy view does not allow the identification of local high load areas which could exceed tool limitations. Although the usefulness of the strain energy has been well established, the benefit of this approach can be maximized if it is considered together with a modification of the critical speed analysis. This additional step introduces tool limitations for bending moment and a frequency dependency, allowing resonance frequency statements.

An optimization formulation, such as the AOVM-Procedure, utilizes this knowledge to select from a range of possible BHA configurations, the one with the smallest cumulative strain energy value. This procedure is solely based on dynamic load scenarios. Therefore, this formulation is integrated into an overall BHA evaluation which incorporates steerability, statics and BHA geometry.

To further reduce the error rate and BHA design efforts, the AOVM-Procedure should be implemented into a MATLAB algorithm. A design engineer should focus on the interpretation of the results and not on the required steps. These steps can be easily done by a fully automated script. Additionally, a script significantly reduces the human error and subjectivity during the selection of optimum BHA configurations. The algorithm should identify the optimum stabilizer position or the optimum location of other geometric properties of a given BHA which can be changed along the BHA length. A basic optimization algorithm would be the “fmin-search” function which is readily implemented into the MATLAB environment. This function is based on an unconstrained nonlinear optimization algorithm. This algorithm finds the minimum of a scalar function, originating from an initial value. The function “fmin-search” relies on the Nelder-Mead simplex algorithm for nonlinear unconstrained optimization as described in (Lagarias et al. 1998; Nelder, Mead 1965).

The overall concept of mitigating lateral vibrations should be introduced into advisory software, providing a sophisticated tool for an enhanced design process. This would allow for a real-time natural frequency determination, in line with drilling parameters changes. The driller would see a continuous critical speed analysis, which allows the driller to adjust the drilling parameters according to the actual downhole environment. The offline modus should be used as a pre-analysis tool for the BHA design phase prior the tool is run in hole. This application builds on the

design criteria defined in this work, for comparing different BHA design based on their vibration susceptibility and is going to be conducted by (Gorelik et al. 2015).

The parameter study should be extended to include more excitation source variations. Random distributions would allow a transfer of the actual excitation source uncertainty from drilling to the simulation environment. An excitation source domain could be used to generate a random excitation input with a probability distribution over the domain. Then, a deterministic computation should be performed on the inputs and the results should be aggregated. These steps are achievable with a Monte Carlo Simulation. A Monte Carlo Simulation is a stochastic procedure which is based on a large number of random experiments. Analytically unsolvable or costly solvable problems are solved numerically with the probability theory. Such experiments can be either achieved in reality or, as for this case, with simulations based on random numbers (Metropolis, Ulam 1949).

More realistic BHA models with actual length and dimensions, reflecting the complex assembly geometry, would enable to further close the gap to the real drilling environment. First attempts in this direction could be the introduction of multiple stabilizers, multiple geometry changes and actual tool dimensions.

The main challenge remains the uncertainty of the excitation source assumptions which induces vibrations in the first place. Excitation location and amplitude considerably affect the vibration response. Excitation source variations can induce different physical amplitudes at different resonance frequencies. The amplitude magnitude defines component failure at any given resonance frequency. Strong deviations of the excitation assumptions from the actual case could lead to misjudgment of the vibration susceptibility and therefore to wrong optimization conclusions. More research should take place on this topic in the near future.

5 Publication bibliography

1. Aadnøy, Bernt S.; Cooper, Iain; Miska, Stefan Z.; Mitchell, Robert F.; Payne, Michael L. (2009): Advanced Drilling and Well Technology. Richardson, Texas: Society of Petroleum Engineers (SPE Textbook Series). 978-1-55563-145-1.
2. Aadnøy, Bernt Sigve (2006): Mechanics of drilling. Aachen: Shaker. 3-8322-4861-7.
3. Aelfers, Florian (10/26/2015): Conflicting BHA Design. Stabilization and Flexibility. Interview with Olof Hummes, Christian Linke. Baker Hughes Celle Technology Center.
4. Aldred, W. D.; Sheppard, M. C. (1992): Drillstring Vibrations: A New Generation Mechanism and Control Strategies. Society of Petroleum Engineers. SPE ACTE Washington D.C. (SPE 24582-MS). DOI: 10.2118/24582-MS.
5. Bailey, Jeffrey R.; Biediger, Erika; Gupta, Vishwas; Ertas, Deniz; Elks, William Curtis, Jr.; Dupriest, Fred E. (2008): Drilling Vibrations Modeling and Field Validation. Society of Petroleum Engineers. SPE/IADC Drilling Conference Orlando, Florida (SPE 112650-MS). DOI: 10.2118/112650-MS.
6. Bailey, Jeffrey R.; Remmert, Stephen M. (2010): Managing Drilling Vibrations Through BHA Design Optimization. In *SPE Drilling & Completion*, pp. 458–471. DOI: 10.2118/139426-PA.
7. Bailey, Jeffrey R.; Wang, Lei; Tenny, Matthew; Armstrong, Neil Robert; Zook, Jason R.; Elks, W. C., Jr. (2010): Design Tools and Workflows To Mitigate Drilling Vibrations. Society of Petroleum Engineers. SPE ATCE Florence, Italy (SPE 135439-MS). DOI: 10.2118/135439-MS.
8. Balke, Herbert (2014): Einführung in die Technische Mechanik. Festigkeitslehre. 3., aktualisierte Aufl. 2014. Berlin, Heidelberg, New York: Springer-Verlag; Springer Berlin (Springer-Lehrbuch). 978-3-642-40980-6.
9. Besaisow, Amjad A.; Payne, Mike L. (1988): A Study of Excitation Mechanisms and Resonances Inducing Bottomhole-Assembly Vibrations. In *SPE Drilling Engineering* 3 (01), pp. 93–101. DOI: 10.2118/15560-PA.
10. Bourgoyne, Adam T.; Millheim, Keith K.; Chenevert, Martin E.; Young, F. S. (1991): Applied Drilling Engineering. Richardson, Texas: Society of Petroleum Engineers (SPE Textbook Series, 2). 1-55563-001-4.
11. Burgess, T. M.; McDaniel, G. L.; Das, P. K. (1987): Improving BHA Tool Reliability With Drillstring Vibration Models: Field Experience and Limitations. Society of Petroleum Engineers. SPE/IADC Drilling Conference, New Orleans, LA (SPE 16109-MS). DOI: 10.2118/16109-MS.
12. Butt, Imran (2015): PDC Bit Steerability. Baker Hughes. Global (Baker Hughes Training Material).

13. Dareing, Don W. (1982): Applied Drill String Mechanics. Houston, Texas: Maurer Engineering Inc.

14. Dubbel, Heinrich; Beitz, Wolfgang; Grote, Karl-Heinrich (2001): Taschenbuch für den Maschinenbau. 20., neubearb. u. erw. Aufl. Berlin [u.a.]: Springer. 3-540-67777-1.

15. Dueber, H. (2008): Stabilizer Design Standard. Baker Hughes. Celle, Germany (BHI Specifications and Standards).

16. Dueber, H.; Gatzen, M. (2013): Mechanical Design Specifications Manual. Baker Hughes. Celle, Germany (BHI Specifications and Standards).

17. Dunayevsky, V. A.; Abbasslan, Fereldoun; Judzis, Arnis (1993): Drilling Stability of Drillstrings Under Fluctuating Weight on Bit. In *SPE Drilling & Completion* 8 (02), pp. 84–92. DOI: 10.2118/14329-PA.

18. Eltrissi, Mohammad Mokhtar (2009): Additional Parameters for better Vibration Control. Society of Petroleum Engineers. SPE/IADC Middle East Drilling Technology Conference, Manama, Bahrain (SPE 125457-MS). DOI: 10.2118/125457-MS.

19. FKM (2012): Rechnerischer Festigkeitsnachweis für Maschinenbauteile aus Stahl, Eisenguss- und Aluminiumwerkstoffen. 6., überarb. Ausg. Frankfurt am Main: VDMA-Verl. (FKM-Richtlinie). 978-3-8163-0605-4.

20. Gasch, Robert; Knothe, Klaus; Liebich, Robert (2012): Strukturdynamik. Diskrete Systeme und Kontinua. 2. Aufl. 2012. Berlin, Heidelberg: Springer (SpringerLink : Bücher). 978-3-540-88977-9. DOI: 10.1007/978-3-540-88977-9.

21. Gorelik, Ilja; Westermann, Henrik; Said, Bilel (2015): On the Concept of a new Lateral Advisor and parameter studies at the Scaled Rig. With assistance of Oliver Höhn. Baker Hughes. Celle, Germany (Technical Report).

22. Gupta, Rajdeep (2008): Rotary Steerable. Baker Hughes. Global (Webinar Presentation).

23. Heisig, G.; Neubert, M. (2000): Lateral Drillstring Vibrations in Extended-Reach Wells. Society of Petroleum Engineers. SPE/IADC Drilling Conference, New Orleans, Louisiana (SPE 59235-MS). DOI: 10.2118/59235-MS.

24. Heisig, Gerald (1993): Braunschweiger Schriften zur Mechanik. Zum statischen und dynamischen Verhalten von Tiefbohrsträngen in räumlich gekrümmten Bohrlöchern. Dissertation. Technical University of Braunschweig, Braunschweig.

25. Herbig, Christian (2015): Hess Tubular Bells #5 (WI-E). 16 1/2 x 19 1/2 Section Analysis. Baker Hughes. Celle, Germany (BHI Customer Presentations).

26. Hohl, Andreas; Hohl, Carsten; Herbig, Christian (2015): A Combined Analytical and Numerical Approach to Analyze Mud Motor Excited Vibrations in Drilling Systems. ASME. ASME Turbine Technical Conference, Montréal, Canada.

27. Hummes, Olof (2010a): Rotary Steerable Systems. Part I: Introduction RSS, AutoTrak Priciples. Baker Hughes. Celle, Germany (BHI Customer Presentations).

28. Hummes, Olof (2010b): Rotary Steerable Systems. Part II: AutoTrak Operation + Service Levels. Baker Hughes. Celle, Germany (BHI Customer Presentations).

29. Jansen, J. D. (1992): Whirl and Chaotic Motion of Stabilized Drill Collars. In *SPE Drilling Engineering* 7 (02), pp. 107–114. DOI: 10.2118/20930-PA.

30. Jürgler, R. (2004): Maschinendynamik. 3., neu bearb. Aufl. Berlin: Springer (VDI-Buch). 3-540-40599-2.

31. Lagarias, Jeffrey C.; Reeds, James A.; Wright, Maragret H.; Wright, Paul E. (1998): Convergence Properties of the Nelder-Mead Simplex Method in Low Dimensions. In *SIAM Journal of Optimization* 9, pp. 112–147.

32. Linke, Christian (2014): Application Engineering. Baker Hughes. Celle, Germany (Baker Hughes Training Material).

33. Linke, Christian; Cardy, Neil (2009): Drilling Optimization & Advanced Vibration Management. Baker Hughes. Celle, Germany (Webinar Presentation).

34. Linke, Christian; Hummes, Olof (2015a): BHASYSPro v2.1 - Dynamics Simulations - Support Information. Section 8—Job Aids. Baker Hughes. Celle, Germany (BHI Operations Manual).

35. Linke, Christian; Hummes, Olof (2015b): Cyclic Bending Load Limits for API Based Thread Connections. Section 6—Specifications. Baker Hughes. Celle, Germany (BHI Operations Manual).

36. Magnus, Kurt (1986): Schwingungen. E. Einf. in d. theoret. Behandlung von Schwingungsproblemen; mit 62 Aufgaben. 4., durchges. Aufl. Stuttgart: Teubner (Teubner-Studienbücher : Mechanik, 3). 3-519-22302-3.

37. Metropolis, Nicholas; Ulam, S. (1949): The Monte Carlo Method. In *Journal of the American Statistical Association* 44 (247), pp. 335–341. Available online at http://links.jstor.org/sici?sici=0162-1459%28194909%2944%3A247%3C335%3ATMCM%3E2.0.CO%3B2-3.

38. Mims, Mike; Krepp, Tony (2003): Drilling Design and Implementation for Extended Reach and Complex Wells. 3rd ed. The Woodlands, Texas: K&M Technology Group, LLC.

39. Mitchell, Robert F.; Miska, Stefan; Aadnøy, Bernt Sigve (2011): Fundamentals of drilling engineering. Richardson, TX: Society of Petroleum Engineers (SPE Textbook Series, v. 12). 978-1-55563-207-6.

40. Nelder, J. A.; Mead, R. (1965): A Simplex Method for Function Minimization. In *Computer Journal* 7, pp. 308–313.

41. Pastor, Miroslav; Binda, Michal; Harcarik, Tomas (2012): Modal Assurance Criterion. In *Procedia Engineering* 48, pp. 543–548.

42. Pastusek, Paul (2014): Stabilizer Selection Guidelines. Exxon Mobil Development. Exxon Mobil.

43. Reckmann, Hanno; Jogi, Pushkar; Kpetehoto, Franck Thierry; Chandrasekaran, Sridharan; Macpherson, John Duncan (2010): MWD Failure Rates Due to Drilling Dynamics. Society of Petroleum Engineers. SPE/IADC Drilling Conference, New Orleans, Louisiana (SPE 127413-MS). DOI: 10.2118/127413-MS.

44. Reckmann, Hanno; Meyer-Heye, Bernhard; Lippert, Tristan; Herbig, Christian (2011): Drilling Control System and Method. Applied for by Baker Hughes Incorporated on 11/10/2011. App. no. 13/293,725. Patent no. US 20120255778A1.

45. Ritter, Axel (2007): Mechanical Strength Assessment Guideline for INTEQ Drilling and MWD/LWD Tools. Baker Hughes. Celle, Germany (BHI Specifications and Standards).

46. Short, J. A. (1993): Introduction to directional and horizontal drilling. Tulsa, Okla.: PennWell Books. 0-87814-395-5.

47. Silva, Clarence W. de (2007): Vibration. Fundamentals and practice. 2nd ed. Boca Raton: CRC/Taylor & Francis. 978-0-849-31987-7.

48. Spanos, P. D.; Payne, M. L. (1992): Advances in Dynamic Bottomhole Assembly Modeling and Dynamic Response Determination. Society of Petroleum Engineers. SPE/IADC Drilling Conference, New Orleans, Louisiana (SPE 23905-MS). DOI: 10.2118/23905-MS.

49. Sugiura, Junichi (2008): Optimal BHA Design for Steerability and Stability with Configurable Rotary-Steerable System. Society of Petroleum Engineers. SPE Asia Pacific Oil and Gas Conference, Perth, Australia (SPE 114599-MS). DOI: 10.2118/114599-MS.

50. Vandiver, Kim J.; Nicholson, James W.; Shyu, Rong-Juin (1990): Case Studies of the Bending Vibration and whirling Motion of Drill Collars. In *SPE Drilling Engineering* 5 (04), pp. 282–290. DOI: 10.2118/18652-PA.

51. Warren, J. E. (1940): Causes, Preventions, and Recovery of Stuck Drill Pipe. American Petroleum Institute. New York (Drilling and Production Practice).

6 Appendix

6.1 Appendix A

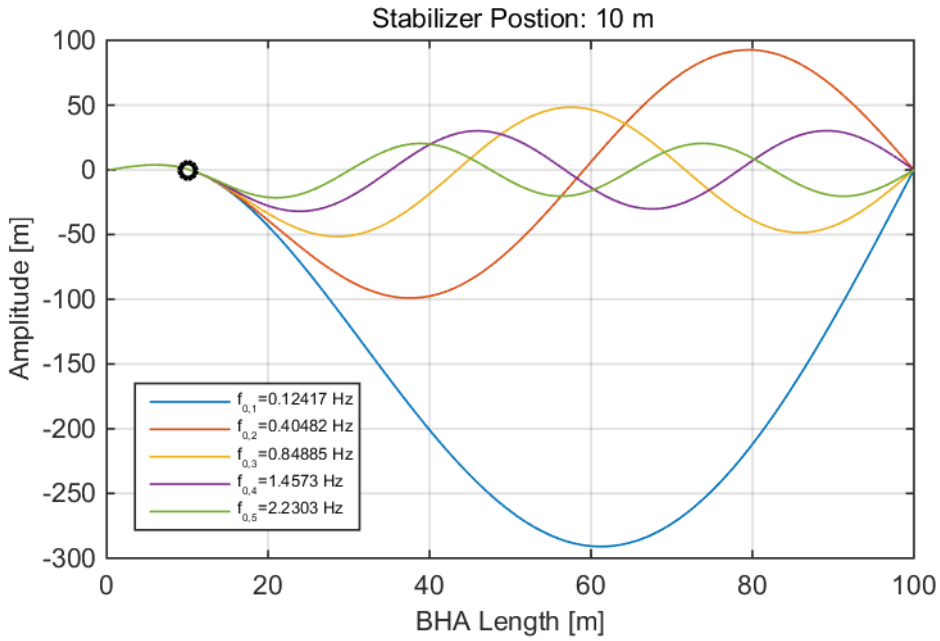

Fig. 6.1: First five natural frequencies and mode shapes for a stabilizer at 10 m.

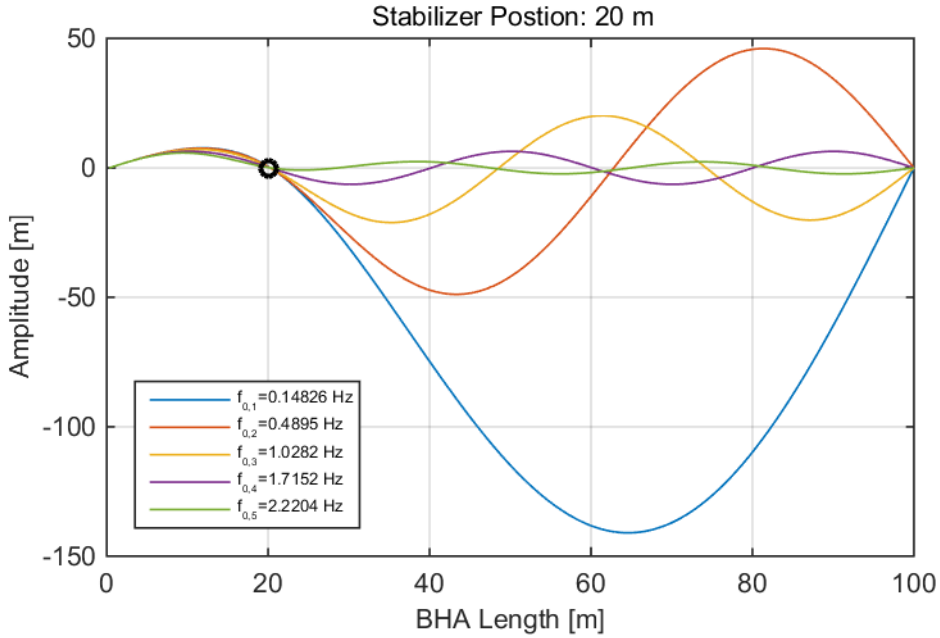

Fig. 6.2: First five natural frequencies and mode shapes for a stabilizer at 20 m.

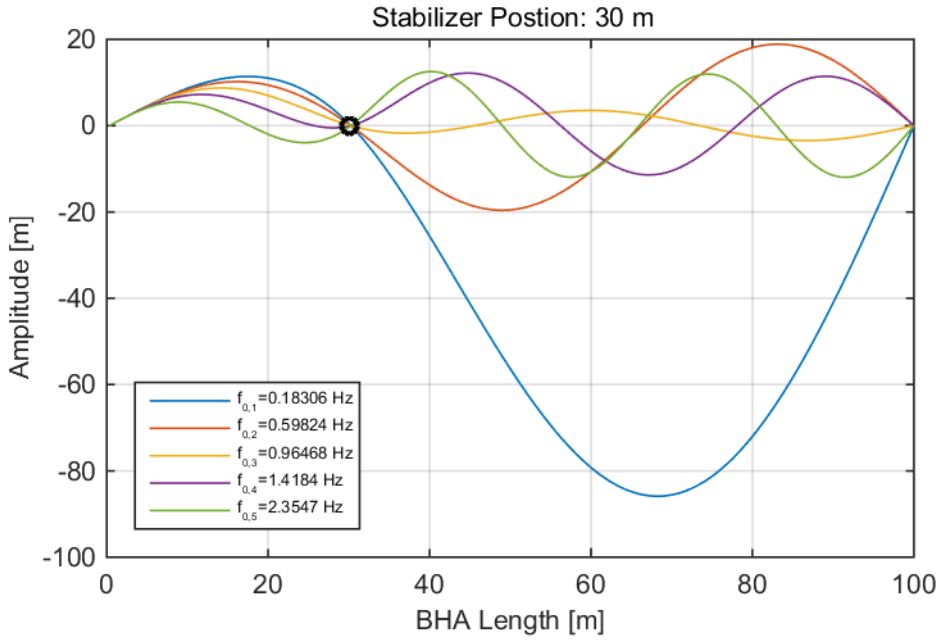

Fig. 6.3: First five natural frequencies and mode shapes for a stabilizer at 30 m.

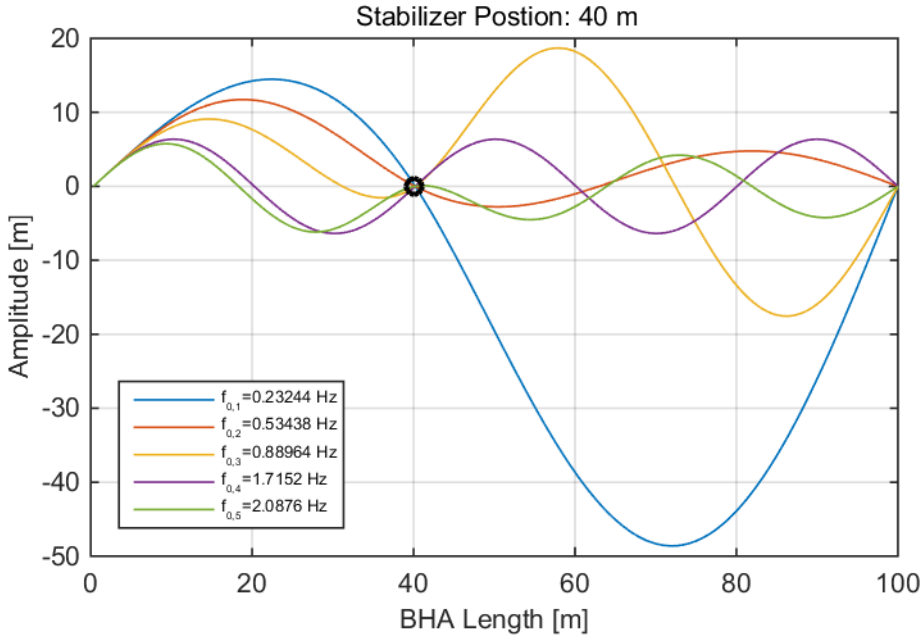

Fig. 6.4: First five natural frequencies and mode shapes for a stabilizer at 40 m.

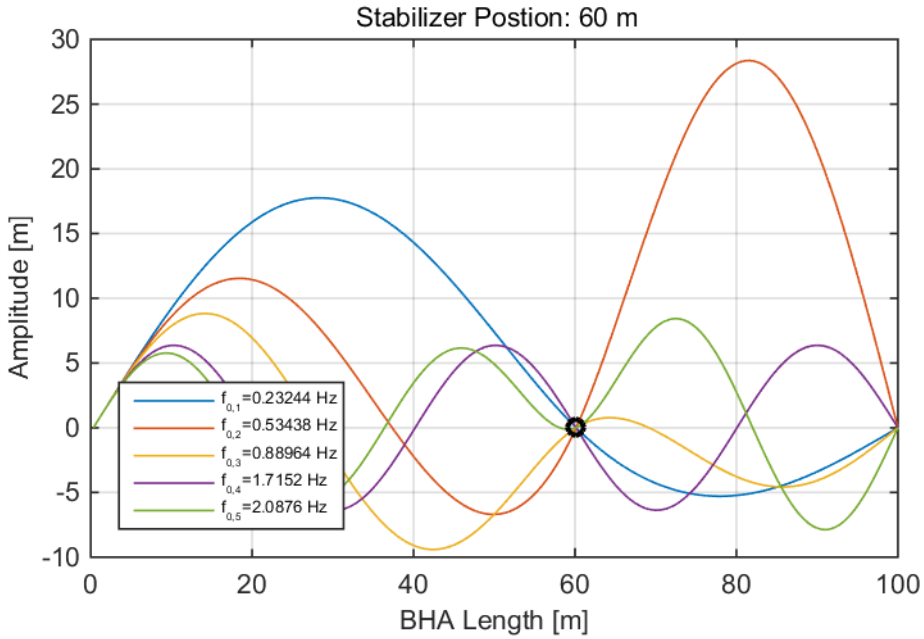

Fig. 6.5: First five natural frequencies and mode shapes for a stabilizer at 60 m.

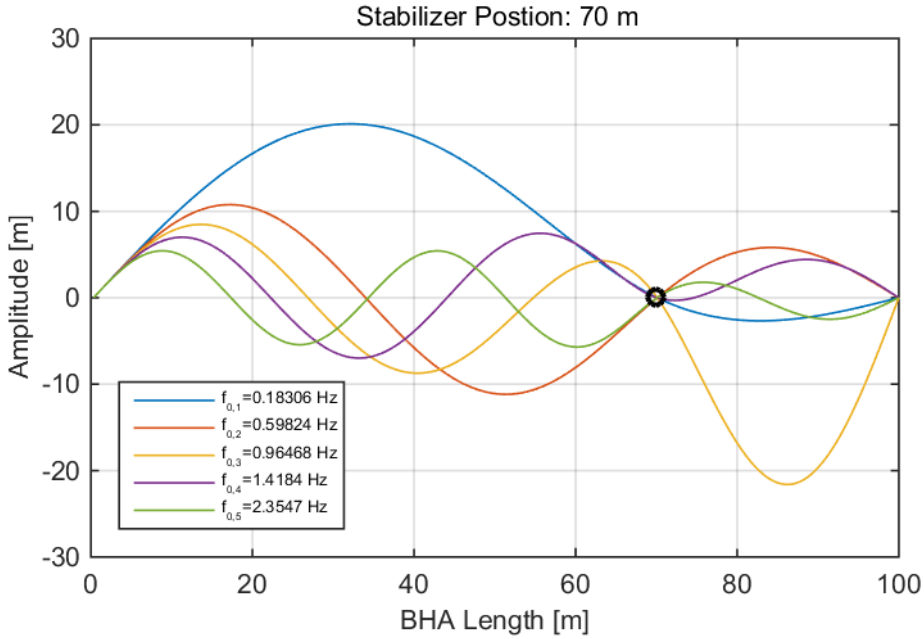

Fig. 6.6: First five natural frequencies and mode shapes for a stabilizer at 70 m.

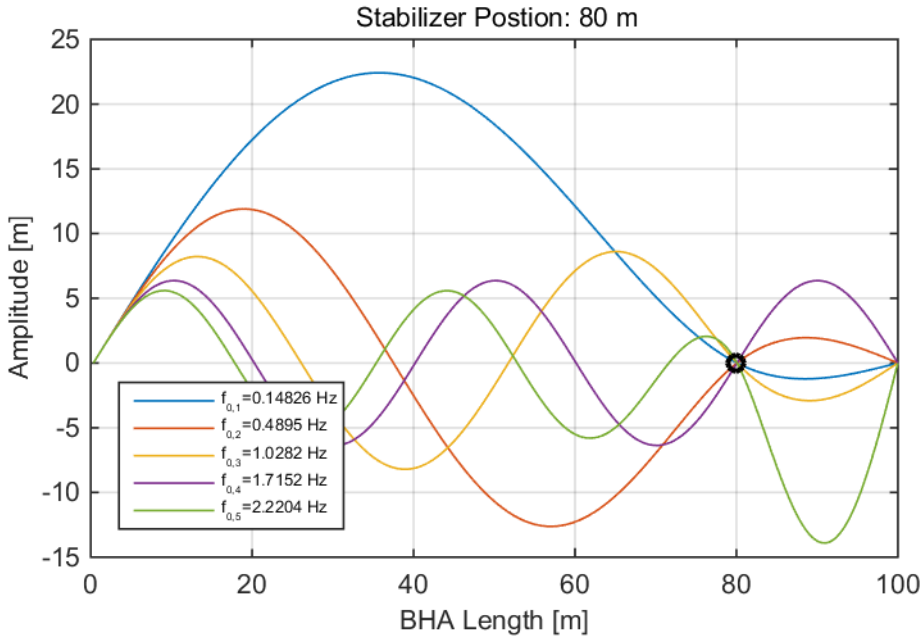

Fig. 6.7: First five natural frequencies and mode shapes for a stabilizer at 80 m.

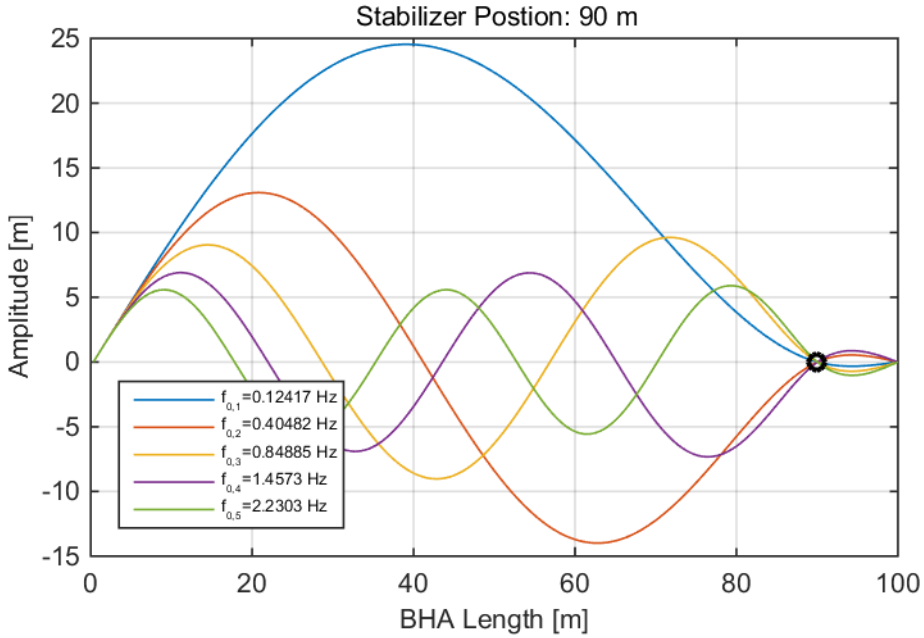

Fig. 6.8: First five natural frequencies and mode shapes for a stabilizer at 90 m.

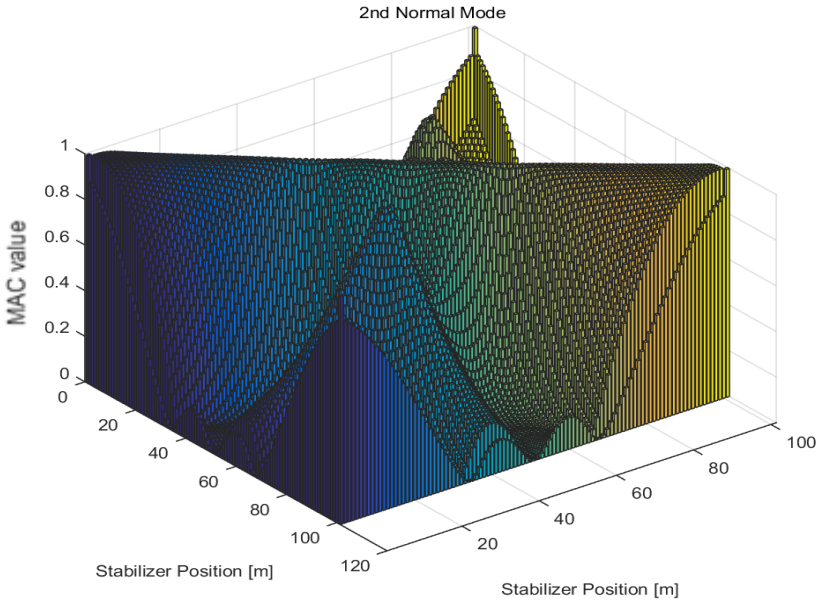

Fig. 6.9: Modal assurance criterion for all 2nd normal modes of every stabilizer position. The elevated values at the edges result from the stabilizer being too close to the boundaries of the model, thus transforming the stabilizer into a clamp which can also bear a moment. A value of one means that the mode shapes are coherent and zero that the shapes are orthogonal. Similarities to the modal assurance plot for all 1st modes exist due to the transformation of previous first modes into second modes through different stabilizer configurations.

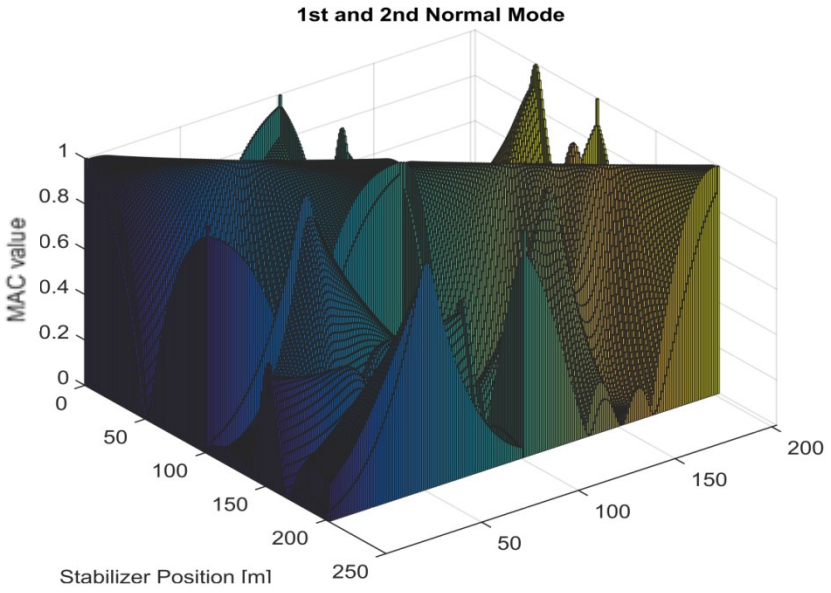

Fig. 6.10: Combination of the modal assurance criteria of the 1st and 2nd normal mode. Note that the x and y axis show the combined length of 200 m, 100 m from every single criterion plot.

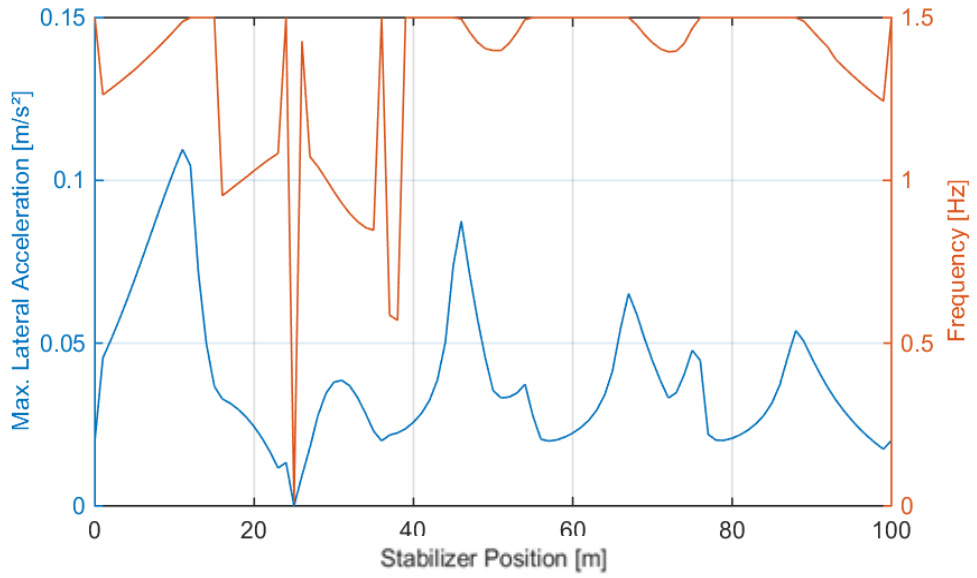

Fig. 6.11: Max. lateral acceleration along the BHA and across all frequencies. The red curve shows the highest resonance frequency for every stabilizer position. This yields only one max. acceleration value for every stabilizer position but neglects other frequencies which could also lead to a harmful displacement.

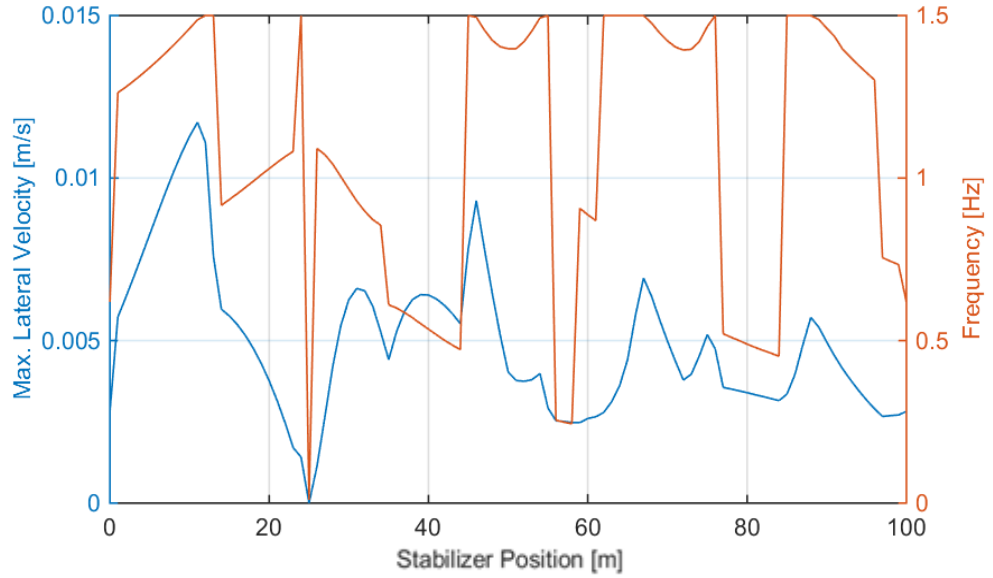

Fig. 6.12: Max. lateral velocity along the BHA and across all frequencies. The red curve shows the highest resonance frequency for every stabilizer position. This yields only one max. velocity value for every stabilizer position but neglects other frequencies which could also lead to a harmful displacement.

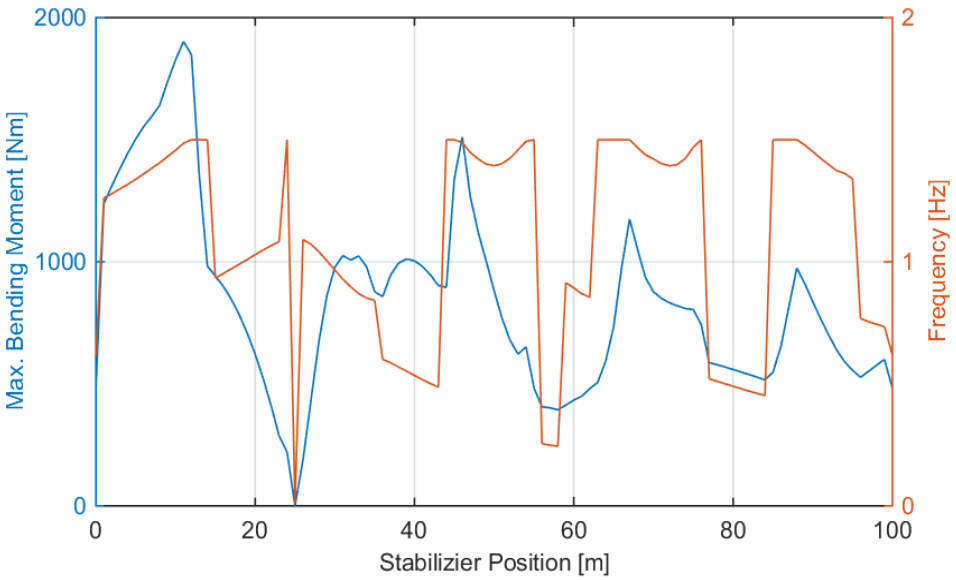

Fig. 6.13: Max. bending moment along the BHA and across all frequencies. The red curve shows the highest resonance frequency for every stabilizer position. This yields only one max. bending moment value for every stabilizer position but neglects other frequencies which could also lead to a harmful displacement.

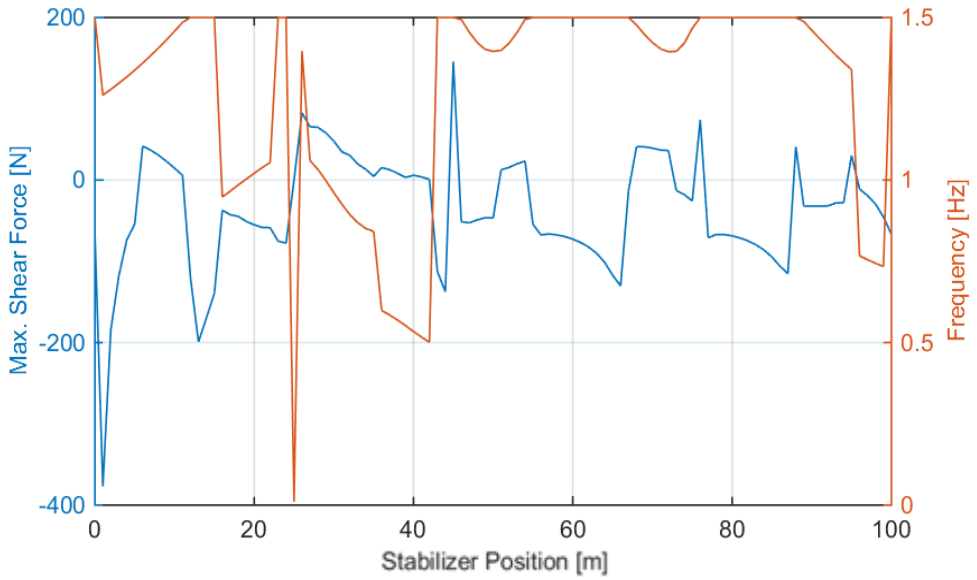

Fig. 6.14: Max. shear force along the BHA and across all frequencies. The red curve shows the highest resonance frequency for every stabilizer position. This yields only one max. shear force value for every stabilizer position but neglects other frequencies which could also lead to a harmful displacement.

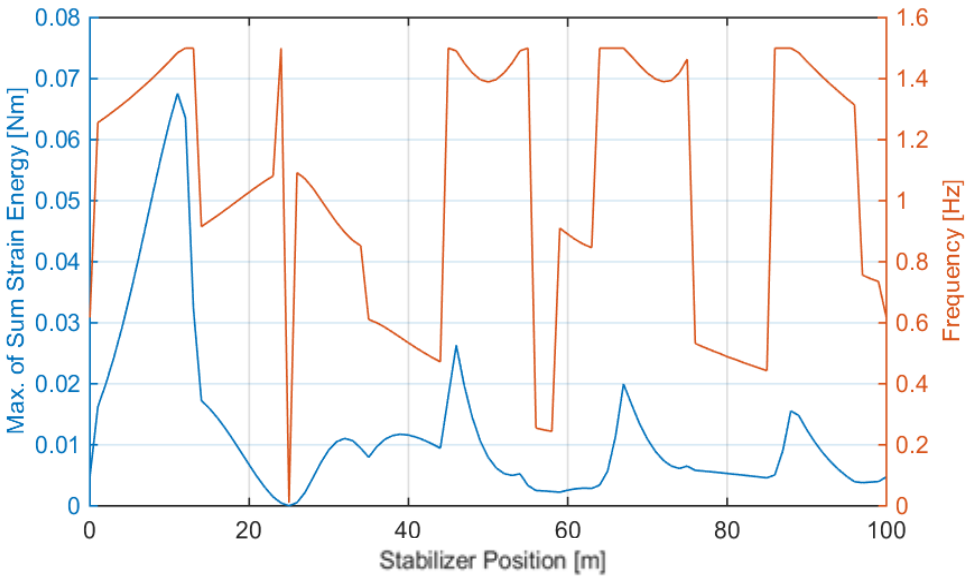

Fig. 6.15: Max. value of the cumulative strain energy across all frequencies. The red curve shows the highest resonance frequency for every stabilizer position. This yields only one result for every stabilizer position but neglects other frequencies which could also lead to a harmful displacement.

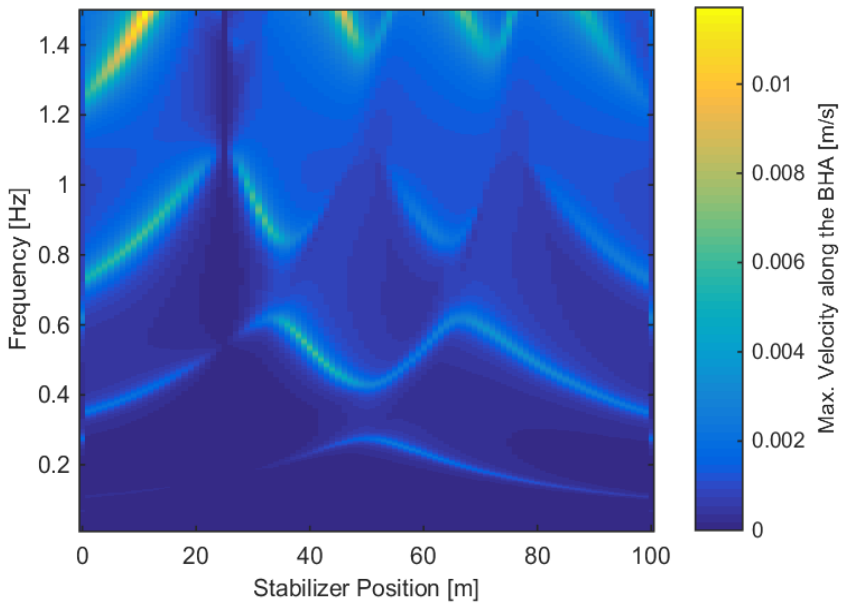

Fig. 6.16: Maximum velocity along the BHA for all stabilizer positions through the whole frequency band. One stabilizer position can have multiple resonance frequencies. The vertical line directly at 25 m marks the position of the excitation force and a stabilizer directly at this point renders the excitation effects to zero. The observable wave form is the frequency response and not related to the mode shapes.

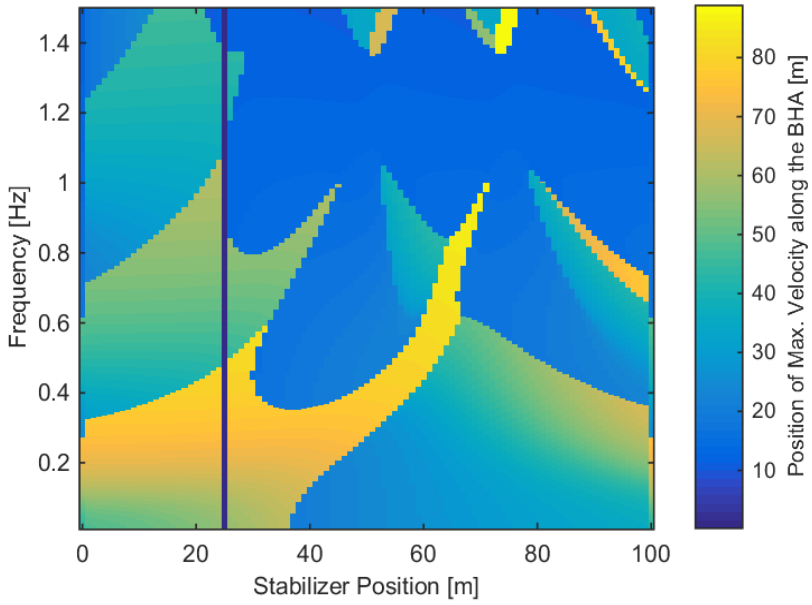

Fig. 6.17: Position of the maximum velocity for every stabilizer position and across the frequencies under investigation.

6.2 Appendix B

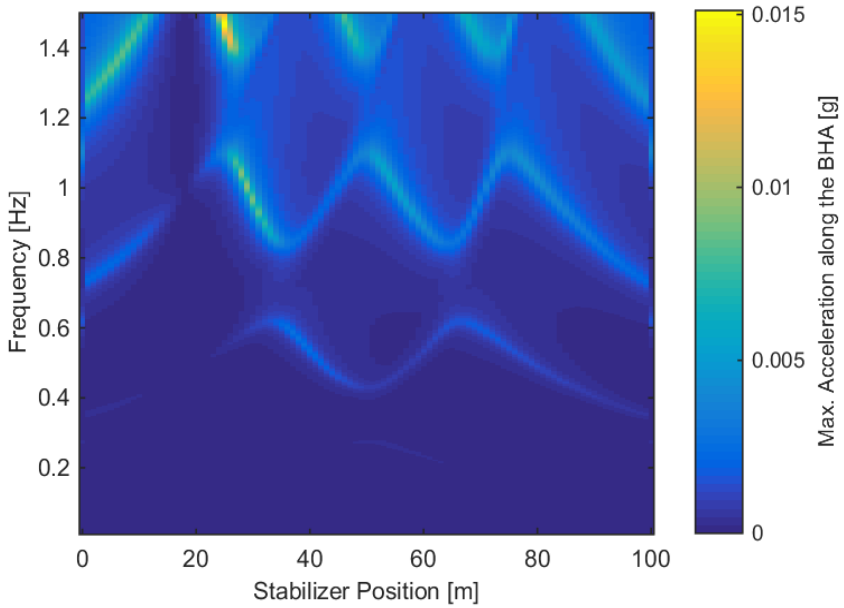

Fig. 6.18: Max. lateral acceleration for all stabilizer positions and and excitation source at 18 m from the bit.

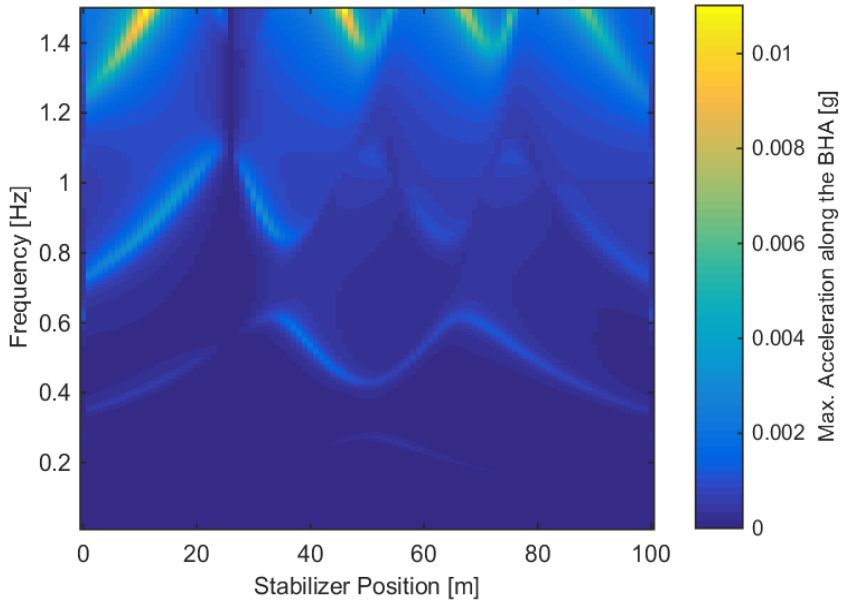

Fig. 6.19: Max. lateral acceleration for all stabilizer positions and an excitation source at 26 m from the bit.

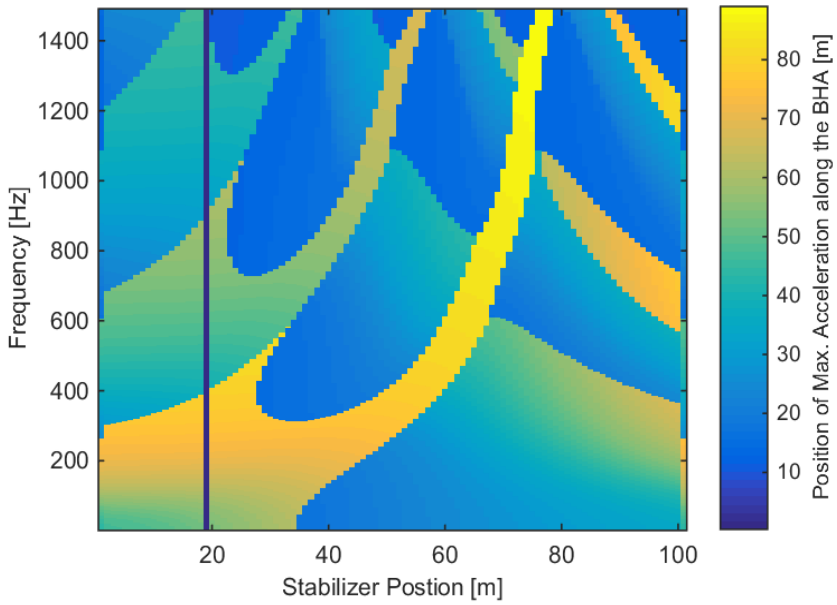

Fig. 6.20: Position of the max. lateral acceleration for all stabilizers and an excitation source at 18 m. Most maxima are located near the bit.

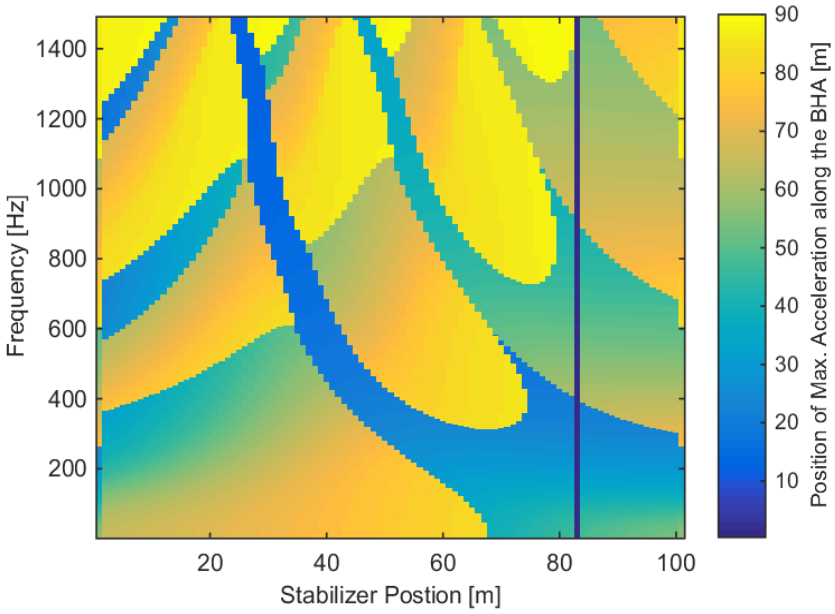

Fig. 6.21: Position of the max. lateral displacement for all stabilizers and an excitation source at 82 m. The maxima are shifted further away from the bit, following the position change of the excitations source.

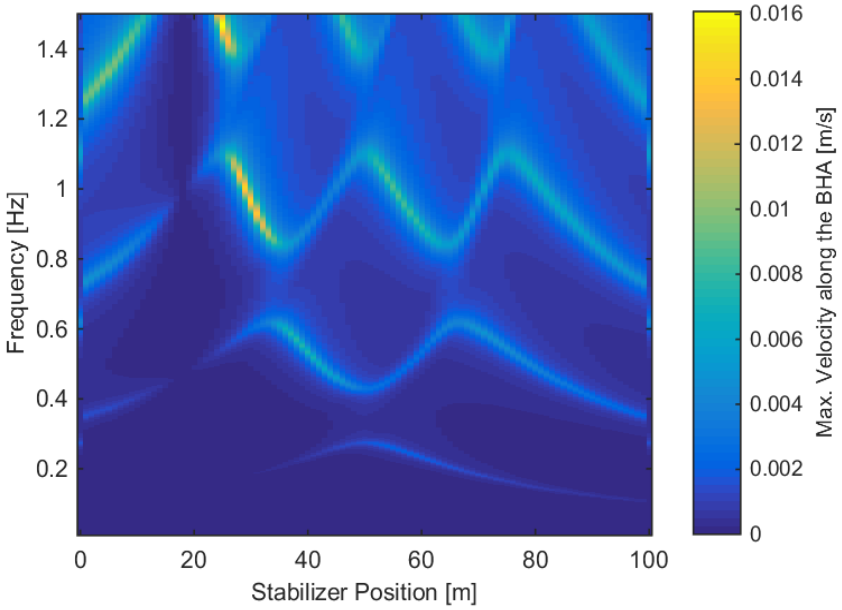

Fig. 6.22: Max. lateral velocity for all stabilizer positions and an excitation source at 18 m from the bit.

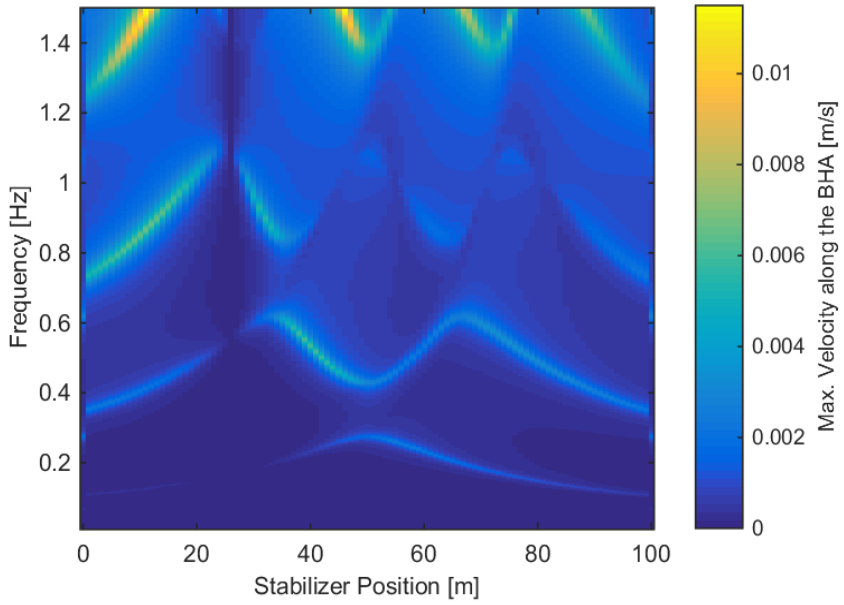

Fig. 6.23: Max. lateral velocity for all stabilizer positions and an excitation source at 26 m from the bit.

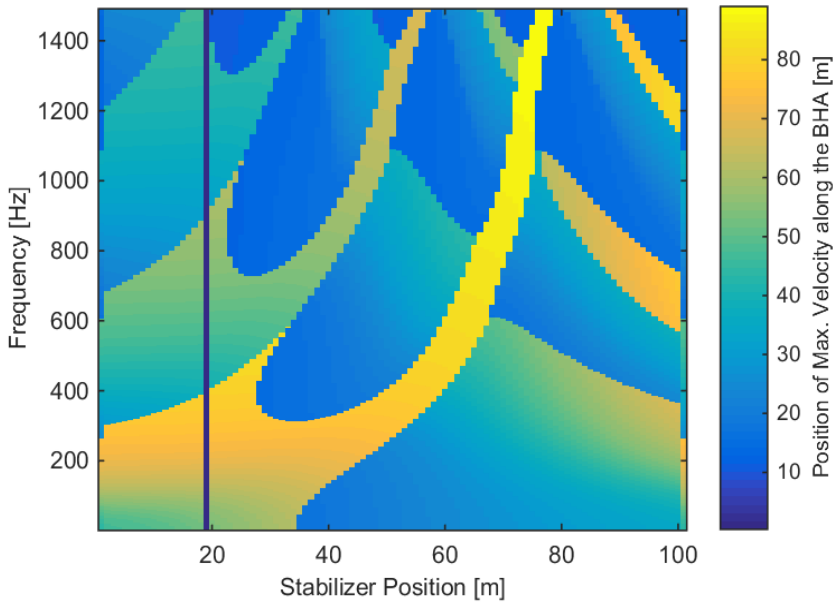

Fig. 6.24: Position of the max. lateral velocity for all stabilizers and an excitation source at 18 m. Most maxima are located near the bit.

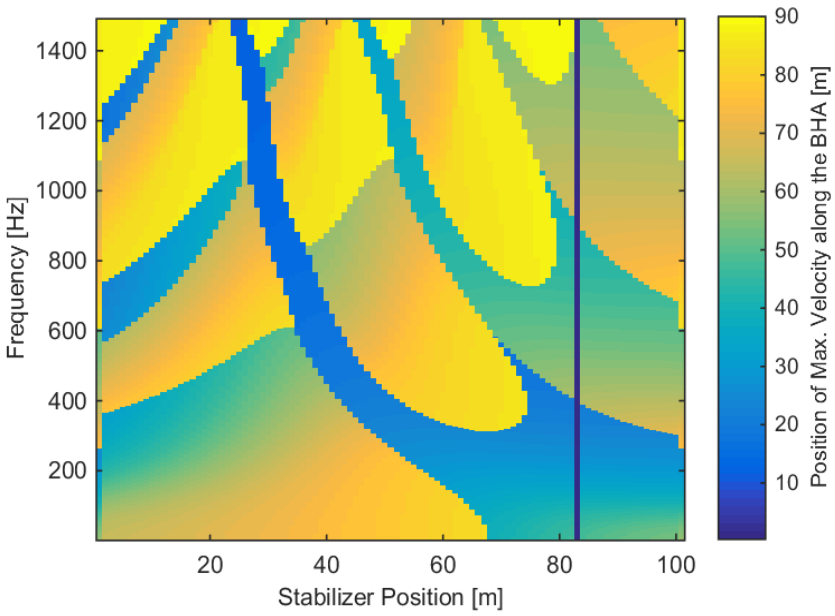

Fig. 6.25: Position of the max. lateral velocity for all stabilizers and an excitation source at 82 m. The maxima are shifted further away from the bit, following the position change of the excitations source.

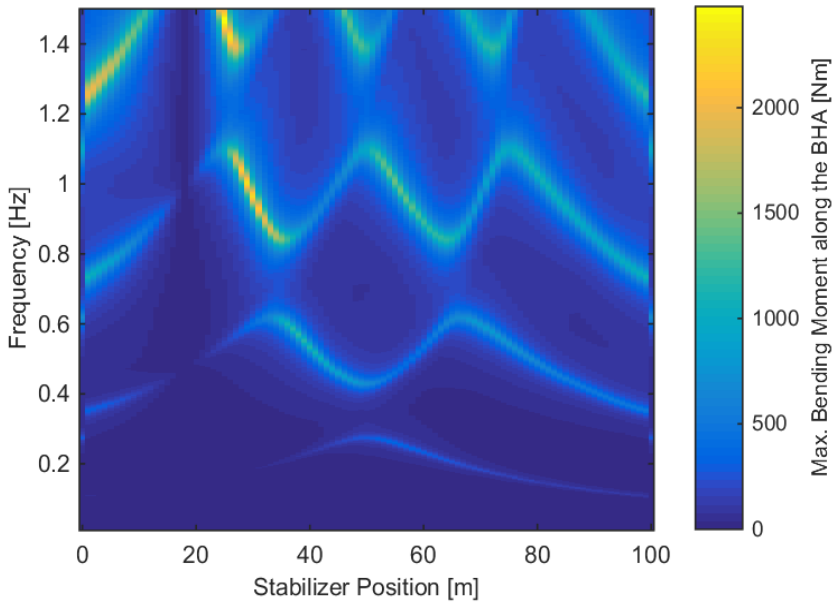

Fig. 6.26: Max. bending moment for all stabilizer positions and an excitation source at 18 m from the bit.

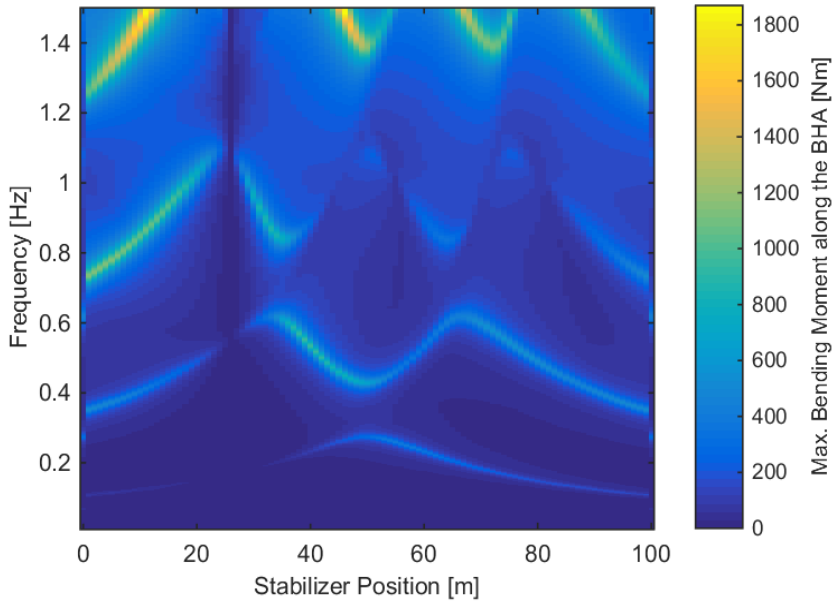

Fig. 6.27: Max. bending moment for all stabilizer positions and an excitation source at 26 m from the bit.

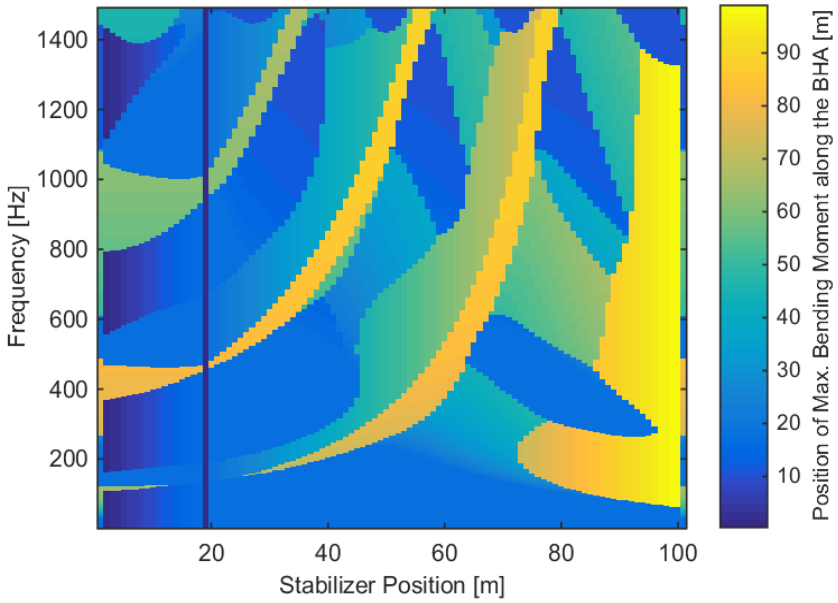

Fig. 6.28: Position of the max. bending moment for all stabilizers and an excitation source at 18 m. Most maxima are located near the bit.

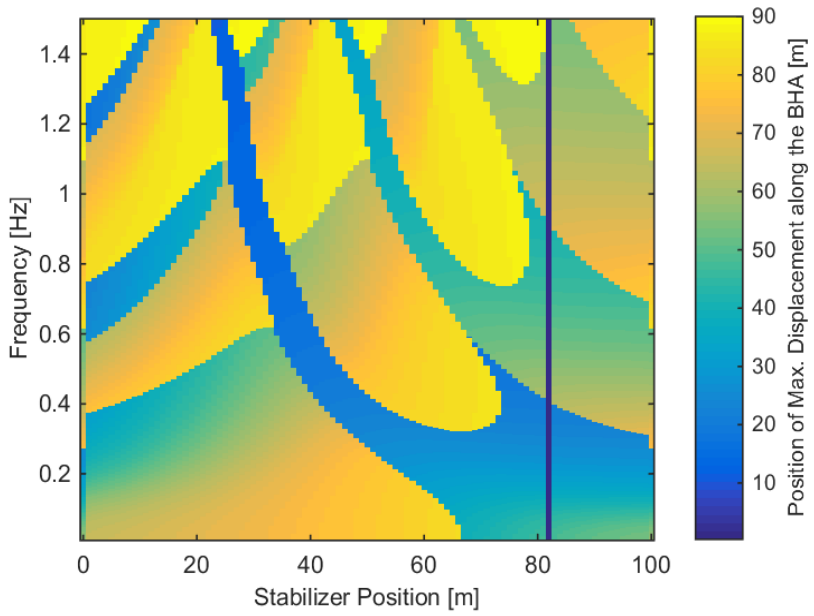

Fig. 6.29: Position of the max. lateral velocity for all stabilizers and an excitation source at 82 m. The maxima are shifted further away from the bit, following the position change of the excitations source.

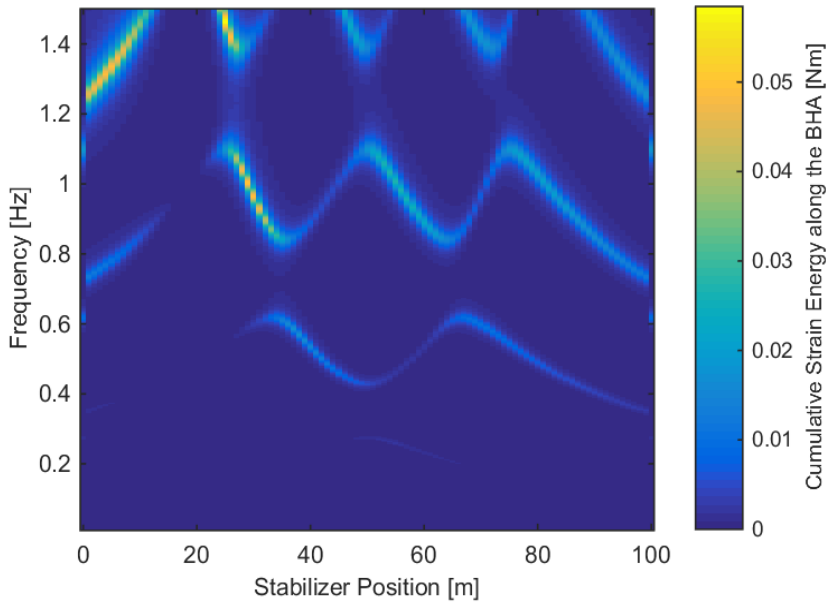

Fig. 6.30: Cumulative strain energy for all stabilizer positions and an excitation source at 18 m from the bit.

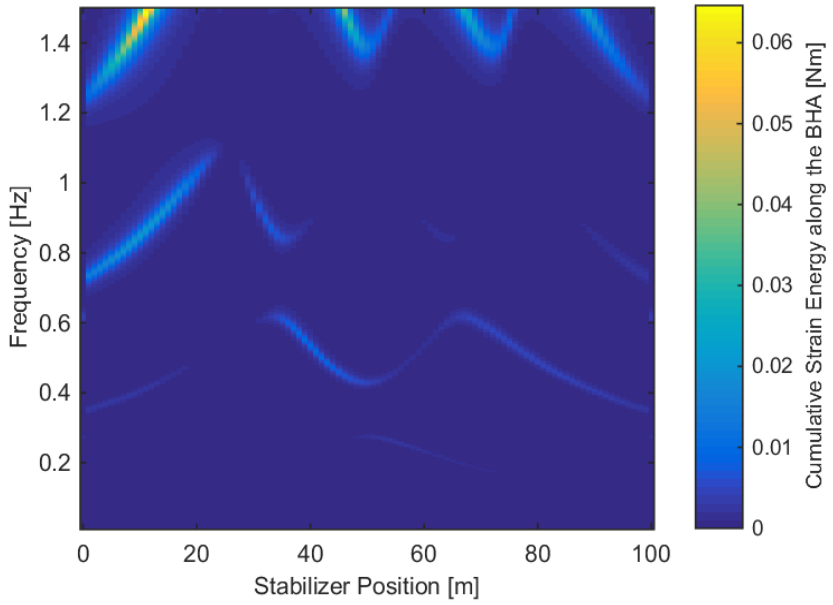

Fig. 6.31: Cumulative strain energy for all stabilizer positions and an excitation source at 26 m from the bit.

6.3 Appendix C

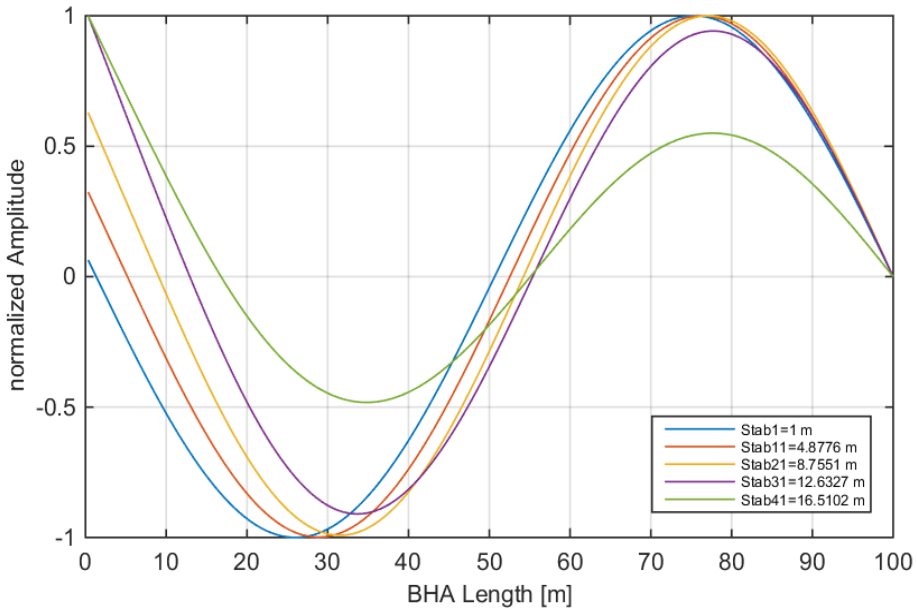

Fig. 6.32: Normalized 2nd normal modes for selected stabilizer positions.

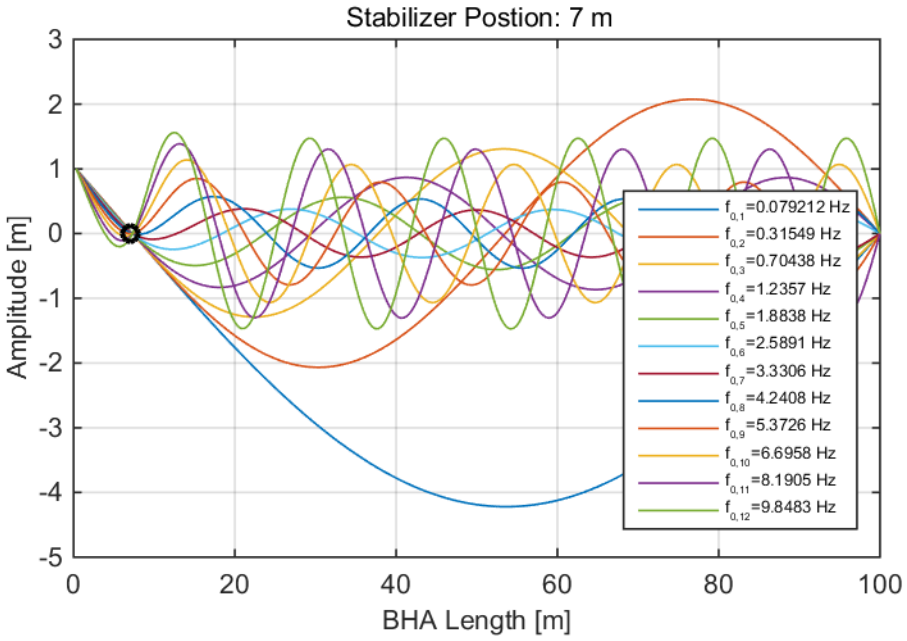

Fig. 6.33: Normal mode shapes and natural frequencies for a stabilizer at 7 m from the bit.

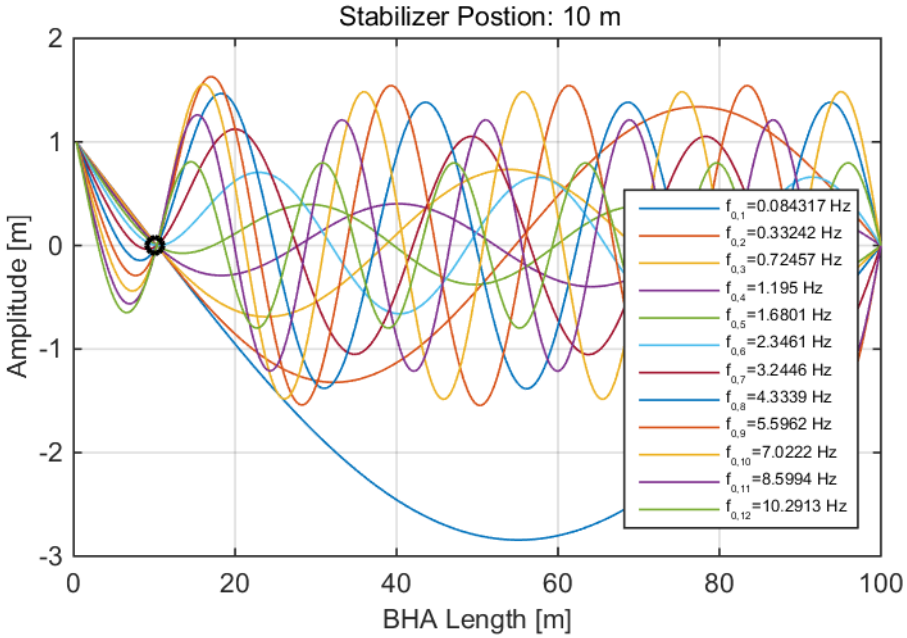

Fig. 6.34: Normal mode shapes and natural frequencies for a stabilizer at 10 m from the bit.

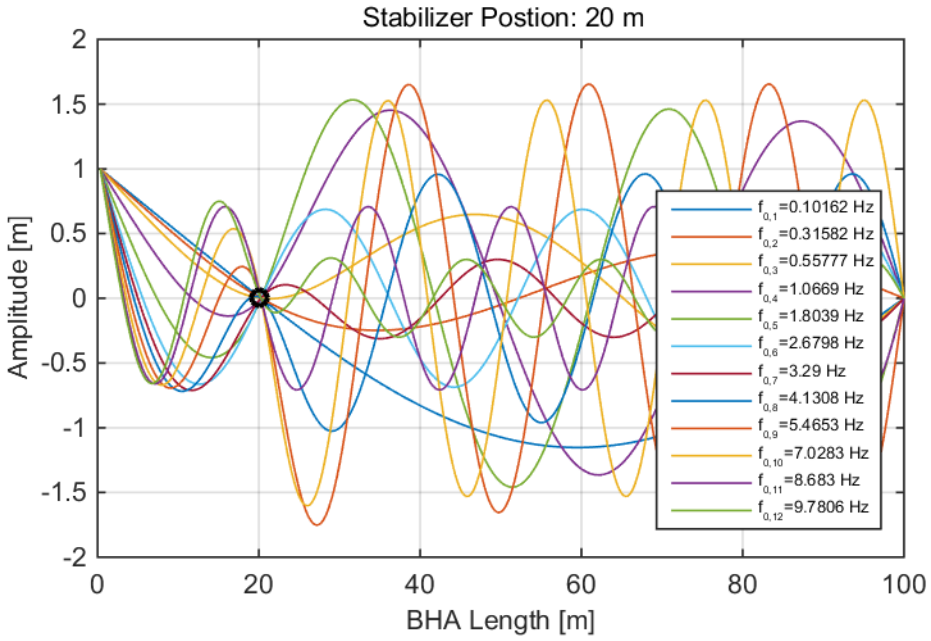

Fig. 6.35: Normal mode shapes and natural frequencies for a stabilizer at 20 m from the bit.

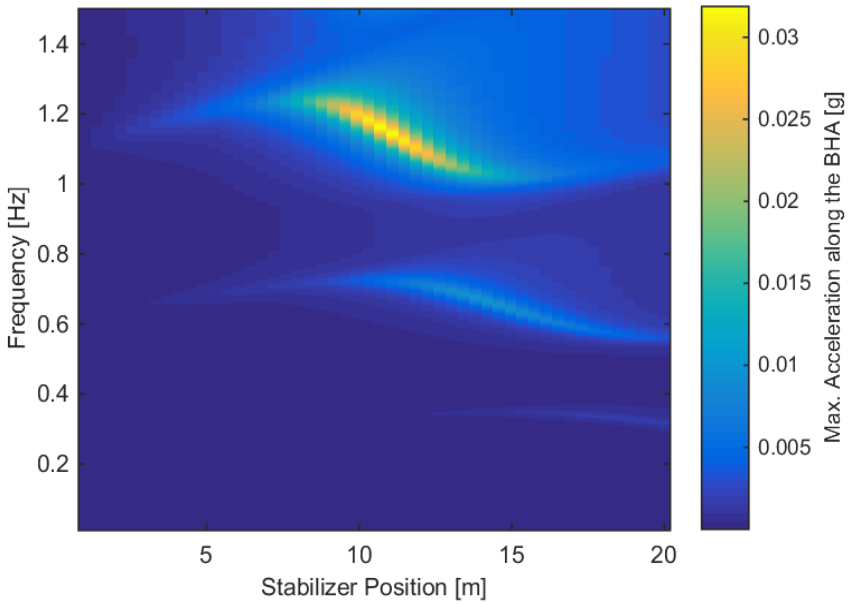

Fig. 6.36: Max. lateral acceleration for all stabilizer positions and every frequency step.

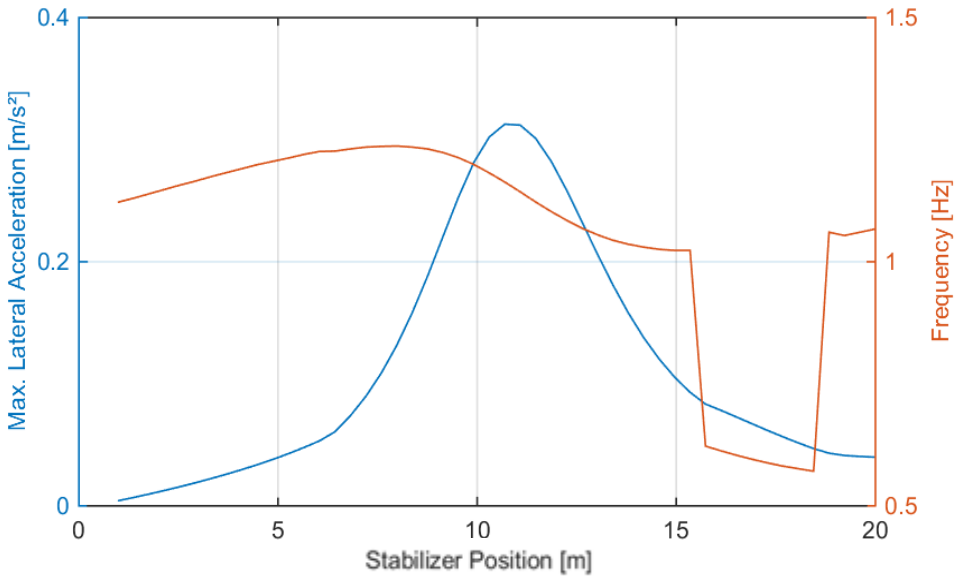

Fig. 6.37: Max. lateral acceleration for all stabilizers across the BHA length and entire frequency range.

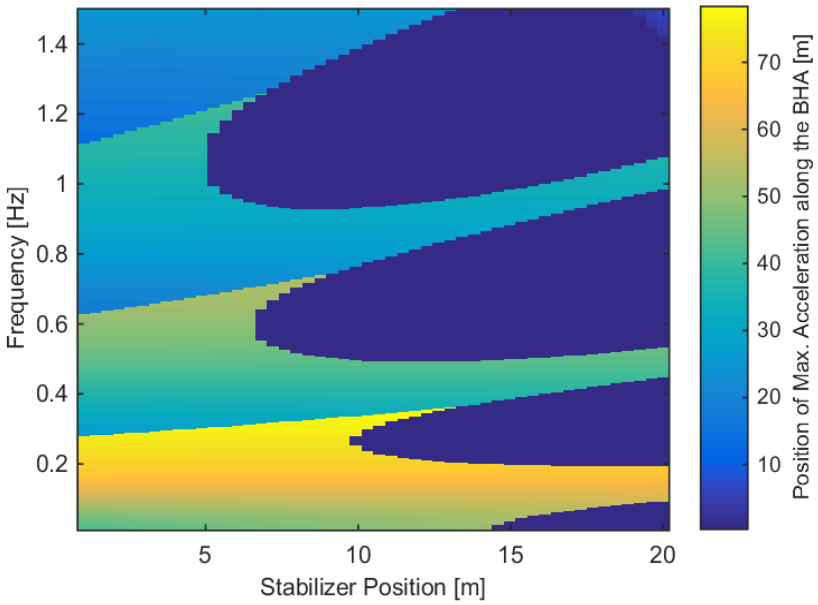

Fig. 6.38: Position of the max. lateral acceleration for all stabilizers and for every frequency step.

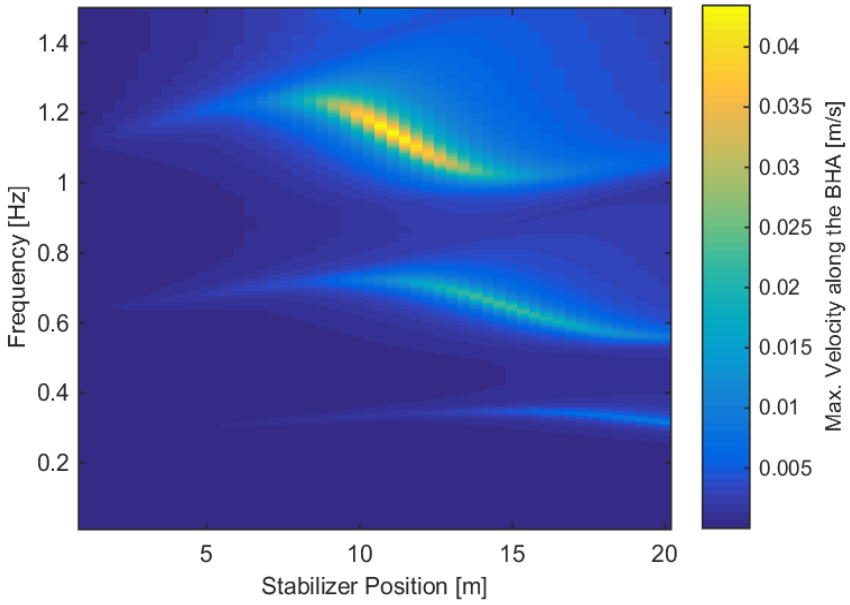

Fig. 6.39: Max. lateral acceleration for all stabilizer positions and every frequency step.

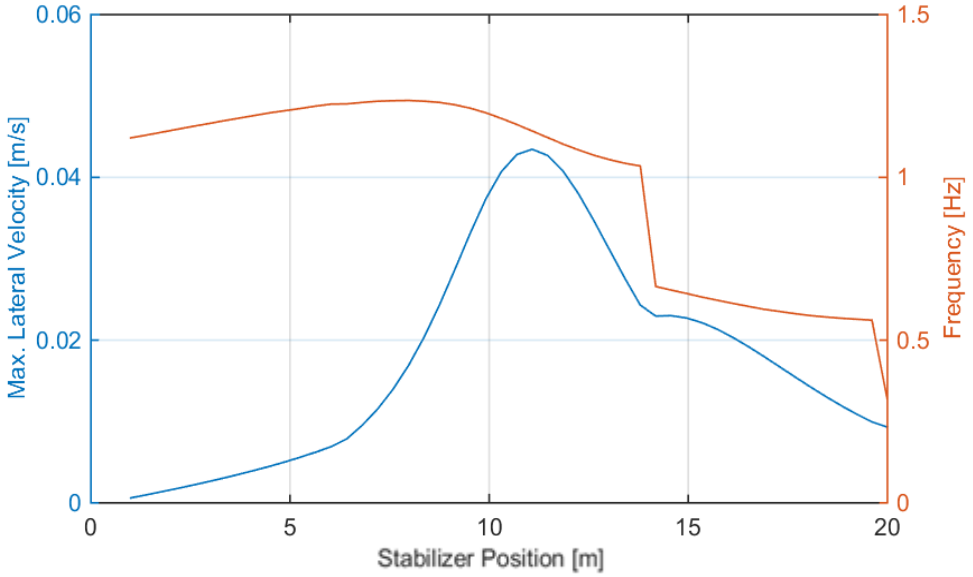

Fig. 6.40: Max. lateral velocity for all stabilizers across the BHA length and entire frequency range.

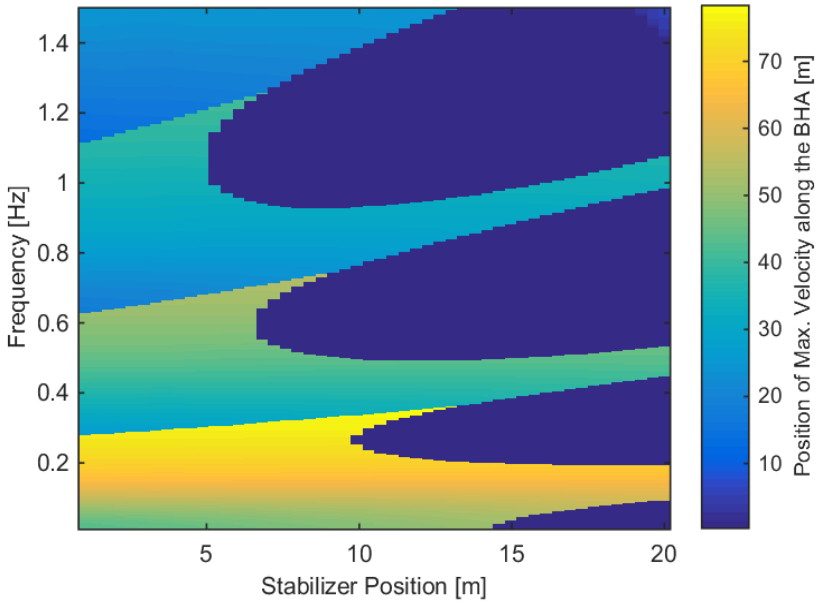

Fig. 6.41: Position of the max. lateral velocity for all stabilizers and for every frequency step.

6.4 Appendix D

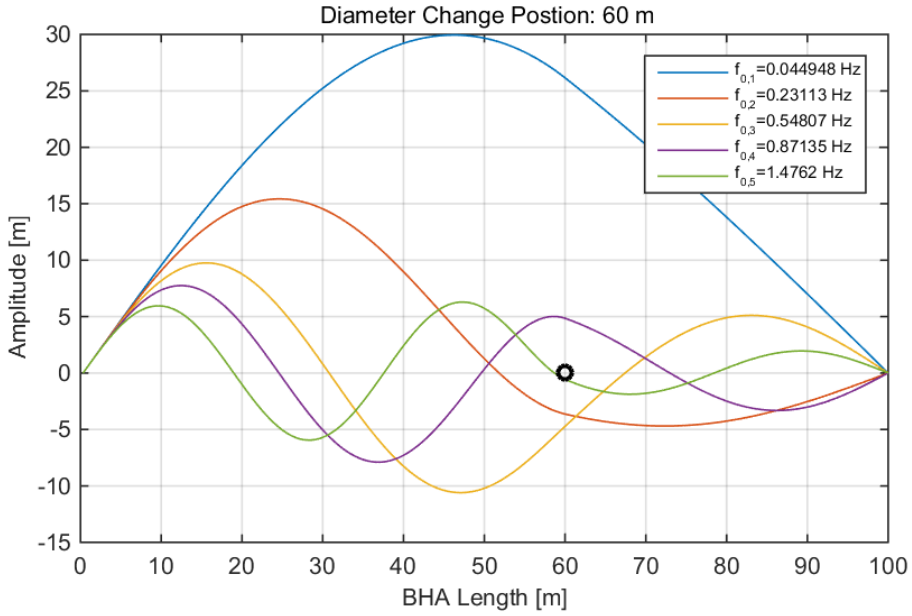

Fig. 6.42: The first 5 normal modes and natural frequencies for a diameter change at 60 m distance from the bit. The previously mentioned compression moves along with the diameter change position as the length of the reduced ID section increases.

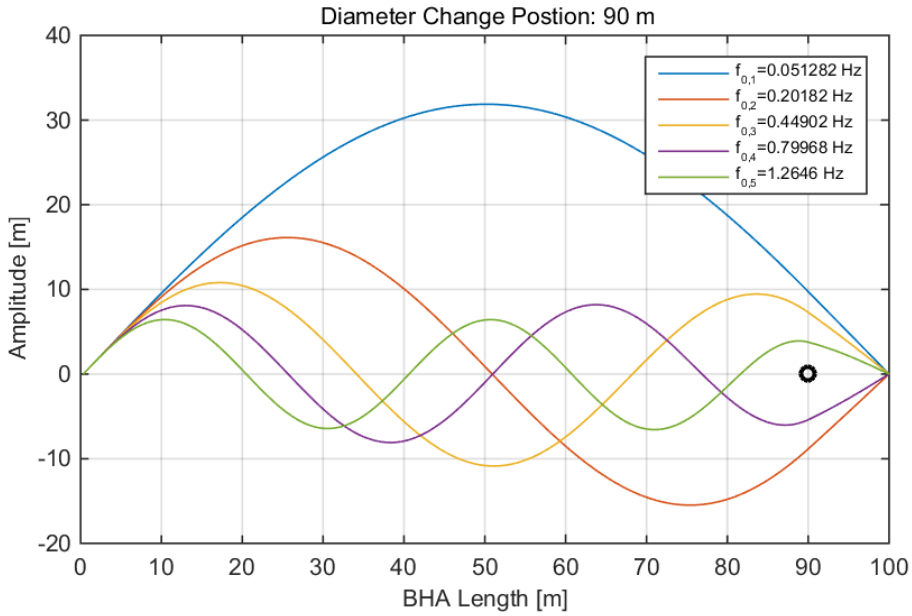

Fig. 6.43: The first 5 normal modes and natural frequencies for a diameter change at 90 m distance from the bit. The normal mode shape does not change significantly over the last few steps. However, most natural frequencies continue to drop until the whole BHA is at an OD of 0.2 m.

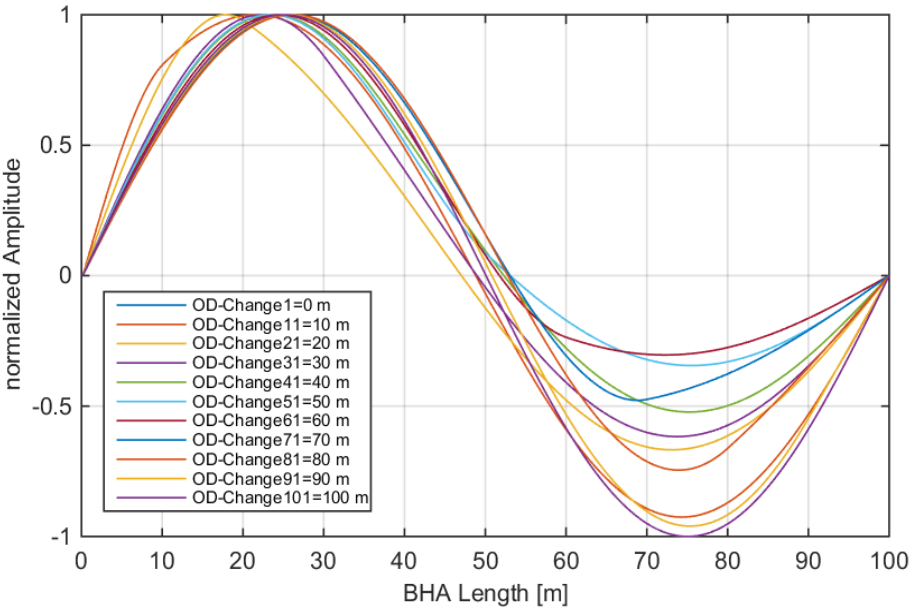

Fig. 6.44: Normalized 2nd normal modes for selected diameter change positions. These mode shapes show the same influence as the 1st modes.

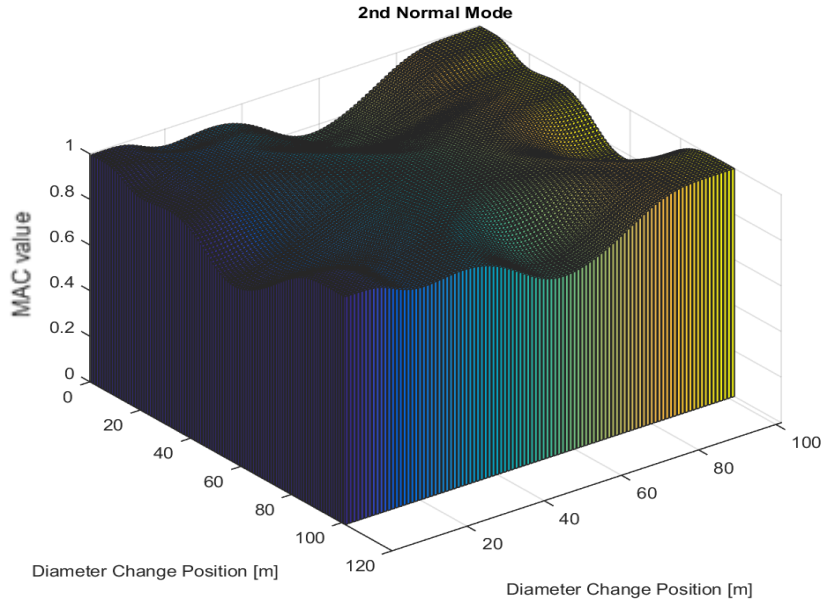

Fig. 6.45: Modal assurance criterion for all 2nd normal mode shapes.

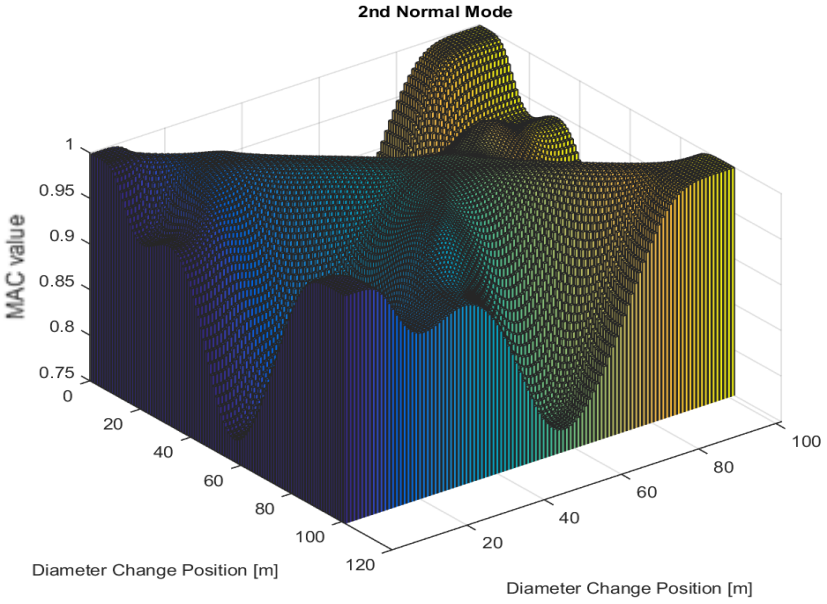

Fig. 6.46: Magnification of Fig. 6.45 to show the small changes in the degree of correspondence.

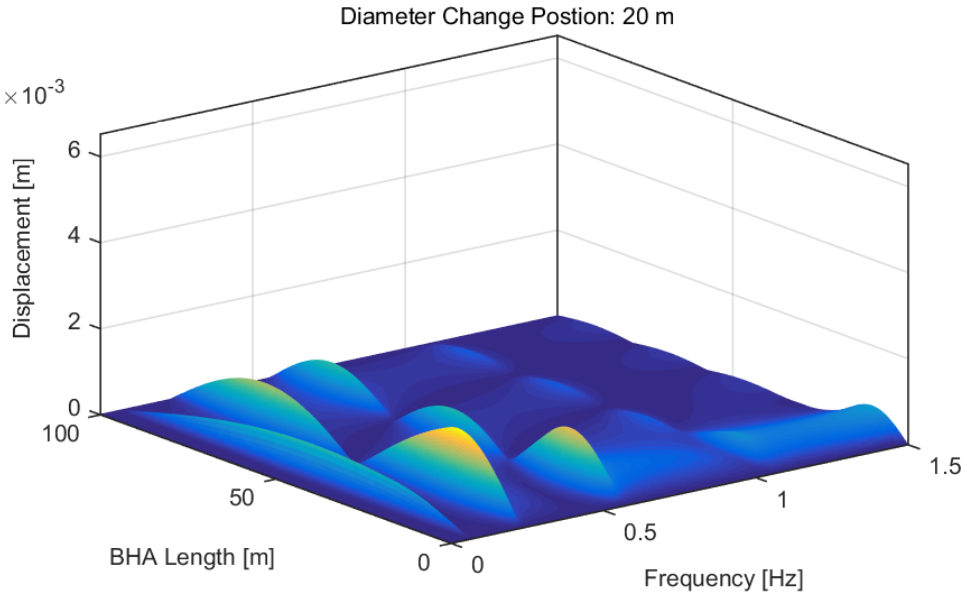

Fig. 6.47: Lateral displacement with a diameter change at 20 m from the bit.

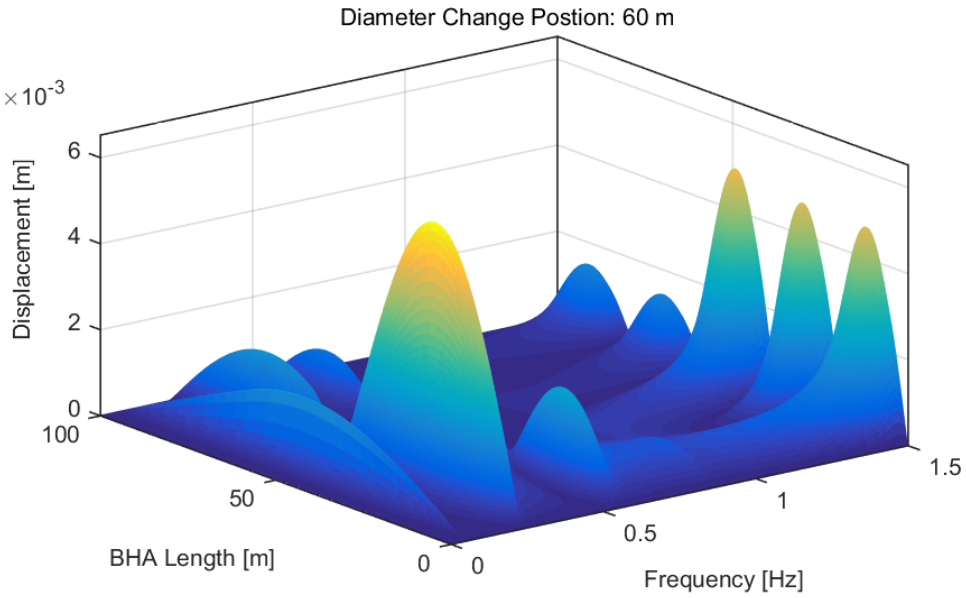

Fig. 6.48: Lateral displacement with a diameter change at 60 m from the bit. The displacement becomes more severe as diameter change progresses and a bigger section of the BHA becomes smaller.

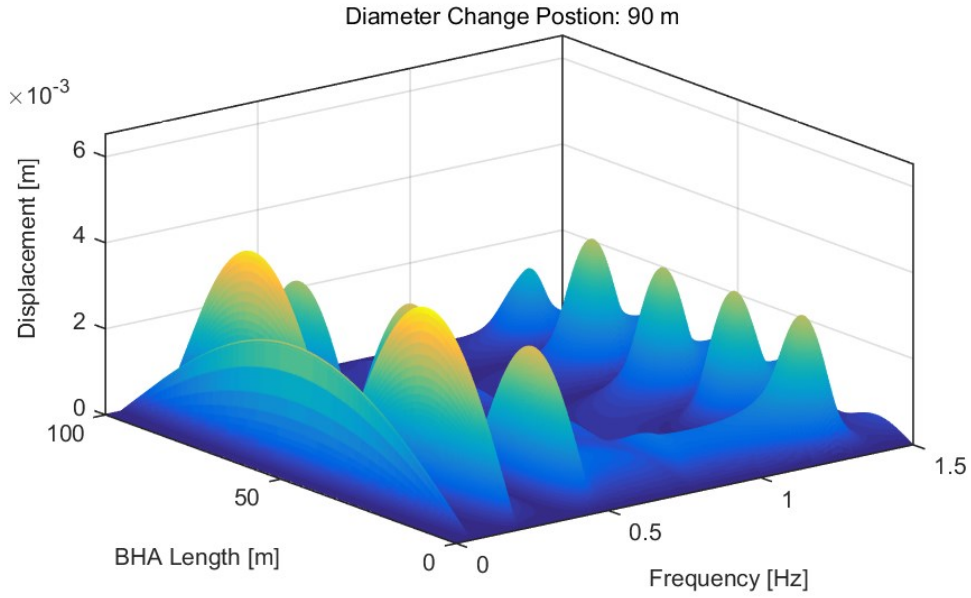

Fig. 6.49: Lateral displacement with a diameter change at 90 m from the bit. The displacement tends to decrease after the diameter change position passes the middle section of the BHA.

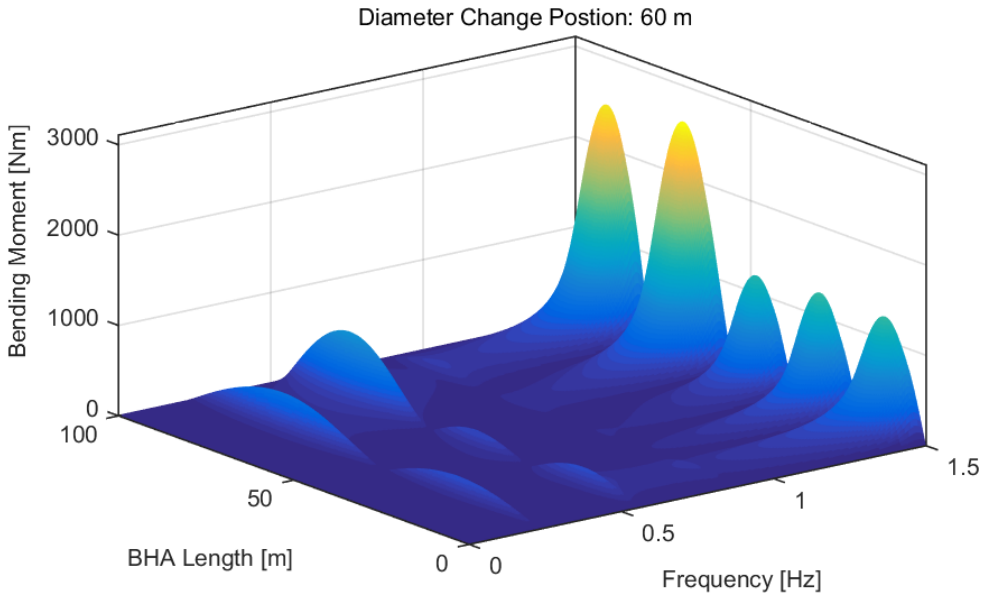

Fig. 6.50: Bending moment for diameter change at 60 m from the bit. The bending moment amplitudes are higher for a BHA model with a shorter, stiffer section.

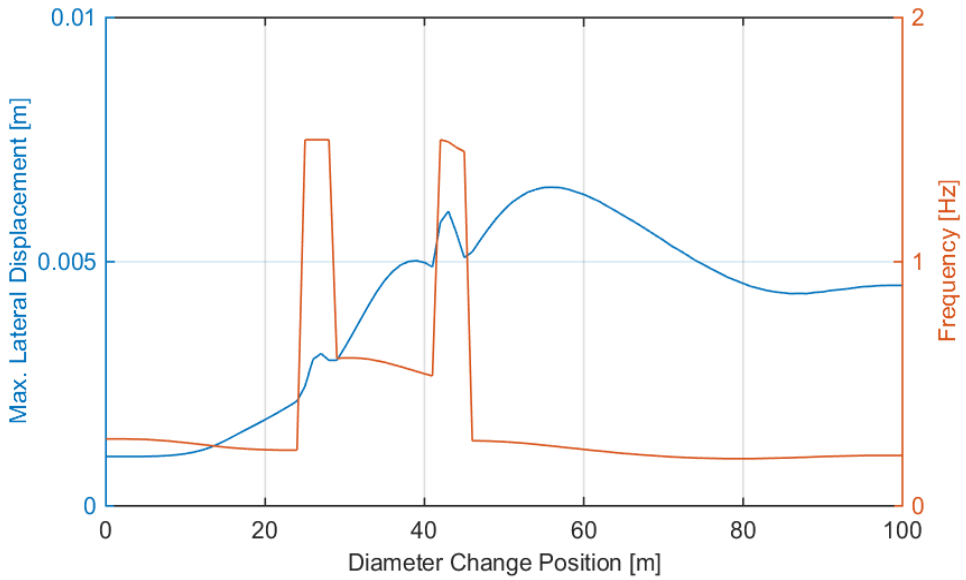

Fig. 6.51: Max. lateral displacement along the BHA and across all frequencies.

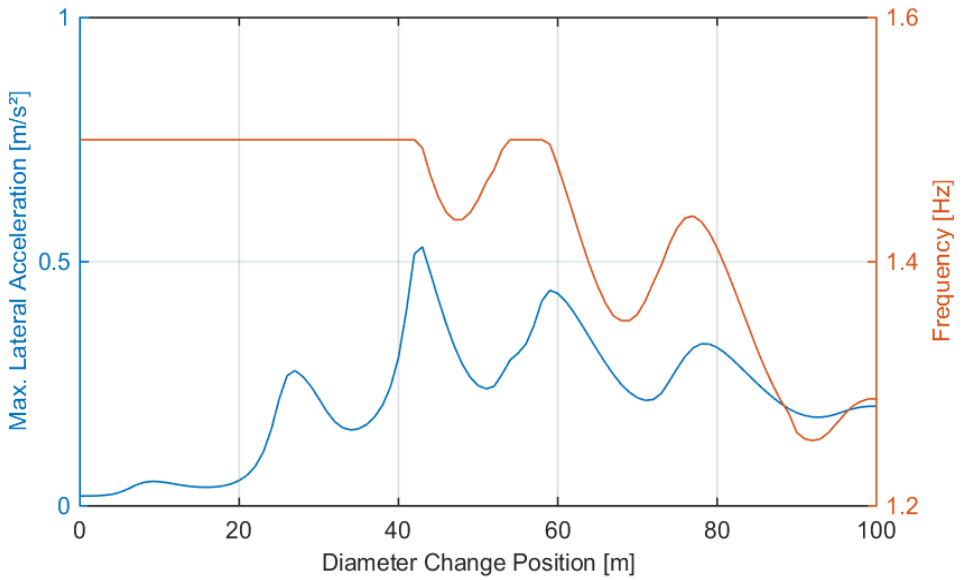

Fig. 6.52: Max. lateral acceleration along the BHA and across all frequencies.

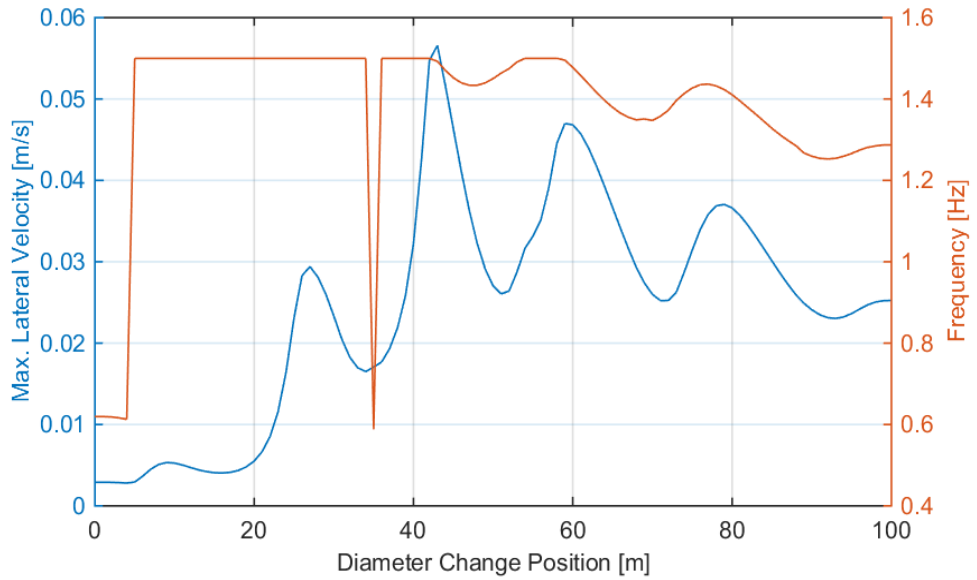

Fig. 6.53: Max. lateral velocity along the BHA and across all frequencies.

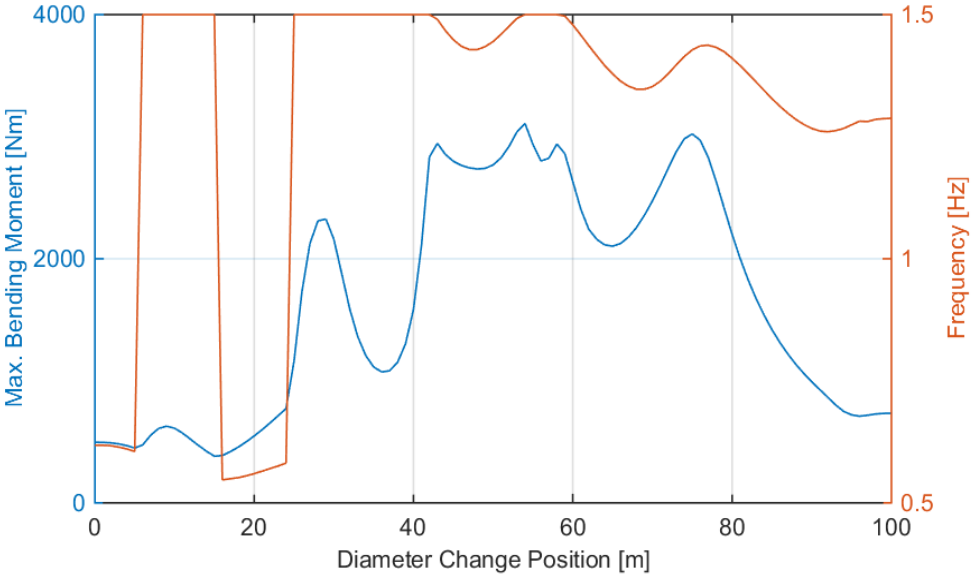

Fig. 6.54 Max. bending moment along the BHA and across all frequencies.

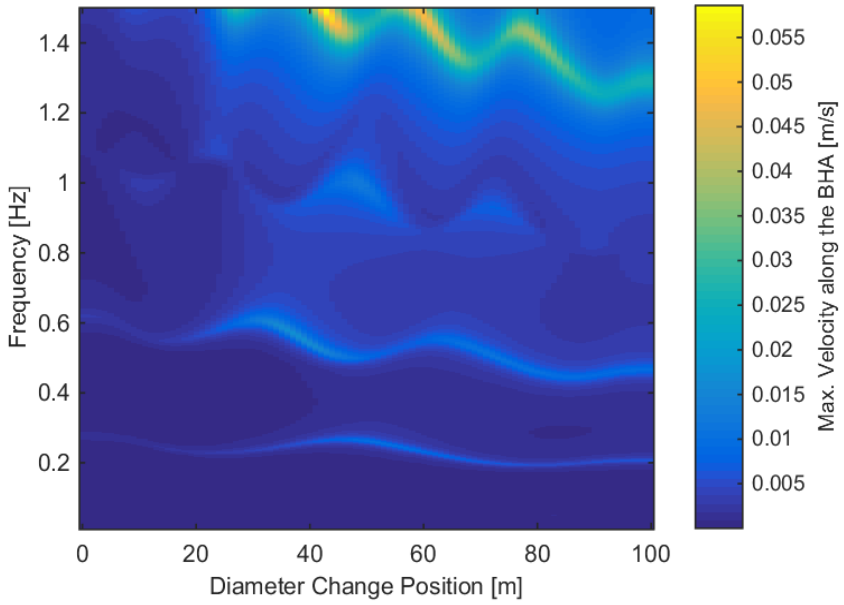

Fig. 6.55: Max. lateral velocity for all diameter change positions. The excitation is located at 25 m.

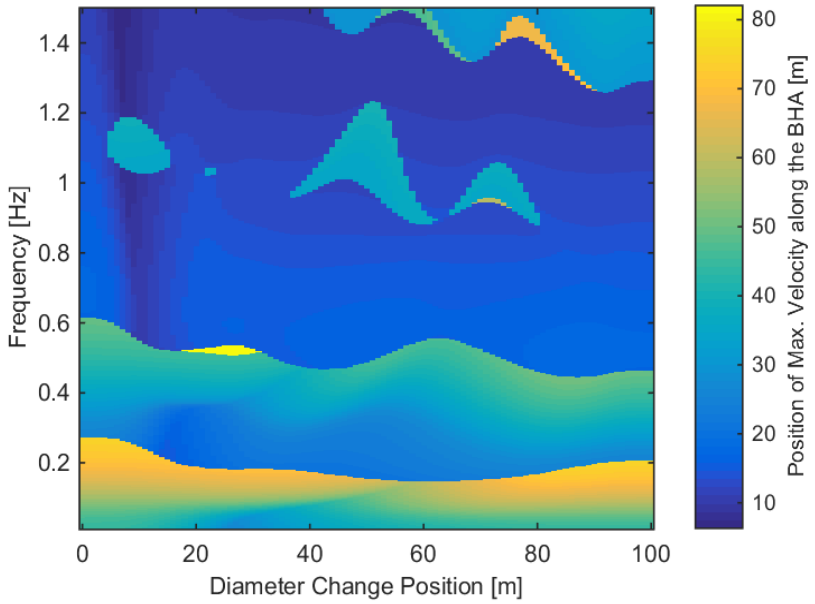

Fig. 6.56: Position of the maximum lateral velocity along the BHA.

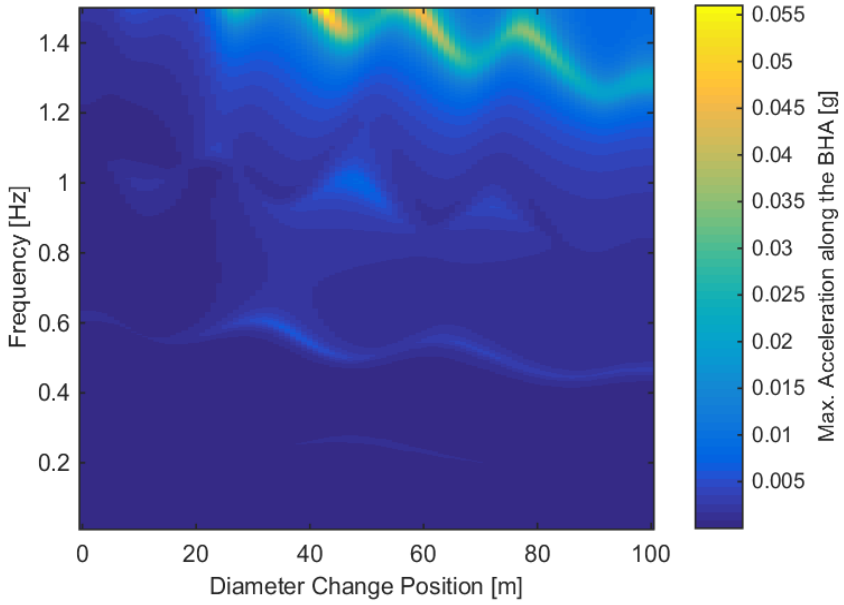

Fig. 6.57: Max. lateral acceleration for all diameter change positions.

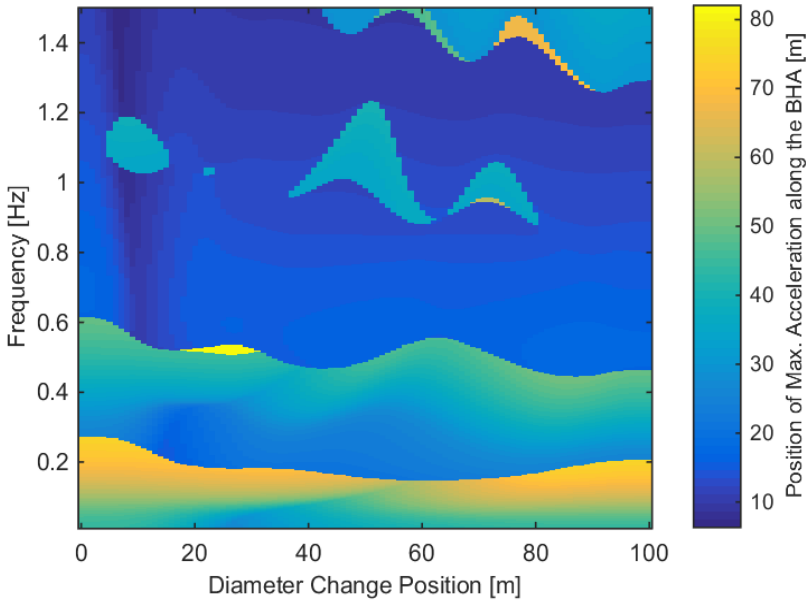

Fig. 6.58: Position of the maximum lateral acceleration along the BHA.

6.5 Appendix E

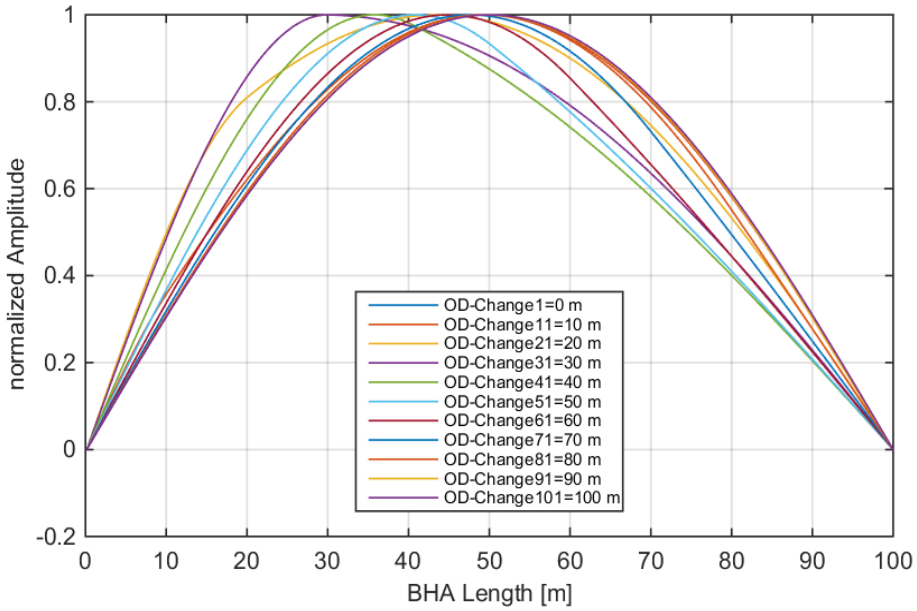

Fig. 6.59: Normalized 1st normal modes for selected diameter change positions.

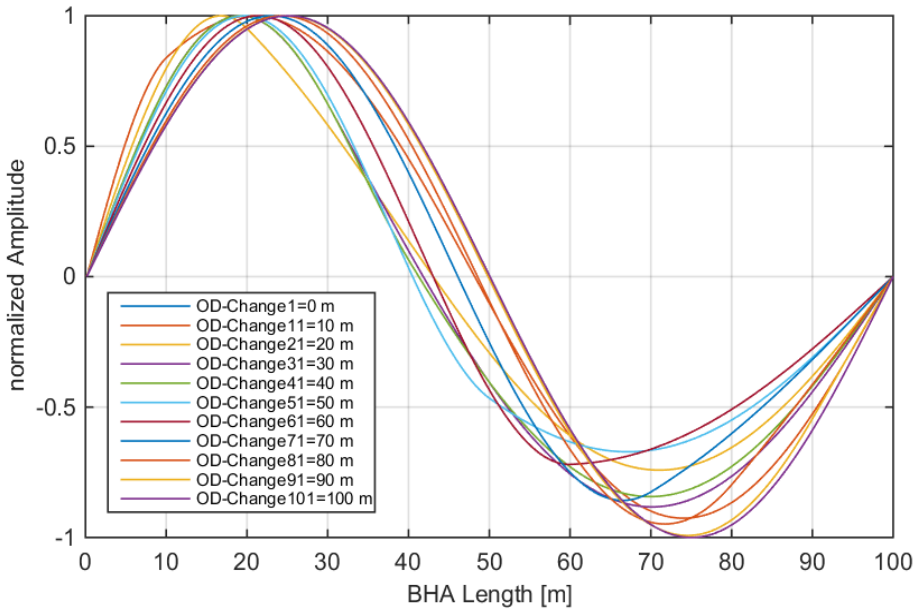

Fig. 6.60: Normalized 2nd normal modes for selected diameter change positions.

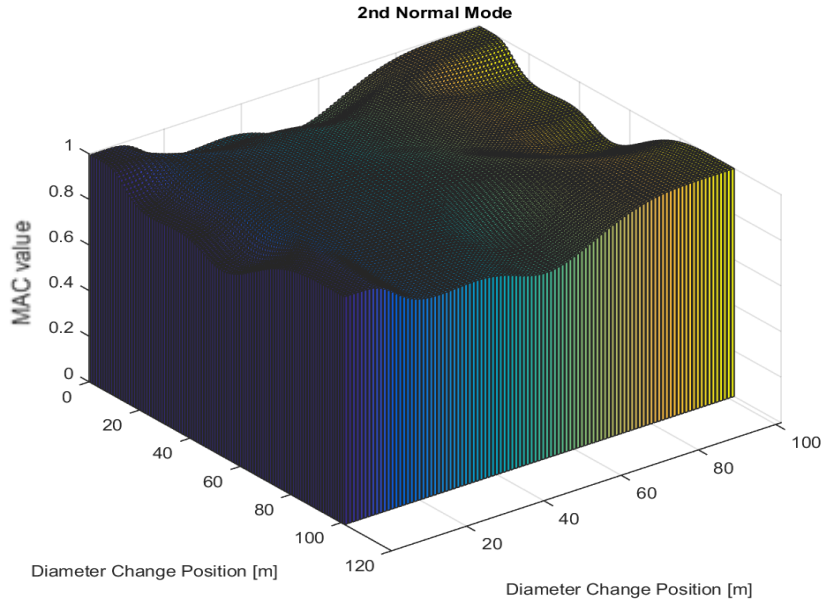

Fig. 6.61: Modal assurance criterion for all 2nd normal mode shapes.

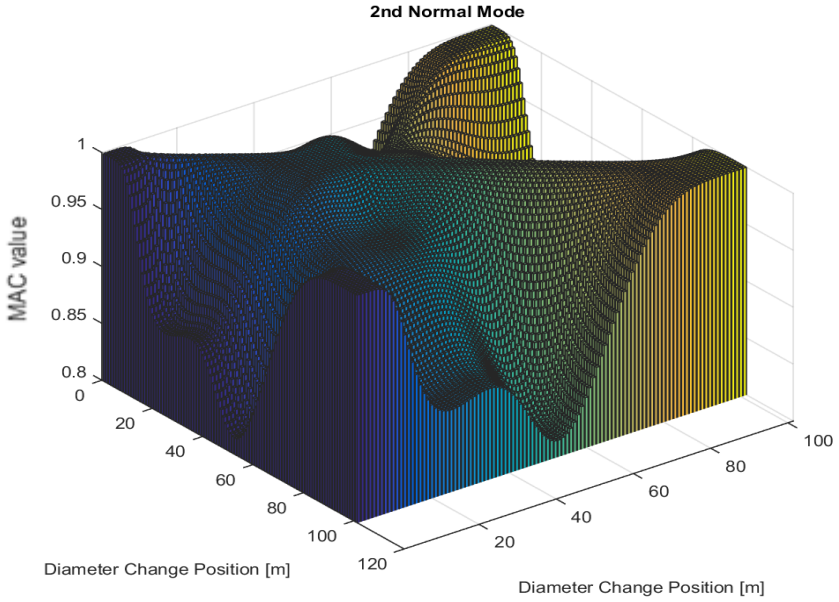

Fig. 6.62: Magnification of Fig. 6.61 to show the small changes in the degree of correspondence.

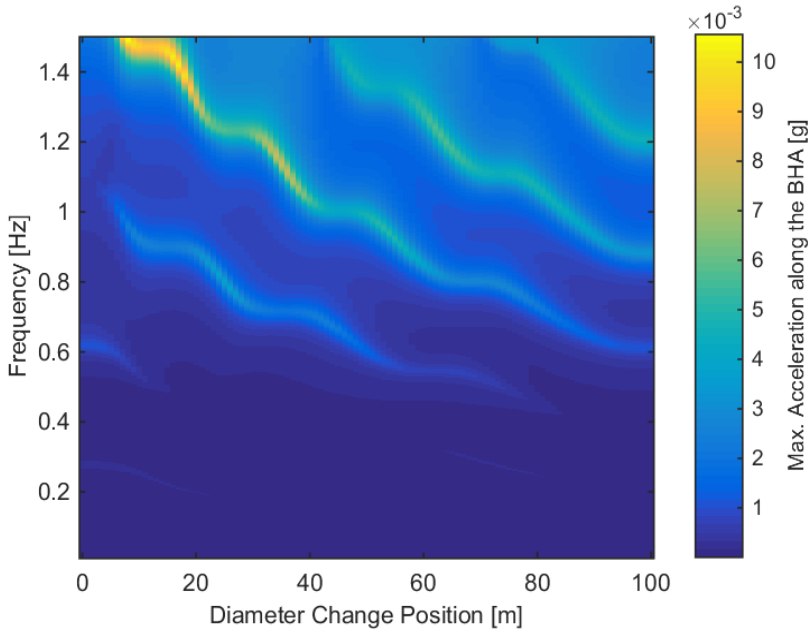

Fig. 6.63: Max. lateral acceleration for all diameter change positions under constant mass considerations.

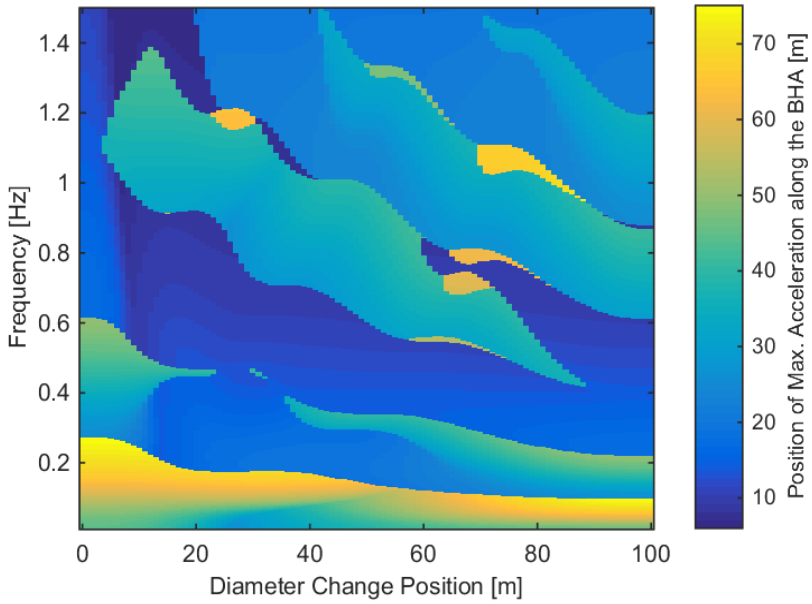

Fig. 6.64: Position of the max. lateral acceleration along the BHA for all diameter change positions under constant mass considerations.

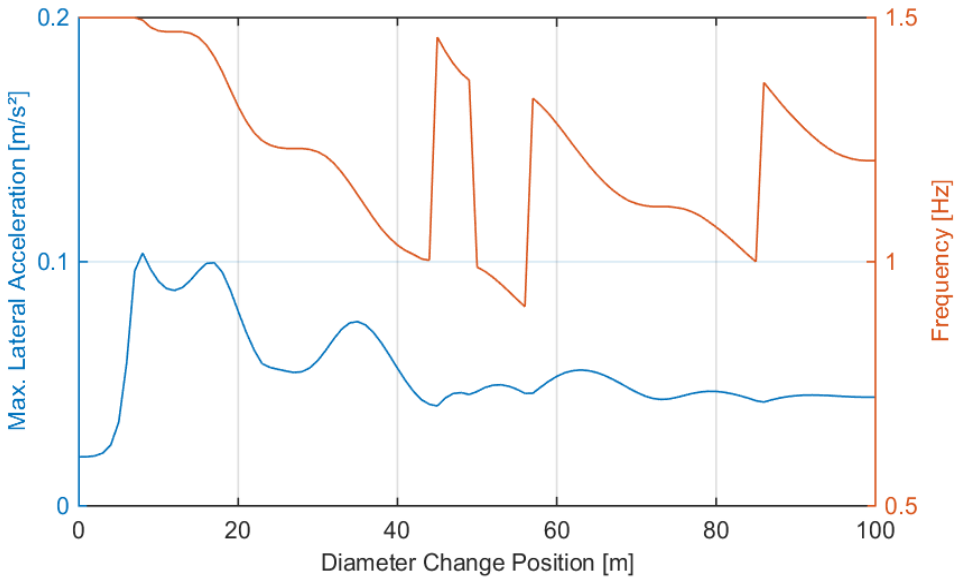

Fig. 6.65: Max lateral acceleration for all diameter change positions and across the whole frequency range.

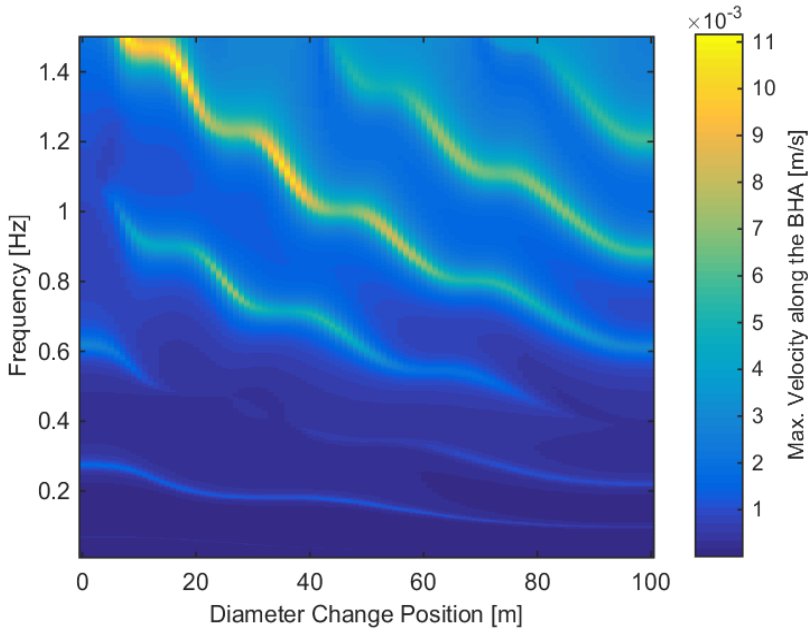

Fig. 6.66: Max. lateral velocity for all diameter change positions under constant mass considerations.

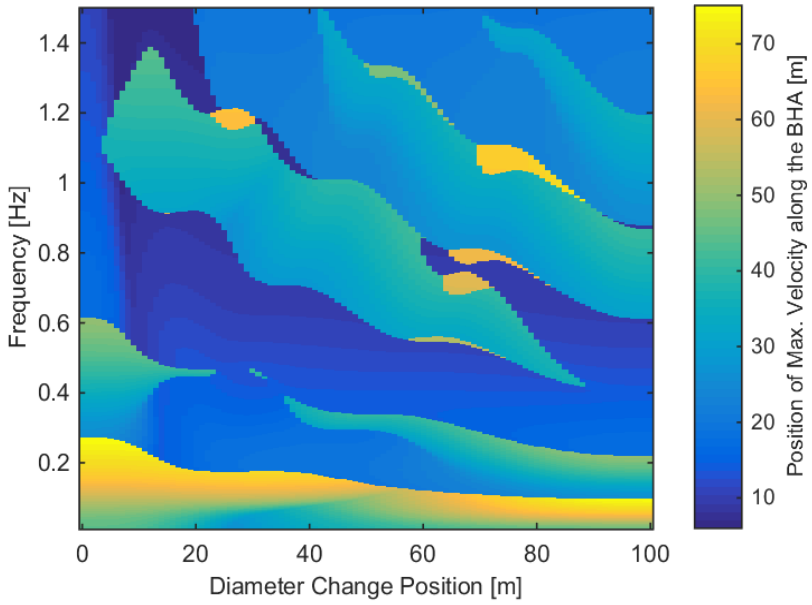

Fig. 6.67: Position of the max. lateral velocity along the BHA for all diameter change positions under constant mass considerations.

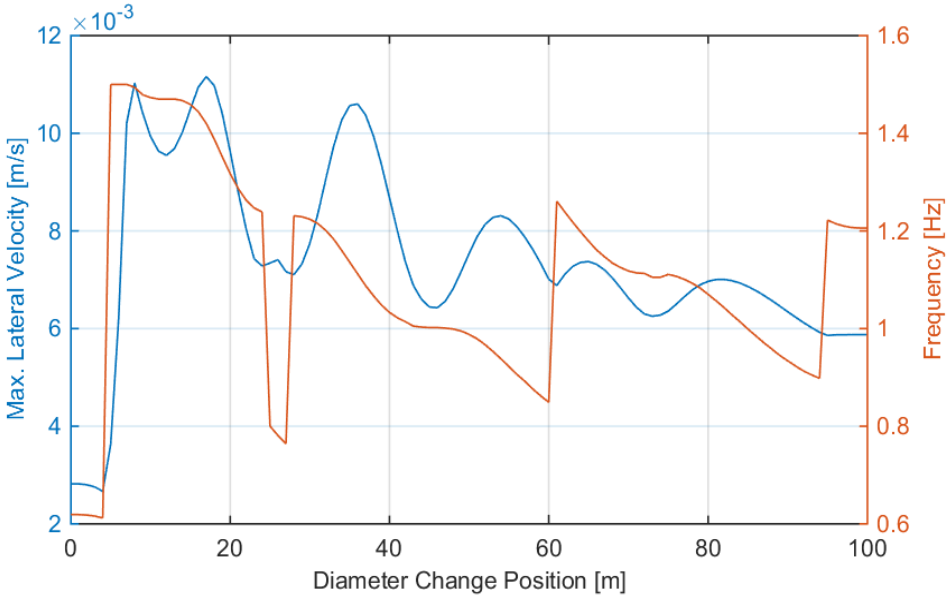

Fig. 6.68: Max lateral velocity for all diameter change positions and across the whole frequency range.

6.6 Appendix F

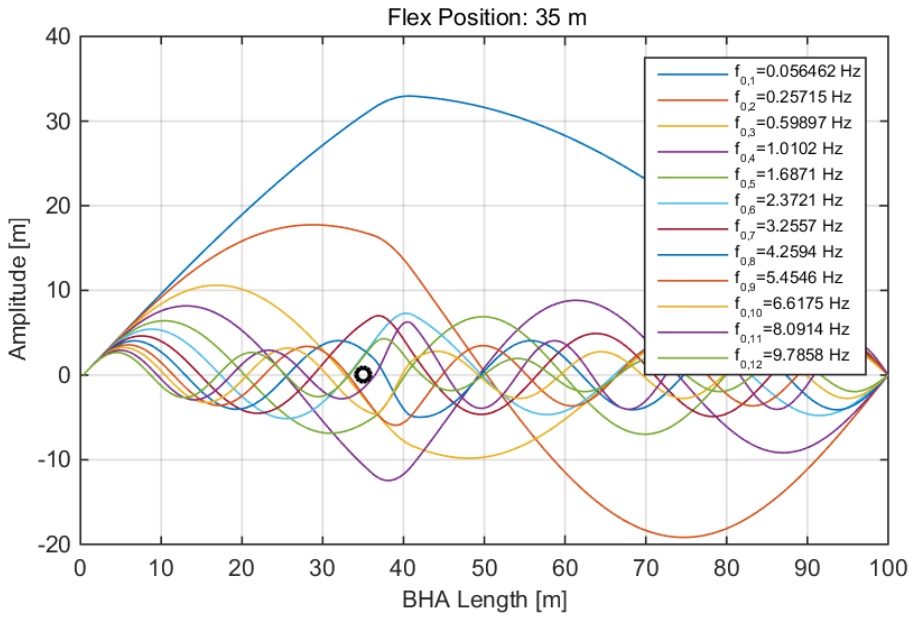

Fig. 6.69: The first five natural frequencies and normal model shapes for a 5 m flex-sub starting at 35 m from the bit and terminating directly at the excitation source location. Note the symmetry to the flex-sub at 65 m in terms of normal mode shape.

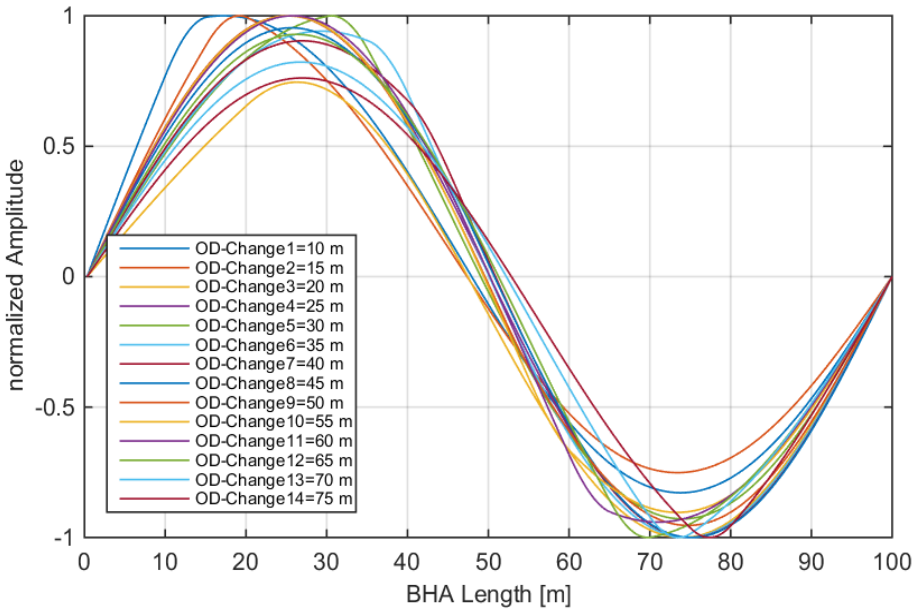

Fig. 6.70: Normalized 2nd normal modes for selected flex-sub positions.

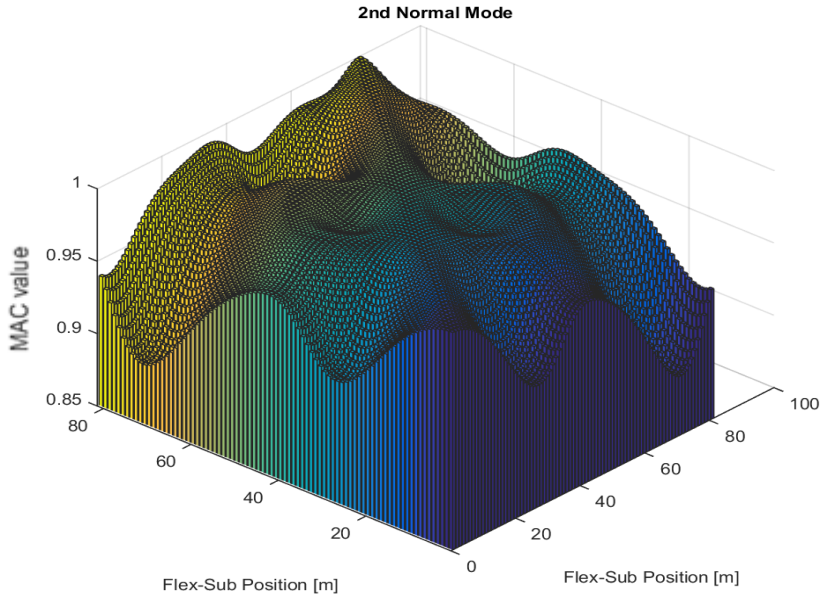

Fig. 6.71: Modal assurance criterion for all 2nd normal modes of all flex-subs.

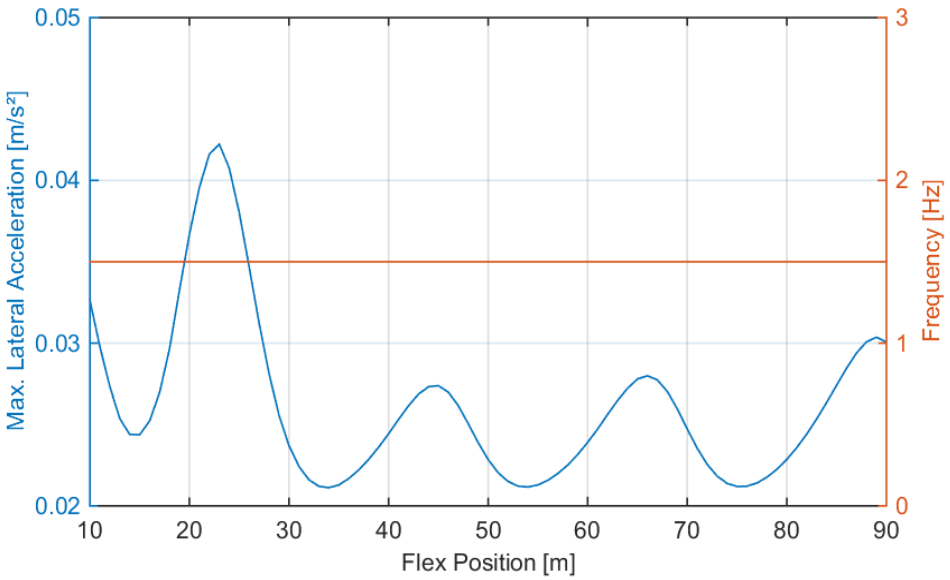

Fig. 6.72: Max. lateral acceleration for all flex-subs and across the whole frequency range.

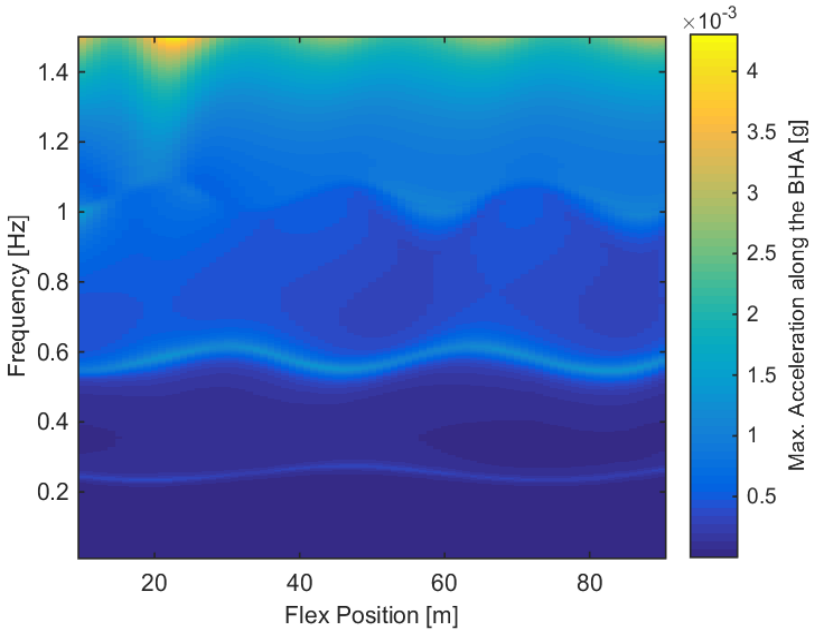

Fig. 6.73: Max. lateral acceleration for all flex-sub positions.

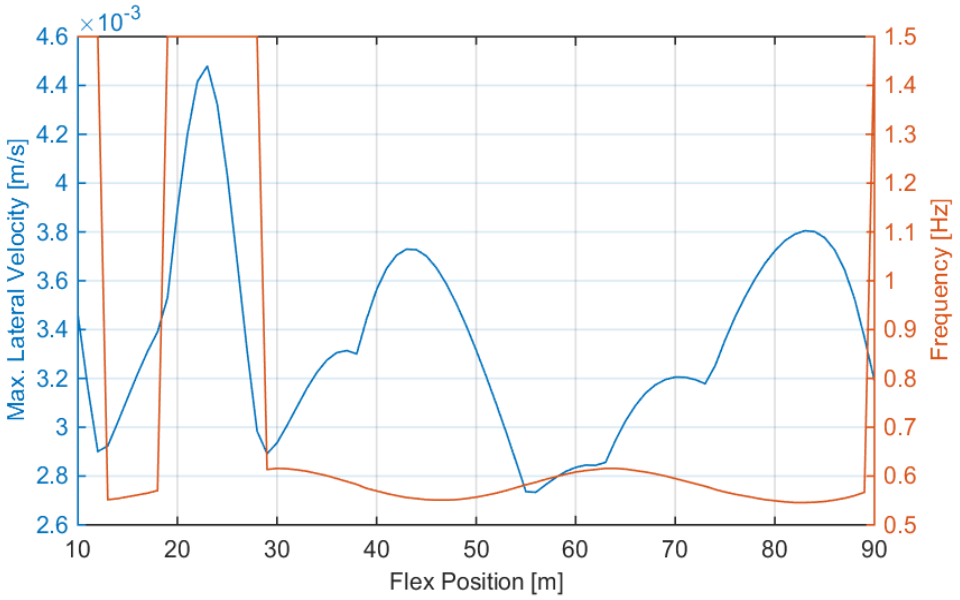

Fig. 6.74: Max. lateral velocity for all flex-subs and across the entire frequency bandwidth.

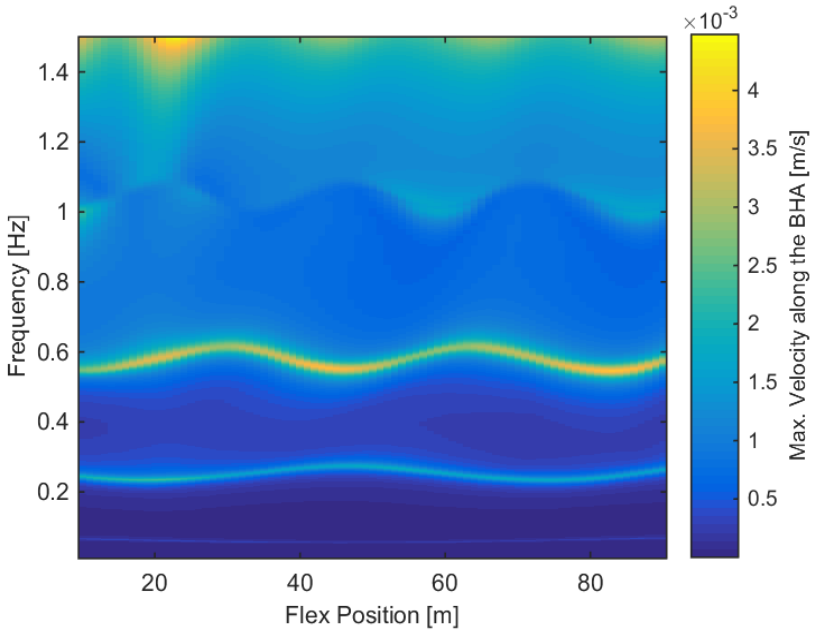

Fig. 6.75: Max. lateral velocity for all flex-sub positions.

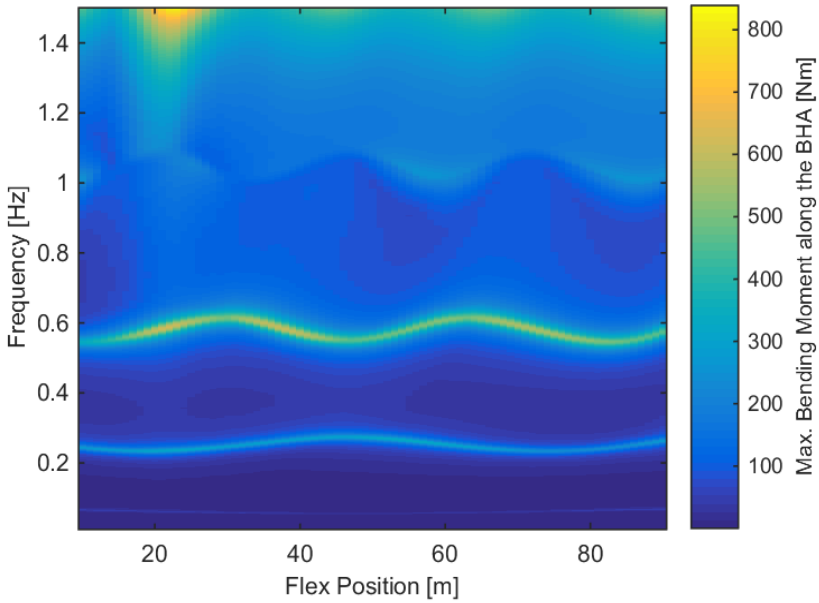

Fig. 6.76: Max. bending moment for all flex-sub positions.

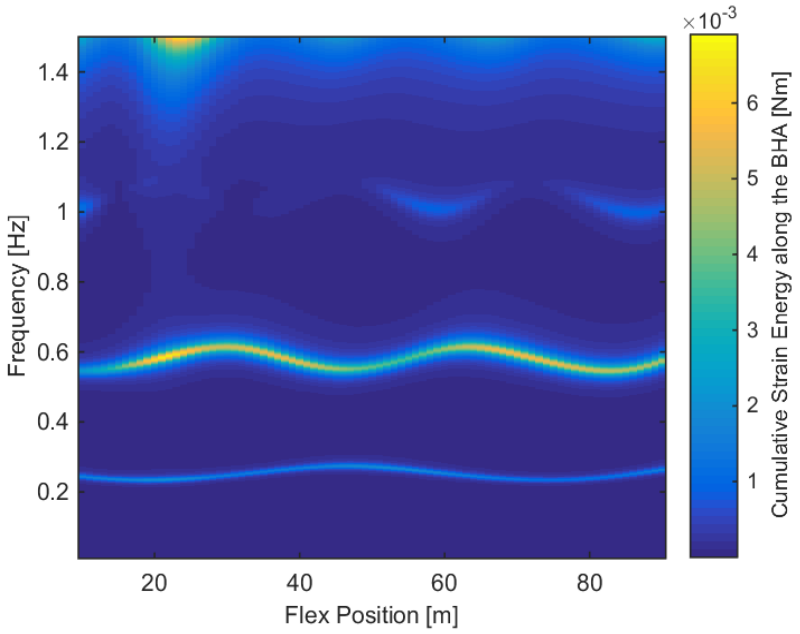

Fig. 6.77: Cumulative strain energy for all flex-sub positions.

6.7 Appendix G

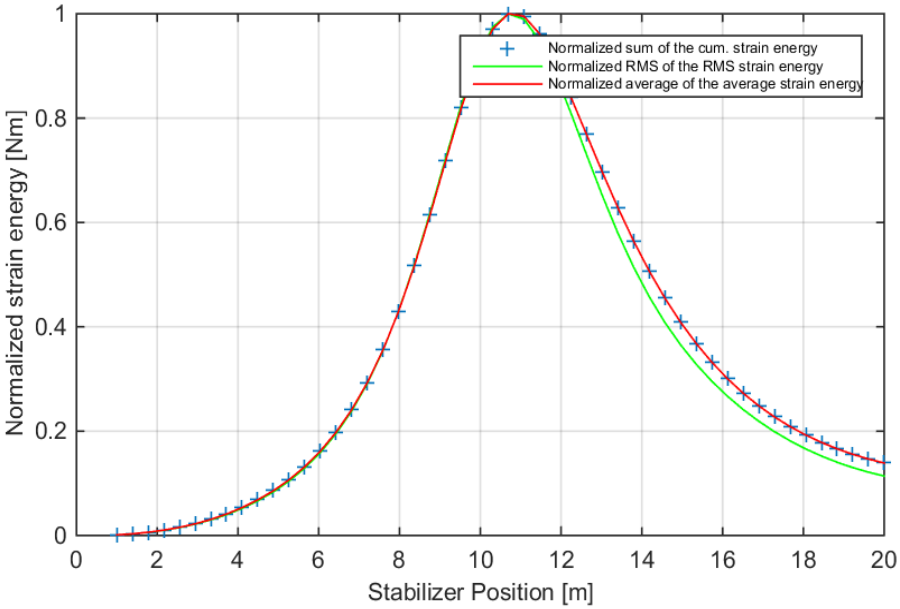

Fig. 6.78: Normalized summated strain energy values across the length and frequency for every configuration under the consideration of an excitation at the bit.

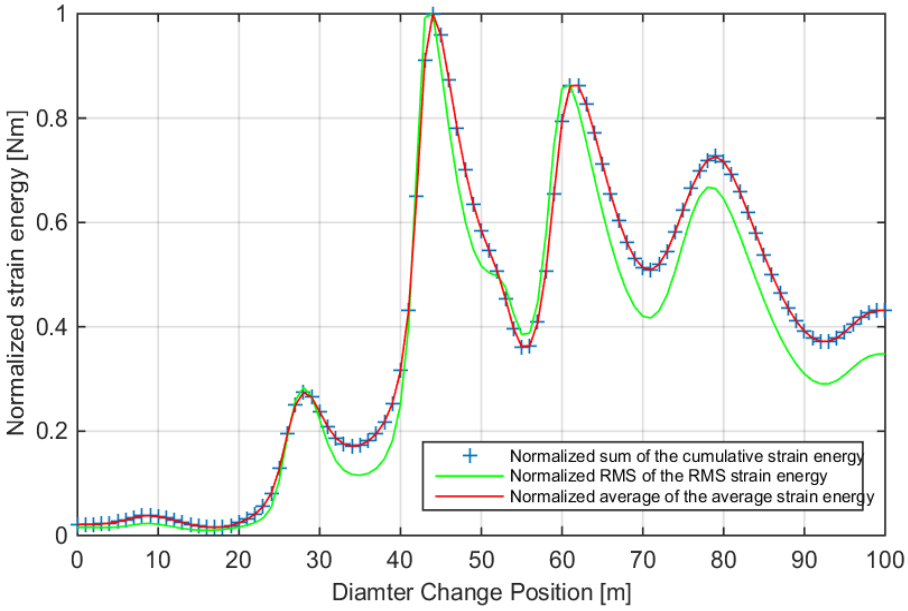

Fig. 6.79: Normalized summated strain energy values across the length and frequency for every diameter change configuration with a component mass which changes with the diameter change accordingly.

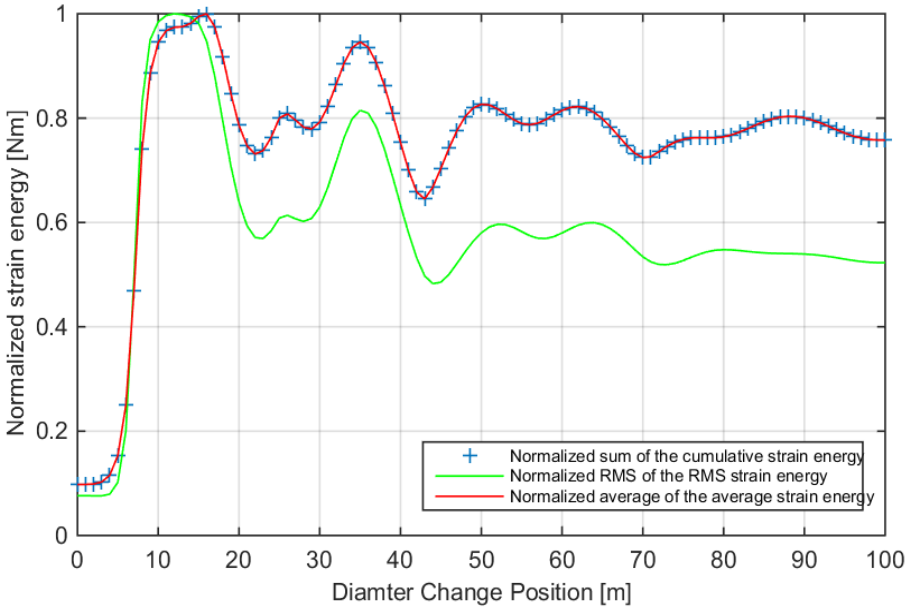

Fig. 6.80: Normalized summated strain energy values across the length and frequency for every diameter change configuration und constant mass considerations.

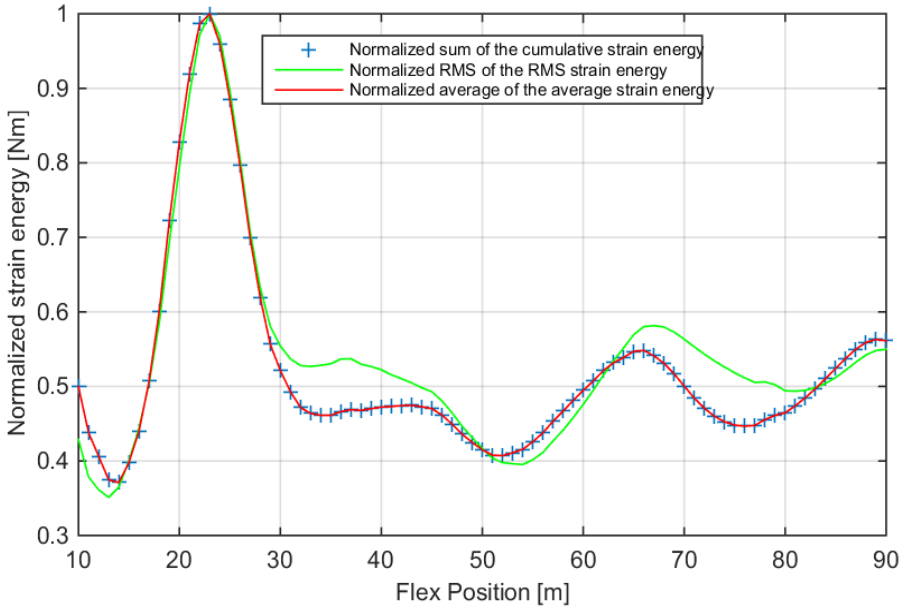

Fig. 6.81: Normalized summated strain energy values across the length and frequency for every flex-sub configuration.